**Design, validation, and application outcomes of a novel Isotopic $N_2O$ monitoring system for field research.**

By

Jordi T. Francis Clar

A dissertation submitted in partial fulfillment of

the requirements for the degree of

Doctor of Philosophy

(Biological Systems Engineering)

at the

UNIVERSITY OF WISCONSIN-MADISON

2021

Date of final oral examination: 04/29/2021

The dissertation is approved by the following members of the Final Oral Committee:

Robert P Anex, Professor, Biological Systems Engineering

Christopher Kucharik, Professor, Agronomy

Matthew Ruark, Professor, Soil Science

Carrie Laboski, Professor, Soil Science

Rebecca Larson, Associate Professor, Biological Systems Engineering

## *I. Abstract*

Nitrous Oxide ($N_2O$) is a global environmental hazard because it is the third most important greenhouse gas (GHG) and the strongest ozone depletion substance in the stratosphere. The concentration of $N_2O$ in the atmosphere has increased from 270±0.1 ppb during pre-industrial times to 333.6±0.1 ppb in 2020. More than three-quarters of the total anthropogenic $N_2O$ production is derived from the use of nitrogen fertilizers in agriculture. Developing mitigation strategies to reduce $N_2O$ soil emissions remains a major challenge due to the lack of $N_2O$ monitoring systems able to capture $N_2O$ emissions with enough temporal and spatial resolution to meaningfully compare the effects of different soil management practices on $N_2O$ emissions.

This dissertation is focused on the design and validation of a state-of-the-art $N_2O$ isotopic monitoring system for in-field research that combines the capabilities of: (1) performing long sampling campaigns with enough temporal and spatial resolution to properly evaluate mitigation strategies; and, (2) measuring changes in the isotope ratios of soil $N_2O$ emissions to elucidate the underlying biological $N_2O$ production and consumption processes. The validation and applicability of this $N_2O$ monitoring for field research went beyond laboratory testing and extended to five years of field research. In addition to assessing the performance of the monitoring system, the goals of the field research were to: (1) improve our understanding of the temporal variability of $N_2O$ soil emissions in highly fertilized crop systems and provide $N_2O$ sampling recommendations to improve the accuracy of $N_2O$ estimates; (2) study the effects of the timing of fall manure application on soil $N_2O$

emissions; and, (3) quantify and compare the overall N losses via $NO_3$ and $N_2O$ from fall manured corn crops in the upper Midwest of the US to identify main N pathway losses and improve fall manure application recommendations.

Recent advances in Laser Absorption Spectroscopy (LAS) have led to the development of trace gas analyzers that provide highly accurate, real-time, simultaneous measurements of $N_2O$ concentration and isotopic composition. Using an LAS instrument that uses Off-Axis Integrated Cavity Output Spectroscopy (OA-ICOS) technology, I designed and built an autonomous in-field system for monitoring $N_2O$ isotope flux during long sampling campaigns with high temporal and spatial resolution (Chapter 2).

While I was developing this new $N_2O$ isotopic flux monitoring system, publications began to appear in the literature that reported on in-field $N_2O$ isotope analysis using different implementations of LAS analyzers. However, the ability of these LAS-based measurement systems to provide consistent, reliable, and accurate *in situ* measurements was only partially evaluated in a few studies. Using laboratory testing, Monte Carlo uncertainty analysis, and soil flux simulations, we assessed the stability and uncertainty of the LAS instrument $N_2O$ isotopic measurements of soil trace gas flux captured in static soil chambers (Chapter 3). This chapter demonstrates that several characteristics of the LAS isotopic instrument make it poorly suited for *in situ* isotopic composition analysis of soil emitted $N_2O$.

The use of our system during one full corn growing season (i.e., 7 months) and four year-round sampling campaigns showed that our system is highly reliable and suitable for long term field research, measuring on average 32 fluxes per day from 4 soil chambers. Analysis

of multiple years of the high temporal resolution $N_2O$ flux-data provided evidence that the diurnal variability of $N_2O$ fluxes changes with flux intensity and that sampling frequently during peak $N_2O$ emissions is essential for an accurate measure of cumulative emissions (and more important than choosing what hour of the day to sample when using infrequent manual sampling).

By quantifying $N_2O$ flux emissions and $NO_3^-$ leachate losses from plots receiving dairy slurry manure early and late in the fall my research demonstrated that time of manure application during the fall has contrasting effects on $N_2O$ and $NO_3^-$ losses and that $NO_3^-$ losses were always larger than $N_2O$ losses.

Collectively this research provides valuable information that can inform ways to reduce the impacts of agriculture on the environment and especially in the mitigation of $N_2O$ soil emissions. My research has done this by designing, implementing, and evaluating a new autonomous $N_2O$ monitoring system that enables the development of $N_2O$ mitigation strategies, and by providing insights into the temporal variability of $N_2O$ emissions and the dynamics of N losses via $NO_3^-$ leaching and $N_2O$ emissions related with fall manure application practices in the Midwestern United States.

## *II. Acknowledgements*

I would like to thank the people who helped me in both my graduate student life and research. First and foremost, I would like to express my sincere appreciation to my advisor Pr. Robert Anex for his tireless guidance, support and encouragement throughout my work. Without his support and help, my thesis would not be a reality today.

I would like to give special thanks Christopher Kucharik, Matthew Ruark, Carrie Laboski, and Rebecca Larson, for serving on my committee, their questions and their constructive comments and feedback.

During the first two years of continuous field experiments studying the trade-off between $NO_3^-$ and $N_2O$ losses my field work was conducted in parallel with an on-going experiment conducted by Pr. Laboski. These two years were crucial in my development as an agricultural field researcher. I am grateful to Pr. Laboski for her support and for giving me the opportunity to work with her team. Special thanks to the Laboski's Lab team members: Todd Andraski, Andy Larson and Anna Teeter which help and support extended beyond our two years of cooperative research. To Todd Andraski, for guiding and helping me through field research and for sharing his invaluable experience and knowledge. To Andy Larson for his dedication, care, and compromise during field work. and to Anna Teeter for her help and for inquisitive research attitude. It was a pleasure and an honor working, learning and laughing with you.

Special thanks to Pr. Ruark and Rebecca Larson for their attention, guidance, and generosity regarding nitrate analysis.

I would also like to thank Mark Allie from the Department of Electrical and Computer Engineering and Kody Habeck (Manager of the Agricultural Engineering Laboratory Shop), their guidance and help was instrumental in the development of the system. Also, thanks to BSE students Ian Rigell, Chris Elwood, Brennan Lunzer, Brian Straub and Dalton Jackson for their help building parts directly and indirectly related to the $N_2O$ monitoring system. I thank also the High School student Braeden B. Anex (now a Mechanical Engineer) for spending part of his summer vacation testing the system.

Special thanks to all the people in my research group and in the Biological Systems Engineering Department for their companionship and support.

Finally, I am grateful to the University of Wisconsin – Madison, especially for supporting the completion of my research via the 'Dissertation Completion Fellow'. The economical and emotional support from UW during the COVID-19 global pandemic was critical in reaching my goals as a student and researcher.

This material is based upon work that was supported by the National Institute of Food and Agriculture, U.S. Department of Agriculture, Hatch project under accession numbers 1001805 and 1009785.

Any opinions, findings, conclusions, or recommendations expressed in this publication are those of the author and do not necessarily reflect the view of the U.S. Department of Agriculture.

***III Table of contents***

I. Abstract i

II. Acknowledgements iv

III Table of contents vi

**Chapter 1: General introduction** 1

References .....13

**Chapter 2: A novel system for high-resolution, near-continuous measurements of soil $N_2O$ isotope fluxes** 19

1. Abstract.....19
2. Introduction .....20
3. Methods – Description of the system .....23
   - 3.1. Isotopic $N_2O$ analyzer ..... 23
   - 3.2. System description ..... 25
4. Results and discussion – System performance .....31
   - 4.1. Flux estimation..... 31
   - 4.2. Minimum Detectable Flux ..... 37
   - 4.3. System Integrity ..... 37
5. Conclusion.....43

6. References .....45

7. Appendix .....49

7.1. Part list..... 49

7.2. Drawings Automatic Soil Chamber ..... 68

7.3. Gas Path Diagram..... 78

7.4. Electrical Diagrams ..... 78

**Chapter 3: Assessing nitrous oxide ($N_2O$) isotopic analyzer performance for in-field use** 87

1. Abstract.....87

2. Introduction .....89

3. Methods and Materials .....95

3.1. LAS analyzer and soil chamber system ..... 95

3.2. Calibration of the LAS ..... 96

3.3. Uncertainty of isotope ratio estimates..... 97

3.4. Soil Flux simulations..... 105

3.5. Soil Chamber flux simulations..... 108

3.6. Isotope ratio δ-concentration dependence correction..... 109

4. Results .....110

4.1. Uncertainty of the isotope ratios ..... 110

4.2. Uncertainty of the isotope ratios .....**Error! Bookmark not defined.**

5. Discussion.....119

6. Uncertainty of the isotope ratios.....119

6.1. Soil Flux simulations..... 123

7. Conclusions .....128

8. References .....130

**Chapter 4: Flux intensity and diurnal variability of soil $N_2O$ emissions in a highly fertilized cropping System** 135

1. Abstract.....135

2. Introduction .....137

3. Materials and methods.....142

3.1. Experimental Site ..... 142

3.2. $N_2O$ fluxes and ancillary measurements ..... 144

3.3. $N_2O$ flux estimation..... 147

3.4. Data selection and statistical analysis ..... 148

4. Results .....152

5. Discussion.....155

6. Conclusion.....160

7. Acknowledgments .....161

8. References .....162

9. Appendix .....165

9.1. Supplement S1..... 165

9.2. Supplement S2..... 167

**Chapter 5: Quantifying trade-offs of nitrogen loss as NO3- and N2O between early and late fall dairy slurry application.** 171

1. Abstract.....171

2. Introduction .....171

3. Materials and Methods .....172

3.1. Experimental Site and set up..... 177

3.2. $NO_3^-$ leaching losses..... 181

3.3. $N_2O$ measurements..... 186

3.4. $N_2O$ flux estimation..... 189

3.5. $N_2O$ data selection..... 191

3.6. Cumulative $N_2O$ emissions ..... 192

3.7. Peak $N_2O$ emissions ..... 193

3.8. Statistical analysis ..... 194

4. Results .....196

4.1. Weather conditions..... 196

4.2. Soil and manure analysis ..... 197

4.3. $NO_3^-$ leaching losses ..... 198

4.4. $N_2O$ measurements ..... 204

4.5. Cumulative $N_2O$ emissions ..... 206

4.6. Peak $N_2O$ emissions ..... 207

4.7. Overall $N_2O$ and $NO_3$- losses ..... 212

4.8. Grain and biomass yields ..... 212

5. Discussion ..... 213

5.1. $NO_3$ leaching losses ..... 213

5.2. $N_2O$ emissions ..... 216

5.3. $N_2O$ and $NO_3^-$ losses ..... 221

6. Conclusions ..... 221

7. References ..... 223

8. Appendix ..... 229

**Chapter 6: General conclusions** 229

References ..... 242

## ***Chapter 1: General introduction***

The detrimental properties of nitrous oxide ($N_2O$) are well known. First, it is a potent greenhouse gas (GHG), with a global warming potential 298 times that of dioxide of carbon ($CO_2$) (Stocker et al., 2013). Second, it is a long-lived gas, with a molecule of $N_2O$ staying in the atmosphere on average 114 years before being removed by a sink or chemically destroyed. Third, it is the single most important depleting substance of stratospheric ozone (Ravishankara et al., 2009). In recent decades, the atmospheric concentration of $N_2O$ broke the natural cyclical trend reaching a global concentration of 330±0.1 ppb, the highest ever observed (IPCC, 2014). In addition, the rate at which the atmospheric concentration is growing is increasing annually. The growth rate between 2015 and 2016 was 20% larger than the mean rate over the previous 10 years (0.89 ppb year $^{-1}$) (WMO, 2016). Agricultural soil, mostly due to the use of nitrogen fertilizers and animal manure, is the largest source of $N_2O$ emissions, accounting for about two-thirds of $N_2O$ emissions worldwide and for about three-quarters of the total anthropogenic U.S. $N_2O$ emissions (Davidson, 2009; IPCC, 2014; Smith, 2017). Reductions in $N_2O$ emissions can be accomplished by improving management (i.e., fertilization, tillage, irrigation) in these cultivated soils (Snyder et al., 2014). The impact of decades of research on $N_2O$ soil emissions have been impeded by two technical barriers: (1) the lack of measuring systems that quantify $N_2O$ emissions accurately enough to compare mitigation practices, and (2) the limitation of current measuring techniques to elucidate the underlying $N_2O$ production pathways during field campaigns with the appropriate temporal and spatial resolution.

## $N_2O$ soil flux measurements

Measuring $N_2O$ emissions accurately during field research has proved to be very challenging because $N_2O$ fluxes from agricultural soils exhibit very large temporal and spatial variation (Ball et al., 2000; Butterbach-Bahl et al., 2013; Giles et al., 2012; Hénault et al., 2012; Molodovskaya et al., 2012). Experimental methods used to measure $N_2O$ emissions in the field are varied and there are no universally accepted standards or guidelines. The two general measurement approaches are micrometeorological techniques and soil chamber techniques (Rapson & Dacres, 2014). Micrometeorological techniques are used to measure changes of $N_2O$ at atmospheric concentrations over large areas between 0.1 and 10 $km^2$. The power of these systems derives from very precise gas Laser Absorption Spectrometry (LAS) analyzers that can detect changes in concentrations at sub-part per billion levels in very short amounts of time. These methods require the construction of a measuring tower of 10 to 20 m height and tri-dimensional measurements of wind direction and speed and other atmospheric variables affecting atmospheric $N_2O$ concentrations (e.g., moisture and temperature). These sophisticated systems allow flux estimation with good temporal resolution. However, they are meant to measure $N_2O$ changes over large surface areas and thus their use to evaluate different $N_2O$ mitigation practices at the plot scale is not recommended (Bai et al., 2018; Smith et al., 1994)

Manual chamber methods are the most widely used methodology to measure $N_2O$ soil emissions, and there is a great deal of variability in the practices used. Nevertheless, there are efforts to create chamber method standards (Grace et al., 2020; Harvey, 2012; Parkin &

Venterea, 2010). In general, an open bottom box (i.e., chamber) is inserted a few centimeters into the soil, bounding the interaction between soil processes and the atmosphere to a specific volume of soil. Typically, several gas samples (3 to 4) are manually taken from the chamber headspace using a hypodermic syringe and needle passed through a septum in the chamber lid. The samples are then transferred to evacuated vials for transport to an analytical instrument. This method has been used widely because it is easy to implement, and manual sampling of this type can be used at any location. Manual chamber methods are affordable because long deployment times (hours) and post sampling analysis allow the use of less sensitive analytical instruments (Harvey, 2012; Mondini et al., 2010; Parkin et al., 2003).

Despite the benefits of this method, it has several limitations. Chamber placement alters environmental factors involved in soil gas production – 'chamber effects' (i.e., alteration of soil temperature, pressure, humidity, and wetting - drying cycles). Long deployment times produce larger chamber effects especially on the $N_2O$ diffusion gradient between soil and chamber headspace which grows smaller after chamber deployment (Duran & Kucharik, 2013; Hutchinson & Livingston, 2001; Rochette & Eriksen-Hamel, 2008; Smith, Keith & Dobbie, 2001; Xu et al., 2006). These chamber effects result in non-linear gas flux data and an underestimation of pre-deployment flux by up to 40% (Anthony et al., 1995). The use of high-precision, high-frequency analytical instruments allow shorter deployment times and thus reduces chamber effects and increases the accuracy and precision of soil trace gas flux estimates (Venterea et al., 2009). Chambers need to be replicated in order to capture spatial variability and have sufficient statistical power to evaluate the effect of mitigation strategies. Soil heterogeneity introduces large differences in $N_2O$ soil emissions due to localized high

microbial activity and small-scale changes is soil properties (Giles et al., 2012; Groffman et al., 2009; Hénault et al., 2012). According to Morris, et al. (2013), the largest increase in statistical power was achieved by the first 3 to 5 chambers per replicated plot (2.5 m by 10 m in size).

High variability of $N_2O$ soil emissions is caused by sporadic and intermittent appearance of high $N_2O$ emission bursts. Single-day events, or 'hot moments', and multi-day events, 'peak events', can contribute up to half of cumulative annual $N_2O$ emissions while representing less than 7% of the total time observed (Molodovskaya et al., 2011). Parkin and Kaspar, (2006) observed in 2003, that 49% of cumulative $N_2O$ flux in corn plots was due to just two intense peaks that occurred 14 days apart. Similarly, Li et al. (2015) found that hot moments accounted for over 50% of $N_2O$ emissions from manure fertilized corn fields in Japan. Manured fields are particularly prone to peak emission events associated with winter and spring freeze-thaw cycles (Wagner-Riddle & Thurtell, 1998). Wagner-riddle, et al. (2007) found fluxes during the non-growing season (Nov-April) in a corn-soybean-wheat rotation comprised 30% to 90% of annual emissions, mostly due to fluxes during soil thawing. Peak emissions are not only associated with thawing events but continue throughout the winter months having been observed in soils at temperatures below 0°C and even after complete soil freezing (Ejack & Whalen, 2021; Singurindy et al., 2009; C. Wagner-Riddle et al., 2010). Elevated $N_2O$ fluxes have been observed to occur in response to specific triggers such as tillage, fertilization, rainfall events and soil freeze-thaw cycles (Baggs et al., 2003; Congreves et al., 2018; Sehy et al., 2003; Wagner-Riddle, 2019).

Regardless of the cause, high temporal variability in $N_2O$ soil emissions has been recognized as a significant challenge. Yet, in most experiments soil $N_2O$ flux is measured only during the growing season, overlooking important winter and spring peak emissions, and annual emissions are often computed from just 15 to 30 flux measurements collected during the growing season (Petersen et al., 2006; Schwager et al., 2016; C. Wagner-Riddle & Thurtell, 1998). In most cases, chamber sampling is performed at 21 days intervals which yields flux estimates within +60%to -40% of the actual cumulative flux computed using with 6h sampling interval (Parkin, 2006). Barton et al. (2015) demonstrated that to obtain annual $N_2O$ fluxes within the 10% of the 'best' estimate, sampling should be performed daily.

There are four components required for accurate and reliable soil $N_2O$ monitoring systems. First, precise analytical tools able to measure small changes in $N_2O$ concentration in real time to overcome the limitations of the soil chamber methodologies. Second, measurement should be performed at temporal frequencies high enough to reflect variations in conditions (e.g., rain, soil moisture, and temperature) influencing bacterial $N_2O$ production rates (e.g., near- continuous systems). Third, systems should be reliable, working over extended periods of time to enable the capturing and quantifying of ephemeral $N_2O$ soil emissions that account for the majority of cumulative emissions (e.g., 'hot moments' and 'peak events'). Fourth, accounting for spatial variations requires replicate experiments, so several soil chamber in close proximity (i.e., the same plots) must be monitored at more or less the same time (e.g., similar ambient conditions).

**Identification of $N_2O$ production pathways in soils**

Although the processes of $N_2O$ production and consumption in soil are not fully understood, it is generally accepted that in agricultural soils $N_2O$ flux is governed by autotrophic nitrification and heterotrophic denitrification (Deppe et al., 2017; Lin et al., 2019). Autotrophic nitrification is a two-step reaction that occurs under aerobic conditions, during which, ammonia ($NH_3$) is oxidized to nitrite ($NO_2$) and nitrate ($NO_3$), and nitrous oxide is formed in the intermediate step as a byproduct of hydroxylamine ($NH_2OH$) oxidation. On the other hand, denitrification is a sub-oxic or anaerobic sequential reaction during which the products of nitrification ($NO_3^-$ and $NO_2^-$) are reduced to dinitrogen ($N_2$) where $N_2O$ is a required intermediate product which can leak out of the heterotrophic cells or become the final product though several mechanisms (i.e., lack/inactivity of the required enzymes in the last step of denitrification or availability of preferred electron acceptors, such as nitrate).

These biological processes are affected differently by soil moisture and aeration, temperature, pH and substrate availability (Henault et al., 2012; Robertson & Groffman, 2015; Sahrawat, 2008; Syakila & Kroeze, 2011). Understanding of the processes responsible for $N_2O$ production and consumption in soils, as well as an understanding of how the relative importance of different production pathways change with time is crucial to develop effective soil management strategies to mitigate $N_2O$ soil emissions while sustaining agricultural productivity. Early approaches for estimating the contribution of denitrification and nitrification to $N_2O$ emissions have mostly relied on acetylene inhibition and isotopic labeling (Baggs, 2008; Groffman et al., 2006). These techniques have important limitations

such as disturbance of the system, short operational time, and uneven distribution of the reagents (Groffman et al., 2006; Ostrom, N. E. & Ostrom, P. H., 2012).

During the last decades stable isotope analysis techniques have been developed that offer a powerful tool for disentangling $N_2O$ production pathways in the environment. The linear molecule of $N_2O$ is formed by two atoms of nitrogen and one atom of oxygen, the four most abundant single atom substituted $N_2O$ isotopocules are $^{14}N^{14}N^{16}O$, $^{14}N^{15}N^{16}O$, $^{15}N^{14}N^{16}O$ and $^{14}N^{14}N^{18}O$. The isotope nomenclature in this document follows the nomenclature rules of The International Union of Pure and Applied Chemistry (IUPAC) and the recommendations of the Commission on Isotopic Abundances and Atomic Weights of the IUPAC (Coplen, 2011).

The heavy-to-light isotope ratios are expressed as relative differences in delta (δ) nomenclature as:

$$\delta^{i}E \quad = \left[\frac{R(^{i}E)_{sample}}{R(^{i}E)_{std}} - 1\right] \times 1000 \qquad (1)$$

Where E denotes $^{15}N^{\alpha}$, $^{15}N^{\beta}$, or $^{18}O$ and R denotes $^{14}N^{15}N^{16}O/^{14}N^{14}N^{16}O$, $^{15}N^{14}N^{16}O/^{14}N^{15}N^{16}O$, or $^{14}N^{14}N^{18}O/^{14}N^{15}N^{16}O$ of the samples and standards (Toyoda et al., 2015; Toyoda & Yoshida, 1999). The extraneous factor 1000 is introduced because the relative difference of isotope ratios (δ), result in very small values ($10^{-3}$) and when they are not multiplied by 1000, they should be written as for example 0.0019 or 1.9 $10^{-3}$ . By convention, delta values are always followed by the symbol ‰ pronounced per mil or per mila.

The subscripts α and β indicate the central and terminal position of the heavy N isotope in the $N_2O$ molecule. The parameters Site Preference (SP) and $^{15}N^{bulk}$ described below (Eq. 2 and 3) are used as illustrative parameters to indicate differences in the relative position of the heavy isotope in the $N_2O$ molecule.

$$SP = \delta^{15}N^{\alpha} - \delta^{15}N^{\beta} \quad (2)$$

$$\delta^{15}N^{Bulk} = \left(\delta^{15}N^{\alpha} + \delta^{15}N^{\beta}\right)/2 \quad (3)$$

SP is especially important because it has been shown to be a useful differentiator of the main $N_2O$ production pathways in soils (i.e., nitrification and denitrification) that is independent of the isotopic composition of the substrates (Decock & Six, 2013; Ostrom, N. E. & Ostrom, P. H., 2017).

The established technology for measuring $N_2O$ isotopocule abundance is Isotope Ratio Mass Spectroscopy (IRMS) (Mohn et al., 2014). While IRMS analyzers yield very accurate measurements, they are not field deployable. Using IRMS to analyze soil trace gas fluxes from field experiments requires manual sampling of gas in the soil chamber headspace and transport of the samples to a spectroscopy laboratory for analysis (Rapson & Dacres, 2014). In addition, IRMS differentiate isotopes based in their molecular mass, as $N_2O$ molecules with different SP have the same molecular mass, SP analysis by IRMS requires additional calibration and corrections that increase the complexity of the process and reduce the accuracy of the measurements (Mohn et al., 2014).

**New Laser Absorption Spectroscopy**

Laser Absorption Spectroscopy (LAS) analyzers allow direct quantification of both $N_2O$ concentration and isotopocule ratios using a tune source of light that targets the specific wavelength of the $N_2O$ isotopocule molecules of interest (Chen et al., 2016; Kong et al., 2017; Petersen et al., 2020; Yamamoto et al., 2017). The strength of optical analyzers is their ability to measure rapidly (i.e., $\approx 10^{-7}$ seconds per spectra measurement) and without sample pre-treatment. Increasing the effective laser path-length from a few centimeters to several kilometers allows highly precise measurements without significantly increasing sampling time. Precision is further increased by averaging many spectral measurements collected over relatively short periods of time (~ 3 minutes). Modern LAS analyzers are highly sensitive and provide interference free isotopocule measurement of $N_2O$ in ambient air (Chen et al., 2016; Kong et al., 2017; Petersen et al., 2020; Yamamoto et al., 2017).

Combining LAS analyzers with automatic soil chambers enables measuring $N_2O$ concentrations and isotopocule abundance ratios accurately many times during short chamber deployments (i.e., 20 minutes). Reducing chamber deployment times minimize chamber effects and increase sampling frequency. Because LAS are field deployable, sampling can be automatic and performed during long sampling campaigns including periods of the year when manual sampling is difficult (i.e., winter) capturing elusive but large contributing peak events.

Measurement systems comprising an LAS analyzer and multiple soil chambers and their ability to measure both, $N_2O$ concentration and its isotope ratios are a promising way to apportion $N_2O$ flux to different production pathways in field experiments.

Despite the advantages of LAS analyzers relative to measurement with IRMS, the use of LAS analyzers with soil chambers for field research is still uncommon. This is because commercially available LAS instruments are relatively new and systems for their use in field experiments are still under development. Although several such systems have been reported in the literature (Chen et al., 2016; Kong et al., 2017; Petersen et al., 2020; Yamamoto et al., 2017), the uncertainty of the isotopocule ratios measured using LAS analyzers through direct soil chambers measurements has not been quantified, and it is unknown if, or under what conditions, these systems are suitable for isotope measurements of soil trace gases collected in a soil chamber headspace for distinguishing between $N_2O$ soil production pathways.

The overall objective of this research was the design and validation of a state-of-the-art Isotopic $N_2O$ monitoring system for field research that can perform long sampling campaigns with enough temporal and spatial resolution to properly evaluate mitigation strategies. And to assess the usability of the $N_2O$ monitoring system to distinguish between $N_2O$ soil production pathways by direct isotope ratio analysis of trace gases collected via soil chamber. The validation process went beyond traditional in-laboratory tests and included assessing the usability and performance of the system for in real-time field experiments in corn production systems in the U.S. Upper Midwest. In addition, the objectives of the in-field $N_2O$ measurements were to improve our understanding of the diurnal and seasonal variability of

soil emissions $N_2O$, evaluate the effect of timing manure application during the fall in $N_2O$ soil emissions and to quantify trade-offs of nitrogen loss as $NO_3$ and $N_2O$ between early and late fall dairy slurry application.

This research was inspired in the need of accurate and reliable, near continuous and high temporal $N_2O$ flux measurements and the commercial availability of newly developed LAS $N_2O$ isotope analyzers that allow, in-field, accurate and in real time $N_2O$ analysis.

***Outline of the dissertation***

Chapter 2 describes the novel monitoring system for autonomous and high-resolution measurements of soil $N_2O$ fluxes. The system is based on a novel Isotopic $N_2O$ analyzer (Isotopic $N_2O$ Analyzer, model 914-0027; - Los Gatos Research Inc (San Jose, CA) (ABB subsidiary)) and comprises a set of custom-made automatic chambers, circulating gas paths and a Digital Logic for system integration and easy flux sampling configuration (i.e., sampling frequency, flux sampling time, etc.,). The system is housed in an insulated and temperature-controlled trailer with a built-in power distribution and control system for field deployment.

Chapter 3 assesses the suitability of the $N_2O$ monitoring system for measuring changes in isotopocule ratios of soil $N_2O$ emissions to elucidate the underlying biological $N_2O$ production processes simultaneously with the $N_2O$ soil flux measuring system described in chapter 2.

Chapter 4 uses the flux measurements collected to perform the first temporal study of $N_2O$ fluxes that analyzes multiyear high temporal flux data that includes multiple peak events (i.e., “hot moments” and “hot periods”). The objective of this chapter was to improve sampling $N_2O$ sampling strategies by providing recommendations to maximize the accuracy in the estimation of cumulative emissions when manual sampling is used.

Chapter 5 uses the monitoring system during a 4 year-round sampling campaign to study the effect of manure application time during the fall in $N_2O$ emissions and to quantify the trade-offs in N-loss as $N_2O$ and nitrate ($NO_3^-$) between early and late fall cow slurry application

## *References*


Baggs, E. M. (2008). A review of stable isotope techniques for N2O source partitioning in soils: recent progress, remaining challenges and future considerations. *Rapid Communications in Mass Spectrometry*, *22*(11), 1664–1672. https://doi.org/10.1002/rcm.3456

Baggs, E. M., Richter, M., Hartwig, U. A. & Cadisch, G. (2003). Nitrous oxide emissions from grass swards during the eighth year of elevated atmospheric pCO2 (Swiss FACE). *Global Change Biology*, *9*(8), 1214–1222. https://doi.org/10.1046/j.1365-2486.2003.00654.x

Bai, M., Suter, H., Lam, S. K., Flesch, T. K. & Chen, D. (2018). Comparison of flux gradient and chamber techniques to measure soil $N_2O$ emissions. *Atmospheric Measurement Techniques Discussions*, 1–16. https://doi.org/10.5194/amt-2018-90

Ball, B. C., Horgan, G. W. & Parker, J. P. (2000). Short-range spatial variation of nitrous oxide fluxes in relation to compaction and straw residues. *European Journal of Soil Science*, *51*(4), 607–616. https://doi.org/10.1046/j.1365-2389.2000.00347.x

Barton, L., Wolf, B., Rowlings, D., Scheer, C., Kiese, R., Grace, P., Stefanova, K. & Butterbach-Bahl, K. (2015). Sampling frequency affects estimates of annual nitrous oxide fluxes. *Scientific Reports*, *5*, 15912. https://doi.org/10.1038/srep15912

Butterbach-Bahl, K., Baggs, E. M., Dannenmann, M., Kiese, R. & Zechmeister-Boltenstern, S. (2013). Nitrous oxide emissions from soils: how well do we understand the processes and their controls? *Philosophical Transactions of the Royal Society of London. Series B, Biological Sciences*, *368*(1621), 20130122. https://doi.org/10.1098/rstb.2013.0122

Chen, H., Williams, D., Walker, J. T. & Shi, W. (2016). Probing the biological sources of soil N 2 O emissions by quantum cascade laser-based 15 N isotopocule analysis. *Soil Biology and Biochemistry*, *100*, 175–181. https://doi.org/10.1016/j.soilbio.2016.06.015

Congreves, K. A., Wagner-Riddle, C., Si, B. C. & Clough, T. J. (2018). Nitrous oxide emissions and biogeochemical responses to soil freezing-thawing and drying-wetting. *Soil Biology and Biochemistry*, *117*, 5–15. https://doi.org/10.1016/J.SOILBIO.2017.10.040

Coplen, T. B. (2011). Guidelines and recommended terms for expression of stable-isotope-ratio and gas-ratio measurement results. *Rapid Communications in Mass Spectrometry*, *25*(17), 2538–2560. https://doi.org/10.1002/rcm.5129

Davidson, E. A. (2009). The contribution of manure and fertilizer nitrogen to atmospheric nitrous oxide since 1860. *Nature Geoscience*, *2*(9), 659–662. https://doi.org/10.1038/ngeo608

Decock, C. & Six, J. (2013). How reliable is the intramolecular distribution of 15N in N2O to source partition N2O emitted from soil? In *Soil Biology and Biochemistry* (Vol. 65, pp. 114–127). Pergamon. https://doi.org/10.1016/j.soilbio.2013.05.012

Deppe, M., Well, R., Giesemann, A., Spott, O. & Flessa, H. (2017). Soil N2O fluxes and related processes in laboratory incubations simulating ammonium fertilizer depots. *Soil Biology and Biochemistry*, *104*, 68–80. https://doi.org/10.1016/j.soilbio.2016.10.005

Duran, B. E. L. & Kucharik, C. J. (2013). Comparison of Two Chamber Methods for Measuring Soil Trace-Gas Fluxes in Bioenergy Cropping Systems. *Soil Science Society of America Journal*, *77*(5), 1601. https://doi.org/10.2136/sssaj2013.01.0023

Ejack, L. & Whalen, J. K. (2021). Freeze-thaw cycles release nitrous oxide produced in frozen agricultural soils. *Biology and Fertility of Soils*. https://doi.org/10.1007/s00374-020-01537-x

Giles, M., Morley, N., Baggs, E. M. & Daniell, T. J. (2012). Soil nitrate reducing processes - drivers, mechanisms for spatial variation, and significance for nitrous oxide production. *Frontiers in Microbiology*, *3*, 407. https://doi.org/10.3389/fmicb.2012.00407

Grace, P. R., der Weerden, T. J., Rowlings, D. W., Scheer, C., Brunk, C., Kiese, R., Butterbach-Bahl, K., Rees, R. M., Robertson, G. P. & Skiba, U. M. (2020). Global research alliance N 2 O chamber methodology guidelines: Considerations for automated flux measurement. *Journal of Environmental Quality*, jeq2.20124. https://doi.org/10.1002/jeq2.20124

Groffman, P. M., Altabet, M. A., Böhlke, J. K., Butterbach-Bahl, K., David, M. B., Firestone, M. K., Giblin, A. E., Kana, T. M., Nielsen, L. P. & Voytek, M. A. (2006). Methods for measuring denitrification: diverse approaches to a difficult problem. *Ecological Applications*, *16*(6), 2091–2122. https://doi.org/10.1890/1051-0761(2006)016[2091:MFMDDA]2.0.CO;2

Groffman, P. M., Butterbach-Bahl, K., Fulweiler, R. W., Gold, A. J., Morse, J. L., Stander, E. K., Tague, C., Tonitto, C. & Vidon, P. (2009). Challenges to incorporating spatially and temporally explicit phenomena (hotspots and hot moments) in denitrification models. *Biogeochemistry*, *93*(1–2), 49–77. https://doi.org/10.1007/s10533-008-9277-5

Harvey, M. (2012). *Nitrous Oxide Chamber Methodology Guidelines* (December 2012 Version 1) Edited by Cecile de Klein and Mike Harvey. Publishing details: Ministry for Primary Industries, Pastoral House, 25 The Terrace, PO Box 2526, Wellington 6140, New Zealand, www.mpi.govt.nz ISBN 978-0-478-40585-9 (online)

Henault, C., Grossel, A., Mary, B., Roussel, M. & Leonard, J. (2012). Nitrous Oxide Emission by Agricultural Soils: A Review of Spatial and Temporal Variability for Mitigation. *Pedosphere*, *22*(4), 426–433. https://doi.org/10.1016/S1002-0160(12)60029-0

Hutchinson, G. L. & Livingston, G. P. (2001). Vents and seals in non-steady-state chambers used for measuring gas exchange between soil and the atmosphere. *European Journal of Soil Science*, *52*(4), 675–682. https://doi.org/10.1046/j.1365-2389.2001.00415.x

Kong, X., Duan, Y., Schramm, A., Eriksen, J., Holmstrup, M., Larsen, T., Bol, R. & Petersen, S. O. (2017). Mitigating N2O emissions from clover residues by 3,4-dimethylpyrazole phosphate (DMPP) without adverse effects on the earthworm Lumbricus terrestris. *Soil Biology and Biochemistry*, *104*, 95–107. https://doi.org/10.1016/j.soilbio.2016.10.012

IPCC. (2014). Climate Change 2014: Synthesis Report. Contribution of Working Groups I, II and III to the Fifth Assessment Report of the Intergovernmental Panel on Climate Change. .

Li, M., Shimizu, M. & Hatano, R. (2015). Evaluation of N2O and CO2 hot moments in managed grassland and cornfield, southern Hokkaido, Japan. *Catena*, *133*, 1–13. https://doi.org/10.1016/j.catena.2015.04.014

Lin, W., Ding, J., Li, Y., Zhang, W., Ahmad, R., Xu, C., Mao, L., Qiang, X., Zheng, Q. & Li, Q. (2019). Partitioning of sources of N2O from soil treated with different types of fertilizers by the acetylene inhibition method and stable isotope analysis. *European Journal of Soil Science*, *70*(5), 1037–1048. https://doi.org/10.1111/ejss.12782

Mohn, J., Wolf, B., Toyoda, S., Lin, C. T., Liang, M. C., Brüggemann, N., Wissel, H., Steiker, A. E., Dyckmans, J., Szwec, L., -, N. E., Casciotti, K. L., Forbes, M., Giesemann, A., Well, R., Doucett, R. R., Yarnes, C. T., Ridley, A. R., Kaiser, J. & Yoshida, N. (2014). Interlaboratory assessment of nitrous oxide isotopomer analysis by isotope ratio mass spectrometry and laser spectroscopy: Current status and perspectives. *Rapid Communications in Mass Spectrometry*, *28*(18), 1995–2007. https://doi.org/10.1002/rcm.6982

Molodovskaya, M., Singurindy, O., Richards, B. K., Warland, J., Johnson, M. S. & Steenhuis, T. S. (2012). Temporal Variability of Nitrous Oxide from Fertilized Croplands: Hot Moment Analysis. *Soil Science Society of America Journal*, *76*(5), 1728. https://doi.org/10.2136/sssaj2012.0039

Molodovskaya, M., Warland, J., Richards, B. K., Öberg, G. & Steenhuis, T. S. (2011). Nitrous Oxide from Heterogeneous Agricultural Landscapes: Source Contribution Analysis by Eddy Covariance and Chambers. *Soil Science Society of America Journal*, *75*(5), 1829. https://doi.org/10.2136/sssaj2010.0415

Mondini, C., Sinicco, T., Cayuela, M. L. & Sanchez-Monedero, M. A. (2010). A simple automated system for measuring soil respiration by gas chromatography. *Talanta*, *81*(3), 849–855. https://doi.org/10.1016/j.talanta.2010.01.026

Morris, S. G., Kimber, S. W. L., Grace, P. & Van Zwieten, L. (2013). Improving the statistical preparation for measuring soil N2O flux by closed chamber. *The Science of the Total Environment*, *465*, 166–172. https://doi.org/10.1016/j.scitotenv.2013.02.032

Ostrom, N. E. & Ostrom, P. H. (2012). The Isotopomers of Nitrous Oxide: Analytical Considerations and Application to Resolution of Microbial Production Pathways. In *Advances in Isotope Geochemistry* (pp. 453–476). Springer Berlin Heidelberg. https://doi.org/10.1007/978-3-642-10637-8_23

Ostrom, N. E. & Ostrom, P. H. (2017). Mining the isotopic complexity of nitrous oxide: a review of challenges and opportunities. *Biogeochemistry*, *132*(3), 359–372. https://doi.org/10.1007/s10533-017-0301-5

Parkin, T. B. (2006). Effect of sampling frequency on estimates of cumulative nitrous oxide emissions. *Journal of Environmental Quality*, *37*(4), 1390–1395. https://doi.org/10.2134/jeq2007.0333

Parkin, T. B. & Kaspar, T. C. (2006). Nitrous oxide emissions from corn-soybean systems in the midwest. *Journal of Environmental Quality*, *35*(4), 1496–1506. https://doi.org/10.2134/jeq2005.0183

Parkin, T. B. & Venterea, R. T. (2010). U.S. Department of Agriculture - Agricultural ressearch service Greenhouse gas Reduction through Agricultural Carbon Enhancement network (USDA-ARS GRACEnet) Project Protocols Chapter 3. Chamber-Based Trace Gas Flux Measurements. *Flux*, *2010*(April 2003), 1–39.

Parkin, T., Mosier, A., Smith, J., Venterea, R., Johnson, J., Reicosky, D., Doyle, G., Mccarty, G. & Baker, J. (2003). *USDA-AR S GRAC Enet Chamber-based Trace Gas Flux Measurement Protocol*.

Petersen, S. O., Regina, K., Pöllinger, A., Rigler, E., Valli, L., Yamulki, S., Esala, M., Fabbri, C., Syväsalo, E. & Vinther, F. P. (2006). Nitrous oxide emissions from organic and conventional crop rotations in five European countries. *Agriculture, Ecosystems & Environment*, *112*(2–3), 200–206. https://doi.org/10.1016/j.agee.2005.08.021

Petersen, S. O., Well, R., Taghizadeh-Toosi, A. & Clough, T. J. (2020). Seasonally distinct sources of N2O in acid organic soil drained for agriculture as revealed by N2O isotopomer analysis. *Biogeochemistry*, *147*(1), 15–33. https://doi.org/10.1007/s10533-019-00625-x

Rapson, T. D. & Dacres, H. (2014). Analytical techniques for measuring nitrous oxide. In *TrAC - Trends in Analytical Chemistry* (Vol. 54, pp. 65–74). Elsevier B.V. https://doi.org/10.1016/j.trac.2013.11.004

Ravishankara, A. R., Daniel, J. S. & Portmann, R. W. (2009). Nitrous oxide (N2O): the dominant ozone-depleting substance emitted in the 21st century. *Science (New York, N.Y.)*, *326*(5949), 123–125. https://doi.org/10.1126/science.1176985

Robertson, G. P. & Groffman, P. M. (2015). Chapter 14 - Nitrogen Transformations. *Soil Microbiology Ecology and Biochemistry*, 421–446. https://doi.org/10.1016/B978-0-12-415955-6.00014-1

Rochette, P. & Eriksen-Hamel, N. S. (2008). Chamber Measurements of Soil Nitrous Oxide Flux: Are Absolute Values Reliable? *Soil Science Society of America Journal*, *72*(2), 331. https://doi.org/10.2136/sssaj2007.0215

Sahrawat, K. L. (2008). Factors Affecting Nitrification in Soils. *Communications in Soil Science and Plant Analysis*, *39*(9–10), 1436–1446. https://doi.org/10.1080/00103620802004235

Schwager, E. A., VanderZaag, A. C., Wagner-Riddle, C., Crolla, A., Kinsley, C. & Gregorich, E. (2016). Field Nitrogen Losses Induced by Application Timing of Digestate from Dairy Manure Biogas Production. *Journal of Environmental Quality*, *45*(6), 1829–1837. https://doi.org/10.2134/jeq2016.04.0148

Sehy, U., Ruser, R. & Munch, J. C. (2003). Nitrous oxide fluxes from maize fields: relationship to yield, site-specific fertilization, and soil conditions. *Agriculture, Ecosystems & Environment*, *99*(1–3), 97–111. https://doi.org/10.1016/S0167-8809(03)00139-7

Singurindy, O., Molodovskaya, M., Richards, B. K. & Steenhuis, T. S. (2009). Nitrous oxide emission at low temperatures from manure-amended soils under corn (Zea mays L.). *Agriculture, Ecosystems and Environment*, *132*(1–2), 74–81. https://doi.org/10.1016/j.agee.2009.03.001

Smith, K. A. (2017). Changing views of nitrous oxide emissions from agricultural soil: key controlling processes and assessment at different spatial scales. In *European Journal of Soil Science* (Vol. 68, Issue 2, pp. 137–155). John Wiley & Sons, Ltd (10.1111). https://doi.org/10.1111/ejss.12409

Smith, Keith A. & Dobbie, K. E. (2001). The impact of sampling frequency and sampling times on chamber-based measurements of N 2 O emissions from fertilized soils. *Global Change Biology*, *7*(8), 933–945. https://doi.org/10.1046/j.1354-1013.2001.00450.x

Snyder, C., Davidson, E., Smith, P. & Venterea, R. (2014). Agriculture: sustainable crop and animal production to help mitigate nitrous oxide emissions. *Current Opinion in Environmental Sustainability*, *9*, 46–54. https://doi.org/10.1016/j.cosust.2014.07.005

Stocker, T.F., Qin, D., Plattner, G.-K., Tignor, M., Allen, S. K., Boschung, J., Nauels, A., Xia, Y., Bex, V. & Midgley, P. M. (eds. ). (2013). *IPCC, 2013: Climate change2013: The Physical Science Basis. Contribution of Working Group I to the Fifth Assesment Report of the Intergovernmental Panel on Climate Change*. https://www.ipcc.ch/report/ar5/wg1/

Syakila, A. & Kroeze, C. (2011). The global nitrous oxide budget revisited. *Greenhouse Gas Measurement and Management*, *1*(1), 17–26. https://doi.org/10.3763/ghgmm.2010.0007

Toyoda, S. & Yoshida, N. (1999). *Determination of Nitrogen Isotopomers of Nitrous Oxide on a Modified Isotope Ratio Mass Spectrometer*. https://doi.org/10.1021/ac9904563

Toyoda, S., Yoshida, N. & Koba, K. (2015). Isotopocule analysis of biologically produced nitrous oxide in various environments. *Mass Spectrometry Reviews*, *36*(2), 135–160. https://doi.org/10.1002/mas.21459

Venterea, R. T., Spokas, K. a. & Baker, J. M. (2009). Accuracy and Precision Analysis of Chamber-Based Nitrous Oxide Gas Flux Estimates. *Soil Science Society of America Journal*, *73*(4), 1087. https://doi.org/10.2136/sssaj2008.0307

Wagner-riddle, C., Furon, A., Mclaughlin, N. L., Lee, I., Barbeau, J., Jayasundara, S., Parkin, G., von Bertoldi, P. & Warland, J. (2007). Intensive measurement of nitrous oxide emissions from a corn-soybean-wheat rotation under two contrasting management systems over 5 years. *Global Change Biology*, *13*(8), 1722–1736. https://doi.org/10.1111/j.1365-2486.2007.01388.x

Wagner-Riddle, C., Rapai, J., Warland, J. & Furon, A. (2010). Nitrous oxide fluxes related to soil freeze and thaw periods identified using heat pulse probes. *Canadian Journal of Soil Science*, *90*(3), 409–418. https://doi.org/10.4141/CJSS09016

Wagner-Riddle, C. & Thurtell, G. W. (1998). Nitrous oxide emissions from agricultural fields during winter and spring thaw as affected by management practices. *Nutrient Cycling in Agroecosystems*, *52*(2/3), 151–163. https://doi.org/10.1023/A:1009788411566

Wagner-Riddle, C. (2019, April 15). Nitrous oxide emissions induced by freeze/thaw: importance and potential mechanisms. *Climate Change, Reactive Nitrogen, Food Security and Sustainable Agriculture* .

WMO. (2016). WMO Greenhouse Gas Bulletin - The State of Greenhouse Gases in the Atmosphere Based on Global Observations through 2014. In *World Meteorological Organization and Global Atmosphere Watch* (Issue 11, pp. 1–4). https://reliefweb.int/report/world/wmo-greenhouse-gas-bulletin-state-greenhouse-gases-atmosphere-based-global-observations

Xu, L., Furtaw, M. D., Madsen, R. A., Garcia, R. L., Anderson, D. J. & McDermitt, D. K. (2006). On maintaining pressure equilibrium between a soil CO 2 flux chamber and the ambient air. *Journal of Geophysical Research*, *111*(D8), D08S10. https://doi.org/10.1029/2005JD006435

Yamamoto, A., Akiyama, H., Nakajima, Y. & Hoshino, Y. T. (2017). Estimate of bacterial and fungal N2O production processes after crop residue input and fertilizer application to an agricultural field by 15N isotopomer analysis. *Soil Biology and Biochemistry*, *108*, 9–16. https://doi.org/10.1016/j.soilbio.2017.01.015

## ***Chapter 2: A novel system for high-resolution, near-continuous measurements of soil $N_2O$ isotope fluxes***

### *1. Abstract*

Measuring soil $N_2O$ flux accurately is a major challenge. Most investigations rely on laborious manual measurement campaigns, which despite the large effort required, often do not provide data with high enough spatial and temporal resolution to capture peak flux events. We have developed a novel measurement system that is able to accurately measure $N_2O$ in soil trace gas flux with high temporal resolution and from multiple chambers. The system comprises a set of automatic chambers, circulating gas paths and a laser spectroscopy-based $N_2O$ isotopic analyzer. Sampling sequence, deployment time, and time between chamber samplings are easy to modify for up to 15 soil chambers. Optional sampling interruption during rain events is customizable at different rain intensities and with different delay options. The system has been deployed to measure soil $N_2O$ emissions during five different long term sampling campaigns in Columbia County (WI). These campaigns include a full growing season (7 months) and four year-round studies during which the system provided on average 8 daily high-resolution flux measurements from four chambers. This measurement system provides precise flux measurements over extended periods, enabling capture of peak events and providing unique insights into microbiological processes governing soil $N_2O$ evolution.

***Keywords.*** Soil trace gas, chamber, nitrous oxide, automated collection.

## *2. Introduction*

Nitrous oxide is the third most important greenhouse gas and is the largest ozone-depleting substance emitted through human activities, fertilized cropping systems are the largest source of anthropogenic $N_2O$ (IPCC, 2014; Snyder et al., 2014).Concerns over the negative impacts of $N_2O$ emissions have fostered keen interest in quantifying $N_2O$ emissions from soil. Unfortunately, estimation of $N_2O$ flux emitted from croplands over the time periods required to evaluate agricultural management practices remains a major challenge (Laville et al. 2011). High temporal and spatial variability make it difficult to cost-effectively measure $N_2O$ fluxes accurately, and this hinders development of predictive estimates of $N_2O$ emissions under different management practices (Bouwman et al. 2002; Cavigelli et al. 2012; Snyder et al. 2009). Estimates of annual soil $N_2O$ emissions are most often based on only 15-30 flux measurements over a full year (Petersen et al. 2006).

The temporal variability of soil $N_2O$ flux has been characterized. Molodovskaya et al. (2011) determined that short "hot moment" peak emission events contributed up to 51% of cumulative annual $N_2O$ emissions, but represented <7% of the total observation time. Parkin and Kaspar, (2006) observed that, 49% of cumulative $N_2O$ flux in corn plots was due to just two intense peaks that occurred 14 days apart. Elevated $N_2O$ fluxes have been observed to occur in response to specific triggers such as tillage, fertilization, rainfall events and soil Freeze Thaw Cycles (FTC) (Christensen, 1983; Machado et al., 2019; Sehy et al., 2003; Wagner-Riddle, 2019). Molodovskaya et al. (2012) report $N_2O$ flux peaks associated with soil moisture, rainfall, and soil temperature, finding that recent N fertilization increased the magnitude of the peak events, but did not cause them independently. The unpredictable episodic nature of $N_2O$ fluxes limits our ability to quantify $N_2O$ emissions.

Automated soil chambers (Ambus and Robertson, 1998; Laville et al. 2011; Parkin, 2008) provide $N_2O$ emission data at frequencies on the order of minutes to hours, but require a dedicated analytical instrument (e.g., gas chromatograph). Measurement of $N_2O$ soil fluxes is most commonly based on the sampling of small flux soil chambers which is labor- and time-intensive (Pattey et al. 2007). Limits on resources available for sampling campaigns often require that a single $N_2O$ soil flux estimate represents the flux over an extended period, ranging from 24 hours up to as long as several weeks (Barton et al., 2015; Parkin, 2008).. The accuracy of cumulative $N_2O$ estimates calculated from these measurements is largely unknown, but the problem has been recognized. Parkin (2008) found that sampling every 3 days yielded flux estimates within ±10% of those based on sampling every 6 hours, but that sampling once every 21 days yielded estimates within +60% and -40% of the actual cumulative flux. Thies et al. (2019) estimated that during 21 days after fertilization the probability to obtain a flux measurement within 20% of the mean daily flux during 80% of the time could be as low as 10% and concluded that to reduce uncertainty in the estimation of $N_2O$ cumulative estimates near continuous measurement systems should be adopted when possible. Although the importance of the high temporal variability of $N_2O$ flux has been recognized, application of this knowledge to guide sampling through time has been overlooked.

Several automated systems to monitor $N_2O$ emissions have been developed during recent years but lack of appropriate technology has been the main limitation to *in situ* high frequency sampling of $N_2O$ fluxes. The main technological difficulties include complicated automation set up, slow sample processing, low measurement sensitivity, spectrum interferences with other trace gases or water vapor, and the necessity of providing consumables to field locations (e.g.

carrier and standard gases) (Mondini et al., 2010; Wang et al., 2011; Savage et al., 2014; Rapson and Dacres, 2014).

A relatively new Laser Absorption Spectroscopy (LAS) technology, known as Off-Axis Integrated Cavity Output Spectroscopy (Off-Axis ICOS) provides significant advantages for *in situ* measurement of soil trace gases. Off-Axis ICOS (OA-ICOS) is highly selective and exhibits minimal cross-interference due to background gases. The off-axis mirror system increases optical path length from 5 to 10 km (e.g. 50 to 100 times larger than previous LAS (Quantum Cascade Laser - QCL)), which improves sensitivity to sub-part per billion precision (0.2 ppb – $N_2O$) within the wide ranges of gas concentrations that characterize $N_2O$ soil emissions (0.3 to 10 ppm - $N_2O$). Integration of the signal in the optical cell reduces laser scan times to milliseconds, increasing frequency rates up to 1000 Hz (e.g. 10 to 100 higher than QCL). In addition, these instruments require low maintenance, minimal calibration and consumables, and can be operated practically without training (Gupta, 2012).In addition, the OA-ICOS instrument measures simultaneously with $N_2O$ concentration its three main $N_2O$ isotope ratios (i.e., $\delta^{15}N^{\alpha}$, $\delta^{15}N^{\beta}$, and $\delta^{18}O$) which have been proved a powerful tool to elucidate the main $N_2O$ production pathways in soils (Decock & Six, 2013).

Although the OA-ICOS instrument has several attractive features for soil trace-gas monitoring, its mode of operation requires a unique gas handling system that circulates soil trace gases from soil chambers in the field and the instrument. The instrument, which incorporates an on-board computer, internal pump, and heater, also requires line-quality electrical power and a controlled temperature environment. The design, fabrication and testing of an automatic gas flux

measurement system built around an OA-ICOS instrument for automated measurement of soil $N_2O$ emissions and its isotope ratios is described.

This $N_2O$ monitoring system have been used in field research during 5 sampling campaigns in corn fields at the University of Wisconsin Arlington Agricultural Research Station (AARS). Providing high quality data to improve our knowledge $N_2O$ flux the diurnal and seasonal patterns and provide recommendations to improve $N_2O$ sampling strategies (Chapter 4). In addition, these $N_2O$ data have been used to compare between different $N_2O$ emissions mitigations strategies (Chapter 5).

## *3. Methods – Description of the system*

### *3.1. Isotopic $N_2O$ analyzer*

Soil chamber methodologies are an intrusive soil trace gas measuring method because their deployment on the soil surface disturbs the natural emissions process, these disturbance effects are known as 'chamber effects' (Davidson et al., 2002; Rochette and Eriksen-Hamel, 2008). It is well known that minimizing time of deployment is the best practice to reduce these disturbances. How short the deployment times can be is limited by the sensitivity and sampling rate of the analytical instrument used to measure the gases collected in the chamber. In general, measurement precision increases with gas concentration, so longer chamber closure times collect more gas emission and provide a more accurate measurement, but also lead to greater disturbance of the soil gas production and diffusion processes.

The Laser Absorption Spectroscopy (LAS) technology, known as Off-Axis Integrated Cavity Output Spectroscopy (Off-Axis ICOS), provides high sensitivity, accuracy and fast measurements which allows short chamber closure times and minimizes chamber effects. The

Isotopic Analyzer measures $N_2O$ concentration continuously and in real time with sub-ppb precision (0.2 ppb) in less than a second (≈ 3 ms), providing measuring rates up to 10Hz. The Los Gatos Enhanced Performance model used in this study (i.e. Isotopic $N_2O$ Analyzer, model 914-0027; - Los Gatos Research Inc (San Jose, CA) (ABB subsidiary)) also measures the four stable nitrous oxide isotopocules ($^{14}N^{14}N^{16}O$, $^{14}N^{15}N^{16}O$, $^{15}N^{14}N^{16}O$ and $^{14}N^{14}N^{18}O$) directly (without pre-concentration) over a wide $N_2O$ dynamic range (i.e. 0.3 to 100 ppm of $N_2O$). The analyzer precision within the aforementioned range is 0.2 ppb for $N_2O$, better than 1‰ for $\delta^{15}N$, $\delta^{15}N^{\beta}$, $\delta^{15}N^{\alpha}$ and $\delta^{18}O$, over 300 seconds for the Nitrogen isotopes and 1000 seconds for the oxygen isotope. Analysis of the isotopic composition of $N_2O$ and particularly the intramolecular distribution ("site preference") of the heavy isotope of nitrogen ($^{15}N$), has been suggested as a powerful tool to trace the geochemical cycle of $N_2O$. This is because many biological and chemical processes have distinct isotopic signatures (Wahlen and Yoshinari, 1985; Yoshida and Toyoda, 2000; Pérez et al., 2001).

The analyzer was calibrated annually as recommended by the manufacturer. During the winters of 2014 and 2015 before the testing and the sampling seasons started, the analyzer was factory calibrated. During the next sampling campaigns the analyzer was calibrated follow the analyzer manufacturer recommendations using gases of known $N_2O$ concentration (Certified Standard $N_2O$, Airgas, Inc. Chicago, IL).

The analyzer can be used to sample small, discrete gas samples if it is equipped with a manual injection port. This model of operation is not, however, practical for in-field, autonomous sample of soil trace gasses. In the standard, "autonomous" mode of operation named in the analyzer manual 'low continuous flow mode', the instrument analyzes a continuous flow of gas through the optical cell. In autonomous mode, a continuous flow of gas, at 100 cc per min, floods the

analyzer optical cell (approximate volume of 1 liter). Two super-reflective mirrors at either end of the cavity increase the laser path length over 10,000 times, similarly increasing the interaction of the targeted species with the tuned laser. Molar fractions of the targeted gases are determined from the measured absorption band using Beer's Law with a period of 3 milliseconds.

Automatic sampling from different sources with a single LGR analyzer can be accomplished using the Multi-port Inlet Unit (MIU) sold by Los Gatos Research (Part Number: 908-0001-0005). The MIU is a multiplex unit; a manifold connected to 16 one-way two-position solenoid valves. The analyzer, attending to user sampling specifications, digitally controls the opening and closing of the MIU valves. The MIU is designed to direct gas from different sources through the analyzer which would typically be vented to the atmosphere.

### *3.2. System description*

#### *System overview*

The system comprises five major parts (Figure 1). The core of the system, the $N_2O$ analyzer (1), is connected through a Gas Path (2) with four soil chambers (5). The Digital Logic System (3) synchronizes these three components according to a user specified sampling sequence and timing. The system is housed in an insulated and temperature controlled mobile shelter (i.e., trailer) (4). Below the different parts of the system are described, the information necessary (i.e., pictures, drawings, schematics and part list) to replicate this system is provided in the appendix.

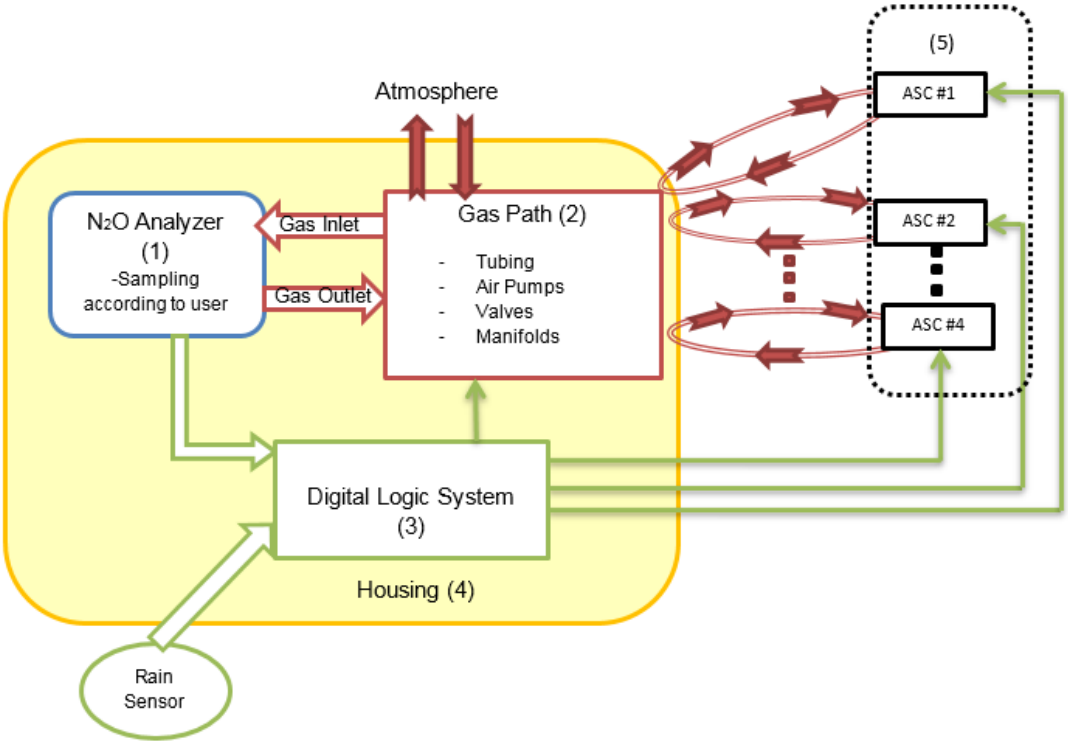


Figure 1. Overview of the $N_2O$ monitoring system. Its five main components and their interactions.

***Gas path***

In the current implementation, the analyzer is connected to four automatic soil chambers with $N_2O$-compatible, nonreactive to $N_2O$ Chemfluor ®FEP tubing (6.35 mm OD, 0.79 mm wall). Two gas path manifolds and a set of associated valves (i.e., distribution blocks) placed at the inlet and the outlet of the analyzer are used to route sampled gas from the soil chambers to the analyzer and back to the soil chambers. The MIU is used as the distribution block at the analyzer inlet, it incorporates 16 solenoid valve inputs, which can accommodate 15 soil chambers and a gas path to flush the system with atmospheric air. This implementation uses only 5 of the MIU solenoid valves. Routing of gas at the analyzer outlet is managed with a custom distribution block designed and built using a stainless steel manifold connected to four 3-way/2-position stainless steel solenoids valves. This distribution block is connected to the analyzer

outlet. Each soil chamber-analyzer gas loop is fitted with a gas pump. Two solenoid valves, place between the analyzer inlet and outlet and the two gas manifolds, isolate the analyzer from the chamber loops, allowing the analyzer optical cell and all the lines (loops) between chamber and analyzer to be flushed simultaneously. In addition, these valves interrupt gas path sampling when precipitation occurs (routing ambient air through the instrument). The length of each chamber-analyzer loop is approximately 30.5 m. Tubing outside of the instrumentation trailer is protected by 19.05 mm ID Full-Coverage Corrugated Wrap-Around Sleeving. All the connections in the gas path are made with stainless steel connectors produced by Swagelok, Inc

During sampling, the distribution blocks (i.e. manifolds, valves and pumps) at the inlet and outlet of the instrument divert gas from a one soil chamber through the analyzer and return the sampled gas back to that chamber. The sampling sequence includes a 10-minute flushing period between sampling from one chamber and the next. During flushing, atmospheric air is used to purge the gas path and the analyzer chamber. The length of time each chamber is sampled and the flushing period are adjustable by the user to match the gas production conditions in a particular experimental design and location.

***Digital logic***

The Digital Logic System is the logic that controls the chamber opening sequence, valves and pumps. The Digital Logic System is embodied in a printed circuit board (PCB) that combines the digital control signals sent by the instrument with precipitation information from an optical rain sensor. This allows synchronization of the different custom parts of the system (i.e., air pumps, valves and soil chambers) during the different operational modes (i.e., sampling and flushing). The system includes automatic sampling interruption during rain events. During a rain event the chambers are all open to allow the area of soil inside the soil chambers to receive

rainfall, the sampling sequence is automatically restarted at the end of a rain event. The PCB design includes optical isolation of signal input and output, to avoid analyzer or digital logic damage in case of power disruption or component failure (i.e., electrical short) .

***Automatic Soil Chambers***

The soil chambers were designed and built following the USDA-ARS GRACEnet protocols for trace gas flux measurements by soil chamber methodology (Parkin & Venterea, 2010). The automatic soil chambers were made from 16 gauge ferromagnetic stainless steel (chemically inert to $N_2O$). Each chamber covers a rectangular area of 0.09 $m^2$ (30 x 30 cm) and has a total height of 20 cm. The top and bottom of the chamber body is open; the bottom edge is sharp to facilitate a 5 cm depth soil incision. When placed in the field chambers have an approximate volume of 18 liters. The top of the chamber wall is finished with a 2.5 cm rim. The chamber lid is made of 12.7 mm thick HDPE (40 x 32 cm) with a custom magnetic gasket (as found on a refrigerator) mounted on the bottom. When the chamber is closed, the magnetic gasket sits on top of the rim of the chamber, sealing it. An auxiliary structure to keep the chamber in place and to support the opening and closing mechanism and controls was built on 3/16 thick angle steel.

The chamber has three sampling ports, two ports accommodate the input and output gas flow of the automated sampling system (6.35 mm OD Stainless Steel Bulkhead Unions, Swagelok®).The third port is a rubber septum built into the chamber lid which can be used for manual sampling using a syringe.

The opening and closing movements are powered by a 12 VDC linear actuator attached to the top of the chamber lid. When the chamber is closed the lid sits on the top rim of the chamber. The linear actuator retracts, pulling the lid backward and upward describing pivoting

movement around the chamber body. The pivoting movement is carried out by two parallel four bar linkages attached to the underside of the lid and to the chamber auxiliary structure. Two limit switches control the end of the linear actuator run during the opening and closing movements. To facilitate servicing, the opening and closing of the chamber can be override using a rocket switched mounted in a washdown electric box attached to auxiliary structure of the soil chamber. The electric controls and protections (i.e., fuses and RC snubber) and housed in that electric box.

Differences in air pressure in the chamber headspace relative to that of the soil and surrounding atmosphere affect the rate of gas diffusion from the soil leading to biased flux measurements (Davidson et al., 2002; Rochette and Eriksen-Hamel, 2008). To equilibrate chamber pressure to atmospheric pressure, a vent made of a loosely coiled 0.15 m length of stainless steel tube ID 2.36 mm was installed in the chamber wall. Two ports accommodate the input and output gas flow of the automated sampling system, in addition, occasional manual sampling using a syringe can be performed through a third sampling port (i.e. rubber septum) built into the chamber lid.

***Mobile housing***

The system is housed in temperature controlled 1.8 by 3 m trailer. Electrical power conditioning, as well as DC and AC power distribution systems are also housed in the trailer. The DC power distribution comprises electrical protection components (i.e., fuses and breakers) a trickle charger and two 12V – 38 Ah batteries which provides surge capacity to supply current draw peaks due to the linear actuator. The AC power distribution comprises electrical protection components (i.e., fuses and breakers) and an Uninterruptible Power Supply (UPS) that is

connected via USB to the analyzer and have been programmed to trigger the analyzer shut-off program when power is interrupted and turn it back on when power is reestablished.

The temperature inside of the trailer is maintained in the analyzer operational range (0 to 45°C) using a differential thermostat a shutter fan and a split air conditioning unit (9000 BTU ≈ 35,714.3 Kcal). When forced ventilation is not enough to keep the temperature below 35°C, the air conditioning unit is automatically activated. During the winter the internal heating elements of the analyzer are sufficient to maintain the temperature of the trailer above freezing.

The full system has a base power requirement of 550 $Wh^{-1}$, with additional load up to a total of 2050 $Wh^{-1}$ depending on cooling requirements. A minimal power supply of 1000 $Wh^{-1}$ is necessary to start the system due to higher power requirements needed to heat up the analyzer to operational temperature (46º C).

***System cost***

Assembling of parts was done at the Biological System Engineering departmental shop (UW-Madison) with the collaboration of the shop manager and several departmental students. The total cost of the materials was approximately $2,320 for each automated soil chamber (x5), $8,000 for the housing (trailer and installations), $2,900 for the gas path (tubing, fittings, valves, pumps) and $450 for the digital logic components, for a total of approximately $23,000 (excluding the $N_2O$ analyzer and the MIU). A complete description and price of all materials and components used for the construction of the system are presented in the Appendix (List of Materials).

## *4. Results and discussion – System performance*

### *4.1. Flux estimation*

Soil gas flux is estimated from the change in gas concentration in the chamber headspace over time. In this study, gas flux per unit soil area is estimated from the slope obtained by least-squares linear regression of *C* ($N_2O$ gas concentration) versus *t* (time) to estimate *dC/dt* , as in equation 1 below.

$$N_2O_{Flux} = H\ \frac{dc}{dt} \quad (1)$$

Where H is the ratio of the internal chamber volume to surface area in contact with soil. $N_2O$ flux is generally expressed in units of mole or mass of N-$N_2O$ per units of area and time (mol N-$N_2O$ $ha^{-1}$ $day^{-1}$ or g N-$N_2O$ $ha^{-1}$ $day^{-1}$). Transformation from parts per million (ppm) (Isotopic $N_2O$ analyzer units) to mol was performed using the ideal gas law (Parkin and Venterea, 2010), as shown Eq. 2 below.

$$n\ (mol) = \frac{P \times V}{R \times T} \quad (2)$$

Where P is pressure in atmospheres and T is temperature in degrees Celsius, both measured in the analyzer internal cell and recorded in the analyzer data output. R is the ideal gas constant (R = 0.08206 L Atm $mol^{-1}$ $°C^{-1}$).V is volume in liters of $N_2O$ which was computed from the concentration of $N_2O$ measured in ppm ( 1ppm = 1L of $N_2O$ /1000000L of Air). Conversion from molar units to g N- $N_2O$ is based on the molecular weight of Nitrogen per molecule of $N_2O$ (14 kg of N per kmole of $N_2O$).

Although gas flux can be estimated with only 3 or 4 gas concentration measures, and is standard practice when chambers are sampled manually, the high sampling frequency of the

ICOS instrument allows us to measure many more samples. With the chamber deployment time implemented I was able to use approximately 44 gas concentration measurements for each flux estimate. Using such a large number of concentration measurements per flux estimate increases the robustness of the linear flux estimate and thus improves the capacity to detect relative differences among $N_2O$ soil fluxes (Venterea et al., 2009). In addition, chamber effects on gas diffusion in the chamber headspace could be detected easily and corrected (by reducing deployment time or the number of data-points used to estimate flux). Having such a large number of measurements allowed us to reliably detect and eliminate chamber effects by testing for linearity in the flux calculation and subsampling the data when necessary to assure flux linearity. The first step in the adaptive linear flux calculation was to estimate the flux (change in chamber headspace $N_2O$ concentration vs. time) and the corresponding coefficient of determination ($r^2$) using all data collected during the effective sampling period. If $r^2$ was smaller than 0.95, a new flux estimate (i.e., slope of $N_2O$ concentration vs. time) and corresponding $r^2$ were calculated using a subsample of the data. Subsamples were created by sequentially eliminating the last $N_2O$ concentration datum until the computed $r^2$ was larger than 0.95, with a minimum of 12 time-concentration data points (10-minute chamber deployment). This Adaptive Linear Regressions (ALR) flux calculation allowed us to minimize chamber effects without compromising the precision or accuracy of the flux estimates. Fluxes with a $R^2$ was smaller than 0.95, were considered as systems failure (i.e., chamber remained open during flux measurement).

***Comparison between the ALR and HMR flux estimation method***

Movement of $N_2O$ from its production site in the soil towards the atmosphere it is influenced by the difference in concentration in $N_2O$ in the soil-air and the atmosphere. Under steady state conditions $N_2O$ soil emissions rates are equal to the soil production rates and the vertical $N_2O$

gradient is constant. Upon Steady State chamber deployment, the $N_2O$ concentration in the chamber headspace increases and the vertical $N_2O$ diffusion gradient between soil-air and atmosphere decreases. Because of this effect, the mean rate of $N_2O$ during a Steady State chamber deployment often underestimates the pre-deployment emission rate. A technique to account for the flux suppression effect of Steady state chambers is the use of non-linear flux estimations methods (i.e., Quadratic, exponential, NDFE, etc.,) which allow estimation of pre-deployment fluxes based on the non-linearity change of $N_2O$ concentration overtime observed in the chamber headspace.

Non-linear models, which are often less biased than linear models, but may display higher sensitivity to measurement error (Hutchinson and Mosier, 1981; Anthony et al., 1995; Pedersen, 2000; Venterea et al., 2009). As a result, the best choice of a flux model method for estimating the pre-deployment $N_2O$ emission rate must be a compromise between precision and accuracy. The accuracy-precision dilemma has been discussed in a number of publications (Hutchinson and Mosier, 1981; Anthony et al., 1995; Pedersen, 2000; Venterea et al., 2009; Levy et al., 2011; Cowan et al., 2013, Venterea et al., 2013, Kandel et al., 2016; Huppi et al., 2018; Venterea et al., 2020). Venterea et al. (2020) provides a “gold standard approach” for application and selection of flux calculation methods, that includes an error analysis tool to quantify the method performance with respect to both accuracy and precision based on chamber dimensions and sampling duration, soil properties, and analytical measurement precision. While Venterea et al. (2020) restates the importance in conducting error-analysis on a site-specific basis, he recognised that it is impossible to evaluate the full universe of potential combinations impacting the flux calculation performance.

Despite the dilemma between accuracy and precision in $N_2O$ flux estimation method still not solved the current research is consistent in that: (1) reducing deployment time minimizes the loss of linearity due to chamber effects (2) that linear regression estimates are more precise than non-linear regressions estimates and (3) that linear estimates tend to underestimate the pre-deployment flux.

As in Venterea et al. (2009) we advocate for rather than impose one method over another to estimate fluxes via linear and non-linear method (analysis of non-linearity) and choose the flux estimation method based in the purpose of the analysis. Venterea et al. (2009) recommends that in cases where the primary objective is to detect differences in $N_2O$ emissions arising from experimental factors, during which $N_2O$ fluxes are traditionally measured with soil chambers, the linear regression will be more robust.

Here we compared our Adaptative Linear Regression (ALR) flux estimation model with the HMR method, the most popular non-linear regression flux calculation procedure on a set of 12,063 fluxes ranging from 0.06 to 2304.57 g $N_2O$-N $ha^{-1}day^{-1}$.

The HMR estimation routine allows estimation flux via HM using a large number of time-concentration points (i.e., $n > 4$) and automatic comparison between linear regression and HM flux estimation. To select the best fitting model and to prevent estimation of false fluxes visual inspection is recommended but the HMR package offers an automatic option in which the criterion selection is based on a single combined mean squared error criterion. Due to the large number of fluxes the automatic criteria selection method was used in our HMR estimations. A more precision description and a link for the free add-on package HMR for the free software R can be found in Pedersen et al. (2010).

One caveat in using the HMR method is that it was not able to detect false fluxes, these were fluxes measured when for example the chamber did not close (See section 'Detection of system malfunction and data selection' below). The ALR, detected 3008 false fluxes that were overlooked by the HMR calculation procedure. Following comparison were only performed in true fluxes. The inability of the HMR to differentiate between true and false fluxes have been observed by others (Cowan et al., 2014; Thomsen et al., 2009).

On average, fluxes estimated by the ALR method were 17.3% smaller than fluxes estimated via HMR method. Flux underestimation by the ALR was always below 2.5 times that of the HMR method. Linear regression analysis indicated a significant (p.value = 0.0036) and negative relationship between the proportion of the flux underestimation ((ALR flux - HM flux) / HM flux) and the magnitude of the flux. The slope of this relationship (m = -0.023), indicated that for each unit that the flux estimated by HMR method increased the underestimation by the ALR decreased by 0.023%. Underestimation by the ARL in fluxes larger than 50 g $N\text{-}N_2O$ $ha^{-1}$ $day^{-1}$ which tend to represent the majority of the cumulative emissions (Chapter 4) was in average 15.5%, and 11.7% when fluxes were greater than 500 g $N\text{-}N_2O$ $ha^{-1}$ $day^{-1}$.

The biggest difference between the ALR and the HMR is in the precision of the flux estimation method. The Standard Error of the fluxes estimated with the HMR is in average 2.5 times greater than that of the fluxes estimated with the ALR method. In average the 95% confidence interval for the HMR method resulted in an uncertainty around the flux of ± 6.8% of the flux while in the case of the ALR the 95% confidence interval yielded fluxes that vary within ± 2.7% of the estimated $N_2O$ soil flux.

As expected, these results show a clear trade-off between accuracy and precision in determining soil fluxes, relative to HM, the ALR method tend to underestimate the pre-deployment flux but results in a higher precision (~x 2.5).

Flux underestimation of linear models respect to non-linear models ranging from 25% up to 70% are common in the literature and the magnitude of these overestimations tend to increase with the magnitude of the flux (Pedersen, 2000; Venterea et al., 2009; Thomsen et al., 2009; Levy et al., 2011; Cowan et al., 2013, Kandel et al., 2016). The average flux underestimation by the ALR method was 17.3%, lower than previously reported; furthermore, in our case the underestimation decreased with flux intensity. During visual observation of large (i.e., > 500 g $N_2O$-N $ha^{-1}$ $day^{-1}$) and fairly linear ($r^2 > 0.95$) flux measurements, I have observed that soil emissions measured by our system do not always exhibit the exponential curvature modelled by the HMR method. As pointed by Cowan et al. (2014) it is possible that flux measurements in field environments are affected by unaccounted errors such as measuring artifacts (i.e., analyzer response, gas mixing during transport, etc.,).

The main goal of $N_2O$ flux measurements by static soil chambers is comparing the effect of soil management practices on $N_2O$ soil emissions rates. The statistical comparison between $N_2O$ flux from different treatments are already hampered by the large spatial and temporal variability of $N_2O$ soil emissions. As the goal of my analyses was to compare flux estimates from different $N_2O$ mitigation practices, I have opted for estimating soil fluxes using the ALR method. I recognize that the ALR method can result in flux underestimation presenting flux values estimated by both flux models ALR and HMR may be useful when comparing our results with studies that have used non-linear flux estimation methods.

### *4.2. Minimum Detectable Flux*

The Minimum Detectable Flux (MDF) is a metric developed by Christiansen, Outhwaite, & Smukler (2015). that indicate the lower limit for flux rates that can be detected with a given methodology, fluxes below the MDF are indistinguishable from zero flux. The MDF is computed by combining the analytical precision of the instrument, the chamber volume, and surface area, and the chamber deployment time. MDF can be used for experimental design and data quality assurance for closed chamber measurements.

A low MDF is beneficial because it allows us to detect small fluxes which occur most of the time. The MDF increases with lower analytical precision, short deployment times and reduced sampling frequency. Under the most unfavorable conditions the values of these variables were 0.2 ppm, 20 seconds, and 5 minutes, (for a minimum deployment time of 10 minutes). under these variables the MDF was $3.7 \times 10^{-4}$ g of $N\text{-}N_2O$ $ha^{-1}$ $day^{-1}$. Increasing deployment time, could be used as a strategy to reduce MDF, for example the MDF for a deployment time of 20 minutes is $9.2 \times 10^{-5}$ g of $N\text{-}N_2O$ $ha^{-1}$ $day^{-1}$.

The MDF $3.7 \times 10^{-4}$ g of $N\text{-}N_2O$ $ha^{-1}$ $day^{-1}$ for a 10 minute deployment time was used for data quality assurance, fluxes below this values were indistinguishable from zero flux and were removed from the flux dataset.

### *4.3. System Integrity*

#### *Chamber effects temperature and pressure*

Temperature impacts soil $N_2O$ production, solubility in soil water and gas diffusion rate through soil. Similarly, pressure differences between the inside and outside of the chamber can cause bulk gas flow, leading to biased flux measurements (Parkin & Venterea, 2010).

Field experiments to measure the chamber effects on temperature and pressure were performed during the last two weeks of July at noon, under sunny conditions in the experimental field in which the corn canopy was fully closed. Three chambers were placed several rows into the field and one was placed in the edge row, exposed to direct sunlight. Temperature and atmospheric pressure were measured with two data loggers based on Arduino Uno single board computers and a Bosch BMP180 chip with an accuracy of 0.01 mbar and 0.1ºC (Bosch Sensortec, 5/4/2013), measurements of the data loggers under identical conditions were within 0.5º C and 0.02 mbars (Brennan Lunzer, 6/25/2014).

In the three chambers under the corn canopy the air temperature variation between inside and outside air during chamber deployment were 3.28 ± 2.57°C (RMSD ± Std Dev), quite small in comparison with the overall air temperature (28 to 35°C). The interior air temperature in these chambers tended to decrease linearly during deployment, with the largest difference in temperature at the end of the deployment time (20 minutes). The average air temperature at the end of deployment was 1.28± 0.87°C lower than the ambient air temperature. Difference between inside and outside air temperature did not follow any pattern in the fourth chamber located at the field edge. The largest difference in air temperature recorded in the fourth chamber was 3.27°C which occurred 10 minutes after deployment. It seemed that due to the short deployment time the change in temperature inside of the soil chamber was mostly driven by soil irradiance. We recognized that the conditions of these experiments do not represent the majority of conditions observed during the year, but it is during the summer when soil chambers were exposed to maximum soil irradiance and air temperature, specially the chamber situated at the edge of the field. Overall, during these experiments differences in air temperature between the

inside and the outside of the soil chambers were small and impact on $N_2O$ production rates across the year is likely insignificant.

The RMSD in chamber-atmosphere pressure was 0.139 ± 0.13 mbar, with pressure inside of the chamber slightly higher than the ambient atmospheric pressure. This is an extremely small pressure difference, barely within the detection limit of this sensitive instrument.

***Integrity of the gas path***

The system requires that gas from the chamber headspace be transported to the analyzer through the gas path. When a chamber is closed and the gas path control system routes gas from the closed chamber to the analyzer, there is a delay related to the gas transport time from chamber to analyzer during which the analyzer is receiving residual atmospheric gas from the system purge. The length of this transport delay was measured using a standard gas tracer and compared to estimates based on pump characteristics and tubing size. Based on tube volume and gas flow rate, the transport delay was expected to be approximately 3 minutes.

Gas transport time was measured by connecting a gas sample bag containing an approximate $N_2O$ concentration of 10 ppm (One part of $N_2O$ 30 ppm (Certified Standard 30 ppm $N_2O$, Airgas Inc. Chicago, IL)) diluted into two parts of zero air (Cryogenic UltraPure Air, Scott-Marrin, Inc, Riverside, CA, USA) to the soil chamber outlet port and monitoring measured $N_2O$ concentration. This “step change” experiment was run repeatedly with measured $N_2O$ concentration rising rapidly and then stabilizing 237±13 seconds (approximately 4 minutes) after introduction of the standard gas. The difference between the predicted 3 minutes and measured lag time likely reflects both diffusion of the highly concentrated standard gas sample during transport and a mixing transient in the measurement cell of the analyzer as the highly

concentrated gas mixed with atmospheric concentrations. Based on these results, transport time was set to 5 minutes to ensure that the increase in [$N_2O$] measured by the analyzer was related with gas from the chamber headspace.

This experiment was also used to test the integrity of the gas path, this is the existence of gas leaks and to assure that the sampling system does not bias the $N_2O$ measurement by introducing volatile organic compounds (VOC) or other substances that have spectral overlap with $N_2O$ in the analyzer. After transport time and once the analyzer measurements were within the 1% of the $N_2O$ concentration measured in the sampling gas bag (i.e., 10 ± 0.1 ppm) the gas path was closed and run for 20 minutes. Changes in $N_2O$ concentration during the 20 minutes were within one standard deviation of the analyzer precision (0.2 ppb). Based on these results the gas path was airtight and the parts involved in gas transport did not affect the precision or accuracy of the analyzer $N_2O$ concentration measurements.

***Detection of system malfunction and data selection***

Soil $N_2O$ flux estimates calculated from the chamber concentration measurements were screened to eliminate unreliable and *de minimis* flux measurements. Estimated fluxes that were below the MDF corresponding to the chamber closure time (e.g. < $3.7 \times 10^{-4}$ g N-$N_2O$ $ha^{-1}$ $day^{-1}$ for 10 minute closure) were indistinguishable from zero flux and were removed from the flux dataset. These fluxes were removed rather than included as zero flux because in this unsupervised system it is impossible to differentiate between fluxes below the MDF and those resulting from a chamber failure. In addition, we screened for unreliable flux estimates resulting from occasional malfunctions of the unsupervised measurement system that occurred when a chamber failed to open or failed to close. For example, a chamber might not close or open if ice build-up blocked the chamber lid linkage during a freezing rain. A flux estimate was deemed

unreliable and rejected due to failure of a chamber to close when the measured chamber $N_2O$ concentrations at the beginning and end of the sampling period were both within ± 2 times the instrument precision (0.4 ppbv) of the ambient atmospheric $N_2O$ concentration. If a chamber failed to open, it would remain closed through a complete 2-hour cycle of sampling all four chambers, and the chamber headspace $N_2O$ concentration would be in equilibrium with the $N_2O$ concentration in the soil or very nearly to. Therefore, a flux estimate was deemed rejected due to failure of a chamber to open when the measured chamber $N_2O$ concentration at the beginning of the sampling period was greater than the ambient atmospheric $N_2O$ concentration by +2 times the instrument precision and the chamber $N_2O$ concentration at the end of the sampling period was within ± 2 times the instrument precision (0.4 ppbv) of the chamber $N_2O$ concentration at the beginning of the sampling period. Ambient atmospheric $N_2O$ concentration was measured by sampling the ambient air 2 m above the instrumentation trailer during the 5 minutes prior to chamber closure.

As explained in the flux estimation section flux are estimated on the assumption that $N_2O$ concentration in the chamber headspace increases linearly with time since the slope of the regression is the flux estimate, fluxes with a $R^2 < 0.95$ where deemed as system malfunction.

Using these strategies to detect malfunction in the system is very useful but regular maintenance (3-4 days) is critical, and observing values of $R^2 \geq 0.95$ does not guarantee correct system operation.

***System autonomy and reliability***

The system has been deployed to measure soil $N_2O$ emissions during five different long term sampling campaigns in Columbia County (WI). These campaigns include a full growing season

(7 months) and four year-round studies during which the system provided on average 8 daily high-resolution flux measurements from four chambers.

The automatic monitoring $N_2O$ system was reliable. During the five sampling campaigns the automatic sampling was only interrupted for more than five consecutive days in four occasions and only three of them were related with failure of the monitoring system (Table 1). The average sampling resolution during the operational time, which includes periods during which sampling was interrupted for less than five consecutive days, was between 6.5 to 10 times per chamber and day across all sampling campaigns (Table 1). This is important because accurate estimation of daily and therefore cumulative $N_2O$ emissions in highly fertilized crop systems requires $N_2O$ measurements at sub-daily frequencies, especially during peak emissions events (Barton et al., 2015; Francis Clar & Anex, 2020). The range of hourly $N_2O$ fluxes measured with this system extend from 0.01 to 3228. g $N\text{-}N_2O$ $ha^{-1}$ $day^{-1}$, these were measured in an incredibly wide range of environmental conditions as one can imagine by the duration and sampling dates represented in table 1. In addition, the ability of this systems in capturing peak emissions events and their relative importance to total cumulative emissions is demonstrated in chapters 4 and 5 of this dissertation.

Table 1. **Performance of the $N_2O$ monitoring for monitoring $N_2O$ fluxes at high temporal resolution during long sampling campaigns. Operational days include sampling interruptions shorter than 5 consecutive days, average sampling resolution was estimated from the total number of fluxes divided by the number of operational days.**

| Sampling campaign | Sampling starts | Sampling ends | Sampling interruptions dates (#days – cause) | Operational time in days | Average sampling resolution (flux measurements $day^{-1}$ $chamber^{-1}$) |
|---|---|---|---|---|---|
| 2015 | 4/2/15 | 10/27/15 | 9/9/15 to 10/3/15 (23 days – electrical short) | 185 | 10 |
| 2016-17 | 9/22/16 | 7/5/17 | 1/18/17 to 2/5/17 (25 – flood/freeze) | 260 | 6.5 |
| 2017-18 | 9/11/17 | 8/22/18 | None | 345 | 6.7 |
| 2018-19 | 9/13/18 | 7/15/19 | 6/4/19 to 6/30/19 (30 - Analyzer fail) | 275 | 7.9 |
| 2019-20 | 9/18/20 | 9/10/20 | 10/19/19 to 11/5/19 (17 - Analyzer fail) | 341 | 7.8 |

## *5. Conclusion*

An automatic soil $N_2O$ isotope monitoring system has been developed and operated continuously over extended periods of time. Accuracy, sensitivity and high sample frequency allowed the system to measure soil gas flux with a very short chamber deployment time (i.e., 10 minutes). Short deployment time did not compromise the accuracy of the flux measurements. Quite the contrary, rapid flux measurements reduced to insignificant levels the chamber effects that are possible with manual sampling. Obtaining flux measurements in such short periods of time allowed increased temporal and spatial resolution, with the current system providing 8 fluxes measurements per day from each of four different soil chambers. Near constant monitoring of $N_2O$ fluxes helps to identify relationships between environmental conditions (e.g. soil moisture and temperature) and $N_2O$ soil production rates. Multiple chambers per plots capture soil heterogeneity and spatial variability, increasing the statistical power of experiments designed to assess differences between soil $N_2O$ mitigation strategies. $N_2O$ flux data obtained

with this system provide the accuracy and sensitive needed to assess differences between $N_2O$ emissions mitigation strategies and also provide data needed to improve soil modelling and our understanding of the evolution of $N_2O$ in agricultural systems.

## *6. References*


Ambus, P. & Robertson, G. P. (1998). Automated Near-Continuous Measurement of Carbon Dioxide and Nitrous Oxide Fluxes from Soil. *Soil Science Society of America Journal*, *62*(2), 394. https://doi.org/10.2136/sssaj1998.03615995006200020015x

Anthony, W. H., Hutchinson, G. L. & Livingston, G. P. (1995). Notes chamber measurement of soil-atmosphere gas exchange: linear vs. diffusion-based flux models. Soil Science Society of America Journal, 59, 1308–1310. https://doi.org/10.2136/sssaj1995.03615995005900050015x

Barton, L., Wolf, B., Rowlings, D., Scheer, C., Kiese, R., Grace, P., Stefanova, K. & Butterbach-Bahl, K. (2015). Sampling frequency affects estimates of annual nitrous oxide fluxes. *Scientific Reports*, *5*(1), 15912. https://doi.org/10.1038/srep15912

Bouwman, A. F., Boumans, L. J. M. & Batjes, N. H. (2002). Emissions of N2O and NO from fertilized fields: Summary of available measurement data. *Global Biogeochemical Cycles*, *16*(4), 6-1-6–13. https://doi.org/10.1029/2001GB001811

Cavigelli, M. a, Grosso, S. J. del, Liebig, M. a, Snyder, C. S., Fixen, P. E., Venterea, R. T., Leytem, A. B., McLain, J. E. & Watts, D. B. (2012). US agricultural nitrous oxide emissions: context, status, and trends. *Frontiers in Ecology and the Environment*, *10*(10), 537–546. https://doi.org/10.1890/120054

Christensen, S. (1983). Nitrous oxide emission from a soil under permanent grass: Seasonal and diurnal fluctuations as influenced by manuring and fertilization. *Soil Biology and Biochemistry*, *15*(5), 531–536. https://doi.org/10.1016/0038-0717(83)90046-9

Christiansen, J. R., Outhwaite, J. & Smukler, S. M. S. M. (2015). Comparison of CO2, CH4 and N2O soil-atmosphere exchange measured in static chambers with cavity ring-down spectroscopy and gas chromatography. *Agricultural and Forest Meteorology*, *211–212*, 48–57.

Davidson, E. A., Savage, K., Verchot, L. V. & Navarro, R. (2002). Minimizing artifacts and biases in chamber-based measurements of soil respiration. *Agricultural and Forest Meteorology*, *113*(1–4), 21–37. https://doi.org/10.1016/S0168-1923(02)00100-4

Decock, C. & Six, J. (2013). How reliable is the intramolecular distribution of 15N in N2O to source partition N2O emitted from soil? In *Soil Biology and Biochemistry* (Vol. 65, pp. 114–127). Pergamon. https://doi.org/10.1016/j.soilbio.2013.05.012

Francis Clar, J. T. & Anex, R. P. (2020). Flux intensity and diurnal variability of soil $N_2O$ emissions in a highly fertilized cropping system. *Soil Science Society of America Journal*, saj2.20132. https://doi.org/10.1002/saj2.20132

Gupta, M. (2012). *Cavity-Enhanced Laser Absorption Spectrometry for Industrial Applications*. Gases & Instrumentation International. May / June www.gasemag.com. http://www.lgrinc.com/documents/CavityEnhanced%20Laser%20Absorption%20Spectrometry%20for%20Industrial%20Applications%20May_June%202012.pdf

Hüppi, R., Felber, R., Krauss, M., Six, J., Leifeld, J. & Fuß, R. (2018). Restricting the nonlinearity parameter in soil greenhouse gas flux calculation for more reliable flux estimates. PLoS ONE, 13(7). https://doi.org/10.1371/journal.pone.0200876

Hutchinson, G. L. & Mosier, A. R. (1981). Improved Soil Cover Method for Field Measurement of Nitrous Oxide Fluxes 1. *Soil Science Society of America , 45*. https://doi.org/10.2136/sssaj1981.03615995004500020017x

IPCC. (2014). Climate Change 2014: Synthesis Report. Contribution of Working Groups I, II and III to the Fifth Assessment Report of the Intergovernmental Panel on Climate Change. In *Ipcc*.

Laville, P., Lehuger, S., Loubet, B., Chaumartin, F. & Cellier, P. (2011). Effect of management, climate and soil conditions on N2O and NO emissions from an arable crop rotation using high temporal resolution measurements. *Agricultural and Forest Meteorology*, *151*(2), 228–240. https://doi.org/10.1016/J.AGRFORMET.2010.10.008

Levy, P. E., Gray, A., Leeson, S. R., Gaiawyn, J., Kelly, M. P. C., Cooper, M. D. A., Dinsmore, K. J., Jones, S. K. & Sheppard, L. J. (2011). Quantification of uncertainty in trace gas fluxes measured by the static chamber method. European Journal of Soil Science, 62, 811–821. https://doi.org/10.1111/j.1365-2389.2011.01403.x

Machado, P. V. F., Wagner-Riddle, C., MacTavish, R., Voroney, P. R. & Bruulsema, T. W. (2019). Diurnal Variation and Sampling Frequency Effects on Nitrous Oxide Emissions following Nitrogen Fertilization and Spring-Thaw Events. *Soil Science Society of America Journal*, *83*(3), 743–750. https://doi.org/10.2136/sssaj2018.10.0365

Mondini, C., Sinicco, T., Cayuela, M. L. & Sanchez-Monedero, M. A. (2010). A simple automated system for measuring soil respiration by gas chromatography. *Talanta*, *81*(3), 849–855. https://doi.org/10.1016/j.talanta.2010.01.026

Molodovskaya, M., Singurindy, O., Richards, B. K., Warland, J., Johnson, M. S. & Steenhuis, T. S. (2012). Temporal Variability of Nitrous Oxide from Fertilized Croplands: Hot Moment Analysis. *Soil Science Society of America Journal*, *76*(5), 1728. https://doi.org/10.2136/sssaj2012.0039

Molodovskaya, M., Warland, J., Richards, B. K., Öberg, G. & Steenhuis, T. S. (2011). Nitrous Oxide from Heterogeneous Agricultural Landscapes: Source Contribution Analysis by Eddy Covariance and Chambers. *Soil Science Society of America Journal*, *75*(5), 1829. https://doi.org/10.2136/sssaj2010.0415

Parkin, T. B. (2008). Effect of Sampling Frequency on Estimates of Cumulative Nitrous Oxide Emissions. *Journal of Environment Quality*, *37*(4), 1390. https://doi.org/10.2134/jeq2007.0333

Parkin, T. B. & Kaspar, T. C. (2006). Nitrous oxide emissions from corn-soybean systems in the midwest. *Journal of Environmental Quality*, *35*(4), 1496–1506. https://doi.org/10.2134/jeq2005.0183

Parkin, T. B. & Venterea, R. T. (2010). U.S. Department of Agriculture - Agricultural ressearch service Greenhouse gas Reduction through Agricultural Carbon Enhancement network (USDA-ARS GRACEnet) Project Protocols Chapter 3. Chamber-Based Trace Gas Flux Measurements. *Flux*, *2010*(April 2003), 1–39.

Pattey, E., Edwards, G. C., Pennock, D. J., Smith, W., Grant, B. & MacPherson, J. I. (2007). Tools for quantifying N2O emissions from agroecosystems. *Agricultural and Forest Meteorology*, *142*(2–4), 103–119. https://doi.org/10.1016/J.AGRFORMET.2006.05.013

Pedersen, A. R. ;, Petersen, S. O. ; & Schelde, K. ; (2010). A comprehensive approach to soil-atmosphere trace-gas flux estimation with static chambers. *European Journal of Soil Science*, *61*(december), 888–902. https://doi.org/10.1111/j.1365-2389.2010.01291.x

Petersen, S. O., Regina, K., Pöllinger, A., Rigler, E., Valli, L., Yamulki, S., Esala, M., Fabbri, C., Syväsalo, E. & Vinther, F. P. (2006). Nitrous oxide emissions from organic and conventional crop rotations in five European countries. *Agriculture, Ecosystems & Environment*, *112*(2–3), 200–206. https://doi.org/10.1016/j.agee.2005.08.021

Pérez, T., Trumbore, S. E., Tyler, S. C., Matson, P. A., Ortiz-Monasterio, I., Rahn, T. & Griffith, D. W. T. (2001). Identifying the agricultural imprint on the global N 2 O budget using stable isotopes. *Journal of Geophysical Research: Atmospheres*, *106*(D9), 9869–9878. https://doi.org/10.1029/2000JD900809

Rapson, T. D. & Dacres, H. (2014). Analytical techniques for measuring nitrous oxide. In *TrAC - Trends in Analytical Chemistry* (Vol. 54, pp. 65–74). Elsevier B.V. https://doi.org/10.1016/j.trac.2013.11.004

Rochette, P. & Eriksen-Hamel, N. S. (2008). Chamber Measurements of Soil Nitrous Oxide Flux: Are Absolute Values Reliable? *Soil Science Society of America Journal*, *72*(2), 331. https://doi.org/10.2136/sssaj2007.0215

Savage, K., Phillips, R. & Davidson, E. (2014). High temporal frequency measurements of greenhouse gas emissions from soils. *Biogeosciences*, *11*(10), 2709–2720. https://doi.org/10.5194/bg-11-2709-2014

Sehy, U., Ruser, R. & Munch, J. C. (2003). Nitrous oxide fluxes from maize fields: relationship to yield, site-specific fertilization, and soil conditions. *Agriculture, Ecosystems & Environment*, *99*(1–3), 97–111. https://doi.org/10.1016/S0167-8809(03)00139-7

Snyder, C., Davidson, E., Smith, P. & Venterea, R. (2014). Agriculture: sustainable crop and animal production to help mitigate nitrous oxide emissions. *Current Opinion in Environmental Sustainability*, *9*, 46–54. https://doi.org/10.1016/j.cosust.2014.07.005

Snyder, C. S., Bruulsema, T. W., Jensen, T. L. & Fixen, P. E. (2009). Review of greenhouse gas emissions from crop production systems and fertilizer management effects. *Agriculture, Ecosystems & Environment*, *133*(3–4), 247–266. https://doi.org/10.1016/j.agee.2009.04.021

Thies, S., Bruggeman, S., Clay, S. A., Mishra, U., Hatfield, G., Kumar, S. & Clay, D. E. (2019). Midmorning point sampling may not accurately represent nitrous oxide emissions following fertilizer applications. *Soil Science Society of America Journal*, *83*(2), 339–347. https://doi.org/10.2136/sssaj2018.08.0313

Thomsen, I. K., Pedersen, A. R., Nyord, T. & Petersen, S. O. (n.d.). Effects of slurry pre-treatment and application technique on short-term N 2 O emissions as determined by a new non-linear approach. "Agriculture, Ecosystems and Environment," 136, 227–235. https://doi.org/10.1016/j.agee.2009.12.001

Venterea, R. T., Spokas, K. a. & Baker, J. M. (2009). Accuracy and Precision Analysis of Chamber-Based Nitrous Oxide Gas Flux Estimates. *Soil Science Society of America Journal*, *73*(4), 1087. https://doi.org/10.2136/sssaj2008.0307

Venterea, R. T., Petersen, S. O., de Klein, C. A. M., Pedersen, A. R., Noble, A. D. L., Rees, R. M., Gamble, J. D. & Parkin, T. B. (2020). Global Research Alliance N2O chamber methodology guidelines: Flux calculations. *Journal of Environmental Quality*, *49*(5), 1141–1155. https://doi.org/10.1002/jeq2.20118

Wagner-Riddle, C. (2019, April 15). Nitrous oxide emissions induced by freeze/thaw: importance and potential mechanisms. *Climate Change, Reactive Nitrogen, Food Security and Sustainable Agriculture* .

Wahlen, M. & Yoshinari, T. (1985). Oxygen isotope ratios in N2O from different environments. *Nature*, *313*(6005), 780–782. https://doi.org/10.1038/313780a0

Wang, W., Dalal, R. C., Reeves, S. H., Butterbach-Bahl, K. & Kiese, R. (2011). Greenhouse gas fluxes from an Australian subtropical cropland under long-term contrasting management regimes. *Global Change Biology*, *17*(10), 3089–3101. https://doi.org/10.1111/j.1365-2486.2011.02458.x

Yoshida, N. & Toyoda, S. (2000). Constraining the atmospheric N2O budget from intramolecular site preference in N2O isotopomers. *Nature*, *405*(6784), 330–334. https://doi.org/10.1038/35012558

# *7. Appendix*

## *7.1. Part list*

Most relevant parts and materials used for the construction of the system are organized along tables 0-1 to 0-15, attending to the part of the system where they belong. Tables provide a general description of the part or material, for what it is used and the number of units needed for the construction of the specific part of the system. Tables include the part number and commercial brand that I used on my design. Unitary price of the parts and total material cost for each of the parts of the system are also included (All prices are in American dollars).

**Table 2.** Approximate cost ($) of the materials and parts used for each one of the parts of the system. Price of the analyzer and the MIU are not included.

| **Part** | **Cost ($)** |
|---|---|
| Automatic Soil Chamber<br>- Battery<br>- Power distribution | 2,320 (x5) |
| Gas Path | 2,900 |
| System Digital Logic | 450 |
| Housing<br>- Temperature control system<br>- Power supply, connections, control and protections | 8,000 |
| Total | 22,950 |

### *Automated soil chambers (Non-Steady State & Flow-Through)*

**Table 3.** Parts used for the construction of the soil chamber body (box)

| General Description | Use | Part # | Brand | Unitary price ($) | Units per Chamber | Price per Chamber ($) |
|---|---|---|---|---|---|---|
| 2 -1/2 x 1-1/2 x 3/16 Angle Bar - ASTM A-36 - (steel) | Mounting /support | | Wiedenbeck Inc. | 2x20 ft | 10ft | 10 |
| 16 gauge ferromagnetic stainless steel | Chamber box | 1-S/S SM 410 AWN 16 GAx48"x120" | Dick's Superior Welding, Inc. | 585.00 | 1/10 | 73.13 |
| 4 bar linkage mechanism | Opening/ closing | Table Lift, Folding Lift Up Top | Amazon | 27.99/pair | 1 | 28 |

**Table 4**. Parts used for the construction of the lid

| General Description | Use | Part # | Brand | Unitary price ($) | Units per Chamber | Price per Chamber ($) |
|---|---|---|---|---|---|---|
| White HDPE Sheeting ½" Thick | Lid | 42599 | United States Plastic Corp. | 126.31 | 16" x 17" | 31.58 |
| Custom Magnetic Gasket – Exterior Dimensions: 7-13/16 x 13-¾ " | Sealing gasket | 02-051 | Refrigeration Hardware Supply Corporation | 3.9 | 1 | 3.90 |
| SS-Steel thin plate - 7-13/16 x 13-¾ " | Hold Gasket | | Scraps | - | - | - |
| Cap screw - hex head - 1/4-20 - 1"length | | 87914743 | MSC Industrial supply Co. | 7.78 | 4 | 1.95 |
| Hex nut 1/4-20 - 7/32 thick | | 71925689 | | 6.33 | 4 | 1.58 |
| Washer | | 87925368 | | 3.78 | 4 | 0.95 |
| Sealing Washer | | 4MZU9 | Grainger | 4.58 | 4 | 2.29 |

**Table 5**. Linear actuator and supplementary parts for its attachment and control

| General Description | Use | Part # | Brand | Unitary price($) | Units per Chamber | Price per Chamber ($) |
|---|---|---|---|---|---|---|
| 12VDC – 12 inch stroke Linear actuator | Lid movement | D12-20A5-18 | Thompson Industries Inc. | 441 | 1 | 441 |
| 7/16"-14 x 4-1/2" Grade 5 Zinc Finish Hex Cap Screw and nuts | Hold LA | 13171 and 36108 | Grainger | 0.95 | 1 | 0.95 |
| 2P2T - 12 Vdc Relay | Switch | 1EJH2 | Grainger | 16.68 | 1 | 16.68 |
| Automotive fuse holder | Automation | 6AYD2 | Grainger | 5.42 | 2 | 10.82 |
| Relay socket square pin 8 | Automation | 6CVE4 | Grainger | 6.45 | 1 | 6.45 |
| H8016 plug in relay 8 pins square 12 VDC | Automation | 6CWAO | Grainger | 8.54 | 1 | 8.54 |
| SPST Rocker Switch | Manual o/c | 6797T21 | Mc Master Car | 12.88 | 1 | 12.88 |
| Compact Limit Switch | Control LA run | 2LNA8 | Automation Direct | 30.69 | 3 | 92.07 |
| Cap screw - socket head #8-32 length 1" | Bolted Unions | 05667100 | MSC Industrial Supply Co. | 9.82 | 2 | 9.82 |
| Machine screw hex nut #8-32 width= 1/8 | | 87925541 | MSC Industrial Supply Co. | 5.77 | 2 | 5.77 |
| EPDM Washer, | | 4PAF1 | Grainger | Use previous surplus | | |

**Table 6** Miscellaneous parts used in the automatic soil chamber

| General Description | Use | Part # | Brand | Unitary price($) | Units per Chamber | Price per Chamber ($) |
|---|---|---|---|---|---|---|
| 14 AWG wire - different colors | Hook-up / Connections | 8054T17 | Mc Master Carr | 11.87 | 1 | 29.6 |
| Wash-down Enclosure 7-1/2" x 7-1/2" x 5" | Housing for chamber electrical controls | 69945K116 | Mc Master Carr | 61.35 | 1 | 61.35 |
| 6 AWG wire - 2 colors (black & red) | Power Supply from trailer to chamber | 6948k71 | Mc Master Carr | 1.51/ft. | 100 ft. | 151 |
| 16 AWG wire | Digital signals from PCB to Soil Chamber | 8054T16 | Mc Master Carr | | 10 ft. | 45.5 |
| 2 AWG Battery cable (black & red) | Battery to power distribution and Charger | 1YPZ1 | Grainger | 57.45/25 ft. | 10 ft. | 14.36 |
| 50 amp Battery Breaker | Protections | CB285-50 | Bussmann | 28.99 | 1 | 28.99 |
| Power distribution block | Power distribution for 12VDC | 5A672 | Grainger | 49.35 | 1 | 49.35 |
| Reusable lever wire clamps | wire connections | 8904T3 | Mc Master Carr | 5.45 | 1 | 5.45 |
| Compact liquid tight cord grip | Chamber - Control Box connections | Several sizes | Mc Master Carr | 3.25 | 8 | 26 |
| Full coverage corrugated wrap-around sleeving | Outdoor Wire & tube protection | 8796T25 | Mc Master Carr | 60.25 | 50 Ft | 30.13 |

| | | | | | | |
|---|---|---|---|---|---|---|
| inline blade style fuse holder | Protect LA & Solenoid | 8110K7 | Mc Master Carr | 5.79 | 3 | 17.37 |
| Blade style low voltage fuses | 10 Amps | | | 31.39/50 uds | 2 | 7.9 |
| Diodes | Varies | 1N4001 | | 3.10/ 10 uds | 1 | 0.8 |
| Battery | Power 12 VDC - Surge Capacity | D51 Yellow top | Optima | 214.99 | 1 | 214.99 |
| Battery Maintainer/Charger | Battery maintainer | IOTA-DLS1215 | IOTA | 154 | 1 | 154 |

***Gas path***

Table 7. Tubbing

| General Description | Use | Part # | Brand | Unitary price($) | Units per Chamber | Price per Chamber($) |
|---|---|---|---|---|---|---|
| 3/16" ID x 1/4" OD x 1/32" Wall Chemfluor® FEP Tubing | Gas Path | 58081 | USPlastics | 1.61 | 1 | 161.00 |
| Flexible Tygon Tubing OD=1/4" ID=1/6"(Aprox) | Gas Path - Pump connection | 56427 | USPlastics | 0.58 | 1 | 58.00 |

**Table 8. Gas path fittings and connectors.**

| General Description | Use | Part # | Brand | Unitary price($) | Units per Chamber | Price per Chamber($) |
|---|---|---|---|---|---|---|
| SS In-Line Particulate Filter, 1/4 in. 2 Micron Pore Size | Analyzer inlet | SS-4F4-2 | Swagelok | 72.93 | 1 | 72.93 |
| 316 Stainless Steel Nut for 1/4 in | Analyzer in/out-let | ss-402-1 | Swagelok | 1.94 | 2 | 3.88 |
| Male Connector, 1/4 in. Tube OD x 1/4 in. Male NPT | 1/4NPT to tube connection | ss-400-1-4 | Swagelok | 7.1 | 4 | 28.4 |
| SS-manifold - 4 out x 1/4 NPT / 1in x 3/8 NPT | Manifold | 2KHL8 | Grainger | 104 | 1 | 104 |
| Male Connector, 1/4 in. Tube OD x 3/8 in. Male NPT | Manifold in/let connections | SS-400-1-6 | Swagelok | 9.2 | 2 | 18.4 |
| Male Connector, 1/4 in. Tube OD x #10-32 Male Thread | Exhaust 3 way valve | SS-400-1-0256 | Swagelok | 18.3 | 1 | 18.3 |
| Male Branch Tee, 1/4 in. Tube OD x 1/4 in. Tube OD x 1/4 in. Male NPT | Chamber /MIU/Chamber | SS-400-3-4TTM | Swagelok | 27.9 | 1 | 4 |
| Female Connector, 1/4 in. Tube OD x 1/4 in. Female NPT | Tee Branch to Tube | SS-400-7-4SC11 | Swagelok | 15.23 | 1 | 15.23 |
| Union, 1/4 in. Tube OD | Union tube-tube | SS-400-6CP | Swagelok | 11.3 | 2 | 22.6 |
| 316 SS 1/4 fittings Ferrule Set | Spare parts | A-400-SET | Swagelok | 1.36 | 1 | 13.6 |

Table 9 Fittings and connectors used on the automatic soil chamber

| General Description | Use | Part # | Brand | Unitary price($) | Units per Chamber | Price per Chamber($) |
|---|---|---|---|---|---|---|
| Bulkhead Union, 1/4 in. Tube OD | in/out-let connections | SS-400-61 | Swagelok | 16.5 | 2 | 33.00 |
| Bulkhead Male Connector, 1/8 in. Tube OD x 1/8 in. Male NPT | Vent connection | SS-200-11-2 | Swagelok | 20.9 | 1 | 20.90 |
| SS 316 tubing OD=1/8 wall=0.016" - 3 feet (15-20cm/chamber) | vent tube | 89995K178 | McMaster | 9.69 | 1 | 9.69 |

**Table 10**. Air pumps and solenoid valves

| General Description | Use | Part # | Brand | Unitary price($) | Units per Chamber | Price per Chamber($) |
|---|---|---|---|---|---|---|
| Air pump: 1060cc/min - 12VDC/105mA - 2.4 psgi | Recirculate air | A120INSNF26PN1 | Sensidyne | 104.98 | 1 | 104.98 |
| SS sol. Valve 3 way/ 2 pos. 2 x 1/4 NPT ( + #13-32 Exhaust) | Gas Path – Solenoid Valve | 3S012-1/4 | STCvalves | 35.99 | 1 | 35.99 |

**Table 11**. Miscellaneous parts used in the implementation of the Gas Path

| General Description | Use | Part # | Brand | Unitary price($) | Units per Chamber | Price per Chamber($) |
|---|---|---|---|---|---|---|
| Tube Rack, 10 Channels, 1/4 In, Black, PK 2 | tube organization | 2HAC1 | Grainger | 4.62 | 1 | 4.62 |
| Thread Sealant Tape, PTFE, 1/4 x 520 In | sealant | 5NTP6 | Grainger | 1.79 | 1 | 1.79 |
| HDPE sheet - 1/4" x 24" x 48" | attachment - organization | 46054 | USPlastics | 31.11 | 1 | 31.11 |
| Self-Laminating Label, 1x2 In | organization | 8PAJ5 | Grainger | 37.3 | 1 | 37.30 |
| Bubble Leak detector | check system | 4E845 | Grainger | 15.74 | 1 | 15.74 |
| Full-Coverage Corrugated Wrap-Around Sleeving (ID 3/8) | Protect tubbing | 8796T26 | McMaster | 75.25 | 1 | 75.25 |

*Digital logic system*

**Table 12** Parts mounted on the PCB

| General Description | Use | Part # | Brand | Unitary price($) | Units | Total Price ($) |
|---|---|---|---|---|---|---|
| High Speed Octocouplers | Isolate Rain sensor signal | TLP2601(F) | Toshiba | 1.69 | 2 | 3.38 |
| Varsistor | Protection overvoltage | F2272-ND | Littelfuse | 0.87 | 2 | 1.74 |
| Buffer | Buffers analyzer signals | CD74ACT541E | Texas Instruments | 0.96 | 2 | 1.92 |
| High Speed Octocouplers | Isolate Analyzer Signals | HCPL-2232-000E | Avago | 8.78 | 10 | 87.8 |
| DC Power connection - PCB 2.1 mm | Power inlet 1 | 163-179PH-EX | kobiconn | 1.04 | 2 | 2.08 |
| Fixed terminal block - 5.08 pitch (3pos) | Connect to Rain sensor | 1729131 | Phoenix contact | 1.42 | 2 | 2.84 |
| Fixed terminal block - 5.08 pitch (2pos) | Power inlet 2 | 1729128 | Phoenix contact | 0.96 | 2 | 1.92 |
| Capacitor 0.1uF-25V | Speed up signals | FK28X7R1E104K | TDK | 0.075 | 100 | 7.5 |
| Polarized Capacitor 47uf-25V | Clean power fluctuations | RDEC71E476MWK1C03B | murata Electronics | 1.51 | 10 | 15.1 |
| Resistors - Through Hole 1/4watt 1Kohms 1% | Pull down signals | CMF551K000FKEA | Visha | 0.176 | 50 | 8.8 |
| Resistors - Through Hole 1/4watt 10Kohms 1% | Pull down signals | 660-MF1/4LCT52R103J | KOA Speer | 0.1 | 20 | 2 |
| Cartridge Fuses 350V 1A SB 2AG PB-FREE | Power 2 Protection | 0209001.MXP | Littelfuse | 0.75 | 5 | 3.75 |

| | | | | | | |
|---|---|---|---|---|---|---|
| Fuse holder | Power 2 Protection | 64600001223 | Littelfuse | 0.76 | 2 | 1.52 |
| Header 24pin(2row) Pitch 2.54 - wire to board | Connection PCB to Relay | 1658621-5 | TE Connectivity | 2.35 | 2 | 4.7 |
| Receptor 24pin(2row) Pitch 2.54 - wire to board | Connection PCB to Relay | 5104338-5 | TE Connectivity | 3.69 | 1 | 3.69 |
| Bipolar Transistors - BJT NPN Gen Pur SS | Rain Signal conditioning | 2N3904 | Central | 0.51 | 1 | 0.51 |
| Logic Gates Quad 2-Input OR | Signal conditioning | M74HC32B1R | ST | 2.8 | 4 | 11.2 |
| Fixed volt Regulator 12 to 5VDC | Volt Regulator | 511-L7805CV | ST | 0.48 | 2 | 0.96 |
| Std LED emitter 2V 10mA | Light indicator | SLR-343VR3F | ROHM | 0.357 | 20 | 7.14 |
| DB 25 Connector - Female to wire | Custom Cable | 1658612-2 | TE Conectivity | 9.64 | 2 | 19.28 |
| DB 25 Connector - Male to wire | Custom cable | 1658608-2 | TE Conectivity | 10.86 | 4 | 43.44 |
| DB 25 Connector - Female - through hole - right | Analyzer to PCB | 745132-2 | TE Conectivity | 9.6 | 1 | 9.6 |
| DB 25 Connector - Male - through hole - right | PCB to MIU | 5745994-4 | TE Conectivity | 14.3 | 1 | 14.3 |
| DB 25 connector Cable Male/female | PCB to MIU | 30-9506MF | AIM-Cambridge | 6.17 | 1 | 6.17 |
| Flat cable 25 conductors 0.05inch pitch | custom cable | 3365/25-CUT-LENGTH | 3M | 0.599 | 10 | 5.99 |

| | | | | | | |
|---|---|---|---|---|---|---|
| BOX ABS GRAY 14.59"L X 10.64"W | PCB housing | NBB-22251 | Bud Industries | 56.2 | 1 | 56.2 |

**Table 13**. General parts of the Digital Logic System

| General Description | Use | Part # | Brand | Unitary price($) | Units | Total Price ($) |
|---|---|---|---|---|---|---|
| Print PCB | 2 layer PCB | N2OcontrolPCB | www.pcbnet.com | 50 | 2 | 50 |
| Optical Rain Sensor | Rain signal Sensor | RG-11 | Hydreon Corporation | 59 | 1 | 59 |
| Optoisolated relay module 12 V - 5v trigger | Output signal distribution | | | 9 | 1 | 9 |

***Housing***

I purchased a 6 by 10 trailer, AFX610SA - FALCON XC SERIES from American Hauler, at a local trailer retailer. I consider that this size is adequate for our installation; two feet shorter or longer will not make a difference, Fig S1 shows the interior of the trailer. Factory made the following modifications for us:

- Wall and ceiling insulation (Keep instrument in the operational temperature range)
- 60” Triple tongue (mount outdoor AC unit)
- Interior reinforcement (mount indoor AC unit)
- 4 Stabilizer Jacks
- No side door

The final price of the trailer was $4.144.

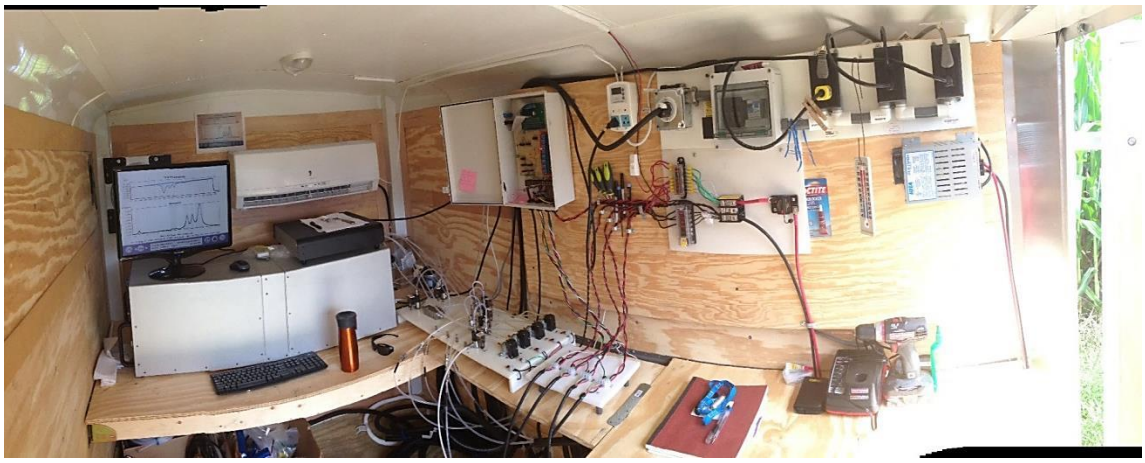

**Figure 2** Interior of the 6x10 ft trailer with all the components of the $N_2O$ monitoring systems except the automated soil chambers which are in the field.

**Table 14.** Parts involved in temperature control

| General Description | Use | Part # | Brand | Unitary price($) | Units | Total Price ($) |
|---|---|---|---|---|---|---|
| Differential Thermostat | Temperature Control | TD300 | Auberins | 99.5 | 1 | 112.44 |
| 10" Shutter Mount Exhaust Fan,115V, HP 1/30 | Exhaust fan | 46Z426 | Airmaster Fan | 232.5 | 1 | 232.5 |
| Single zone wall mount AC unit | Split AC unit 9000BTU | MW09C1H | Friedrich | 987 | 1 | 987 |
| Outdoor unit AC unit | | MR09C1H | | | | |
| Insulated Line set for AC 15 ft D = -1/4" + 3/8" | AC line | T32150 | Friedrich | 108 | 1 | 108 |

**Table 15**. Electrical distribution panel

| General Description | Use | Part # | Brand | Unitary price($) | Units | Total Price ($) |
|---|---|---|---|---|---|---|
| Type 1 Surge protection | Surge protection | SDSA1175 | Square D | 25 | 1 | 25 |
| GFCI Outlet 115V 15Amp | Power Outlet | | Local | 30 | 5 | 300 |
| Power Inlet - Socket | Power Inlet | | Local | 50 | 1 | 50 |
| DIM Breaker 20 Amp-120V | General Breaker | QOU120 | Allie | 31.83 | 2 | 63.66 |
| DIM Breaker 10 Amp-120 V | AC Protection | QOU110 | Allie | 31.83 | 2 | 63.66 |
| DIM Breaker 10 Amp-120V | Analyzer + MIU Protection | QOU110 | Allie | 31.83 | 1 | 31.83 |
| DIM Breaker 5 Amp-120V | Fan Protection | 1BU5R | Allie | 11.6 | 1 | 23.2 |
| Power Cord 4 wires-10AWG | Feed Power to system | 8248K24 | Mc Master Carr | 331 | 1 | 331 |
| Locking Power cord connections | | | Local | 50 | 3 | 150 |
| Breaker Enclosure DIM Style - clear cover | Breaker enclosure | | Allie | 53.16 | 1 | 53.16 |
| Uninterrupted power supply | Electrical protection | SMT1500 | APC | 497 | 1 | 497 |

**Table 16.** Parts used to accommodate trailer installations. All of them were locally bought at the same trailer dealer or at local hardware stores

| General Description | Use | Unitary Price ($) | Units | Total Price($) |
|---|---|---|---|---|
| Flexible Cap, Elastomeric PVC, 3 In | Pass-through connections | 7.41 | 4 | 29.64 |
| Snap-in cleanout assembly 3 inch | Pass-through connections | 5.56 | 3 | 16.68 |
| 2 by 4 Standard lumber | Tables | 3.28/10ft | 4 | 13.12 |
| Plywood 4 by 8 ft | Tables | 20 | 2 | 40 |
| Wood Screws Varies | | | | |
| E-Track trailer system (5 inches) | Hold tables - attaching | 32.51 | 3 | 97.53 |
| E-Track Beam Socket | Hold tables - attaching | 6 | 8 | 48 |
| E-Track Tie Down Stripes 15 ft | Hold Instrumentation when moving | 10 | 4 | 40 |
| Tri-Max Coupler Lock | Burglar trailer protection | 40.7 | 1 | 40.7 |

### *7.2. Drawings Automatic Soil Chamber*

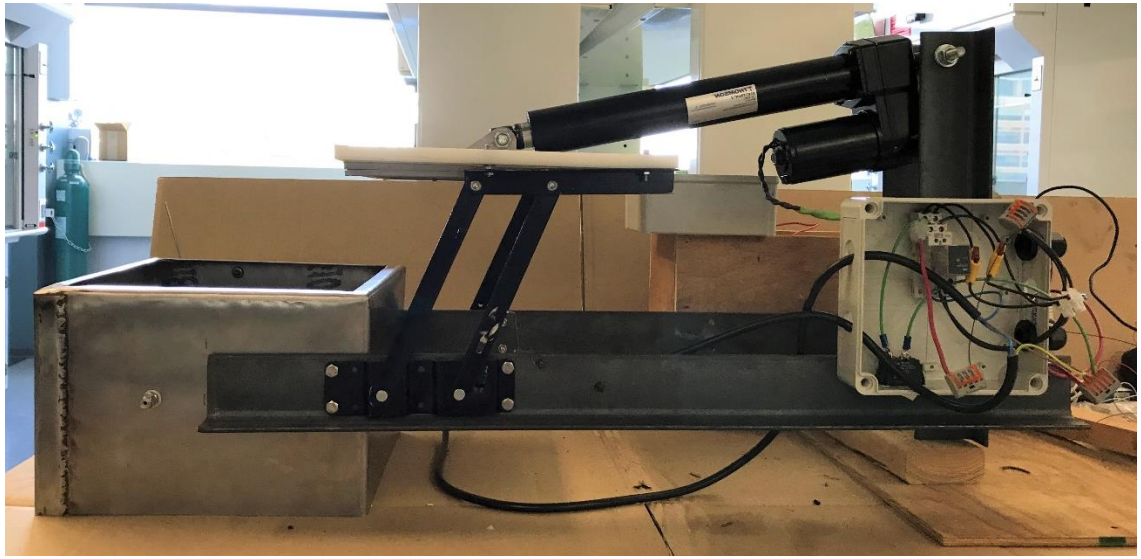

**Figure 3. Automatic soil chamber general view**

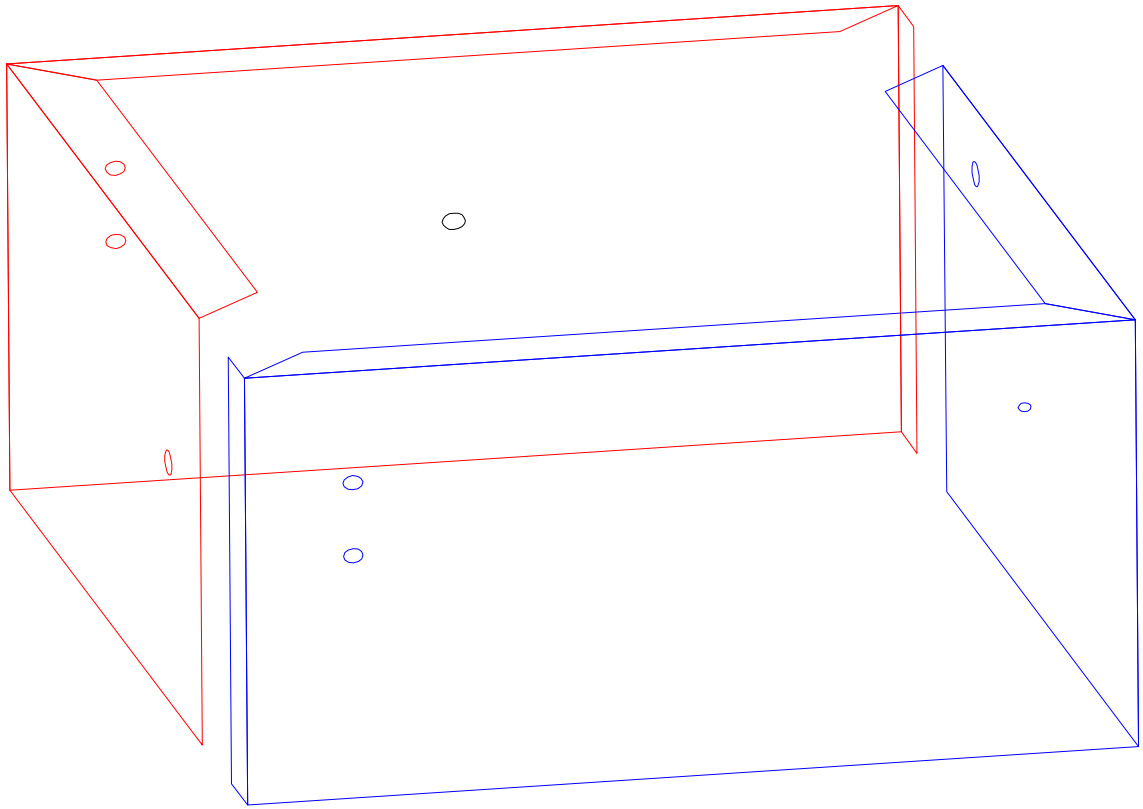

**Figure 4. Drawing – Chamber Box**

| |
|---|
| Drawing title: Chamber box |
| Number: 1 |
| Material: ferromagnetic SS 16 gauge |
| Notes: All holes are through |

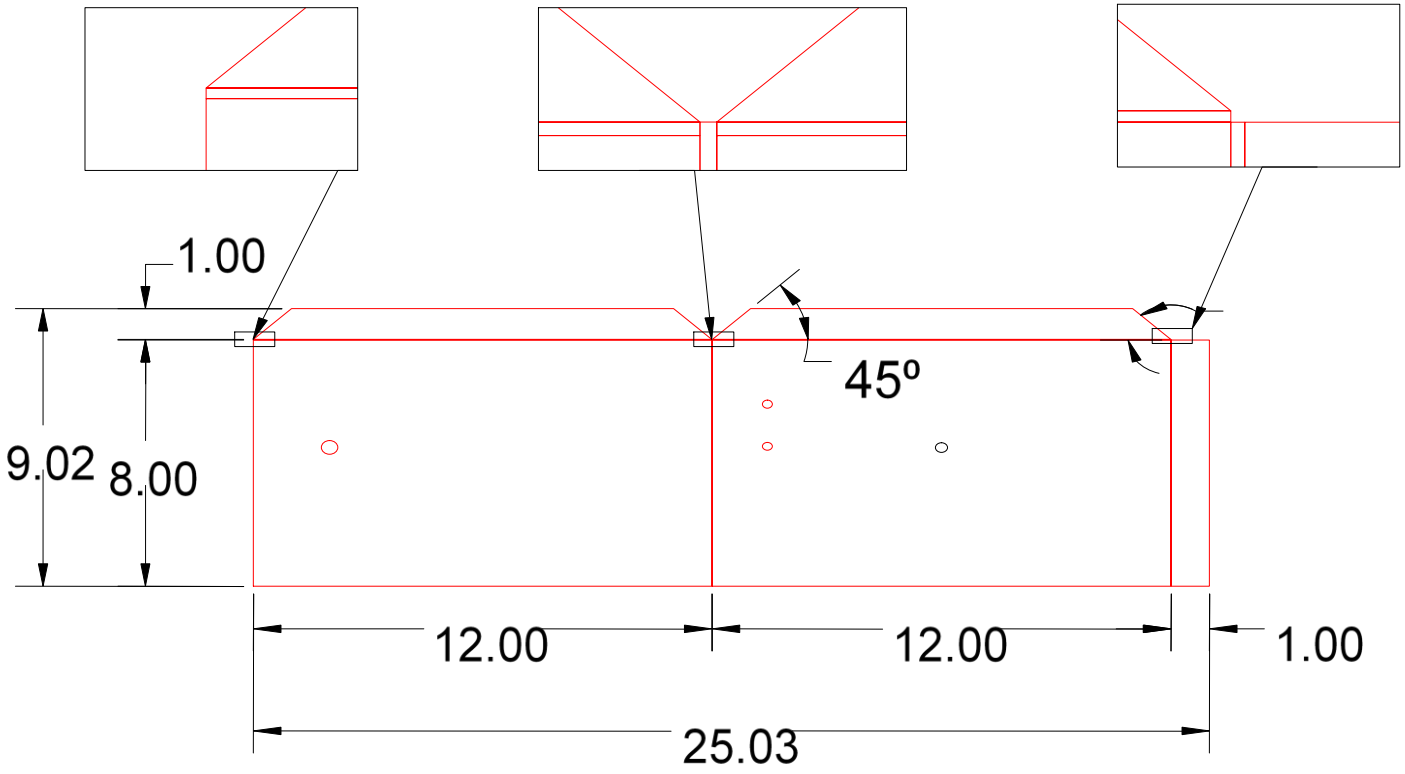


**Figure 5. Chamber box – Unfolded**

| |
|---|
| Drawing title: Chamber box – unfolded |
| Number: 2 |
| Material: ferromagnetic SS 16 gauge |
| Notes: All holes are through – all angles are 45 – bend towards you – material consumed in bending 0.015 inches |
| Measurements are in inches |

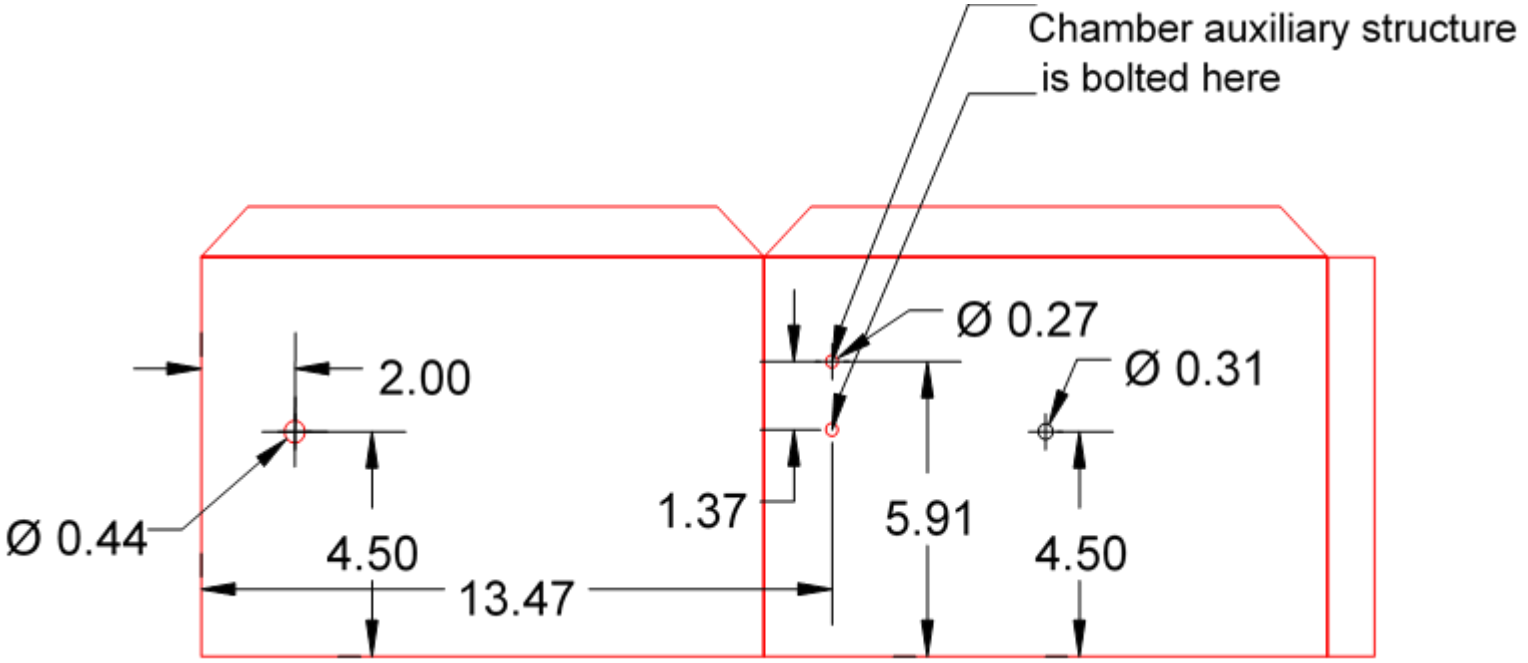


**Figure 6. Chamber Box Unfolded**

| |
|---|
| Drawing title: Chamber box – unfolded |
| Number: 3 |
| Material: ferromagnetic SS 16 gauge |
| Notes: All holes are through – all angles are 45 – bend towards you - material consumed in bending 0.015 inches |
| Measurements are in inches |

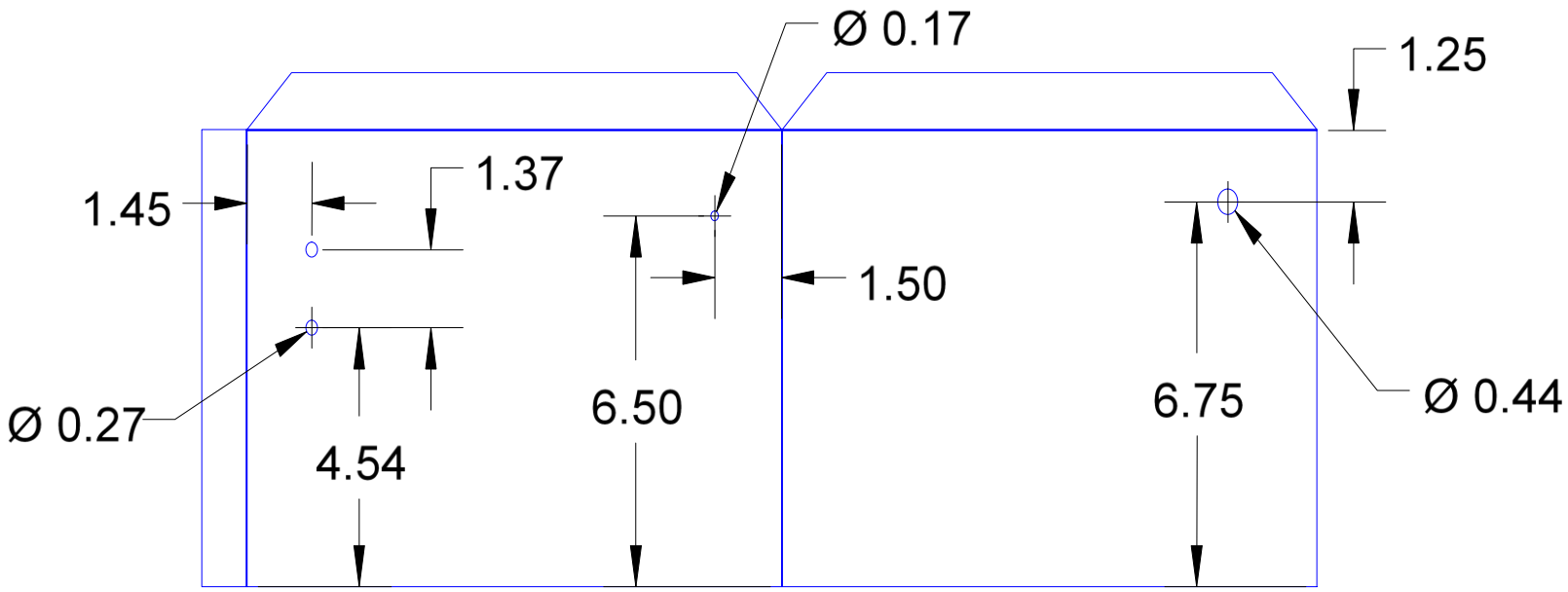


**Figure 7. Chamber box – Unfolded**

| |
|---|
| Drawing title: Chamber box – unfolded |
| Number: 4 |
| Material: ferromagnetic SS 16 gauge |
| Notes: All holes are through – all angles are 45 – bend you - material consumed in bending 0.015 inches |
| Measurements are in inches |

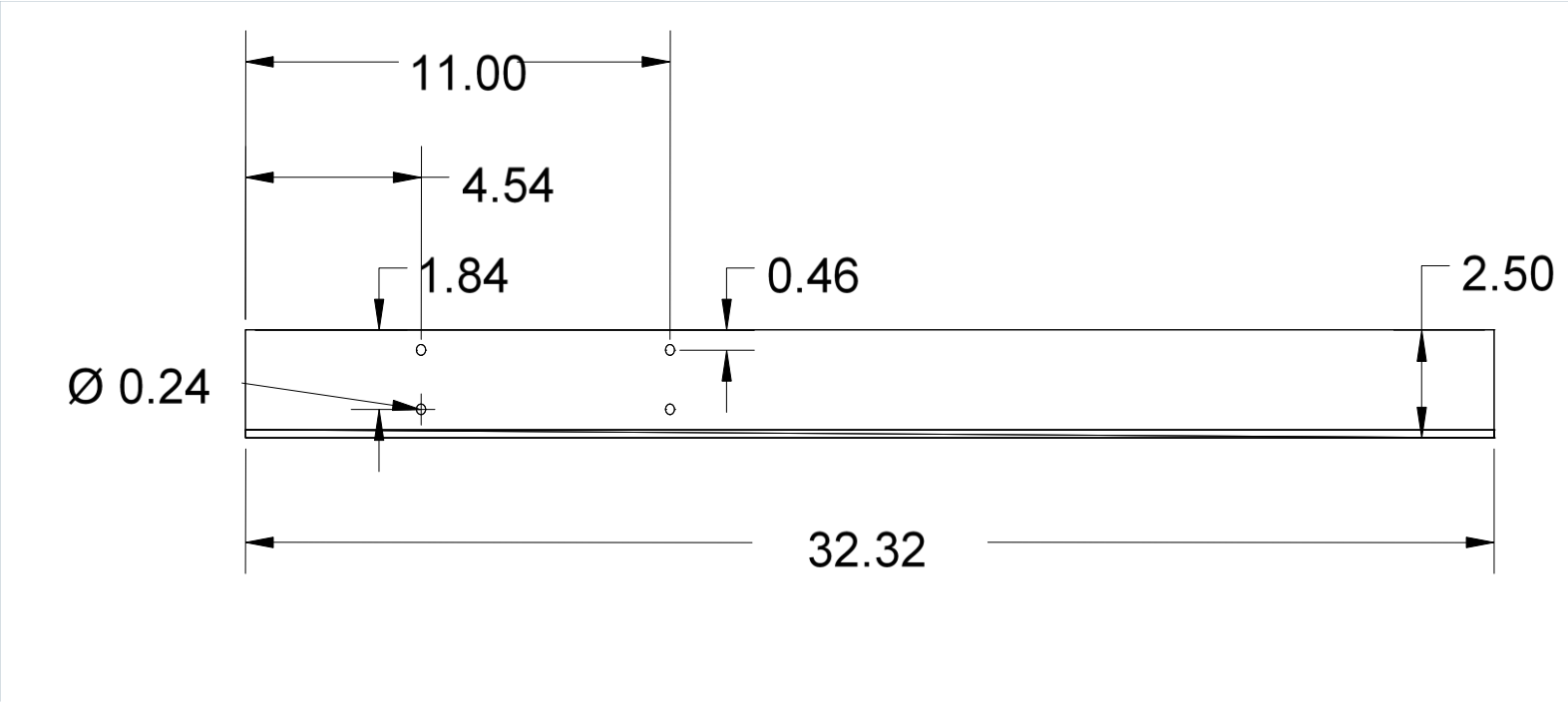


*Figure 8. Auxiliary structure – Part 1*

| |
|---|
| Drawing title: Auxiliary structure - Part 1 |
| Number: 5 |
| Material: Steel angle |
| Notes: Passing holes for ¼ Nut bolts – bolted to chamber and 4 bar mechanism<br>Build a mirrored copy for the opposite side of the chamber |
| Measurements are in inches |

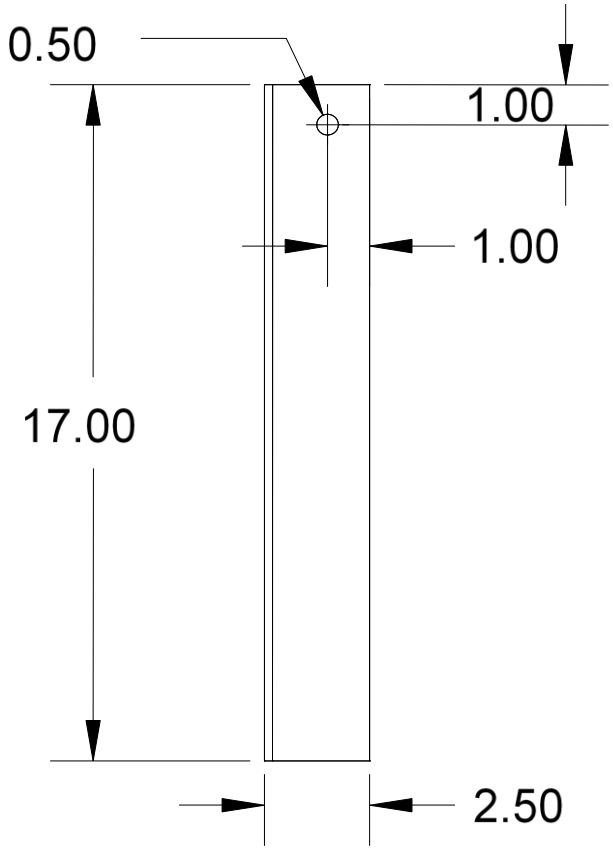


*Figure 9 Auxiliary structure – Part 2*

| |
|---|
| Drawing title: Auxiliary structure - Part 2 |
| Number: 6 |
| Material: Steel angle |
| Notes: Passing holes<br>Build a mirrored copy for the opposite side of the chamber |
| Measurements are in inches |

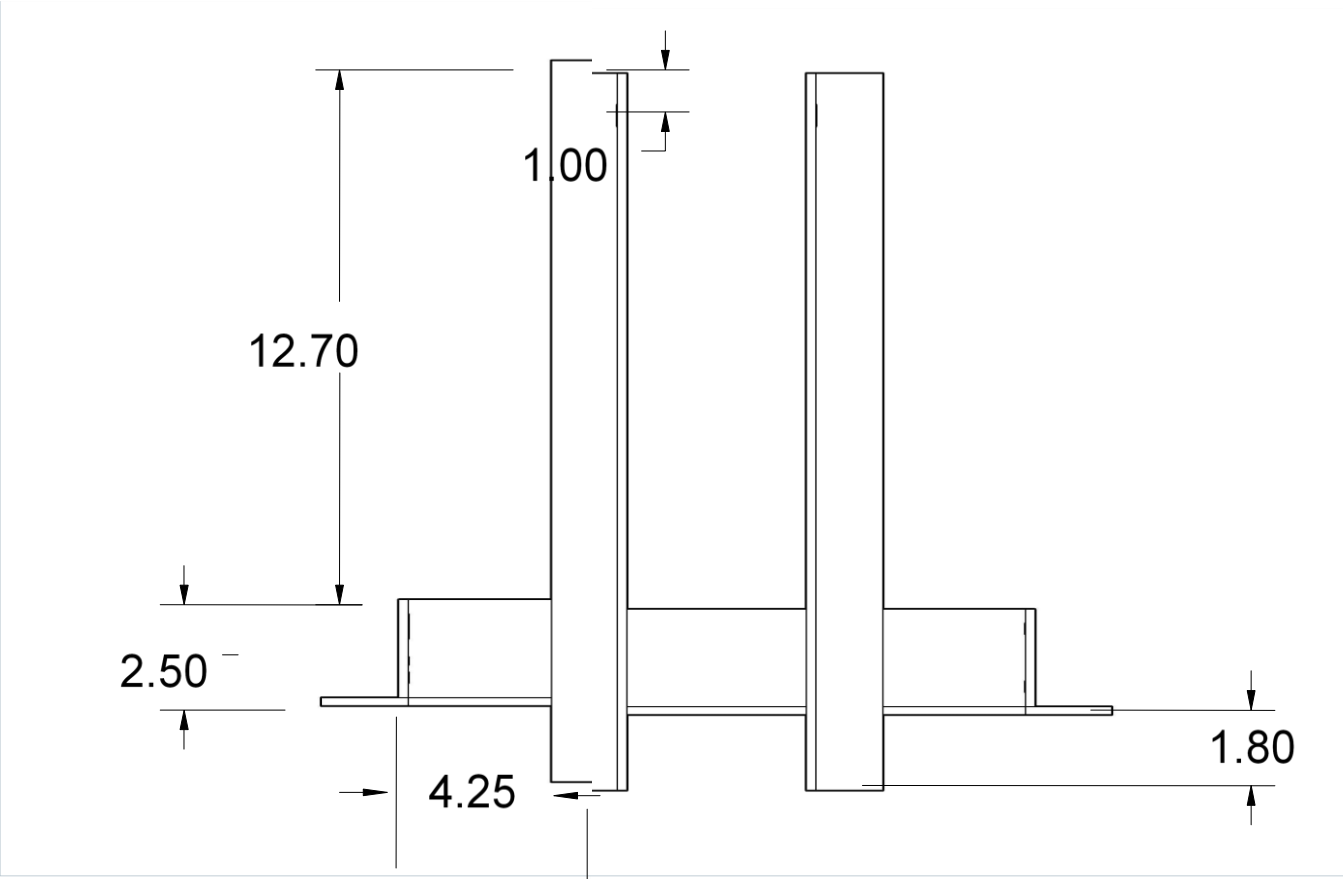


*Figure 10 Auxiliary structure – Back View*

| |
|---|
| Drawing title: Auxiliary structure – Back View |
| Number: 7 |
| Material: Steel angle |
| Notes: Passing holes |
| Measurements are in inches |

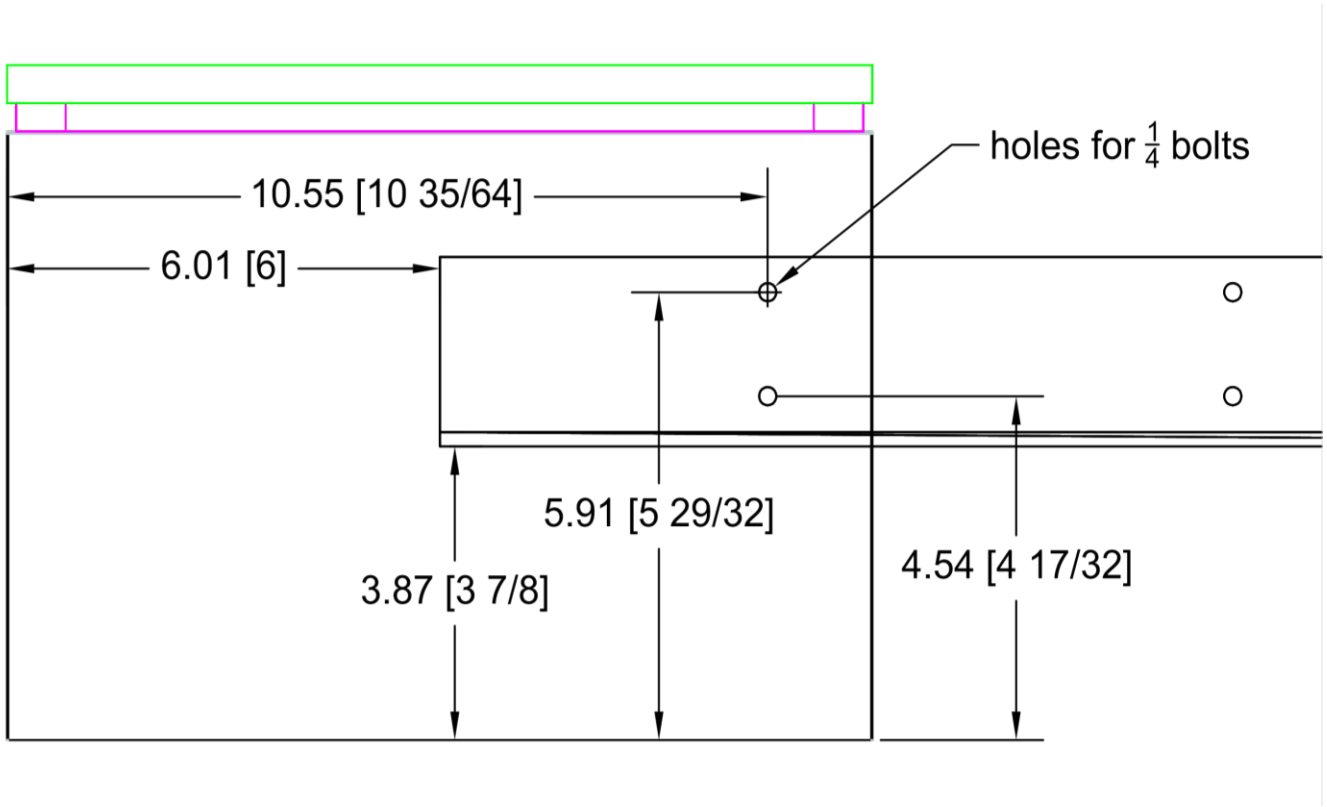


*Figure 11. Detail attachment auxiliary structure to chamber body*

| |
|---|
| Drawing title: Detail attachment auxiliary structure to chamber body |
| Number: 8 |
| Material: |
| Notes: Passing holes |
| Measurements are in inches |

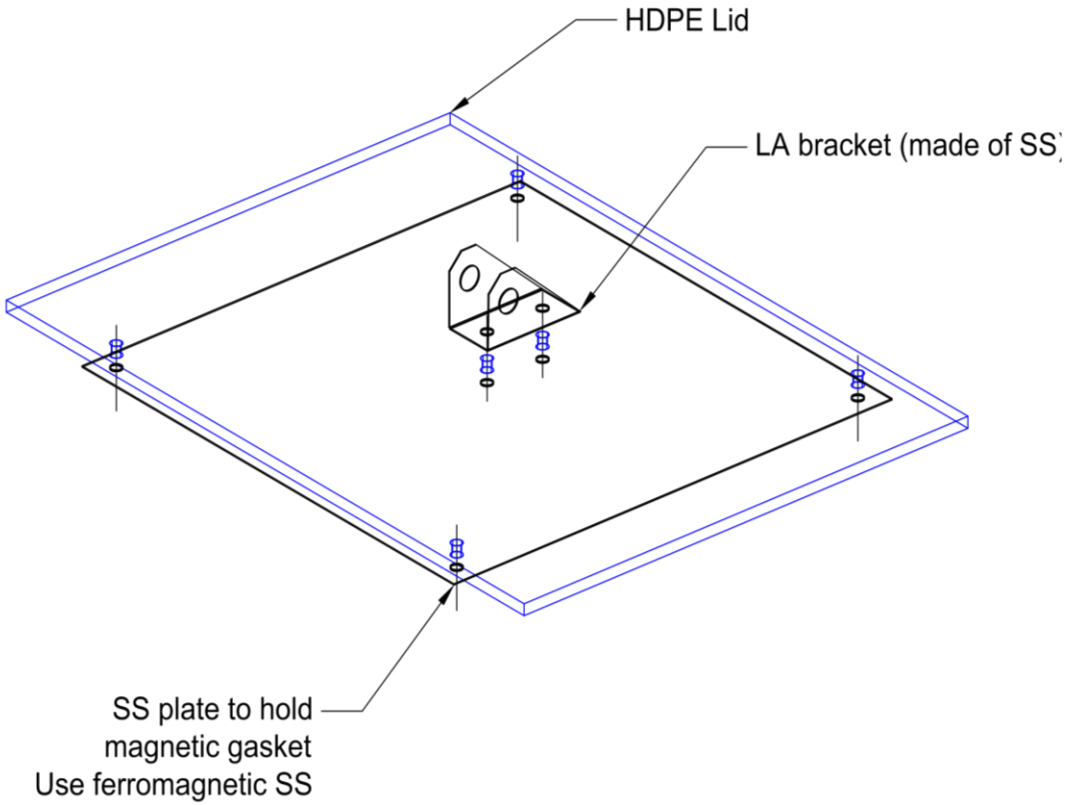


*Figure 12. Lid*

| |
|---|
| Drawing title: Lid |
| Number: 9 |
| Material: HDPE and SS |
| Notes: Passing holes – ¼ bolts all<br>SS plate same dimensions than the gasket |
| Measurements are in inches |

### *7.3. Gas Path Diagram*

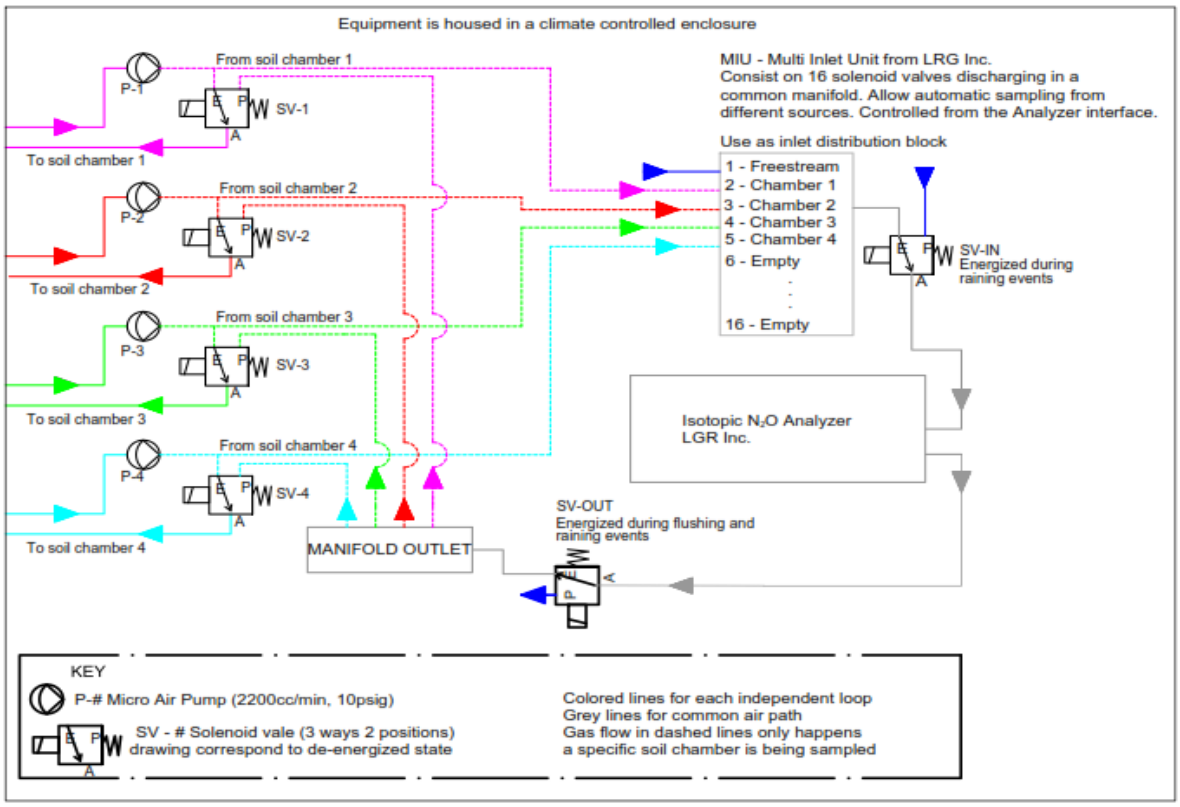


**Figure 13. Dynamic gas path** Gray lines represent the common gas path. Colored lines represent the independent gas loop between each of the chambers and the Analyzer. When a solenoid valve - SV-# was energized, gas flew through dashed colored lines including the analyzer in the gas loop. During flushing, all the air pumps (SV-IN, SV-OUT and MIU valve 1) were energized, while SV-# remained de-energized and soil chambers were open. For simplification, soil chamber and outdoor gas path are not included in the diagram. The system is housed in a climate-controlled enclosure attending the Isotopic $N_2O$ Analyzer requirements.

### *7.4. Electrical Diagrams*

#### *Printed circuit board – Digital Logic System*

Altium Designer version 15 was the software used for the design of the PCB, files generated by this software including ordering specifications for reproduction will be shared upon request. I used through hole components, because soldering them to the PCB is easy and fast and only require the use of a soldering station and a pair of tweezers. PCD schematics are shown below in Fig. 14, and a picture of the final product in Fig 15.

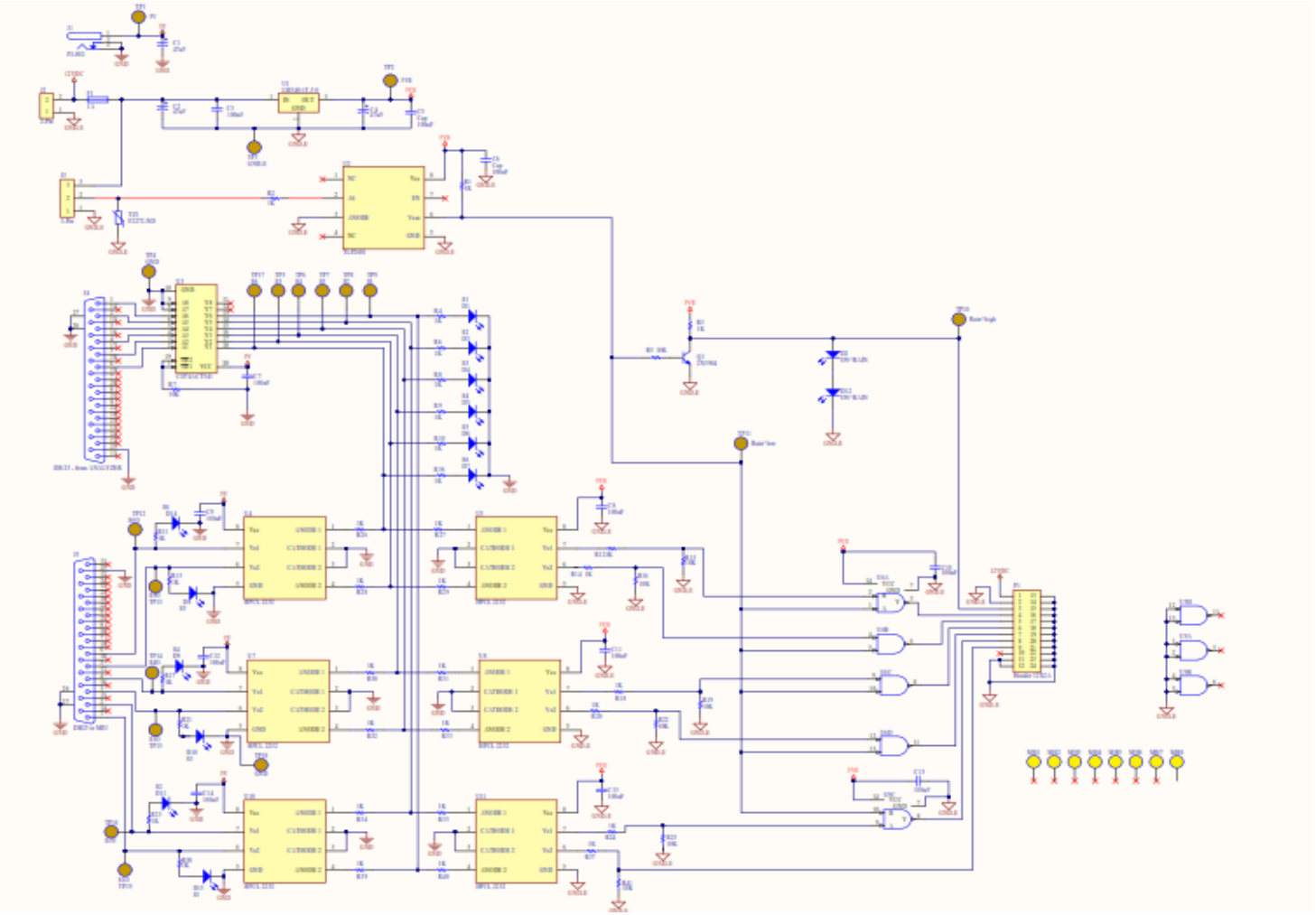

**Figure 14 PCB schematics,** with 7 outputs, sampling sequence are link to outputs 4 to 8 allowing to control 5 different chambers, output 9 controls flushing and output 3 is assigned to raining. These outputs need to be connected through a 24 channels (2 rows) square connector to the 8-relay module as shown in Fig. S19 and then distributed to the rest of the system. Link to high resolution Image below or here https://uwmadison.box.com/s/p43ssa8tcr7q9uaj9o1stteo1xifvd7b

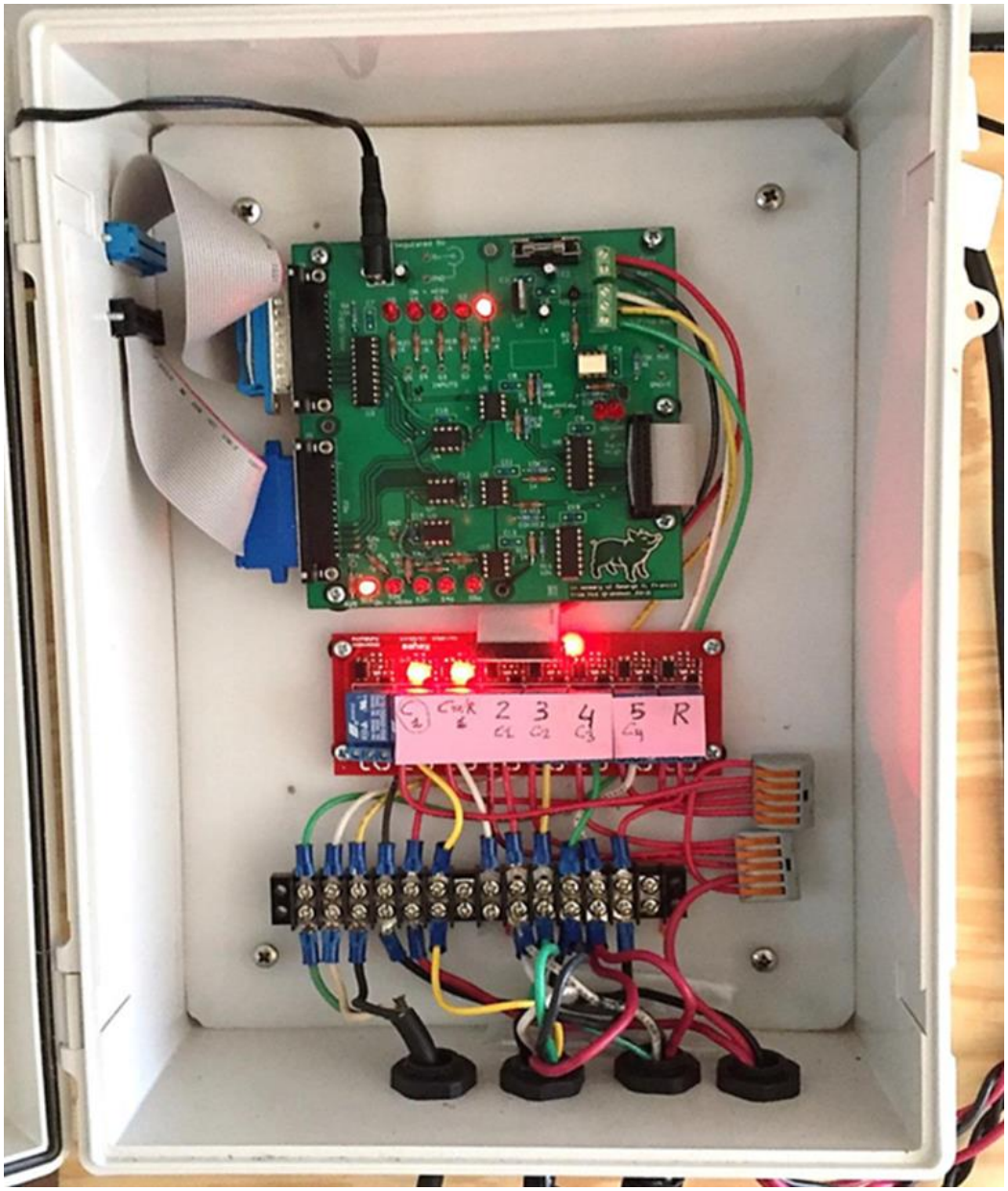


**Figure 15 Picture of the complete Digital Logic System**, PCB and relay module. Starting from the right side the outputs of the relay module are: Channel 5 (Rain, marked as R), Channels 2 to 4 (Chambers, marked as numbers 2 to 4), Channel 1(Flushing, marked as C w/r (cleaning without rain subordination)), Channel 0 (marked as C1) could be used to flush the analyzer internal chamber using standard gases, last relay is not used.

***Gas path wiring diagram***

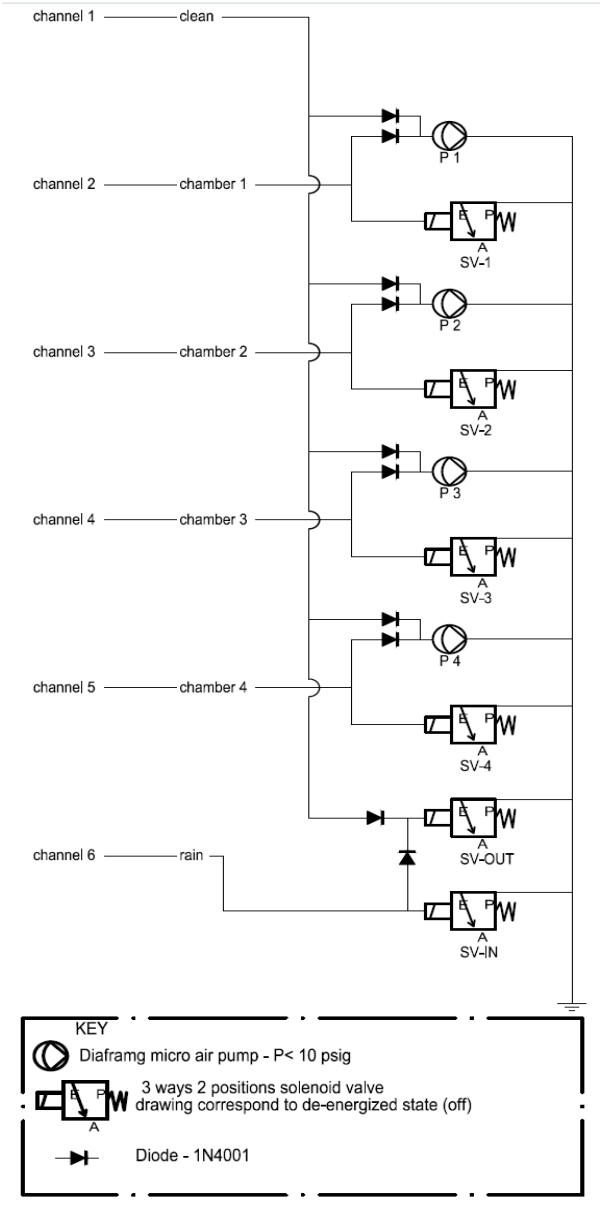


**Figure 16** Outlet distribution block, wiring diagram. Signals come from the module relay, PCB outlet, at 12 VDC.

### *Automatic soil chamber controls*

Electric controls of the Automated Soil Chamber are housed in a wash-down with enclosure attached to the auxiliary structure of the chamber. Power is provide by the 12V deep cycle battery housed in the trailer by 2, 6 AWG wires, signal to trigger opening and

closing mechanism travels on a 12 AWG wire. Figure 17, bellow shows the location of the different electrical components on the ASC.

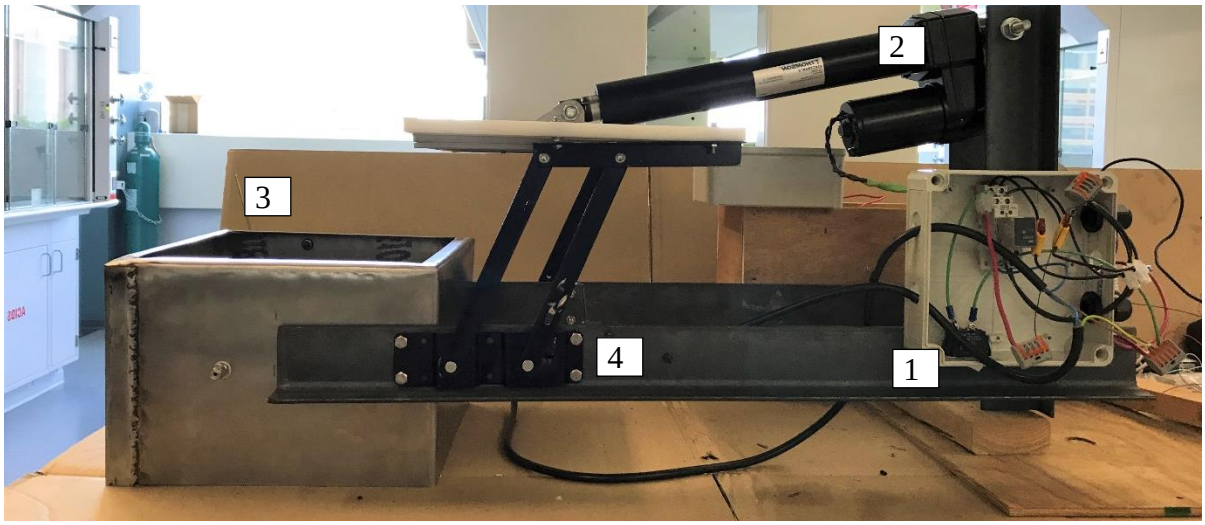


**Figure 17.** Location of the different electrical components on the ASC.- side view (1) Wash-down electrical enclosure, (2) Linear Actuator (3) Limit switch – End Run (closing) (opposite side of the chamber, not visible), (4) Limit switch – End Run (Opening) (behind steal bar, not visible)

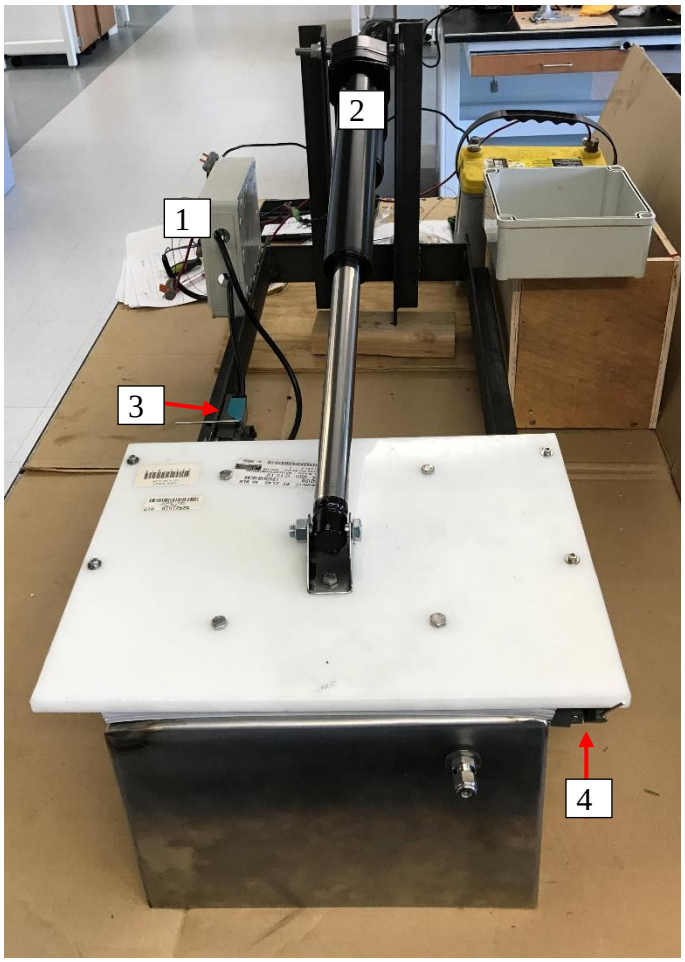


**Figure 18** Location of the different electrical components on the ASC, front view (1) Wash-down electrical enclosure, (2) Linear Actuator (3) Limit switch – End Run (closing), (4) Limit switch – End Run (Opening).

### *Linear actuator controls*

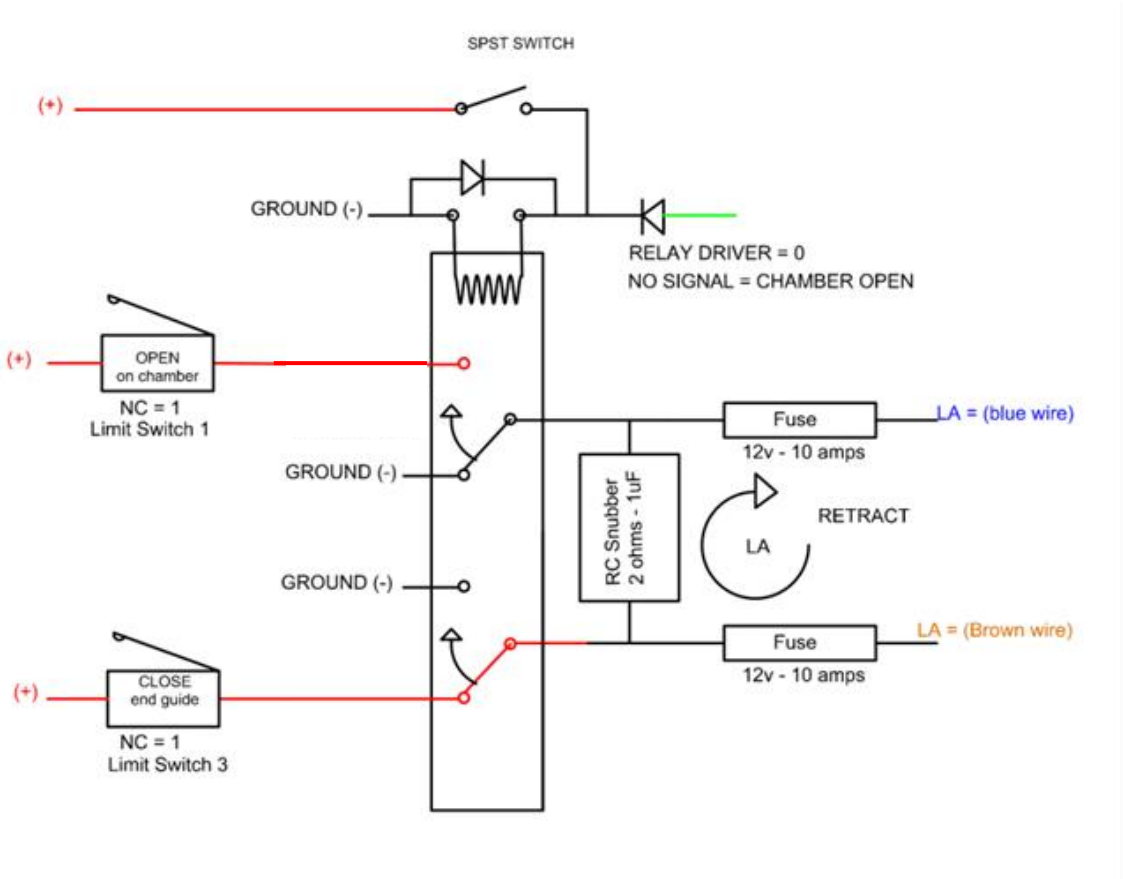


**Figure 19. Wiring diagram of the linear actuator controls**. Red (+) and Black (-) wires are connected to a distribution block which supply power for the battery. Green line, represents the triggering signal, when is low (0), chamber remains open. The RC Snubber is made by wiring in series a 2 Ohms resistor and a 1μF capacitor between the LA connections. Limit switches are labeled (red numbers) according to fig 4-7.

## *Housing distribution panels*

## *AC Distribution panel*

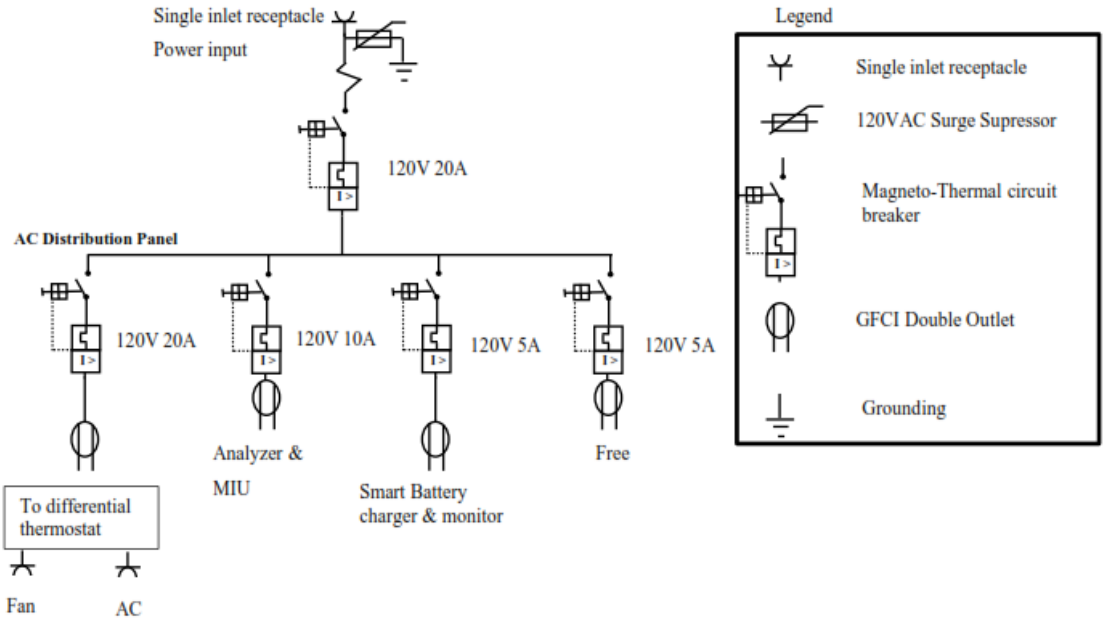


**Figure 20. Alternate current distribution panel**, power consume fluctuated between 550W to 1450 W an hour depending mostly on weather.

### *DC Distribution panel*

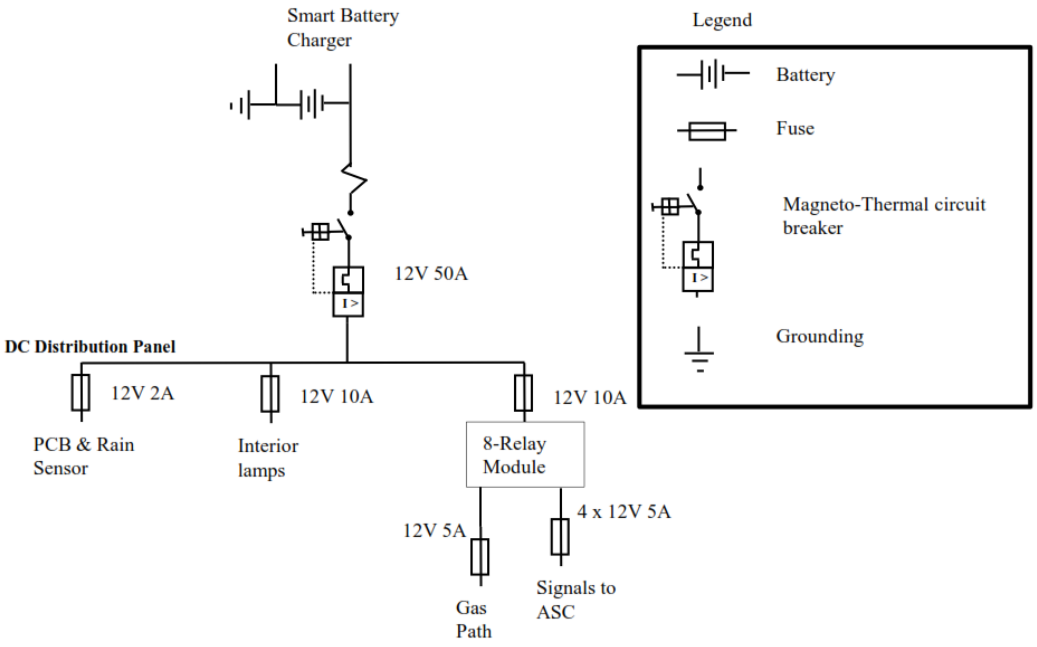


**Figure 21. Direct current distribution panel**

.

# ***Chapter 3: Assessing nitrous oxide ($N_2O$) isotopic analyzer performance for in-field use***

## *1. Abstract*

Analysis of the isotope ratios of $N_2O$ ($^{15}N^{\alpha}$, $^{15}N^{\beta}$, and $^{18}O$) is a promising tool for improving our understanding of biologically controlled nitrogen transformations in soil. Understanding which biological pathways result in $N_2O$ production under particular soil conditions can guide development of effective mitigative soil management strategies. During *in situ* studies, measurement with Laser Absorption Spectroscopy (LAS) has advantages over Isotope Ratio Mass Spectrometry (IRMS) for real-time isotopic measurements of $N_2O$, including high spatial- and temporal-resolution sampling and reduced labor through use of automation in an integrated measurement system.

Recent advances in Laser Absorption Spectroscopy (LAS) have led to the development of affordable analytical instruments that enable simultaneous high frequency measurements of $N_2O$ concentration and $N_2O$ isotope ratios. Reports of studies using LAS $N_2O$ isotopic instruments to collect in-field measurement of soil emitted $N_2O$ are appearing more frequently in the literature. However, the ability of these LAS-based measurement systems to provide consistent, reliable, and accurate *in situ* measurements has not previously been evaluated fully.

The goal of this study was to assess the stability and uncertainty of LAS $N_2O$ isotopic measurements of soil trace gas flux captured in static soil chambers and analyzed using the Keeling plot method. We calibrated, corrected, and characterized LAS measurements over the range of $N_2O$ concentrations representative of those observed during *in situ* experiments, and applied Monte Carlo simulation to find the uncertainty of isotope ratios estimated using Keeling

plot analysis of LAS measurement of headspace gas for multiple combinations of chamber closure duration and soil flux rates representative of typical field experiment conditions. We tested the accuracy LAS-based *in situ* measurement of $N_2O$ isotope ratios through a series of soil flux simulations. The simulations used soil trace gases emitted during soil incubations that were released into a soil chamber headspace, measured using an LAS isotopic analyzer, and interpreted using the Keeling plot method to yield $N_2O$ isotope ratio data which were then compared to measurements of the trace gas isotope ratios measured using IRMS.

We demonstrate that several characteristics of the LAS isotopic instruments, including high measurement variability at low [$N_2O$], nonlinear measurement biases associated with isotopologue concentration, and measurement interference by non-analyte gases, make these instruments poorly suited for *in situ* source partitioning of $N_2O$ emitted from soil. Reliable in-field use will require development of new compensatory techniques including interferent gas scrubbers, identification of interferent gases in gas samples, and adaptive correction functions.

## *2. Introduction*

Nitrous oxide ($N_2O$) is a potent greenhouse-gas and the most important ozone depleting substance in the stratosphere (Portmann et al., 2012; Stocker et al., 2013). Reducing $N_2O$ emissions from agriculture is an important contribution to mitigating climate change. Agricultural fields account for more than 60% of total $N_2O$ anthropogenic emissions (IPCC, 2014). Reductions in $N_2O$ emissions can be accomplished by improving management (i.e., fertilization, tillage, irrigation) in these cultivated soils (Snyder et al., 2014). Obtaining information about the underlying $N_2O$ production pathways in soils is essential for developing sound management practices to reduce $N_2O$ soil emissions.

Recently, changes relative to the natural abundance of the $N_2O$ isotope ratios, $\delta^{15}N^{\alpha}$, $\delta^{15}N^{\beta}$, and $\delta^{18}O$, have been recognized as useful indicators for distinguishing among the sources and sinks of $N_2O$ (Ostrom et al., 2007; Well et al., 2006; Yoshida & Toyoda, 2000). Isotopic effects that occur during $N_2O$-producing processes in soils make it possible to distinguish these processes by the site-specific isotopic ratios of $^{15}N/^{14}N$ in the alpha ($\alpha$) and beta ($\beta$) positions of $N_2O$. For example, $N_2O$ from nitrification is depleted in $^{15}N$, the heavy isotope of nitrogen, which is reflected in a lower value of $\delta^{15}N^{bulk}$, defined as $(\delta^{15}N^{\alpha} + \delta^{15}N^{\beta})/2$. Similarly, the nitrification reaction sequence leads to an enrichment of $^{15}N$ in the $\alpha$ position and depletion in the $\beta$ position, resulting in higher site preference ($SP = \delta^{15}N^{\alpha} - \delta^{15}N^{\beta}$). These isotopic signatures of $N_2O$ have been recommended and applied as differentiators of the main $N_2O$ production pathways in soils (i.e., nitrification and denitrification) (Decock & Six, 2013; N.E., Ostrom & P.H., Ostrom, 2017; Petersen et al., 2020; Bracken et al., 2021).

In plot- or field-scale experiments, soil chambers are generally used to capture soil $N_2O$ fluxes for analysis (Rapson & Dacres, 2014). A soil chamber is an open-ended box that constrains the gas exchange at the soil-atmosphere interface. Upon chamber closure, the $N_2O$ concentration and its isotope ratios shift from those of ambient-air toward those of the soil-produced $N_2O$. Obtaining accurate estimates that allow comparison between different management practices requires measurements from multiple soil chambers several times per day (Henault et al., 2012). Calculating soil $N_2O$ flux and its isotope ratios requires that multiple gas samples be collected from the chamber headspace over the deployment time (Parkin et al., 2012).

The established technology for measuring $N_2O$ isotopocule abundance is Isotope Ratio Mass Spectroscopy (IRMS) (Mohn et al., 2014). While IRMS analyzers yield very accurate measurements, they are not field deployable. Using IRMS to analyze soil trace gas fluxes from field experiments requires manual sampling of gas in the soil chamber headspace and transport of the samples to a spectroscopy laboratory for analysis (Rapson & Dacres, 2014). Manual sampling of soil chambers is time consuming and due to time and budget constraints, can usually only be performed infrequently or on a small number of chambers, which is insufficient to capture spatial and temporal variation with enough resolution to accurately compare $N_2O$ emissions associated with different soil management practices (Groffman et al., 2006; Morris et al., 2013).

Laser Absorption Spectroscopy (LAS) analyzers are field deployable and allow direct, real time quantification of both $N_2O$ concentration and isotope ratios. Combining LAS analyzers with automatic soil chambers enables measuring $N_2O$ concentrations and

isotopocule abundance ratios many times per chamber deployment. Measurement systems comprising an LAS analyzer and multiple soil chambers are an attractive option for near-continuous in-field monitoring of $N_2O$ flux and $N_2O$ isotopocules with high spatial resolution and much reduced labor compared with discrete sample collection (Chen et al., 2016; Kong et al., 2017; Petersen et al., 2020; Yamamoto et al., 2017; Yu et al., 2020).

Despite the advantages of LAS analyzers relative to discrete sampling and measurement with IRMS, the use of LAS analyzers with soil chambers for in-field research is still uncommon. This is because commercially available LAS instruments are relatively new and systems for their use in field experiments are still under development. Although several such systems have been reported in the literature, the uncertainty of the isotope ratios measured using LAS analyzers through direct soil chambers measurements has not been quantified, and it is unknown if, or under what conditions, these systems can achieve the level of accuracy that is required to differentiate among soil $N_2O$ production pathways (Decock & Six, 2013; Mohn et al., 2014).

The isotopic composition of soil emitted $N_2O$ collected using soil chambers can be found using a two-end-component mixing model such as the Keeling plot (Keeling, 1958; Chen et al., 2016) or Miller-Tans methods (Miller and Tans, 2003). The commonly used Keeling plot method involves fitting a linear equation relating the isotope ratio to the reciprocal $N_2O$ concentration to measurements made of the air the chamber headspace (Keeling, 1958). Assessing the suitability of LAS measurements for apportioning of soil $N_2O$ emissions to different source pathways requires quantifying the uncertainty of the $N_2O$ isotope ratios found using these methods. The uncertainty of the Keeling plot method has been analyzed

previously for isotopes of $CO_2$ measured by LAS and Eddy Covariance (EC) (Wehr & Saleska, 2017; Zobitz et al., 2006), but not for the extraction of isotopic signatures of $N_2O$ soil fluxes using LAS measurements and soil chambers. Ibraim, et al. (2019) compared the Keeling plot and Miller-Tans methods for extracting the isotopic composition of soil emitted $N_2O$ and found that the two methods agreed within the reported uncertainties and without systematic deviations. Unlike $CO_2$ LAS analyzers that are insensitive to analyte concentration, the analytical precision of $N_2O$ LAS analyzers varies with $N_2O$ concentration. When soil chambers are used to measure trace gas emissions, the concentration of $N_2O$ in the chamber headspace changes significantly over time according to soil flux rate and chamber dimensions (Parkin & Venterea, 2010).

Calculating the uncertainty of $N_2O$ isotope ratios using Keeling plots with an LAS analyzer and soil chambers requires first characterizing the precision of LAS $N_2O$ isotope ratio measurements in the range of $N_2O$ concentrations present in the soil chamber headspace during field experiments. Because of the variability of LAS measurement precision with $N_2O$ concentration and evolution of $N_2O$ concentration in the chamber headspace over time according to soil flux rate, the uncertainty of $N_2O$ isotope ratios obtained via Keeling plots must be calculated for multiple combinations of $N_2O$ soil fluxes and chamber closure times; each combination representing a particular set of $N_2O$ concentrations and isotope ratios that change over time in the soil chamber headspace during the field measurement.

Commercially available LAS analyzers make use of different types of lasers and detection schemes to measure analyte gases (Harris et al., 2020). The strength of optical analyzers is their ability to measure rapidly (i.e. $\approx 10^{-7}$ seconds per spectra measurement) and

without sample preparation (Griffith et al., 2012). Recent studies have shown, however, that the accuracy of LAS isotope ratio measurements is affected both by changes in the $N_2O$ concentration and variation in the composition and concentration of background gases in sampled air (Erler et al., 2015; Harris et al., 2020). These two sources of uncertainty in LAS isotope ratio measurements are of particular interest because they are not reported in the instrument performance specifications and are often overlooked in the literature describing the application of LAS to in-field measurement of soil trace gases.

Pronounced deviations in LAS isotope ratio measurements from IRMS-measurements have been observed when analyte concentrations vary (Braden-Behrens et al., 2017; Erler et al., 2015; Harris et al., 2020; Joseph et al., 2019). This loss of accuracy in LAS isotope ratio measurements with changes in concentration is referred to here as the "δ-concentration dependence effect". Obtaining accurate isotopocule measurements across a range of $N_2O$ concentrations, such as those measured during soil chamber deployments, requires accounting and correcting for δ-concentration dependence effects. Corrections for the δ-concentration dependence of LAS measurement of $N_2O$ isotope ratio have been developed previously (Erler et al., 2015; Harris et al., 2020; Wassenaar et al., 2018), but it remains uncertain whether these corrections provide $N_2O$ isotope ratio measurements that are sufficiently accurate to differentiate between $N_2O$ production pathways when the LAS is used for in-field experiments.

Interference in $N_2O$ isotopocule measurements resulting from the presence of interferent gases in the background of a gas sample is another important source of error in LAS isotope ratio measurements (Gralher et al., 2016; Nara et al., 2012; Rella et al., 2015). Gas species

often found in soil gas emissions (e.g., $H_2$, $N_2$, $O_2$, $H_2O$, $CH_4$, $CO_2$, NO), may exhibit absorbance at the light wavelength targeted for measurement of the $N_2O$ isotopocule molecules. Changes in the concentrations of these interferant gases resulting from changes in soil biogeochemistry complicates measures to correct for the interference effects and impacts the accuracy of LAS isotope ratio measurements. In laboratory studies, Erler et al. (2015) and Harris et al. (2020) investigated the effect of changes in the concentration of several interferant gases on $N_2O$ LAS isotope ratios measurements. The interferent gases examined in their experiments, however, did not represent the complexity of the soil trace gas samples (i.e., diversity of interferent gas species and their concentrations) expected to be observed during in-field experiments.

The goal of this study is to assess the suitability of LAS isotopic analyzer measurement of soil trace gases collected in a soil chamber headspace for distinguishing between $N_2O$ soil production pathways. To achieve this goal we: (1) characterize the precision of LAS measurements over the range of $N_2O$ concentrations representative of those observed in soil chamber experiments; (2) calculate the uncertainty of isotope ratios estimated using the Keeling plot method for different chamber deployment times and $N_2O$ flux rates; (3) account and correct for δ-concentration dependence effects; and, (4) estimate the isotope ratio of soil emitted $N_2O$ captured in the headspace of a soil chamber during soil flux simulations using the Keeling plot method and calibrated and δ-concentration dependence corrected LAS isotopic measurements, the Keeling plot results were compared with the isotope ratio measured with IRMS.

## *3. Methods and Materials*

### *3.1. LAS analyzer and soil chamber system*

All experiments were carried out using a Los Gatos Research (LGR) model 914-0027 LAS analyzer connected to automatic soil chambers through a continuous gas path. The LAS was operated in 'low continuous flow mode' in which a continuous stream of gas flows through the analyzer internal measuring cell at 100 sccm. Nitrous oxide measurements ([$N_2O$], SP, $\delta^{15}N^{Bulk}$, and $\delta^{18}O$) were recorded every 2 seconds, the highest rate possible with this analyzer. The measurement system, which is described in detail in Francis Clar & Anex (2020), has been used to monitor soil $N_2O$ emissions in field experiments since 2015. The LAS analyzer and the soil chambers are the components of the measurement system that directly influence the uncertainty of $N_2O$ isotope ratio measurements.

The Isotopic $N_2O$ analyzer uses Off-Axis Integrated Cavity Output Spectroscopy (OA-ICOS) technology (Baer et al., 2002), a laser detection configuration commonly used in commercially available LAS analyzers (Harris et al., 2020). All experiments described were performed in a temperature-controlled laboratory and the enhanced version of the instrument used in this study controls the temperature of the measurement cell to provide ultra-stable, minimal-drift measurements, so measurement variability due to temperature change is not a consideration. The device used in this study was built in 2014. In April 2016, the instrument's hard drive and internal computer stack were updated by the manufacturer. During all experiments, the instrument was running the most recently available software (Manual document No. 914-0027-0000-ULR5 revision AA (4/12/2017)).

The soil chambers were designed, built, and operated following the USDA-ARS GRACEnet protocols for trace gas flux measurements by soil chamber methodology (Parkin & Venterea, 2010). The soil chambers had a planform area of 0.09 $m^2$ and a volume of 18 L. The soil chambers were equipped with a vent to minimize diffusive loss of soil trace gases out of the chamber while maintaining atmospheric chamber pressure to avoid altering the rate of diffusion of trace gases from the soil. The soil chambers were operated with a maximum closure time of 90 minutes. Based on 3 years of $N_2O$ flux data from field experiments in highly fertilized corn (Francis Clar & Anex, 2020), a flux of 200 g N-$N_2O$ $ha^{-1}day^{-1}$ was taken to be representative of a very high $N_2O$ soil flux that could be expected to be observed in such experiments. Based on this flux rate, the soil chamber dimensions, and maximum deployment time, the $N_2O$ concentration expected in the chamber headspace were calculated to range from that of ambient air (approximately 0.3 ppm) to 10 ppm.

### *3.2. Calibration of the LAS*

The manufacturer recommends calibrating the LAS analyzer annually. The LAS instrument was calibrated according to the manufacturer's recommended procedure the day before the first experiment described here. All measurements reported in this manuscript were made within 6 weeks of this calibration. The calibration gas was created by diluting an $N_2O$ reference gas (Certified Standard 30 ppm $N_2O$ Airgas, Chicago, IL) with ultrapure synthetic air (Cryogenic UltraPure Air, Scott-Marrin, Inc, Riverside, CA, USA). According to gas supplier-provided specifications, the gases were composed of high purity (99.99%) synthetic air (21% $O_2$ and 79% $N_2$) and neither of the constituent gases contained trace gases that are known to interfere with LAS measurements. Dilution was done in 10 L Tedlar gas

sampling bags (Part #22053, Restek Inc.). During calibration of the LAS analyzer a Tedlar gas sampling bag containing the calibration gas was connected to the analyzer inlet and the internal calibration routine as initialized.

The concentration and isotopocule composition of the calibration gas was determined by Isotopic Ratio Mass Spectroscopy (IRMS) analysis at the Stable Isotope Facility (SIF), University of California-Davis. The IRMS measurements are referenced to international standards. For nitrogen, the isotopic ratio $^{15}N/^{14}N$, used to calculate SP and $\delta^{15}N^{Bulk}$, was referenced to the $^{15}N/^{14}N$ isotope ratio of $N_2$ in tropospheric air ($N_2$-Air), the international standard reference material. For oxygen, the $^{18}O/^{16}O$ isotope ratio used to calculate $\delta^{18}O$, was referenced to the $^{18}O/^{16}O$ isotope ratio of $O_2$ in Vienna Standard Mean Ocean Water (VSMOW) (Mohn et al., 2014). The calibration gas was sampled by extracting 8 samples from the Tedlar sampling bag using a gastight syringe (Hamilton Company, Reno, NV USA). Samples were placed in 12 ml soda glass vials (Labco-Exetainer ® part#739W, Labco Limited, Lampeter, Wales, UK) and shipped to the SIF. The calibration gas had an $N_2O$ concentration of 2024.93 ppb and isotope ratios ($\mu \pm \sigma$, n = 8) of 25.79 ± 0.92, 1.06 ± 0.08, and 45.61 ± 0.26 ‰ for SP, $\delta^{15}N^{Bulk}$, and $\delta^{18}O$, respectively.

### *3.3. Uncertainty of isotope ratio estimates*

In field experiments in which soil trace gases are collected using soil chambers, isotope ratios are estimated using the Keeling plot method (Chen et al., 2016). If LAS isotope ratio measurements have been calibrated and corrected for $N_2O$ concentration dependency ("δ-concentration dependence"), then the uncertainty of isotope ratios estimated using Keeling plots is the result of the of the LAS instrument variability propagated through the Keeling

plot method. The isotopic $N_2O$ measurements (SP, $\delta^{15}N^{Bulk}$, or $\delta^{18}O$) are not strictly "isotope ratios" but are often referred to as such and we will do the same. The equations developed below apply equally and individually to each of these three $N_2O$ isotope ratios (SP, $\delta^{15}N^{Bulk}$, or $\delta^{18}O$), which for convenience are generically referred to in these equations as "δ".

The basis of the Keeling plot method is the conservation of mass in a binary mixing model as shown in equation 1, in which *n* represents the number of moles of $N_2O$ and subscripts *h*, *s* and *a*, are the chamber headspace, soil, and ambient air respectively. Thus, in equation 1, $n_{h,t}$ is the number of moles of $N_2O$ in the chamber headspace at *t*, the time since chamber closure. $n_{h,t}$ is the sum of the moles of $N_2O$ from the ambient air contained in the chamber volume at closure, $n_a$, and the moles of $N_2O$ that have been added from the soil since chamber closure, $n_{s,t}$ .

$$n_{h,t} = n_a + n_{s,t} \quad (1)$$

Similarly, for a particular isotope ratio (e.g., SP, $\delta^{15}N^{Bulk}$, or $\delta^{18}O$) of the trace gas molecules in the chamber headspace, $\delta_{h,t}$ , is the weighted sum of the isotope ratio of the trace gas molecules contributed by the ambient air $\delta_a$, and that of the trace gas molecules added from the soil during the chamber closure, $\delta_{s,t}$, in which the weightings are the number of moles of $N_2O$ from each source (Well et al., 2006):

$$\delta_{h,t} \cdot n_{h,t} = \delta_a \cdot n_a + \delta_s \cdot n_{s,t} \quad (2)$$

Substituting (2) into (1) and simplifying yields:

$$\delta_{h,t} = (\delta_a \cdot n_a - \delta_s \cdot n_a)\, {}^{1}/_{n_{h,t}} + \delta_S \quad (3)$$

Converting numbers of moles to concentrations gives equation 4, in which $\delta_{h,t}$ and $c_{h,t}$, are respectively the isotope ratio and $N_2O$ concentration of the gas in the chamber headspace at time *t*.

$$\delta_{h,t} = (\delta_a \cdot c_a - \delta_s \cdot c_a) \, {}^{1}\!/_{c_{h,t}} + \delta_s \quad (4)$$

Plotting $\delta_{h,t}$ versus $1/c_{h,t}$ at each measurement time during the chamber deployment gives a Keeling plot of the form shown in Figure 1. Assuming the rate of $N_2O$ flux from the soil and its site-specific isotope ratios remain constant over the chamber deployment, the slope and intercept of equation 4 are found by computing the least squares regression line (Wehr & Saleska, 2017; Zobitz et al., 2006). The intercept of this line is the isotope ratio of the $N_2O$ emitted from the soil, $\delta_s$ (Pataki et al., 2003).

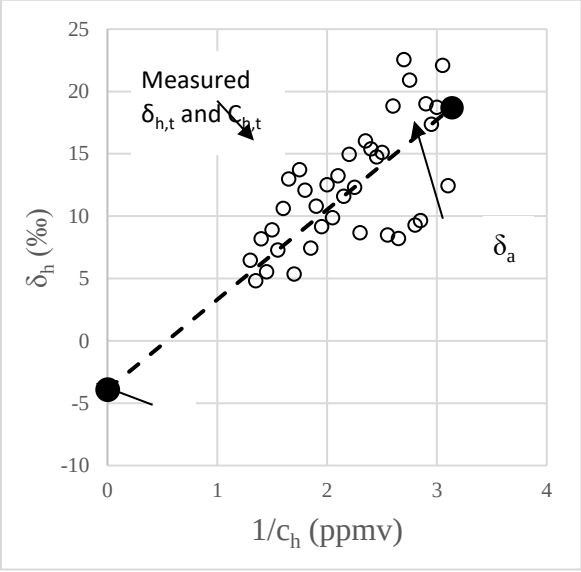


**Figure 1.** Typical Keeling plot used to estimate isotope ratios from measurements of isotope ratios and $[N_2O]$ in the soil chamber headspace. If the chamber dimension, deployment time and flux rate remain constant, error in the estimation of isotope ratio results from random variation in the LAS measurements.

***Variability of LAS measurements.***

It has been previously observed that the variability of LAS [$N_2O$] measurements is smallest near ambient $N_2O$ concentration and increases linearly with increasing [$N_2O$] (i.e., $\sigma_{[N_2O]} \approx [N_2O] / 15{,}000$) (Harris et al., 2020; Lebegue et al., 2016). Conversely, the variability of LAS isotope ratio measurements (SP, $\delta^{15}N^{Bulk}$, and $\delta^{18}O$) is largest near ambient $N_2O$ concentration and decreases more than linearly with increasing [$N_2O$]. The variability of the LAS measurements was characterized as the standard deviation of repeated measurements made at $N_2O$ concentrations from 0.3 to 10 ppm. Relationships describing the standard deviation of the LAS measurements as functions of [$N_2O$] were developed from [$N_2O$], SP, $\delta^{15}N^{Bulk}$, and $\delta^{18}O$ data that were collected simultaneously. Due to the rapid decrease in standard deviation of the isotope ratios with increasing [$N_2O$], stratified sampling was employed. The standard deviation of each of the measured isotope ratios was computed at 10 evenly spaced $N_2O$ concentrations across the range from 0.3 to 3 ppm, at 4 concentrations between 3.6 to 6 ppm, and at 3 concentrations between 6.6 to 10 ppm. In total, the standard deviation of each of the LAS isotope ratios was measured at 17 different $N_2O$ concentrations across the range from 0.3 to 10 ppm. At each [$N_2O$] the standard deviation was computed from 90 measurements of each [$N_2O$], SP, $\delta^{15}N^{Bulk}$, and $\delta^{18}O$.

The 17 [$N_2O$] gas samples were prepared by diluting an $N_2O$ reference gas in ultrapure synthetic air in a 10 L Tedlar gas sampling bags, as described in section 2.2. A gas sampling bag was then connected for 15 minutes to the LAS analyzer running in continuous mode. The first 12 minutes of each measurement run was used to condition the LAS measuring chamber (Wassenaar et al., 2018). Measurements made during the subsequent 3 minutes of each run

were used to calculate the measurement variability of the LAS instrument. Three minutes is the measurement duration the manufacturer recommends for maximum measurement stability. Between each 15-minute measurement run the analyzer measuring cell was flushed with ambient air for 15 minutes.

LAS measurements (i.e., [$N_2O$], SP, $\delta^{15}N^{Bulk}$, and $\delta^{18}O$) at a particular [$N_2O$] were assumed to be normally distributed. Normality of the measured data at each [$N_2O$] was verified using the Kolmogorov-Smirnoff test at the 95% confidence level.

Relationships describing the standard deviation of the LAS measurements as functions of [$N_2O$] were found for each of the four LAS measurements [$N_2O$], SP, $\delta^{15}N^{Bulk}$, and $\delta^{18}O$ using the MATLAB Curve Fitting Toolbox (MATLAB version R2020a). The variation of the isotope ratios (i.e., SP, $\delta^{15}N^{Bulk}$, and $\delta^{18}O$) with [$N_2O$] was best described by an exponential function of the form of $\sigma_\delta = e^{a+b\cdot([N_2O])}$, in which $a$ and $b$ are the coefficients found to minimize the mean square error. The variation of [$N_2O$] was described by a linear function of the form $\sigma_{N_2O} = c + d \cdot ([N_2O])$. The goodness of fit between the measured data and each of the four functions ([$N_2O$], SP, $\delta^{15}N^{Bulk}$, and $\delta^{18}O$) was evaluated using the coefficient of determination, $R^2$.

***Isotopocule uncertainty calculations***

This study used Monte Carlo simulation to examine the influence of the accuracy of the LAS measurements ([$N_2O$] and isotope ratio) on the uncertainty of isotope ratios estimated using the Keeling plot method. As described previously, the variability of the LAS measurements is a function of [$N_2O$] in the chamber headspace which increases over the

course of a chamber deployment. Thus, the uncertainty of isotope ratios estimated from the data collected during a soil flux measurement depends on the LAS measurement accuracy, the chamber dimensions, the flux intensity, and the chamber deployment time. It is assumed in this analysis that LAS isotope ratio measurements have been calibrated and corrected for δ-concentration dependence effects, so the primary source of error in estimates of the isotope ratios made by the Keeling plot method is the LAS measurement variability that was characterized as described in the previous section.

The Monte Carlo investigation of the influence of soil $N_2O$ flux rate and chamber closure time on the uncertainty of isotope ratios estimated using the Keeling plot method comprised a series of soil flux simulations each representing a particular combination of soil flux isotope ratio, soil flux rate, and chamber closure time. Each soil flux simulation represents the [$N_2O$] and isotope ratios in the headspace at two second intervals from chamber closure until the end of the chamber closure period, and the simulated measurements are then used to estimate the $N_2O$ isotope ratio of the soil $N_2O$ flux via the Keeling plot method (Equation 4).

The number of moles of $N_2O$ entering the chamber headspace during each two-second simulation interval is calculated directly from the soil flux rate (g N-$N_2O$ $ha^{-1}$ $day^{-1}$), chamber planform area, and $N_2O$ molar mass. The number of moles of $N_2O$ in the chamber headspace at a given simulation interval is then calculated as the sum of the moles of $N_2O$ contributed by ambient air in the chamber at closure and the moles of $N_2O$ contributed from the soil (Equation 1), where the soil flux contribution is the product of soil flux over one time and the number of time intervals since chamber closure.

The deterministic trajectories of the number of moles of $N_2O$ and isotope ratios in the chamber headspace can be calculated at each flux simulation time step using equation 2 and the assumed isotope ratios of the ambient air and soil flux. Soil flux simulations were carried out using two soil flux $N_2O$ isotope ratios ($\delta_s$ in equation 2) representing the commonly accepted isotope ratios of soil $N_2O$ produced entirely by nitrification or denitrification. The $N_2O$ isotope ratios for denitrification were taken to be -3.9‰, 10.7‰ and 21‰ for SP, $\delta^{15}N^{Bulk}$, and $\delta^{18}O$, respectively; the values for nitrification were 34.8‰, -65‰, and 43.6‰ for SP, $\delta^{15}N^{Bulk}$, and $\delta^{18}O$, respectively (Lewicka-Szczebak et al., 2017; Wolf et al., 2015). The accepted isotope ratios of $N_2O$ in ambient air $\delta_a$ are 18.7‰, 7‰ and 47.7‰ for SP, $\delta^{15}N^{bulk}$, and $\delta^{18}O$, respectively (Yoshida & Toyoda, 2000).

The deterministic trajectories of the number of moles of $N_2O$ and isotope ratios in the chamber headspace define the expected values of the LAS measurements at each time step. At each time step the simulated LAS measurements ($[N_2O]$ and the isotope ratios) were random variates drawn from Gaussian distributions. For $[N_2O]$ the Gaussian distributions had parameters $N(\mu_{N_2O}, \sigma_{N_2O})$, where, $\mu_{N_2O}$ was the expected $[N_2O]$ and $\sigma_{N_2O} = c + d \cdot ([N_2O])$. Similarly, for each isotope ratio the Gaussian distributions had parameters $(\mu_\delta, \sigma_\delta)$, where, $\mu_\delta$ was the expected isotope ratio and $\sigma_\delta = e^{a+b([N_2O])}$, where there are unique values of $a$ and $b$ for each isotope ratio ($\delta$) representing SP, $\delta^{15}N^{Bulk}$, or $\delta^{18}O$. At the completion of each soil flux simulation, $N_2O$ isotope ratios were estimated using the Keeling plot method. Each soil flux simulation represents one iteration of the Monte Carlo simulation and resulted in one estimate of each of the three soil isotope ratios. The estimation error of each of the isotope ratios was calculated as the difference between the $\delta_s$ estimated by the

Keeling plot method and the known isotope ratio of the $N_2O$ source (nitrification or denitrification).

Each Monte Carlo experiment evaluated 10,000 soil simulations describing one combination of flux rate, deployment time, and soil flux $N_2O$ isotope ratio. The error in the 'measured' value of each isotope ratio as estimated by the Keeling plot method was calculated as the difference between the estimated value and the input (deterministic) value of the $N_2O$ source, $\delta_s$. From the resulting probability distributions of the output isotope ratio measurement error, uncertainties were retrieved as the threshold values associated with the probabilities of 0.05 and 0.95 and reported as a 90% confidence interval.

Monte Carlo simulations were carried out for 16 combinations of flux rate, deployment time, and $N_2O$ isotope ratios representative soil $N_2O$ production pathways of nitrification and denitrification. The four flux rates (4, 18, 66, and 200 g $N\text{-}N_2O$ $ha^{-1}$ $day^{-1}$) represented the median, the average, the $75^{th}$, and the $90^{th}$ percentile of flux rates measured during a 3-year experiment (n > 20,000 fluxes) in a highly fertilized corn system in the Midwest of US (Francis Clar & Anex, 2020). Deployment times were 30, 60 and 90 minutes, chosen based on $N_2O$ chamber methodology guideline recommendations (Venterea et al., 2020). These combinations of flux rate and chamber closure time are typical of those used in practice. Figure 2 enumerates the combinations of Monte Carlo simulation parameters.

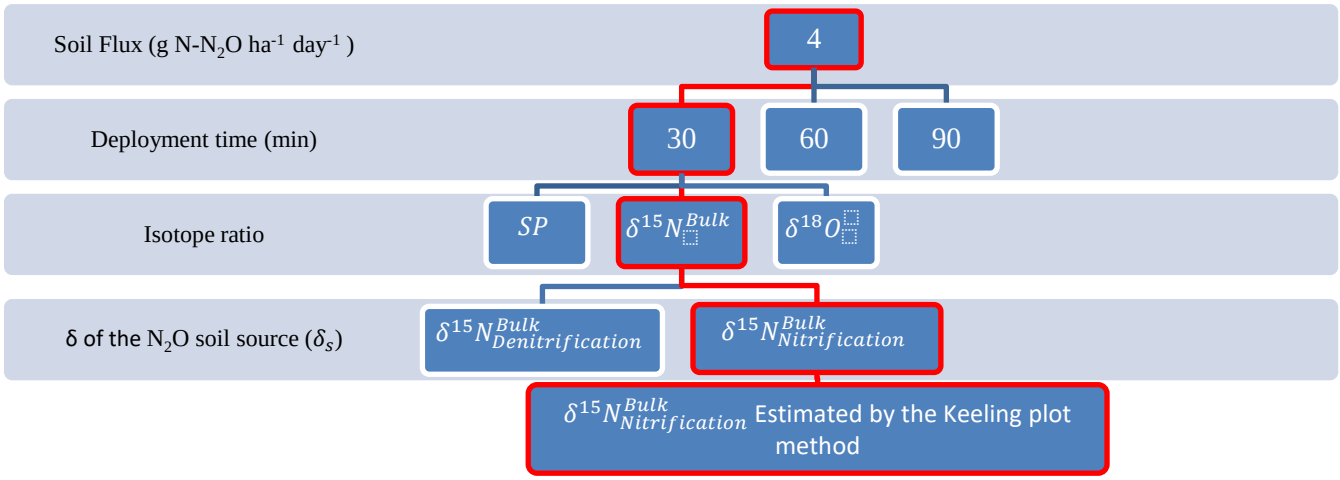


**Figure 2.** Decision tree showing the decision path in red for one of the 64 different combinations in which the isotopocule composition of soil emitted $N_2O$ was computed. For each of the 64 combinations, 10,000 values of $N_2O$ soil emitted isotope ratio were computed.

### *3.4. Soil Flux simulations*

To verify the results of the Monte Carlo investigation of measurement under field conditions, a series of experimental soil flux simulations was undertaken using soil chambers into which were introduced controlled fluxes of trace gases generated through soil incubation experiments. The trace gases generated during the soil incubations are referred to here as the "source gases". The isotope ratios of the source gases were estimated from LAS measurements using the Keeling plot method and compared with the isotope ratios of the source gases obtained by IRMS.

#### *Production of soil emitted $N_2O$ – Source gas*

The source gases were generated through a series of soil incubations designed to simulate soil conditions typical of a field used for production agriculture. The soil incubations were carried out under conditions favoring one of the two main $N_2O$ production pathways that are distinguishable through isotope ratio analysis, nitrification (N) and denitrification (D) (Decock & Six, 2013). Soil incubations were carried out in duplicate, resulting in a total of 4

source gases, two produced under nitrification-favoring conditions (N1 and N2) and two under denitrification-favoring conditions (D1 and D2).

To produce the most representative soil trace gases, soil samples were incubated following the methods described by Chen, et al. (2016) and Well, et al. (2006). The soil was collected from the top layer (0.1m) of an agricultural field used for corn production at the University of Wisconsin Agricultural Research Station - Arlington (ARS-A) (43°17'41.2"N 89°21'28.1"W), in Columbia County (WI). The field had previously been cropped in a maize-soybean rotation with pre-planting shallow tillage (i.e., 0.1 m depth) and had a history of no manure application during the previous three years. The soil was a Plano silt loam soil and Ringwood slit loam complex (fine-silty, mixed, superactive, mesic Typic Argiudoll). The collected soil was screened (4 mm) to remove large stones and other debris and air dried to a Water Filled Pore Space (WFPS) below 5%. A sample of this soil was analyzed at the University of Wisconsin Soil and Forage Lab (Marshfield, WI) for Total Nitrogen, $NO_3$-N, $NH_4$-N, Total Organic Carbon and a wide range of basic elements (Appendix 1, Table A5).

Each soil incubation used 2 kg of dry soil that were thoroughly mixed with water and amendments. The amendments for soil incubations favoring the denitrification pathway were 0.72 mg $KNO_3$ and 2 mg of glucose per g of dry soil; the volume of water was calculated to reach a soil WFPS of 90%. The amendments for soil incubations favoring the denitrification pathway were 0.94 mg $NH_4$ as $(NH_4)_2SO_4$ and 2 mg of glucose per g of dry soil, and the volume of water was calculated to reach a soil WFPS of 50%. After mixing the soil with the water and amendments it was packed to a bulk density of 1400 kg $m^{-3}$ (1.4 g $cm^{-3}$) in 3.8 L airtight glass containers. The lid of the container was equipped with two quarter-turn valves

(Nylon Bulkhead female Luer adapter threated into one-way stopcock Luer lock valves, Masterflex fittings, Masterflex Gelsenkirchen, Germany). Soil samples were incubated for 5 days in a dark room at 20ºC.

After 5 days, the gas in the headspace of each container was transferred to a 10 L Tedlar sampling bag (Part # 22053, Restek Inc.) The source gas was transferred from the glass container to the gas bag by connecting the bag to one of the glass container's valves and by pumping approximately 10 L of ultrapure synthetic air (Cryogenic UltraPure Air from Scott-Marrin, Inc, Riverside, CA) into the glass container through the other valve. The connections between the glass container, the gas cylinder and the gas sampling bag were made with 1-meter-long polytetrafluoroethylene (PTFE) tubes (5.3 mm outer diameter). Three gas samples were retrieved from each sampling gas bag; two samples were used to analyze $N_2O$ concentration and its isotope ratios by IRMS, the third gas sample was used to measure $CO_2$ and $CH_4$ concentrations using a gas chromatograph (7890A GC System, Agilent Technologies, Santa Clara, CA, USA).

Soil temperature and Volumetric Water Content (VWC) were measured from each soil container at the beginning and the end of the soil incubations during at least 5 minutes using a soil probe (5TM, Decagon Inc., Pullman, WA). The soil prove was installed in the container with the soil, at the beginning of the soil incubation and retrieved after collecting the gas from the container's headspace. The data was collected with an em50 data logger (Decagon Inc.). The Water Filled Pore Space was calculated from the measured VWC and the value of soil density at which the soil was packed in the containers (Bilskie, 2001).

***Soil Chamber flux simulations***

The skirt of the soil chamber, which during field sampling is inserted into the soil, was sealed onto a 0.1 m thick sheet of High-Density Polyethylene (HDPE) using commercial, food grade silicone adhesive. The soil chamber ports were connected to the inlet and outlet of the LAS analyzer using Swagelok stainless steel fittings (Swagelok, Solon OH) and 1-meter-long polytetrafluoroethylene (PTFE) tubes (6.35 mm outer diameter). Eight soil fluxes were simulated by pumping source gas at a known rate from a 10L Tedlar gas sampling bag into the headspace of the soil chamber using a peristaltic pump (MasterFlex L/S Economy Peristaltic Pump 07554-90 w, Masterflex Gelsenkirchen, Germany).

The gas sampling bag was connected to the soil chamber using a 1-meter-long PharMed® BPT (Saint-Gobain Performance Plastics Corporation, Courbevoie, France) tube (Interior diameter 3.1 mm). One end of the PharMed® BPT tubing was connected to the sampling port on the Tedlar sampling gas bag, the other to a PTFE half turn valve mounted on the chamber lid. The midsection of the PharMed® BPT tubing was installed on the peristaltic pump.

The rotational speed of the peristaltic pump was adjusted to simulate fluxes at 66 and 200 g $N\text{-}N_2O$ $ha^{-1}$ $day^{-1}$. As explained in the '*Uncertainty calculations*' section, these flux rates represented approximately the $75^{th}$ and the $90^{th}$ percentile of flux rates measured during 3-years of field experiments (Francis Clar & Anex, 2020). In the description and discussion of the soil flux simulation experiments, the 66 and 200 g $N\text{-}N_2O$ $ha^{-1}$ $day^{-1}$ flux rates are referred to as "low" and "high" flux, respectively. Pump flow rates were calculated for each flux simulation according to the $N_2O$ concentration of the source gas using the equation suggested

by Parkin & Venterea (2010) for estimating $N_2O$ soil fluxes using soil chambers. For all experimental flux simulations the targeted deployment time was 90 minutes.

Soil $N_2O$ gas flux was estimated from the LAS [$N_2O$] measurements as the change in [$N_2O$] in the chamber headspace over time (Parkin & Venterea, 2010). The isotopocule composition of the source gas was calculated using the LAS [$N_2O$] and isotope ratio measurements using the Keeling plot method. Before the Keeling plot analysis, the isotope ratios measured by the LAS were corrected for δ-concentration dependency effects using the correction factors that were found as described in following section.

***Isotope ratio δ-concentration dependence correction***

The δ-concentration dependency correction is calculated is the difference (Δδ) between the isotope ratio of the standard gas as obtained by IRMS ($\delta_{IRMS}$) and the LAS-measured isotope ratio ($\delta_{LAS}$), so $\Delta\delta = (\delta_{IRMS} - \delta_{LAS})$. This correction factor was estimated for each isotope ratio over a range of [$N_2O$] from 0.3 to 10 ppm. The isotope ratios of the standard gas were measured as explained in section 2.2. Measurement of LAS isotope ratios was performed as described in section 2.3. The stability of the δ-concentration dependency over time was analyzed by taking four sets of LAS measurements at one-week intervals over one month. The same reference gases were used for each set of measurements and all measurements were made in a temperature-controlled laboratory.

For each isotope ratio (SP, $\delta^{15}N^{Bulk}$, and $\delta^{18}O$), δ-concentration dependency correction functions were calculated by fitting first- to sixth-order polynomials relating [$N_2O$] and Δδ, and a first-order polynomial relating 1/[$N_2O$] and Δδ, using the MATLAB Curve Fitting Toolbox (MATLAB version R2020a). Polynomials were fit to the data collected on

individual days as well as to the entire data set (data collected on 4 days at one-week interval over one month). The δ-concentration dependency correction functions derived from the full data set thus represent the best fit across the temporal variability of the available LAS isotope ratio measurements. For each isotope ratio, the polynomial function that best described the δ-concentration dependency correction function was chosen using the Akaike Information Criterion (Glatting et al., 2007).

## *4. Results*

### *4.1. Uncertainty of the isotope ratios*

***Variability of the LAS measurements.***

At ambient $N_2O$ concentration (~ 0.3 ppm) the standard deviation of LAS measurements of SP, $\delta^{15}N^{Bulk}$ and $\delta^{18}O$ were found to be 26‰, 21‰, and 61‰ respectively. The standard deviation decreased rapidly with increasing [$N_2O$], falling to 4‰ for SP and $\delta^{15}N^{bulk}$, and 7‰ for $\delta^{18}O$ when [$N_2O$] was 3 ppm (Figure 3). The highest LAS isotopocule measurement precision was observed in the range of [$N_2O$] between 3 ppm and 10 ppm. In this range the standard deviation decreased only slightly as [$N_2O$] increased. At 10 ppm the standard deviation for all 3 isotopocules was approximately 3‰ (Figure 3). The change in variability of the LAS isotope ratio measurements with [$N_2O$] was best described by exponential functions of the form $\sigma_\delta = e^{a+b\cdot([N_2O])}$, where δ refers to either SP, $\delta^{15}N^{Bulk}$, or $\delta^{18}O$. The coefficients *a* and *b,* and the corresponding coefficients of determination ($R^2$) are presented in table A1 of the appendix for each of the isotope ratio functions.

The standard deviation of the LAS [$N_2O$] measurements increased linearly with [$N_2O$] at constant rate of approximately 1/1200 (ppm/ppm). Measurements of [$N_2O$] were collected at 2 second intervals for three minutes (90 measurements) at each concentration. The standard deviations of the LAS [$N_2O$] measurements at the end-points, 0.3 and 10 ppm, were 2.59 x $10^{-4}$ and 8.54 x $10^{-3}$ ppm, respectively. The best fit linear function was $\sigma_{N_2O} = 4.145 \times 10^{-3} + 8.502 \times 10^{-4} \cdot [N_2O]$, with $R^2 = 0.99$.

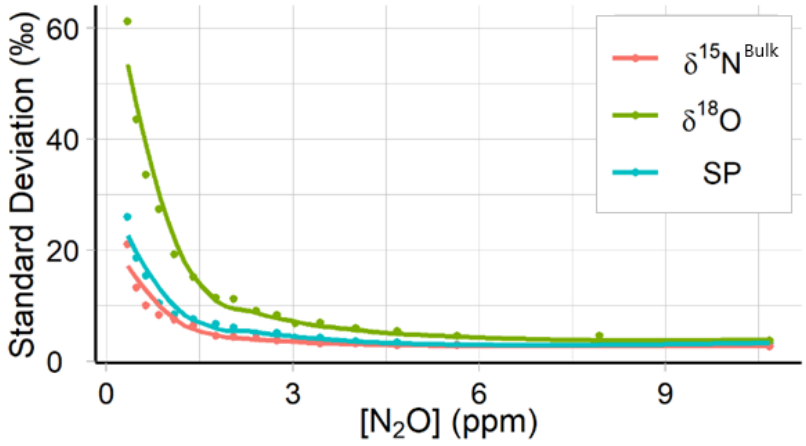


**Figure 3.** Standard deviation of SP, $\delta^{15}N^{Bulk}$, and $\delta^{18}O$ measured at [$N_2O$] from 0.3 ppm to 10 ppm by the LAS analyzer. At each [$N_2O$] the standard deviation was calculated from 90 measurements. The standard deviation of the LAS isotopocule measurements decreased rapidly between 0.3 ppm to 3 ppm, and decreased more slowly at higher [$N_2O$].

***Isotopocule uncertainty results***

The Monte Carlo investigation of the influence of soil $N_2O$ flux rate and chamber closure time on the uncertainty of isotope ratio estimates produced probability distributions of the isotope ratio measurement error for 16 combinations of flux rate, deployment time, and soil $N_2O$ production pathway.

The resulting probability distributions were symmetrical about zero uncertainty. The uncertainty of each estimated isotope ratio (i.e., SP, $\delta^{15}N^{Bulk}$, and $\delta^{18}O$) is reported as the absolute value of the 90% confidence interval (i.e., absolute error value at probabilities 0.05 and 0.95) of these probability distributions (Table 1). There were no differences between the isotope ratio uncertainty distributions for the two soil $N_2O$ production pathways (e.g., nitrification and denitrification).

The uncertainty of $N_2O$ isotope ratio estimates decreased with increasing flux rates and deployment times (Table 1). Uncertainties smaller than 1‰ were achieved for SP and $\delta^{15}N^{Bulk}$ isotopocule estimates at the highest simulated soil flux rate of 200 g N-$N_2O$ $ha^{-1}day^{-1}$ and with deployment times equal to or greater than 60 minutes. The percentage reduction in uncertainty between a flux rate of 200 g N-$N_2O$ $ha^{-1}day^{-1}$ and a flux rate of 4 g N-$N_2O$ $ha^{-1}day^{-1}$ was nearly the same for all the isotope ratios, as well as at each deployment time (i.e., 85% – 95%). For all isotope ratios and at all flux rates, the percentage reduction in uncertainty between a 60-minute deployment and a 30-minute deployment was larger than the change between a 90-minute deployment and a 60-minute deployment. For SP and $\delta^{15}N^{Bulk}$ the difference was an approximately 20% larger reduction between 30-minute and 60-minute deployments across all flux rates.

The soil flux rates and deployment times at which the uncertainty of SP and $\delta^{15}N^{Bulk}$ isotopocule estimates were smallest were also those with the highest $N_2O$ concentration in the soil chamber at the end of the deployment. Concentrations of $N_2O$ above 3 ppm, and particularly between 6 ppm and 10 ppm, are the conditions under which LAS isotope ratio measurements are most precise. Conversely, the larger isotope ratio uncertainties were

mostly associated with $N_2O$ concentration at the end of the chamber deployments that were well below 3 ppm, except for the combination of a 200 g N-$N_2O$ $ha^{-1}day^{-1}$ soil flux rate and a 30-minute deployment time, for which the terminal [$N_2O$] was 3.34 ppm (Table 1).

**Table 1.** Uncertainty, as the 90% confident interval for SP, $\delta^{15}N^{Bulk}$, and $\delta^{18}O$ estimated by Keeling plots at deployment times of 30, 60, and 90 minutes and flux rates of 4,18, 60, and 200 g N-$N_2O$ $ha^{-1}day^{-1}$. $N_2O$ tf indicates $N_2O$ concentration in the chamber headspace at the end of the deployment time. Isotopocule estimates at a precision of 1‰ or better were only calculated for SP and $\delta^{15}N^{Bulk}$ (bold values) during high flux rates and long deployment times.

| **Deployment time (No. points fit)** | **Flux (g N-$N_2O$ $ha^{-1}day^{-1}$)** | **Uncertainty as 90% Confidence Interval around the true value (± ‰)** | | | **[$N_2O$]$t_f$ (ppm)** |
|---|---|---|---|---|---|
| | | **SP** | **$\delta^{15}N^{Bulk}$** | **$\delta^{18}O$** | |
| 30 min (900) | 4 | 42.80 | 24.03 | 52.44 | 0.38 |
| | 18 | 11.52 | 6.29 | 14.31 | 0.59 |
| | 66 | 4.18 | 2.28 | 5.67 | 1.32 |
| | 200 | 1.73 | 1.16 | 3.75 | 3.34 |
| 60 min (1800) | 4 | 16.15 | 9.73 | 22.89 | 0.44 |
| | 18 | 4.78 | 2.86 | 6.46 | 0.86 |
| | 66 | 1.82 | 1.15 | 3.00 | 2.32 |
| | 200 | 0.82 | 0.84 | 2.77 | 6.37 |
| 90 min (2700) | 4 | 9.33 | 5.82 | 13.75 | 0.50 |
| | 18 | 2.86 | 1.80 | 4.11 | 1.14 |
| | 66 | 1.14 | 0.83 | 2.86 | 3.32 |
| | 200 | 0.55 | 0.76 | 2.08 | 9.39 |

### *4.2. Soil Flux simulations*

The soil incubations favoring nitrification (N1 and N2) and denitrification (D1 and D2) produced $N_2O$ with significantly different isotope ratios (Table 2). The average soil WFPS at the beginning and at the end of the soil incubations was within 15% of the targeted values (i.e., 50% and 90% for incubations favoring nitrification and denitrification, respectively). The concentrations of $CO_2$ and $CH_4$ in the gas emissions from N1 and N2 were significantly different from the concentrations of $CO_2$ and $CH_4$ in the ambient air (Table 2). The $CO_2$ and $CH_4$ concentrations in the gas emissions from D1

and D2 were not measured. The concentration $N_2O$ in the gas produced from soil incubations N1 and N2 was 62.5 and 33.34 ppm, respectively, while from D1 and D2 it was approximately 200 ppm (Table 2).

**Table 2.** $N_2O$ concentration and isotope ratios (SP, $\delta^{15}N^{Bulk}$, and $\delta^{18}O$) measured by IRMS of the gas produced during soil incubations and used to simulate soil flux in the soil chamber headspace. Concentration of $CO_2$ and $CH_4$ was measured by electron capture detector - Gas Chromatography. Average and standard deviation of soil WFPS and soil temperature.

| | Ambient Air* | N1 | N2 | D1 | D2 |
|---|---|---|---|---|---|
| **SP (‰)** | 21.61 ± 0.63 | 0.65 | 0.95 | 10.58 | 10.39 |
| **$\delta^{15}N^{Bulk}$ (‰)** | 10.80 ± 0.32 | -40.72 | -36.76 | 7.66 | 9.95 |
| **$\delta^{18}O$ (‰)** | 42.86 ± 0.19 | 27.04 | 29.40 | 46.69 | 50.37 |
| **$N_2O$ [ppm]** | 0.46 ± 0.1 | 62.50 | 33.34 | 398.64 | 217.80** |
| **$CO_2$ [ppm]** | 583.54 ± 1.03 | 11,964.58 | 10,798.92 | Not meas. | Not meas. |
| **$CH_4$ [ppm]** | 2.03 ± 0.04 | 1.32 | 1.13 | Not meas. | Not meas. |
| **WFPS (%)†** | - | 37±3 | 42±3 | 89±3 | 105±2 |
| **Temp (°C)** | - | 20±2 | 20±2 | 20±2 | 20±2 |

*Averaged from 4 samples taken the day of the soil flux simulations.

**Estimated value. Sample 2D was diluted with $N_2O$ free gas before analysis, its $N_2O$ concentration was estimated from the measured value times the dilution factor.

† Although WFPS cannot exceed 100%, measurement error can lead to calculated WFPS > 100%

### *Soil Chamber flux simulations*

For each source gas, we intended to set the rotational speed of the peristaltic pump to simulate one low soil flux at 66 g N-$N_2O$ $ha^{-1}$ $day^{-1}$ and one high flux at 200 g N-$N_2O$ $ha^{-1}$ $day^{-1}$. In practice, adjusting the rotational speed of the peristaltic pump to obtain these specific flux rates was not possible. The resulting flux simulations included one high (H) and one low (L) flux for each source gas, but the specific flux rates varied. The $N_2O$ flux rates achieved in the eight soil flux simulations ranged from 21.84 to 558.63 g N-$N_2O$ $ha^{-1}day^{-1}$ (Table 3). Consequently, chamber deployment times were constrained by the limited amount of source gas available and ranged from 44 to 83 minutes (Table 3). The variation in flux rates and chamber closure times did not impact the quality of the experimental results or limit the conclusions drawn from these results.

**Table 3.** $N_2O$ flux rate, chamber deployment time, $N_2O$ concentration at the end of the chamber deployment ($t_f$) for the 8 soil flux simulations.

| | $N_2O$ flux (g N-$N_2O$ $ha^{-1}day^{-1}$) | Deployment time (min) | $N_2O$ $t_f$ [ppm] |
|---|---|---|---|
| **N1-L** | 77.78 | 78 | 1.75 |
| **N2-L** | 21.84 | 83 | 0.82 |
| **N1-H** | 558.63 | 44 | 5.03 |
| **N2-H** | 132.99 | 74 | 2.44 |
| **D1-L** | 58.25 | 80 | 1.35 |
| **D2-L** | 130.29 | 72 | 2.27 |
| **D1-H*** | 300.62 | 69 | 4.35 |
| **D2-H*** | 331.12 | 78 | 5.67 |

*Simulated at more than 200 g N-$N_2O$ $ha^{-1}day^{-1}$ and with chamber deployment longer than 60 minutes

The discrepancies between the IRMS measured isotope ratios and the values estimated from the soil flux simulations using LAS measurements and the Keeling plot method were larger than expected from the results of the Monte Carlo investigation (Table 1) and significantly larger than 1‰ (Figure 4, bottom panel).

The magnitude of the discrepancies calculated for $\delta^{15}N^{Bulk}$ was the smallest among the 3 isotope ratios, followed by those of SP which were approximately twice those observed for $\delta^{15}N^{Bulk}$ (Figure 4). Discrepancies in $\delta^{18}O$ were the largest, being three times those of SP and twice those of $\delta^{15}N^{Bulk}$.

The discrepancies in the SP estimates from soil flux simulations made with source gas from D1 and D2 were smaller than those made with source gas from N1 and N2. The discrepancies in $\delta^{15}N^{Bulk}$ and $\delta^{18}O$ did not vary with source gas. Comparing the discrepancies among similar flux rates and attending to chamber deployment time, does not reveal any relationship between the size of the discrepancy and the deployment time. Similarly, we did not observe a pattern when comparing the magnitude of the discrepancies between low (L)

and high (H) flux rates. The size of the discrepancies for all three isotope ratios seem to be independent of flux rate and deployment time (Figure 4).

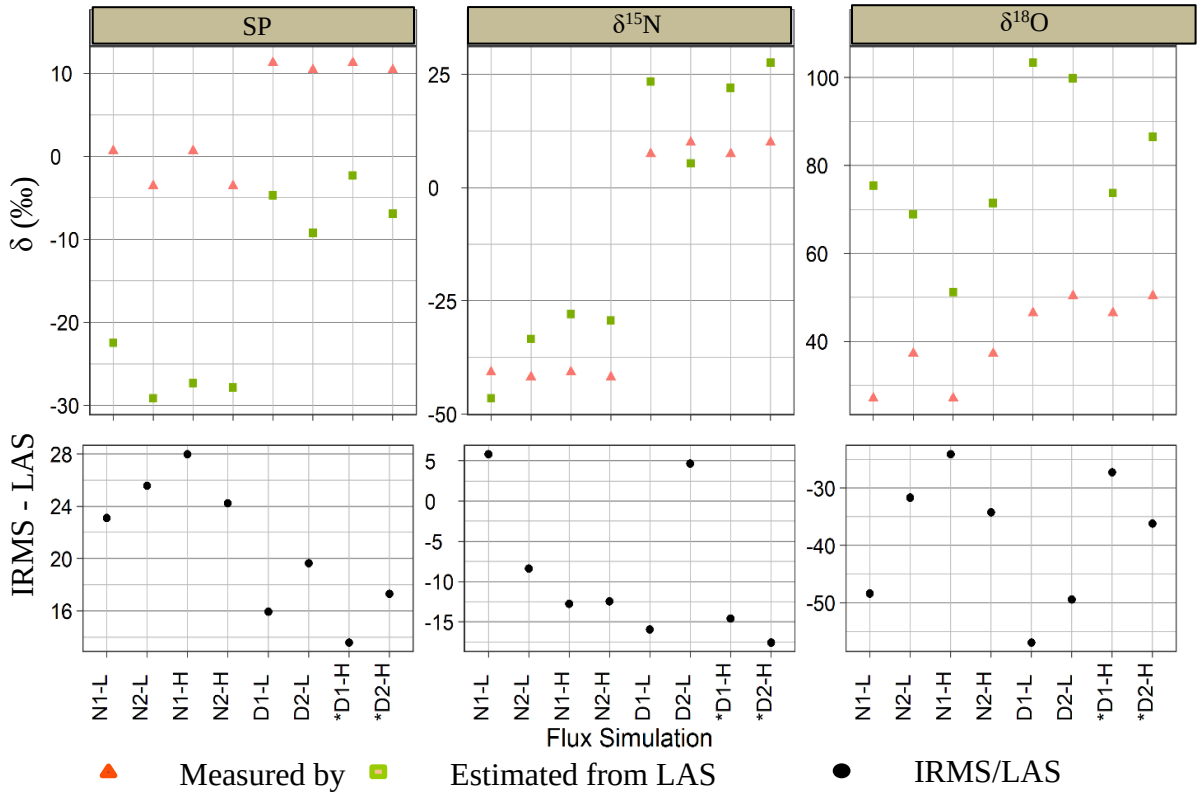


**Figure 4.** Isotope ratios (SP, $\delta^{15}N^{Bulk}$, and $\delta^{18}O$) of the soil produced $N_2O$ measured by IRMS (orange triangles) and estimated via Keeling plots of δ-concentration corrected LAS direct measurements from soil chambers during 8 flux simulations (green squares) (top panels). Discrepancies of the LAS estimated isotope ratios, calculated as the absolute difference in isotope ratios measured by IRMS and estimated from LAS measurements (bottom panels). *D1-H and *D2-H were simulated flux rates greater than 200 g $N\text{-}N_2O$ $ha^{-1}day^{-1}$ and chamber closures longer than 60 minutes, these should have resulted in estimates of SP and $\delta^{15}N^{Bulk}$ within 1‰ of the IRMS measured values.

### *Isotope ratio δ-concentration dependence correction*

The δ-concentration dependency corrections were found to be substantial and varied with the day on which they were calculated (Figure 5). Over the range of $[N_2O]$ examined, the difference between the isotope ratios measured by IRMS and the 3-minute average of the weekly LAS measurements ($\Delta\delta = \delta_{IRMS} - \delta_{LAS}$) ranged from, -20.8 to 11.5 ‰, -29.4 to 50.9

‰, and -77.7 to 344.17 ‰, for SP, $\delta\ ^{15}N^{Bulk}$ and $\delta^{18}O$, respectively (Figure 5, upper plots). The error bars in Figure 5, represent one standard deviation of the 3-minute LAS isotope ratio measurements.

The δ-concentration dependency correction function polynomials were fit to the data collected on individual days as well as to the entire data set (i.e., data collected on 4 days at one-week intervals over one month). The resulting correction functions for each isotope ratio (SP, $\delta^{15}N^{Bulk}$, and $\delta^{18}O$), are first- to sixth-order polynomials relating $\Delta\delta$ to $1/[N_2O]$. In figure 5, the δ-concentration dependency correction functions representing the best fit to data collected on a single day are represented by colored lines while the correction functions fit to the entire data set (4 days at weekly intervals) are represented by the solid black lines. The polynomial equations can be found in Appendix A (Equations A1, A2 and A3) along with the polynomial coefficients and adjusted $R^2$ values (Tables A2, A3 and A4).

After corrected using the function fit to the entire data set, the residuals computed from the daily measurements ranged from -12.1 to 12.4‰, -5.3 to 5.6‰ and -17.1 to 46.2 ‰ for SP, $\delta\ ^{15}N^{Bulk}$ and $\delta^{18}O$, respectively (Figure 5, lower plots). Unsurprisingly, applying the δ-concentration correction function for a specific day to correct data gathered on that same day resulted in smaller residuals than if the δ-concentration dependence correction functions fit to the entire data set were used. For example, a correction function fit to data collected on 8/24, yielded residuals for that day ranging from -2.3 to 1.9‰, -1.9 to 2.4‰ and -5.6 to 4.5 ‰ for SP, $\delta\ ^{15}N^{Bulk}$ and $\delta^{18}O$, respectively (Figure 5, lower plots). For this specific day, the residuals for SP, $\delta\ ^{15}N^{Bulk}$ and $\delta^{18}O$ were approximately factors of 6, 2, and 10 less than the

residuals calculated using the δ-concentration dependence correction function derived from the data collected on all four days.

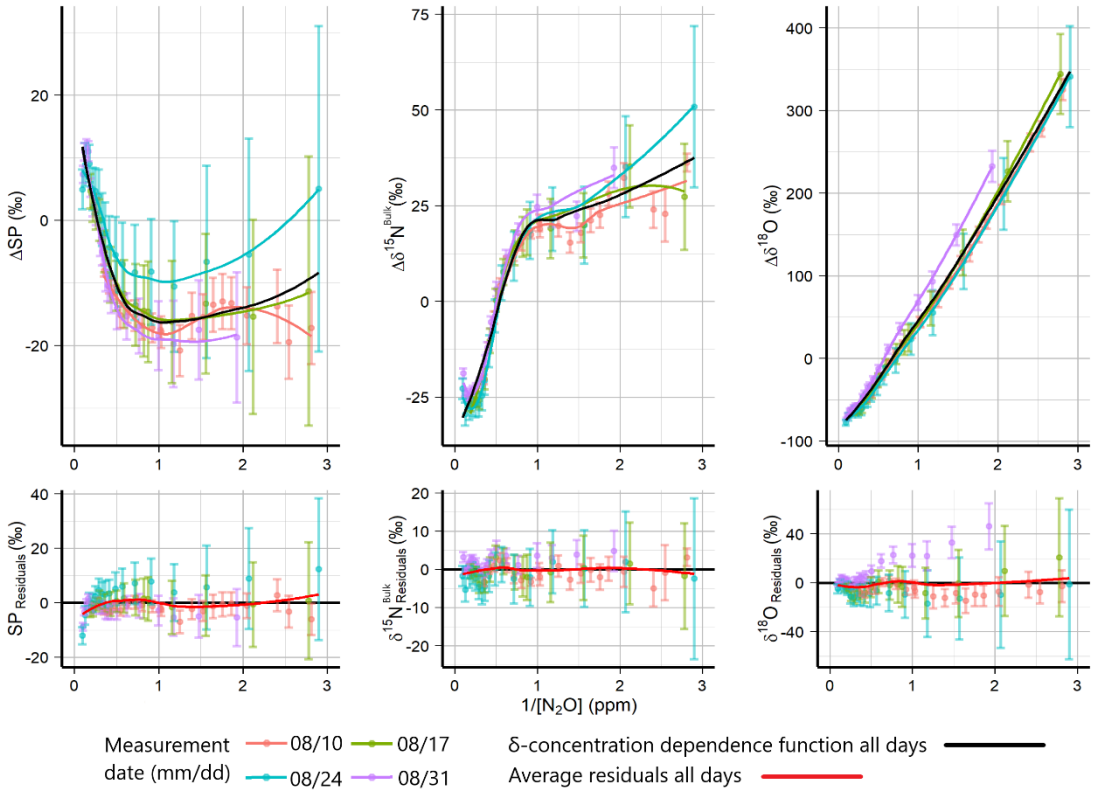


**Figure 5**. δ-concentration effects (upper plots) and residuals of the corrected measurements (lower plots). Differences in SP, δ $^{15}N^{Bulk}$ and $\delta^{18}O$ between the IRMS and the LAS analyzer measurements (y-axis) at different $N_2O$ concentrations, $1/[N_2O]$ (x-axis). Measurements were repeated once a week for four weeks (colored). LAS isotopocule measurements lasted 3-minute (n = 90), points represented average value and error bars represent the standard deviation. δ-concentration functions were computed for each day, colored lines, and for the whole data set, black line. Red line represents the average residual value computed for all data using the function fitted to the whole data set, black line. The δ-concentration effects described non-linear patterns that were different on different days.

## *5. Discussion*

### *5.1. Uncertainty of the isotope ratios*

***Variability of the LAS measurements.***

For all three isotope ratios SP, $\delta^{15}N^{Bulk}$, and $\delta^{18}O$, the variability of the LAS isotope ratio measurements, reported as a standard deviation, decreased with increasing [$N_2O$]. Near ambient $N_2O$ concentrations, the variability decreased rapidly as [$N_2O$] increased and more slowly at higher [$N_2O$] (Figure 3). The standard deviations of the SP and $\delta^{15}N^{Bulk}$ measurements were similar. This is expected because SP and $\delta^{15}N^{Bulk}$ are computed as the difference and average of the $\delta^{15}N^{\alpha}$ and $\delta^{15}N^{\beta}$ isotopomers Butterbach-Bahl, et al. (2013).

The only mention in the literature of the variability of LAS measurements with $N_2O$ concentration was by Harris et al. (2020). Using the same model of analyzer used in this study (Los Gatos Research, model 914-0027), Harris et al. (2020) calculated the variability of five-minute averages of measurements collected over 30-h periods of continuous measurement using standard gases at three $N_2O$ concentrations. The resulting standard deviations are not directly comparable to our results because the long averaging time and very long run time greatly reduce the observed variability, however, the trends reported are reproduced in our results. Harris et al. (2020) reported a decrease in the standard deviations of SP, $\delta^{15}N^{Bulk}$, and $\delta^{18}O$ with increasing [$N_2O$] in the same proportions that we observed (Figure 3). Similarly, Harris et al. (2020) also reported standard deviations of the 5-minute averages of SP and $\delta^{15}N^{Bulk}$ that were approximately one-half those of the $\delta^{18}O$ averages.

The variability of measured [$N_2O$] increased linearly with [$N_2O$] but was only 8.54 x $10^{-3}$ ppm at 10 ppm $N_2O$. This is similar to values reported by (Butterbach-Bahl et al., 2013). Given that the concentration of $N_2O$ observed in the soil chamber headspace will vary from the $N_2O$ concentration of ambient air (~ 0.3 ppm) to as high as 10 ppm, this change in variability with changing $N_2O$ concentration is extremely small, and in this context and can be neglected. For example, when the soil flux rate is 4 g N-$N_2O$ $ha^{-1}day^{-1}$, which occurred in field experiments reported by Francis Clar & Anex (2020) 50% of the time, the change in [$N_2O$] in the chamber headspace over a 30 min closure time will be 200 times greater than the [$N_2O$] measurement variability observed at 0.3 ppm.

***Isotope ratio uncertainty results***

The isotope ratio uncertainties, calculated as the 90% confidence interval of the probability distributions of the output isotope ratio measurement error, reveal that the magnitudes of the uncertainties depend on a complex interplay between $N_2O$ flux rate, chamber deployment time, and the change in the variability of the isotope ratio measurements with [$N_2O$] in the chamber headspace (Table 1). Although clear trends are evident, the uncertainty of an isotope ratio derived using the Keeling plot method and *in situ* LAS measurements of the soil chamber headspace depend on multiple factors.

In the Keeling plot method isotope ratio data are plotted versus the reciprocal of [$N_2O$], so as concentration increases the data are more closely spaced. Error about the reciprocal is likewise not symmetric, so low concentration data have greater influence on the least-squares solution. LAS measurements at low concentration are, unfortunately, also the measurements

with the highest variability (Figure 3), so these data are associated with the largest residuals and simultaneously have high leverage.

Intuitively, a wider range of $N_2O$ in the measured gas samples for a given Keeling plot should provide a better estimate of the intercept and similarly increasing the number measurements should result in smaller error (Pataki et al., 2003). When deployment time is short and $N_2O$ flux rate is small, the number of measurements is small, and the measurements are all of relatively low $N_2O$ concentration gas and will thus have relatively high variability. When deployment time is long and $N_2O$ flux rate is large, higher $N_2O$ concentration is achieved in the chamber headspace and more of the measurements will have low variability, but because they are plotted versus the reciprocal of $[N_2O]$, these data are spaced more closely to each other and so individually have reduced influence on the isotope ratio estimate. What is more, when the $N_2O$ flux rate is large, the $[N_2O]$ in headspace rises more rapidly so there are fewer of these more variable measurements and their sampling variability is thus not reduced by increased sample size.

It is possible that use of a different mixing model might better complement the LAS analyzer uncertainty characteristics. The Miller-Tans mixing model (Miller and Tans, 2003) results in linear equation in which the unknown isotope ratio appears as the slope of the regression line of $\delta_h \times [N_2O]$ versus $[N_2O]$ rather than the intercept of $\delta_h$ versus $1/[N_2O]$ as in the Keeling method. In the Miller-Tans model error about concentration are symmetric so the leverage of individual data points is independent of $[N_2O]$. We did not investigate use of the Miller-Tans model with LAS $N_2O$ isotopic measurements in this study.

To provide context for the size of the uncertainty values reported in Table 1 we can consider the idealized case suggested by Decock and Six (2003) in which the $N_2O$ flux is entirely from nitrification ($N_2O_N$) and denitrification ($N_2O_D$) in the absence of $N_2O$ reduction to $N_2$. The fractional contribution of denitrification, $f_D = N_2O_D/N_2O_{total}$ , can be found from $f_D = (SP_{total} - SP_N)/(SP_D - SP_N)$, where $SP_D$ and $SP_N$ are the *SP* values observed for $N_2O_N$ and $N_2O_D$ in pure cultures; and $SP_{total}$ is the site preference value for the soil emitted $N_2O_{total}$ found using a Keeling plot and chamber headspace measurements. Using the pure culture values (section 2.3) suggested by Lewicka-Szczebak et al. (2017) plus and minus standard deviation of 4‰ as reported by Decock and Six (2003), $SP_D$ and $SP_N$ are -3.9 ± 4‰ and 34.8 ± 4‰, respectively. The uncertainty of $SP_{total}$ , $SP_D$ , and $SP_N$ can then be propagated through to give the uncertainty around $f_D$. If the standard deviation of $SP_{total}$ is 0.31 (corresponding to the smallest 90% confidence uncertainty in Table 1 of 0.55), which results from the combination of a 90-minute deployment and a flux of 200 g $N\text{-}N_2O$ $ha^{-1}day^{-1}$, the average uncertainty around $f_D$ is 26%. If the standard deviation of $SP_{total}$ is 9.60, corresponding to a 60-minute deployment and a flux of 4 g $N\text{-}N_2O$ $ha^{-1}day^{-1}$, the average uncertainty around $f_D$ is 57%. A flux of 4 g $N\text{-}N_2O$ $ha^{-1}day^{-1}$ occurred in field experiments reported by Clar & Anex (2020) 50% of the time and a 60-minute deployment is a relatively long-duration closure (Charteris et al., 2020). As noted by Decock and Six (2003), this very large uncertainty is a conservative estimate because this idealized case does not account for $N_2O$ reduction or the wider range of SP values that will be seen outside of pure cultures.

This investigation of isotope ratio uncertainty also intentionally excludes errors that result from the δ-concentration dependence and interferent gas sensitivities that effect LAS

instruments, but can (theoretically) be eliminated through calibration and correction. The estimates of isotope ratio uncertainty in Table 1 result from the LAS instrument measurement variability only and are thus the best result that is possible when using this LAS instrument for *in situ* soil flux measurement.

### *5.2. Soil Flux simulations*

#### *Isotope ratio δ-concentration dependence correction*

Differences between IRMS and LAS δ measurements (SP, $\delta\ ^{15}N^{Bulk}$ and $\delta^{18}O$) as the result of δ-concentration dependence effects were large, exhibiting non-linear patterns that were different on different days. Precise estimation of the isotopocule composition of soil emitted $N_2O$ will require rigorous δ-concentration dependency correction.

The δ-concentration dependence effects were best described by polynomial regressions of degree four for SP and $\delta^{18}O$, and degree six for $\delta\ ^{15}N^{Bulk}$ (Figure 5, see appendix A for correction functions and their coefficients). Effective correction of the δ-concentration dependency requires correction function polynomials of this relatively high-order due to the highly nonlinear nature of the LAS δ-concentration dependence. Accurate fitting of these polynomials requires IRMS and LAS isotope ratio comparisons at small [$N_2O$] increments (i.e., 0.2 to 3 ppm) to provide sufficient data. Previous work by Erler et al. (2015), Wassenaar et al. (2018) and Winther et al. (2018) also found that δ-concentration dependence effects are best described by polynomial functions and that accurate parametrization of the polynomial functions requires characterization of the δ-concentration dependence effects at small concentration steps. Harris et al. (2020) characterized δ-concentration dependence effects of multiple LAS analyzers using linear functions and large [$N_2O$] steps but recognized that

using non-linear functions, specially at [$N_2O$] close to ambient air would improve the results of the δ-concentration dependence correction models that were developed.

Correction functions for δ-concentration dependence would typically be developed during LAS calibration which may be only done once or twice a year. Our results showed that the pattern of δ-concentration dependence varied significantly over the span of a week (Figure 5, Appendix A - tables A2, A3 and A4). Residuals of the isotope ratios corrected using data collected over multiple days were between 2 and 10 times larger than those corrected with δ-concentration dependence corrections from data collected on the same day. This suggests that to be effective corrections for δ-concentration dependence must be performed frequently (e.g., daily). Although quantitative data were not reported, Harris et al. (2020) also observed the temporal variability of δ-concentration dependence and recommend performing correction frequently (e.g., daily). Developing δ-concentration dependence correction functions through comparison of a large number of LAS and IRMS measurements on a daily or even weekly basis would be difficult under any circumstances and impractical for a field-deployed instrument.

***Production of soil emitted $N_2O$ – Source gas***

The $N_2O$ gas produced via soil incubations exhibited isotope ratios (Table 2) that are representative of values reported in the literature for $N_2O$ production observed during field experiments. The range of SP of the soil emitted $N_2O$ (0.65‰ to 21.6‰) is similar to the SP values found in the literature by Decock & Six (2013) for both soil incubations and field experiments (-1.6±3.8 to 32.8±4 ‰). The ranges of measured $\delta^{15}N$ and $\delta^{18}O$ have also been

observed in field and soil incubations experiments (Lin et al., 2019; Toyoda et al., 2011; Verhoeven et al., 2019).

The $N_2O$ produced by all four soil incubations had SP signatures in the range associated with $N_2O$ production dominated by denitrification Butterbach-Bahl, et al. (2013). Denitrification is most common under anaerobic conditions, most frequently occurring due to high soil moisture (WFPS > 80%). The soils in N1 and N2 had average WFPS of 37% and 42% respectively, and the emitted gas samples had SP of 0.65‰ and 0.95‰, respectively. Although N1 and N2 exhibited low WFPS, $N_2O$ production may have occurred primarily in soil microsites that were anaerobic or anoxic. Butterbach-Bahl, et al. (2013) suggest that because $N_2O$ production rates via denitrification are much higher than those of nitrification, it is possible for $N_2O$ production via denitrification in small soil microsites to dominate the production of $N_2O$ in low WFPS soil conditions. Low SP has been observed in emissions from relatively dry soils before. In an incubation with 55% WFPS, Well et al. (2006) observed $N_2O$ SP signatures of 1.9±8.4‰ , similarly in soil at 16% WFPS, Pérez et al. (2012) observed SP signatures of 4.2±8.4‰.

Incubations D1 and D2 had average WFPSs of 89% and 105% (WFPS values > 100% are the result of measurement error). Although these conditions favor denitrification and low SP, the D1 and D2 measured SP was 10.58‰ and 10.39‰, respectively. A possible explanation of the elevated SP signatures of D1 and D2 is isotopic fractionation that occurs during the further reduction of $N_2O$ to $N_2$. During $N_2O$ reduction the lighter N-O bonds are cleaved preferentially which tends to enrich $^{15}N$ at the $\alpha$ position of the remaining un-reduced $N_2O$, leading to an increase in SP (Buchen et al., 2018; Lewicka-Szczebak et al., 2016; Wolf et al.,

2015; Wu et al., 2016). SP values higher than those associated with pure culture denitrification have been observed under anaerobic conditions in soils with WFPS of 65-100%. Wu et al. (2016) observed SP signatures of 6.1 ± 6.6‰, similarly Chen et al. (2015) observed SP ranging between 7.13 to 16.69‰ in soil with 80-90% WFPS.

***Soil chamber flux simulations***

The observed discrepancies between the IRMS measured isotope ratios and those estimated from soil flux simulations using LAS measurements and the Keeling plot method were 2 to 10 times larger than those predicted by Monte Carlo simulation (Table 1, Figure 4). Furthermore, the isotope ratio disparities observed in the flux simulations did not exhibit the expected pattern that longer chamber deployment times and larger soil flux rates result in lower uncertainty. The soil simulation results did echo the Monte Carlo simulation in that discrepancies associated with $\delta^{15}N^{Bulk}$ were smaller than those of SP which were in turn smaller than those of $\delta^{18}O$ (Figure 4, lower panel). The observed discrepancies follow no other discernable pattern.

A likely explanation for the large observed discrepancies between the IRMS measured isotope ratios and those estimated from soil flux simulations using LAS measurements and the Keeling plot method is the presence of interferent gases in the soil trace gas flux with absorbance in the same spectral region as the $N_2O$ isotopes. Gases that cause these laser interferences are known to be present in soil trace gases (Erler et al., 2015; Harris et al., 2020). This hypothesis is supported by the differences observed in the discrepancies of SP and $\delta^{15}N^{Bulk}$. The SP values estimated from LAS measurements were uniformly smaller than those measured by IRMS, while the LAS-measured $\delta^{15}N^{Bulk}$ values are generally larger than the

corresponding IRMS measurements. This is consistent with the interferent effects of $CO_2$ on LAS $N_2O$ isotope ratio measurements reported by Harris et al. (2020).

Using the same model of analyzer used here, Harris et al. (2020) observed that the effects on LAS measurements of $\delta^{15}N^{\alpha}$ and $\delta^{15}N^{\beta}$ from an increase in [$CO_2$], were a reduction in $\delta^{15}N^{\alpha}$ and an increase in $\delta^{15}N^{\beta}$ that was approximately twice as large. Thus, an increase in [$CO_2$] is expected to result in a negative bias in SP ( = $\delta^{15}N^{\alpha}$ - $\delta^{15}N^{\beta}$) and a positive bias in $\delta^{15}N^{Bulk}$ (= ($\delta^{15}N^{\alpha}$ + $\delta^{15}N^{\beta}$)/2) as measured by LAS. The [$CO_2$] of the N1 and N2 source gases was up to 20 larger than that of ambient air. Based on the flux rates used in the N1 flux simulation, the [$CO_2$] in the chamber headspace at the end of the simulation was approximately twice that of ambient air.

Our results cannot be compared quantitatively with those of Harris et al. (2020) who used pure gases at fixed concentrations, whereas the sources gases used in our soil flux simulations contained a poorly defined mixture of soil trace gases the concentrations of which changed continuously in the chamber headspace during a flux simulation. The magnitude of the $\delta^{15}N^{\alpha}$, $\delta^{15}N^{\beta}$, and $\delta^{18}O$ measurement biases are known to be affected by [$CO_2$] and [$N_2O$], both of which change continuously but at different rates during a flux simulation according to their concentrations in the source gas. The impact of other interferent gases that may have been present in the source gases (i.e., $CO_2$, $H_2O$, $CH_4$, etc.,) and the combined effects of multiple interferent gases on LAS measurements are unknown.

Efforts have been made to identify and quantify the effect of individual trace gases on the accuracy of LAS $N_2O$ isotope ratio measurements, but the number of trace gases

investigated, and the range of concentrations examined has been limited. Furthermore, there is no information about the effects on the LAS accuracy that will result from *in situ* measurement of soil-derived gases in which multiple trace and possible interfering gases may coexist. Future research should investigate the use soil flux simulations like those described here with chemical scrubbers and pre-concentration systems to remove interferent gases. These types of systems have proved effective for removing interferent gases during laboratory experiments (Ibraim et al., 2018; Kantnerová et al., 2019; Mohn et al., 2012).

## *6. Conclusions*

We assessed the suitability of an LAS isotopic analyzer for in-field, real-time measurement of the isotopic signatures of soil-emitted $N_2O$. Our analysis demonstrates that the measurement uncertainty characteristics of these instruments severely limit their applicability to *in situ* systems that use soil chambers and mixing model analysis to extract the isotopic signature of soil trace gas emissions. Because the measurement variability of the $N_2O$ isotope ratios is very high at low [$N_2O$] these instruments are ill-suited for analysis of chamber headspace data using the Keeling plot method in which low concentration data have a particularly strong influence on the linear regressions that yield the isotopic ratios of the soil emitted $N_2O$. The pronounced deviations in LAS isotope ratio measurements from IRMS-measurements (δ-concentration dependence) further complicates extraction of isotopic signatures from in-field experiments since [$N_2O$] changes dramatically during soil chamber deployments. Correction functions for δ-concentration dependence change significantly over short periods, so corrections must be made frequently (e.g., daily), and developing these correction functions for in-field experiments is difficult but necessary. The large

discrepancies observed between the LAS-derived and IRMS-measured isotope ratios point to the complicated impact on LAS isotopic measurements of interferent gases present in soil gas emissions. Development of more complete models of the LAS measurement bias resulting from interference by the full range of trace gases common in soils (e.g., $H_2$, $N_2$, $O_2$, $H_2O$, $CH_4$, $CO_2$, NO) and their combinations is recommended. Therefore, *in situ* isotopic measurement of soil emitted gases using LAS instruments is likely to remain a qualitative tool for $N_2O$ source partitioning, most useful in combination with other indicators like water filled pore space or soil matric potential.

## *7. References*


Arévalo-Martínez, D. L., Beyer, M., Krumbholz, M., Piller, I., Kock, a., Steinhoff, T., Körtzinger, a. & Bange, H. W. (2013). A new method for continuous measurements of oceanic and atmospheric $N_2O$, CO and $CO_2$: performance of off-axis integrated cavity output spectroscopy (OA-ICOS) coupled to non-dispersive infrared detection (NDIR). *Ocean Science Discussions*, *10*(4), 1281–1327. https://doi.org/10.5194/osd-10-1281-2013

Baer, D. S., Paul, J B & Gupta, M. (2002). Lasers and Optics Applied Physics B Sensitive absorption measurements in the near-infrared region using off-axis integrated-cavity-output spectroscopy. *Appl. Phys. B*, *75*, 261–265. https://doi.org/10.1007/s00340-002-0971-z

Bilskie, J. (2001). *Soil water status: content and potential*. Copyright © 2001 Campbell Scientific, Inc., 815 W. 1800 N., Logan, UT 84321-1784. App Note 2S-I. https://s.campbellsci.com/documents/us/technical-papers/soilh20c.pdf

Bracken, C. J., Lanigan, G. J., Richards, K. G., Müller, C., Tracy, S. R., Grant, J., Krol, D. J., Sheridan, H., Lynch, M. B., Grace, C., Fritch, R. & Murphy, P. N. C. (2021). Source partitioning using N2O isotopomers and soil WFPS to establish dominant N2O production pathways from different pasture sward compositions. *Science of The Total Environment*, 146515. https://doi.org/10.1016/j.scitotenv.2021.146515

Braden-Behrens, J., Yan, Y. & Knohl, A. (2017). A new instrument for stable isotope measurements of 13C and 18O in CO2 - Instrument performance and ecological application of the Delta Ray IRIS analyzer. *Atmospheric Measurement Techniques*, *10*(11), 4537–4560. https://doi.org/10.5194/amt-10-4537-2017

Buchen, C., Lewicka-Szczebak, D., Flessa, H. & Well, R. (2018). Estimating N 2 O processes during grassland renewal and grassland conversion to maize cropping using N 2 O isotopocules. *Rapid Communications in Mass Spectrometry*, *32*(13), 1053–1067. https://doi.org/10.1002/rcm.8132

Butterbach-Bahl, K., Baggs, E. M., Dannenmann, M., Kiese, R. & Zechmeister-Boltenstern, S. (2013). Nitrous oxide emissions from soils: how well do we understand the processes and their controls? *Philosophical Transactions of the Royal Society of London. Series B, Biological Sciences*, *368*(1621), 20130122. https://doi.org/10.1098/rstb.2013.0122

Charteris, A.F., Chadwick, D.R., Thorman, R.E., Vallejo, A., de Klein, C.A., Rochette, P. and Cárdenas, L.M., 2020. Global Research Alliance $N_2O$ chamber methodology guidelines: Recommendations for deployment and accounting for sources of variability. *Journal of Environmental Quality*, *49*(5), pp.1092-1109. https://doi.org/10.1002/jeq2.20126

Chen, H., Williams, D., Walker, J. T. & Shi, W. (2016). Probing the biological sources of soil N 2 O emissions by quantum cascade laser-based 15 N isotopocule analysis. *Soil Biology and Biochemistry*, *100*, 175–181. https://doi.org/10.1016/j.soilbio.2016.06.015

Decock, C. & Six, J. (2013). How reliable is the intramolecular distribution of 15N in N2O to source partition N2O emitted from soil? In *Soil Biology and Biochemistry* (Vol. 65, pp. 114–127). Pergamon. https://doi.org/10.1016/j.soilbio.2013.05.012

Erler, D. v., Duncan, T. M., Murray, R., Maher, D. T., Santos, I. R., Gatland, J. R., Mangion, P. & Eyre, B. D. (2015). Applying cavity ring-down spectroscopy for the measurement of dissolved nitrous oxide concentrations and bulk nitrogen isotopic composition in aquatic systems: Correcting for interferences and field application. *Limnology and Oceanography: Methods*, *13*(8), 391–401. https://doi.org/10.1002/lom3.10032

Francis Clar, J. T. & Anex, R. P. (2020). Flux intensity and diurnal variability of soil N $_2$ O emissions in a highly fertilized cropping system. *Soil Science Society of America Journal*, 84:1983-1994. https://doi.org/10.1002/saj2.20132

Glatting, G., Kletting, P., Reske, S. N., Hohl, K. & Ring, C. (2007). Choosing the optimal fit function: Comparison of the Akaike information criterion and the F-test. *Medical Physics*, *34*(11), 4285–4292. https://doi.org/10.1118/1.2794176

Gralher, B., Herbstritt, B., Weiler, M., Wassenaar, L. I. & Stumpp, C. (2016). Correcting Laser-Based Water Stable Isotope Readings Biased by Carrier Gas Changes. *Environ. Sci. Technol*, *50*, 33. https://doi.org/10.1021/acs.est.6b01124

Griffith, D. W. T., Deutscher, N. M., Caldow, C., Kettlewell, G., Riggenbach, M. & Hammer, S. (2012). Atmospheric Measurement Techniques A Fourier transform infrared trace gas and isotope analyser for atmospheric applications. *Atmos. Meas. Tech*, *5*, 2481–2498. https://doi.org/10.5194/amt-5-2481-2012

Groffman, P. M., Hardy, J. P., Discoll, C. T. & Fahey, T. J. (2006). Snow depth, soil freezing, and fluxes of carbon dioxide, nitrous oxide and methane in a northern hardwood forest. *Global Change Biology*, *12*(9), 1748–1760. https://doi.org/10.1111/j.1365-2486.2006.01194.x

Harris, S. J., Liisberg, J., Xia, L., Wei, J., Zeyer, K., Yu, L., Barthel, M., Wolf, B., Kelly, B. F. J., Cendón, D. I., Blunier, T., Six, J. & Mohn, J. (2020). N2O isotopocule measurements using laser spectroscopy: Analyzer characterization and intercomparison. *Atmospheric Measurement Techniques*, *13*(5), 2797–2831. https://doi.org/10.5194/amt-13-2797-2020

Henault, C., Grossel, A., Mary, B., Roussel, M., Leonard, J. (2012). Nitrous Oxide Emission by Agricultural Soils: A Review of Spatial and Temporal Variability for Mitigation. *Pedosphere*, *22*(4), 426–433. https://doi.org/10.1016/S1002-0160(12)60029-0

Ibraim, E., Harris, E., Eyer, S., Tuzson, B., Emmenegger, L., Six, J. & Mohn, J. (2018). Development of a field-deployable method for simultaneous, real-time measurements of the four most abundant N2O isotopocules*. *Isotopes in Environmental and Health Studies*, *54*(1), 1–15. https://doi.org/10.1080/10256016.2017.1345902

Ibraim, E., Wolf, B., Harris, E., Gasche, R., Wei, J., Yu, L., Kiese, R., Eggleston, S., Butterbach-Bahl, K., Zeeman, M. and Tuzson, B., 2019. Attribution of $N_2O$ sources in a grassland soil with laser spectroscopy based isotopocule analysis. *Biogeosciences*, *16*(16), pp.3247-3266. https://doi.org/10.5194/bg-16-3247-2019

IPCC. (2014). Climate Change 2014: Synthesis Report. Contribution of Working Groups I, II and III to the Fifth Assessment Report of the Intergovernmental Panel on Climate Change. Retrieved from https://www.ipcc.ch/site/assets/uploads/2018/02/SYR_AR5_FINAL_full.pdf.

Joseph, J., Külls, C., Arend, M., Schaub, M., Hagedorn, F., Gessler, A. & Weiler, M. (2019). Application of a laser-based spectrometer for continuous in situ measurements of stable isotopes of soil CO 2 in calcareous and acidic soils. *SOIL*, *5*(1), 49–62. https://doi.org/10.5194/soil-5-49-2019

Kantnerová, K., Tuzson, B., Emmenegger, L., Bernasconi, S. M. & Mohn, J. (2019). Quantifying isotopic signatures of N2O using quantum cascade laser absorption spectroscopy. *Chimia*, *73*(4), 232–238. https://doi.org/10.2533/chimia.2019.232

Keeling, C. D. (1958). The concentration and isotopic abundances of atmospheric carbon dioxide in rural areas. In *Geochimica et Cosmochimica Acta* (Vol. 13).

Kong, X., Duan, Y., Schramm, A., Eriksen, J., Holmstrup, M., Larsen, T., Bol, R. & Petersen, S. O. (2017). Mitigating N2O emissions from clover residues by 3,4-dimethylpyrazole phosphate (DMPP) without adverse effects on the earthworm Lumbricus terrestris. *Soil Biology and Biochemistry*, *104*, 95–107. https://doi.org/10.1016/j.soilbio.2016.10.012

Lebegue, B., Schmidt, M., Ramonet, M., Wastine, B., Kwok, C. Y., Laurent, O., Belviso, S., Guemri, A., Philippon, C., Smith, J. & Conil, S. (2016). Comparison of nitrous oxide (N 2 O) analyzers for high-precision measurements of atmospheric mole fractions. *Atmos. Meas. Tech*, *9*, 1221–1238. https://doi.org/10.5194/amt-9-1221-2016

Lewicka-Szczebak, D., Augustin, J., Giesemann, A. & Well, R. (2017). Quantifying N2O reduction to N2 based on N2O isotopocules-validation with independent methods (helium incubation and 15N gas flux method). *Biogeosciences*, *14*(3), 711–732. https://doi.org/10.5194/bg-14-711-2017

Lewicka-Szczebak, D., Dyckmans, J., Kaiser, J., Marca, A., Augustin, J. & Well, R. (2016). Oxygen isotope fractionation during N2 O production by soil denitrification. *Biogeosciences*, *13*(4), 1129–1144. https://doi.org/10.5194/bg-13-1129-2016

Lin, W., Ding, J., Li, Y., Zhang, W., Ahmad, R., Xu, C., Mao, L., Qiang, X., Zheng, Q. & Li, Q. (2019). Partitioning of sources of N2O from soil treated with different types of fertilizers by the acetylene inhibition method and stable isotope analysis. *European Journal of Soil Science*, *70*(5), 1037–1048. https://doi.org/10.1111/ejss.12782

Miller, J.B. and Tans, P.P., 2003. Calculating isotopic fractionation from atmospheric measurements at various scales. *Tellus B: Chemical and Physical Meteorology*, *55*(2), pp.207-214. https://doi.org/10.3402/tellusb.v55i2.16697

Mohn, J, Tuzson, B., Manninen, A., Yoshida, N., Toyoda, S., Brand, W. A. & Emmenegger, L. (2012). Site selective real-time measurements of atmospheric N2O isotopomers by laser spectroscopy. In *Atmospheric Measurement Techniques* (Vol. 5, Issue 7, pp. 1601–1609). https://doi.org/10.5194/amt-5-1601-2012

Mohn, J., Wolf, B., Toyoda, S., Lin, C. T., Liang, M. C., Brüggemann, N., Wissel, H., Steiker, A. E., Dyckmans, J., Szwec, L., Ostrom, N. E., Casciotti, K. L., Forbes, M., Giesemann, A., Well, R., Doucett, R. R., Yarnes, C. T., Ridley, A. R., Kaiser, J. & Yoshida, N. (2014). Interlaboratory assessment of nitrous oxide isotopomer analysis by isotope ratio mass spectrometry and laser spectroscopy: Current status and perspectives. *Rapid Communications in Mass Spectrometry*, *28*(18), 1995–2007. https://doi.org/10.1002/rcm.6982

Morris, S. G., Kimber, S. W. L. W., Grace, P. & van Zwieten, L. (2013). Improving the statistical preparation for measuring soil N2O flux by closed chamber. *The Science of the Total Environment*, *465*, 166–172. https://doi.org/10.1016/j.scitotenv.2013.02.032

Nara, H., Tanimoto, H., Tohjima, Y., Mukai, H., Nojiri, Y., Katsumata, K. & Rella, C. W. (2012). Effect of air composition (N2, O2, Ar, and H 2O) on CO2 and CH4 measurement by wavelength-scanned cavity ring-down spectroscopy: Calibration and measurement strategy. *Atmospheric Measurement Techniques*, *5*(11), 2689–2701. https://doi.org/10.5194/amt-5-2689-2012

Ostrom, N. E. & Ostrom, P. H. (2017). Mining the isotopic complexity of nitrous oxide: a review of challenges and opportunities. *Biogeochemistry*, *132*(3), 359–372. https://doi.org/10.1007/s10533-017-0301-5

Ostrom, N. E., Pitt, A., Sutka, R., Ostrom, P. H., Grandy, A. S., Huizinga, K. M. & Robertson, G. P. (2007). Isotopologue effects during $N_2O$ reduction in soils and in pure cultures of denitrifiers. *Journal of Geophysical Research*, *112*(G2), G02005. https://doi.org/10.1029/2006JG000287

Parkin, T. B., Venterea, R. T. & Hargreaves, S. K. (2012). Calculating the detection limits of chamber-based soil greenhouse gas flux measurements. *Journal of Environmental Quality*, *41*(3), 705–715. https://doi.org/10.2134/jeq2011.0394

Parkin, Timothy B & Venterea, R. T. (2010). U.S. Department of Agriculture - Agricultural ressearch service Greenhouse gas Reduction through Agricultural Carbon Enhancement network (USDA-ARS GRACEnet) Project Protocols Chapter 3. Chamber-Based Trace Gas Flux Measurements. *Flux*, *2010*(April 2003), 1–39.

Pataki, D. E., Ehleringer, J. R., Flanagan, L. B., Yakir, D., Bowling, D. R., Still, C. J., Buchmann, N., Kaplan, J. O. & Berry, J. A. (2003). The application and interpretation of Keeling plots in terrestrial carbon cycle research. *Global Biogeochemical Cycles*, *17*(1). https://doi.org/10.1029/2001GB001850

Pérez, T., Garcia-montiel, D., Trumbore, S., Tyler, S., De, P., Applications, S. E. & Dec, N. (2012). Nitrous Oxide Nitrification and Denitrification $^{15}N$ Enrichment Factors from Amazon Forest Soils nitrous oxide nitrification and denitrification 15n enrichment factors from amazon forest soils. *Ecological Applications*, *16*(6), 2153–2167. https://doi.org/10.1890/1051-0761(2006)016[2153:NONADN]2.0.CO;2

Petersen, S. O., Well, R., Taghizadeh-Toosi, A. & Clough, T. J. (2020). Seasonally distinct sources of N2O in acid organic soil drained for agriculture as revealed by N2O isotopomer analysis. *Biogeochemistry*, *147*(1), 15–33. https://doi.org/10.1007/s10533-019-00625-x

Portmann, R. W., Daniel, J. S. & Ravishankara, A. R. (2012). Stratospheric ozone depletion due to nitrous oxide: influences of other gases. *Philosophical Transactions of the Royal Society B: Biological Sciences*, *367*(1593), 1256–1264. https://doi.org/10.1098/rstb.2011.0377

Rapson, T. D. & Dacres, H. (2014). Analytical techniques for measuring nitrous oxide. In *TrAC - Trends in Analytical Chemistry* (Vol. 54, pp. 65–74). Elsevier B.V. https://doi.org/10.1016/j.trac.2013.11.004

Rella, C. W., Hoffnagle, J., He, Y. & Tajima, S. (2015). Local- and regional-scale measurements of CH4, Δ13CH4, and C2H6 in the Uintah Basin using a mobile stable isotope analyzer. *Atmospheric Measurement Techniques*, *8*(10), 4539–4559. https://doi.org/10.5194/amt-8-4539-2015

Snyder, C., Davidson, E., Smith, P. & Venterea, R. (2014). Agriculture: sustainable crop and animal production to help mitigate nitrous oxide emissions. *Current Opinion in Environmental Sustainability*, *9*, 46–54. https://doi.org/10.1016/j.cosust.2014.07.005

Stocker, T.F., Qin, D., Plattner, G.-K., Tignor, M., Allen, S. K., Boschung, J., Nauels, A., Xia, Y., Bex, V. & Midgley, P. M. (eds. ). (2013). *IPCC, 2013: Climate change2013: The Physical Science Basis. Contribution of Working Group I to the Fifth Assesment Report of the Intergovernmental Panel on Climate Change*. https://www.ipcc.ch/report/ar5/wg1/

Toyoda, S., Yano, M., Nishimura, S., Akiyama, H., Hayakawa, A., Koba, K., Sudo, S., Yagi, K., Makabe, A., Tobari, Y., Ogawa, N. O., Ohkouchi, N., Yamada, K. & Yoshida, N. (2011). Characterization and production and consumption processes of N 2 O emitted from temperate agricultural soils determined via isotopomer ratio analysis . *Global Biogeochemical Cycles*, *25*(2), n/a-n/a. https://doi.org/10.1029/2009gb003769

Venterea, R. T., Petersen, S. O., de Klein, C. A. M., Pedersen, A. R., Noble, A. D. L., Rees, R. M., Gamble, J. D. & Parkin, T. B. (2020). Global Research Alliance N2O chamber methodology guidelines: Flux calculations. *Journal of Environmental Quality*, *49*(5), 1141–1155. https://doi.org/10.1002/jeq2.20118

Verhoeven, E., Barthel, M., Yu, L., Celi, L., Said-Pullicino, D., Sleutel, S., Lewicka-Szczebak, D., Six, J. & Decock, C. (2019). Early season N 2 O emissions under variable water management in rice systems: source-partitioning

emissions using isotope ratios along a depth profile. *Biogeosciences*, *16*, 383–408. https://doi.org/10.5194/bg-16-383-2019

Waechter, H., Mohn, J., Tuzson, B., Emmenegger, L. & Sigrist, M. W. (2008). Determination of N_2O isotopomers with quantum cascade laser based absorption spectroscopy. *Optics Express*, *16*(12), 9239. https://doi.org/10.1364/oe.16.009239

Wang, Z., Fu, P. & Chao, X. (2019). Laser Absorption Sensing Systems: Challenges, Modeling, and Design Optimization. *Applied Sciences*, *9*(13), 2723. https://doi.org/10.3390/app9132723

Wassenaar, L. I., Douence, C., Altabet, M. A. & Aggarwal, P. K. (2018). N and O isotope (δ15Nα, δ15Nβ, δ18O, δ17O) analyses of dissolved NO3− and NO2− by the Cd-azide reduction method and N2O laser spectrometry. *Rapid Communications in Mass Spectrometry*, *32*(3), 184–194. https://doi.org/10.1002/rcm.8029

Wehr, R. & Saleska, S. R. (2017). Corrigendum to "The long-solved problem of the best-fit straight line: application to isotopic mixing lines." *Biogeosciences*, *14*, 17–29. https://doi.org/10.5194/bg-14-17-2017-corrigendum

Well, R., Kurganova, I., de Gerenyu, V. L. & Flessa, H. (2006). Isotopomer signatures of soil-emitted N2O under different moisture conditions - A microcosm study with arable loess soil. *Soil Biology and Biochemistry*, *38*(9), 2923–2933. https://doi.org/10.1016/j.soilbio.2006.05.003

Winther, M., Balslev-Harder, D., Christensen, S., Priemé, A., Elberling, B., Crosson, E. & Blunier, T. (2018). Continuous measurements of nitrous oxide isotopomers during incubation experiments. *Biogeosciences*, *15*, 767–780. https://doi.org/10.5194/bg-15-767-2018

Wolf, B., Merbold, L., Decock, C., Tuzson, B., Harris, E., Six, J., Emmenegger, L. & Mohn, J. (2015). First on-line isotopic characterization of $N_2O$ emitted from intensively managed grassland. *Biogeosciences Discussions*, *12*(2), 1573–1611. https://doi.org/10.5194/bgd-12-1573-2015

Wu, D., Köster, J. R., Cárdenas, L. M., Brüggemann, N., Lewicka-Szczebak, D. & Bol, R. (2016). N2O source partitioning in soils using 15N site preference values corrected for the N2O reduction effect. *Rapid Communications in Mass Spectrometry*, *30*(5), 620–626. https://doi.org/10.1002/rcm.7493

Yamamoto, A., Akiyama, H., Nakajima, Y. & Hoshino, Y. T. (2017). Estimate of bacterial and fungal N2O production processes after crop residue input and fertilizer application to an agricultural field by 15N isotopomer analysis. *Soil Biology and Biochemistry*, *108*, 9–16. https://doi.org/10.1016/j.soilbio.2017.01.015

Yoshida, N. & Toyoda, S. (2000). Constraining the atmospheric N2O budget from intramolecular site preference in N2O isotopomers. *Nature*, *405*(6784), 330–334. https://doi.org/10.1038/35012558

Yu, L., Harris, E., Lewicka-Szczebak, D., Barthel, M., Blomberg, M. R. A., Harris, S. J., Johnson, M. S., Lehmann, M. F., Liisberg, J., Müller, C., Ostrom, N. E., Six, J., Toyoda, S., Yoshida, N. & Mohn, J. (2020). What can we learn from N 2 O isotope data? – Analytics, processes and modelling. *Rapid Communications in Mass Spectrometry*, *34*(20). https://doi.org/10.1002/rcm.8858

Zobitz, J. M., Keener, J. P., Schnyder, H. & Bowling, D. R. (2006). Sensitivity analysis and quantification of uncertainty for isotopic mixing relationships in carbon cycle research. *Agricultural and Forest Meteorology*, *136*(1–2), 56–75. https://doi.org/10.1016/j.agrformet.2006.01.003

## ***Chapter 4: Flux intensity and diurnal variability of soil $N_2O$ emissions in a highly fertilized cropping System***

* Note: This chapter was published in the Soil Science Society of America Journal on 05 August 2020.

Jordi T. Francis Clar[1], Robert P. Anex[1]

[1]Department of Biological Systems Engineering, University of Wisconsin, Agricultural Building, 460 Henry Mall, Madison, 53706, USA

### *1. Abstract*

Manual sampling of nitrous oxide soil fluxes is labor intensive and sampling frequencies are often insufficient to capture daily variability of $N_2O$ soil flux, compromising the accuracy of emissions estimates. Knowledge of the diurnal fluctuation of $N_2O$ flux has been used to choose a flux sampling time that maximizes the accuracy of $N_2O$ flux estimates and thereby reduces the required sampling frequency, but the results of previous studies are inconsistent. We analyzed $N_2O$ soil emissions measured quasi-continuously over three years from a highly fertilized (> 200 kg N $ha^{-1}$) Corn (*Zea mays L.*) system grown in southern Wisconsin, USA. This is the first study of $N_2O$ flux temporal variability that includes multiple, difficult-to-measure peak emission events ("hot moments") and estimates the relative contribution of hot moments to cumulative emissions. The relationship between the observed hourly average flux and the mean daily flux was assessed using linear regression, using all measured data (≈ 22,000 fluxes) as well as using subsets of the data grouped by flux magnitude. Results show that diurnal variation in $N_2O$ soil flux was closely associated with normalized flux size. During low emission periods, $N_2O$ soil fluxes exhibited a diurnal pattern such that $N_2O$ flux

measured at particular times of day, “Preferred Measuring Times” (PMTs), were not significantly different from the mean daily flux. During high emissions periods $N_2O$ flux did not exhibit a diurnal pattern and there was no PMT. High emissions periods included difficult-to-measure hot moments that did not exhibit a PMT and contributed up to 50% of the cumulative emissions, therefore, high temporal resolution flux measurements were required to estimate cumulative emissions accurately.

**Abbreviations:** PMT, preferred measuring time; MDF, minimum detectable flux, HCC, high cumulative contribution; LCC, low cumulative contribution.

**Core ideas:**

- $N_2O$ fluxes were measured at two hour intervals over 3 years
- $N_2O$ emissions from fertilized corn were highly episodic
- Short, high-emissions periods accounted for approximately 50% of total $N_2O$ emissions
- During peak periods emissions did not exhibit a diurnal pattern or trend
- Accurate estimation of cumulative flux requires high frequency measurements during peak events

## *2. Introduction*

Understanding the patterns of nitrous oxide ($N_2O$) emissions from agricultural soils is a priority in the context of mitigating global warming. Nitrous oxide is a long-lived greenhouse gas (GHG) with a global warming potential 289 times that of carbon dioxide (IPCC, 2011) and its breakdown in the atmosphere is a major source of stratospheric nitric oxide which destructively reacts with the stratospheric ozone layer. Agriculture is estimated to contribute around 80% of global anthropogenic $N_2O$ emissions, more than half of which comes from agricultural soils (Syakila and Kroeze 2011) and the atmospheric concentration of $N_2O$ is increasing at 0.6 – 0.9 ppbv $yr^{-1}$ (WMO, 2014).

Measurement of $N_2O$ soil fluxes is most commonly based on the sampling of small flux chambers which is labor- and time- intensive (Pattey et al. 2007). Limits on resources available for sampling campaigns often require that a single $N_2O$ soil flux estimate represents the flux over an extended period, ranging from 24 hours up to as long as several weeks (Barton et al., 2015; Parkin, 2008). This makes choosing a flux measurement that accurately represents the average soil flux during the interval between samples very important.

Nitrous oxide fluxes in soils are the result of complex biological processes which, while linked to a wide range of physical and chemical factors, are strongly influenced by soil temperature (Maag & Vinther, 1996). Nitrous oxide fluxes are therefore expected to follow the diurnal pattern of soil temperature, increasing during the day and decreasing during the night. When present, this diurnal pattern of $N_2O$ fluxes means that there are particular times of day at which the measured flux will not be significantly different from the mean daily flux. We will refer to these times as Preferred Measuring Times (PMTs). If PMTs can be

identified, sampling at these times would increase the accuracy of soil $N_2O$ flux estimates or reduce the necessary frequency of flux measurements by implementing intermittent sampling schedules (e.g. weekly, biweekly, monthly). Unfortunately, there is considerable disagreement in the literature about the existence and timing of diurnal patterns of soil $N_2O$ flux (the relevant literature is summarized in Table S1 in supplement S1).

When diurnal patterns of $N_2O$ emissions have been observed previously, they have usually been based on fluxes measured in unfertilized crops or on small data sets (i.e. several weeks) that did not capture emissions variability across the year or fluxes. Cosentino, Fernandez, Figueiro, & Taboada (2012) measured $N_2O$ fluxes in an unfertilized soybean crop in Argentina every three hours over three days using five soil chambers, resulting in a total of 120 flux measurements. They observed that $N_2O$ emissions exhibited a diurnal pattern and the PMT was from 09:00 to 12:00. Alves et al., (2012) studied diurnal variability of $N_2O$ emissions at Seropedica, Brazil in an unfertilized native grassland and at Edinburg, Scotland in unfertilized crop land used to grow potatoes and vegetables. In Edinburg, $N_2O$ rates were measured every four hours over 30 days, yielding 180 flux measurements. In Seropedica, $N_2O$ rates were measured every three hours over five days from five soil chambers, yielding 200 flux measurements. A similar diurnal $N_2O$ emission pattern was observed at both Seropedica and Edinburg, with PMTs from 09:00 to 10:00 and from 21:00 to 22:00. Laville, Lehuger, Loubet, Chaumartin, & Cellier, (2011) measured $N_2O$ emissions every 90 minutes from 6 soil chambers in a highly fertilized maize crop in the north of France. Soon after each N application and coinciding with rainfall, $N_2O$ emissions spiked. Diurnal variability was studied from a total of 864 flux measurements taken during 9 consecutive days when it did

not rain between the spikes in emissions. PMTs were found to be from 07:30 to 09:00 and from 18:00 to 19:30. Cumulative emissions computed using a single flux measurement taken each day at 08:15 or weekly at 12:45 were within 10% of the cumulative emissions computed using fluxes measured at 90 minute intervals.

Studies supporting the evidence of a diurnal pattern of $N_2O$ soil emissions based on large data sets of fluxes measured in fertilized crops concluded that the diurnal variability of the fluxes across different days or replicates (i.e. soil chambers) were not always the same. Due to the variability in diurnal patterns, the PMTs found in these studies are long periods of time, up to 12 hours a day. Reeves and Wang (2015) first reported diurnal variability of $N_2O$ emissions using a multiyear data set. Fluxes were measured every 2.5 hours over 3 consecutive years using three soil chambers, collecting approximately 25,000 fluxes. Soil $N_2O$ emissions were measured in southern Queensland, Australia in a wheat/barley rotation with conventional tillage and stubble retention management, receiving 90 Kg of N at planting. Diurnal emission patterns were observed during emissions rates higher than 20 g of $N\text{-}N_2O$ $ha^{-1}$ $day^{-1}$, usually occurring after rain and lasting for weeks. Diurnal fluctuations followed different patterns on different days and patterns were not consistent across replicates. However, the variation from the daily mean in emissions higher than 20 g of $N\text{-}N_2O$ $ha^{-1}$ $day^{-1}$ demonstrated a pronounced sinusoidal diurnal pattern. PMTs were found to be from 09:00 to 12:00 and from 18:00 to 24:00. Machado, Wagner-Riddle, MacTavish, Voroney, & Bruulsema, (2019) studied the diurnal variability of $N_2O$ soil emission from fields under different management practices during two periods of the year when $N_2O$ emissions were large. Data were collected from 2000 to 2006 and during 2015 in Ontario,

Canada and the fluxes selected for diurnal variability analysis belong to the 30 days period after the major spring-thaw events and the 45 day period after N fertilization or planting. During these periods $N_2O$ fluxes followed the diurnal pattern of soil temperature variation at 5-cm depth and PMTs were found in 12 hours of the day, from 09:00 to 12:00 and from 17:00 to 02:00

There is disagreement in the literature about the timing of PMTs, but also whether a PMT exists when fluxes are high. In highly fertilized systems, ephemeral $N_2O$ bursts, or *'hot moments'*, may last from hours to days, contribute to a large fraction of cumulative emissions, and often occur in response to triggers such as tillage, fertilization and rainfall (Baggs et al., 2003; Molodovskaya et al., 2012; Sehy, Ruser, & Munch, 2003; Yanai, Toyota, & Okazaki, 2004).

Fluxes measured in systems that received high amounts of nitrogen tended to result in high and variable fluxes which did not exhibit a diurnal pattern and no PMTs were found. In a series of short experiments, with measurement intervals varying from one to two hours and experimental periods ranging from one to five days, Blackmer, Robbins, & Bremner (1982) measured $N_2O$ emission rates using one soil chamber each in maize and fallow fields in Iowa. The measured fluxes were high and variable, ranging from 1 to 150 g of $N\text{-}N_2O$ $ha^{-1}$ $day^{-1}$. Blackmer et al. (1982) concluded that although they observed isolated and varying diurnal patterns, they could not find a single short period of time in each day that consistently yielded the smallest difference between the measured flux and the mean daily emission. Van der Weerden, Clough, & Styles, (2013) measured $N_2O$ emissions between 8 to 12 times per day over 22 to 28 days from four soil chambers placed on a pasture following bovine urine

fertilization. Urine was applied to 3 plots at N loadings of 486, 501 and 508 Kg N $ha^{-1}$. Peak emissions ranging from 120 up to 450 g of N-$N_2O$ $ha^{-1}$ $day^{-1}$ were observed in all plots and occurred soon after fertilization and following precipitation events. Three sampling seasons yielded a total of 1850 flux measurements. During the three sampling seasons a diurnal pattern was only observed during 12 of the 71 observed days. During a sampling campaign of 8 days, Laville, Jambert, Cellier, & Delmas (1999) measured $N_2O$ fluxes in highly fertilized maize plots in the south-east of France, beginning 6 days after injection of anhydrous ammonia. The maximum hourly flux measured was more than 600 g N-$N_2O$ $ha^{-1}$ $day^{-1}$ and often exceeded 175 g N-$N_2O$ $ha^{-1}$ $day^{-1}$. Laville et al. (1999) concluded that across the 8 sampling days there was no PMT and there was very high variation in the size and timing of the observed $N_2O$ fluxes.

Measuring soil emissions during short high emissions periods is only possible with intensive, high-frequency flux monitoring, so the literature on diurnal variability of $N_2O$ fluxes during high emission periods is limited and most of the short sampling campaigns that target such ‘hot periods’ do not provide information about the contribution of these ‘hot moments’ to the total annual cumulative emissions. Assessing the importance of $N_2O$ diurnal patterns during high emissions events requires capturing multiple high emissions periods during long-term sampling campaigns.

It is unclear from prior studies if, or under what circumstances, a PMT exists for $N_2O$ emissions from fertilized crop systems. Answering this question is important because sampling at a PMT could reduce the required frequency and cost of sampling, while maintaining or improving the accuracy of $N_2O$ emissions estimates. The literature is also

inconclusive about whether, when a PMT does exist, it varies over time or with the size of $N_2O$ flux. Previous studies have been unable to address these questions because generally they used limited data from short sampling campaigns that did not capture the large, episodic flux events which are a distinctive characteristic of $N_2O$ flux from highly fertilized crop lands. We answer these questions using high-frequency flux data collected over three years from highly fertilized corn grown in southern Wisconsin, USA. This analysis characterized diurnal variability to identify the existence of a PMT across seasons, years, and flux size regimes and quantitatively assessed the impact on cumulative emissions estimates of sampling at the PMT as influenced by flux magnitude and sampling frequency.

## *3. Materials and methods*

### *3.1. Experimental Site*

Soil $N_2O$ emissions were measured during three sampling campaigns at the University of Wisconsin Agricultural Research Station - Arlington (ARS-A) (43°17'41.2"N 89°21'28.1"W) in Columbia County (WI). To avoid interference from previous manure amendments the experiments were performed at different sites every year, the selected sites had a no manure application history during at least the three years immediately preceding our experiment. The three sites were within close proximity of one another (< 2.25 km). The soil at the three sites was a well-drained Plano silt loam soil (fine-silty, mixed, superactive, mesic Typic Argiudolls). The three sites had previously been cropped in a maize-soybean rotation with pre-planting shallow tillage (i.e., 0.1 m depth).

During the first sampling campaign in 2015, flux measurements were taken from April 2$^{nd}$ to October 25$^{th}$. Corn was planted on May 13$^{th}$ at a rate of 86000 seeds per ha (Renk Seed

ID# RK791SSTX) and the space between rows was 0.75 m. The crop received a total of 215 kg N $ha^{-1}$ in two applications: at planting and at vegetative growth stage 6 (V6). At planting, 68 kg N $ha^{-1}$ in the form of granular urea was applied in a fertilization band located 5 cm to the side and 5 cm below the seed. Fertilization at V6 was on June 10$^{th}$, at a rate of 147 kg N $ha^{-1}$ in the form of urea ammonium nitrate (UAN) 28% solution (30% urea, 40% ammonium nitrate and 30% water) applied between rows with knife injectors at a depth of 5 to 7 cm. Corn was harvested for grain on October 22$^{nd}$, yielding 14,400 kg of grain per ha. We will refer to this sampling campaign as 2015.

During the second and third campaigns, most nitrogen fertilizer was applied as dairy slurry manure at two different times during the fall. The second sampling campaign occurred from September 16$^{th}$ 2016 to July 5$^{th}$ 2017. We refer to this sampling campaign as 2016-2017. Dairy slurry was applied on September 15$^{th}$ in the early application plot and in November 16$^{th}$ in the late application plot. Corn was planted on May 8$^{th}$ and harvested on October 23$^{rd}$ 2017. The third sampling campaign occurred from September 12$^{th}$ 2017 to August 22$^{nd}$ 2018. We refer to this sampling campaign as 2017-2018. Dairy slurry was applied on September 11$^{th}$ in the early application plot and in November 13$^{th}$ in the late application plot. Corn was planted on May 8$^{th}$ and harvested on October 29$^{th}$.

The $N_2O$ fluxes measured during the 2016-2017 and 2017-2018 sampling campaigns are part of an ongoing experiment studying the effect of manure application timing on soil $N_2O$ emissions. During these two campaigns, fluxes were measured simultaneously from two contiguous plots, receiving the same amount of dairy slurry (65500 l $ha^{-1}$) either in mid-September (early) or mid-November (late). Manure slurry was collected from a single pit

which had been mixed thoroughly prior to collection on the same day of the application. The quantity of total N applied ranged from 95 to 155 kg N $ha^{-1}$ due to manure composition variability. The slurry was incorporated within 24 hours after application using a soil finisher (i.e., 0.1 m depth). Slurry application methods and rates were based on the Nutrient Application Guidelines for Crops in Wisconsin (Laboski & Peters, 2011). During both sampling campaigns corn was planted at a rate of 86000 seeds per ha (Pionner Seed ID# P0157AMX) and the space between rows was 0.75 m. At planting, 11 kg N $ha^{-1}$ in the form of granular urea was applied in a fertilization band located five cm to the side and five cm below the seed.

### *3.2. $N_2O$ fluxes and ancillary measurements*

Soil $N_2O$ emissions were measured at least every 2 hours using an automatic flux measurement system, which comprises a Los Gatos Research model 914-0027 $N_2O$ analyzer and four automatic soil chambers (Francis Clar et al., 2015; Anex, Francis Clar & Anex, 2015).

The ability to measure $N_2O$ concentration at both high rate and precision was key to keeping deployment times short (i.e., 10 to 20 minutes) and thereby obtaining high temporal resolution flux data. In continuous flow mode, the analyzer computes in 'real time' the $N_2O$ concentration of a gas stream (i.e., 100 cc $min^{-1}$) by integrating multiple laser absorption measurements (<3 milliseconds) over a user selected averaging time. An averaging time of 20 seconds was used, yielding a measurement precision (i.e., one standard deviation) of 1/1500 of the measured gas concentration ($1\sigma < 0.2$pbb at $[N_2O] \approx 300$ ppb). With these settings (sampling rate, deployment time and analytical precision) and the chamber

dimensions described below, the Minimum Detectable Flux (MDF) of the system is 9.2 x $10^{-5}$ g of N-$N_2O$ $ha^{-1}$ $day^{-1}$ for deployment times of 20 minutes and 3.7 x $10^{-4}$ g of N-$N_2O$ $ha^{-1}$ $day^{-1}$ for deployment times of 10 minutes. MDFs were computed following the method of Christiansen, Outhwaite, & Smukler (2015).

Four soil chambers were distributed over an area of approximately 40 $m^2$. During the 2015 sampling seasons two chambers were placed between plant rows directly on top of the fertilization band and the other two directly on the row. During the sampling seasons of 2016-2017 and 2017-2018 two chambers were used per plot, one placed between plant rows and one directly on the plant row. The chambers were only removed from the field during planting and fertilization and were placed back in their original position as soon as feasible (a few hours to two days) after planting or fertilizing. Any vegetation that grew within the chambers was removed by hand. The chambers were 0.35 m long by 0.20 m wide by 0.25 m tall ferromagnetic stainless steel open-ended boxes pressed into the soil approximately 0.05 m. Chamber tops were finished with a 25 mm rim to accommodate a magnetic gasket mounted on the underside of the chamber lids. Lids were made of a 12.7 mm thick HDPE plate which was supported by four levers, two at each side. Each pair of levers was mounted on steel tracks attached to both sides of the soil chambers. The opening and closing movements relied on an electrical linear actuator attached to the lid and a pull-solenoid controlling the rotation of the four levers (Francis Clar et al., 2015; Francis Clar & Anex, 2018).

After the 2016-2017 sampling season the soil chambers were rebuilt. The redesigned chamber volume was slightly larger and incorporated an improved closing mechanism.

Chambers used in the sampling campaign of 2017-2018 were 0.30 m long by 0.30 m wide by 0.20 m tall and the chamber lid levers were redesigned as two parallel four bar linkages.

The analyzer was connected to each of the four soil chambers with a gas path composed of two manifold valve assembles at the inlet and the outlet of the analyzer which diverted the continuous gas flow from the analyzer to the soil chambers and vice versa via a 30-meter-long closed loop made of Chemfluor ®FEP tubing (6.35 mm OD, 0.79 mm wall). Vents were installed in all chambers, no significant differences in pressure between the inside and the outside of the chamber were observed (Hutchinson & Livingston, 2001).

Synchronization between the soil chambers, the valve assemblies, and the analyzer was controlled by digital logic that allowed the user to customize the sampling sequence and the duration of the flushing and sampling periods. The digital logic included an interruption sequence triggered by an optical rain sensor that opened all chambers during precipitation events. The measurement system was flushed before each measurement to eliminate residual gas from the previous chamber sampling. During the flushing periods all chambers remained open (i.e. lids were retracted) and the gas path and the analyzer were flushed with ambient air for 10 minutes. Chamber sampling time was set to 20 minutes, except for short periods when high flux emissions were observed. During high emission periods a 10 minute sampling time was used, yielding temporal resolutions of 12 and 18 flux measurements per chamber per day for 20 and 10 minute sampling periods, respectively.

In addition to $N_2O$ flux measurements, soil temperature and moisture and weather data were recorded following Kladivko et al. (2014). Soil temperature and moisture were

measured at the quarter-row position (less than 4 meters radius from the soil chambers) every 15 minutes using five soil probes (5TM, Decagon Inc.) installed at depths of 10, 20, 40, 60 and 100 cm. Soil measurements were recorded using an em50 data logger (Decagon Inc.). Air temperature and rainfall measurements taken each 30 minutes were obtained from the Arlington-ARS Weather Station (43°17'48.0"N 89°23'03.4"W) located less than 2 km from the experimental sites.

### *3.3. $N_2O$ flux estimation*

Soil $N_2O$ gas flux was estimated from the change in gas concentration in the chamber headspace over time. Gas flux per unit soil area was estimated from the slope obtained by least-squares linear regression of the concentration of [$N_2O$] versus time (t) to estimate d[$N_2O$]/dt, as in Eq. (1).

$$N_2O_{flux} = H \frac{d[N_2O]}{dt} \quad (1)$$

where H is the ratio of the internal chamber volume to area of soil surface enclosed by the chamber. Flux of $N_2O$ is generally expressed in units of mole or mass of N-$N_2O$ per units of area and time (e.g., mol N-$N_2O$ $ha^{-1}$ $day^{-1}$ or g N-$N_2O$ $ha^{-1}$ $day^{-1}$) (Parkin et al., 2003).

Use of the high-precision, cavity enhanced laser absorption spectroscopy instrument, capable of measuring near-ambient levels of $N_2O$ enabled very short chamber deployment times (<0.25 h) and use of a linear flux calculation. Estimates of soil gas flux using surface chambers tend to underestimate actual emission rates because as the concentration of $N_2O$ in the headspace increases, the vertical concentration gradient driving diffusion of $N_2O$ into the chamber necessarily decreases (referred to as the ‘chamber effect’). The error resulting from

this inherent nonlinearity of $N_2O$ flux is minimized by using a nonlinear flux calculation or by maintaining a low $N_2O$ concentration in the chamber through short deployment times as done here (Venterea Spokas, & Baker, 2009; Parkin, Venterea, & Hargreaves, 2012).

Total chamber closure times used were either 20 minutes or 10 minutes, depending on flux intensity, the corresponding effective chamber deployment (i.e., sampling) times were 15 or 5 minutes respectively, after accounting for gas transport time in the sampling system. The analyzer sampling rate was set to 20 seconds yielding an approximate precision of 0.2 ppb and recording 45 or 15 $N_2O$ concentration measurements per a 15 or 5 minute chamber deployment time, respectively. Having such a large number of measurements allowed us to reliably detect and eliminate chamber effects by testing for linearity in the flux calculation and subsampling the data when necessary to assure flux linearity. The first step in the adaptive linear flux calculation was to estimate the flux (change in chamber headspace $N_2O$ concentration vs. time) and the corresponding coefficient of determination ($r^2$) using all data collected during the effective sampling period. If $r^2$ was smaller than 0.95, a new flux estimate (i.e., slope of $N_2O$ concentration vs. time) and corresponding $r^2$ were calculated using a subsample of the data. Subsamples were created by sequentially eliminating the last $N_2O$ concentration datum until the computed $r^2$ was larger than 0.95, with a minimum of 6 time-concentration data points. This adaptive linear flux calculation allowed us to minimize chamber effects without compromising the precision or accuracy of the flux estimates.

### *3.4. Data selection and statistical analysis*

Soil $N_2O$ flux estimates calculated from the chamber concentration measurements were screened to eliminate unreliable and *de minimis* flux measurements prior to statistical

analysis. Estimated fluxes that were below the MDF corresponding to the chamber closure time (e.g. < 3.7 x $10^{-4}$ g N-$N_2O$ $ha^{-1}$ $day^{-1}$ for 20 minute closure) were indistinguishable from zero flux and were removed from the flux dataset. These fluxes were removed rather than included as zero flux because in this unsupervised system it is impossible to differentiate between fluxes below the MDF and those resulting from a chamber failure. In addition, we screened for unreliable flux estimates resulting from occasional malfunctions of the unsupervised measurement system that occurred when a chamber failed to open or failed to close. For example, a chamber might not close or open if ice build-up blocked the chamber lid linkage during a freezing rain. A flux estimate was deemed unreliable and rejected due to failure of a chamber to close when the measured chamber $N_2O$ concentrations at the beginning and end of the sampling period were both within ± 2 times the instrument precision (0.4 ppbv) of the ambient atmospheric $N_2O$ concentration. If a chamber failed to open, it would remain closed through a complete 2 hour cycle of sampling all four chambers, and the chamber headspace $N_2O$ concentration would be in equilibrium with the $N_2O$ concentration in the soil or very nearly to. Therefore, a flux estimate was deemed rejected due to failure of a chamber to open when the measured chamber $N_2O$ concentration at the beginning of the sampling period was greater than the ambient atmospheric $N_2O$ concentration by +2 times the instrument precision and the chamber $N_2O$ concentration at the end of the sampling period was within ± 2 times the instrument precision (0.4 ppbv) of the chamber $N_2O$ concentration at the beginning of the sampling period. Ambient atmospheric $N_2O$ concentration was measured by sampling the ambient air 2 m above the instrumentation trailer during the 5 minutes prior to chamber closure. After data filtering no negative fluxes were observed.

Capturing the daily variability of $N_2O$ fluxes is essential to testing the hypothesis that sampling at one particular time of the day is a reasonable approximation of the mean daily flux. Consequently, only days with a minimum of 6 flux measurements and with gaps between flux measurements of no more than 4 hours were included in the analysis. That is, only the high time-resolution flux data were analyzed.

The '*daily flux'* of $N_2O$ at each chamber (g $N\text{-}N_2O$ $ha^{-1}day^{-1}$) was computed as the integral over 24 hours of the individual flux estimates at that chamber on a specific day. '*Mean daily flux'* at a chamber was calculated as the daily flux at that chamber divided by 24. The annual '*cumulative flux'* at each chamber was computed as the sum of the daily fluxes over a year.

The similarity between the mean daily flux and a flux recorded at a specific hour of the day was assessed through a linear regression following the methods of Alves et al., 2012; and Cosentino et al., 2012. All estimated fluxes were binned into one of 24, one-hour, intervals according to the hour of the day when the chamber deployment began (the '*sampling interval*'). The common logarithm of all fluxes recorded during a particular sampling interval (the *'hourly fluxes'*) were regressed on the common logarithm of the corresponding mean daily flux and chamber using least squares regression with zero intercept, Eq. (2). Logarithmic transformation was necessary to meet linear model assumptions (i.e. normality and heteroscedasticity) and allowed inclusion in the analysis of very large fluxes that would otherwise be identified as outliers. The logarithmic transformation reduces the relative importance of the larger fluxes in the regression analysis.

$$log_{10}(mean\ daily\ flux_{chamber,day}) = \beta_{hour} \times log_{10}(hourly\ flux_{chamber,day,hour}) \quad (2)$$

The regression coefficient β is referred to as the '*deviation coefficient'* or simply 'β'. The statistical significance of the difference between the mean daily flux and the flux measured during a particular sampling interval was tested (t-test, p value < 0.05) by comparing the regression coefficient β to a value of 1.

The magnitude of soil $N_2O$ flux can be highly variable on weekly, monthly, seasonally and annual scales due to variations in the levels of available oxygen, nitrogen, and carbon in the soil. The mechanisms controlling the availability of these limiting resources, and therefore the size of the soil $N_2O$ flux, are expected to vary both seasonally and with events like precipitation, tillage and fertilization. Therefore statistical analysis was performed using all available flux estimates and subsequently using subsets of the individual flux estimates grouped by normalized size of cumulative daily flux.

The normalized cumulative daily flux size was calculated for each chamber and each year as the ratio between the daily flux and the cumulative flux. To create the data subsets we computed a new variable referred to here as 'cumulative contribution'. Cumulative contribution was computed as the result of successive additions of normalized cumulative daily fluxes that were sorted by size in descending order. For example, if the 3 top normalized daily fluxes were 2%, 1.5% and 1% the resulting cumulative contributions for each successive normalized daily flux would be 2%, 3.5% and 4.5%. Using values of cumulative contribution as breaking points we created four subsamples of flux estimates:

75% High Cumulative Contribution (HCC), 50% HCC, 25% HCC and 50% Low Cumulative Contribution (LCC). In an HCC sample, the fluxes included in the subsample are from days that are above the cumulative contribution threshold while the fluxes included in the LCC subsample are from days below the cumulative contribution threshold. For example, the 50% HCC includes all estimated fluxes from the days included in the set of largest daily fluxes which sum to 50% of the cumulative flux. Similarly, the 50% LCC includes all estimated fluxes from the days included in the set of the smallest daily fluxes which sum to 50% of the cumulative flux.

## *4. Results*

The number of flux estimates that were below the MDF or deemed to be unreliable due to a sampling system malfunction represented 13%, 48% and 15% of the total measured fluxes during 2015, 2016-2017 and 2017-2018, respectively. From the remaining 23,793 fluxes, 21,865 were estimated with high temporal resolution, accounting for 551, 373 and 1,093 chamber-days of high frequency flux measurements, gathered during the 2015, 2016-2017 and 2017-2018 sampling seasons, respectively (Fig 1). In sum, high temporal resolution flux measurements represented 2,017 days with an average temporal resolution of 11 fluxes per day. The average number of data pairs (mean daily flux and hourly flux) used to estimate the deviation coefficients (β) for the whole data set and across the 24-hour intervals was 912. The 50% and 25% HCC subsamples contained the fewest flux measurements (Fig. 1, panel (d) left plots), for these subsamples β values were, on average, computed from 55 and 27 measurements, respectively.

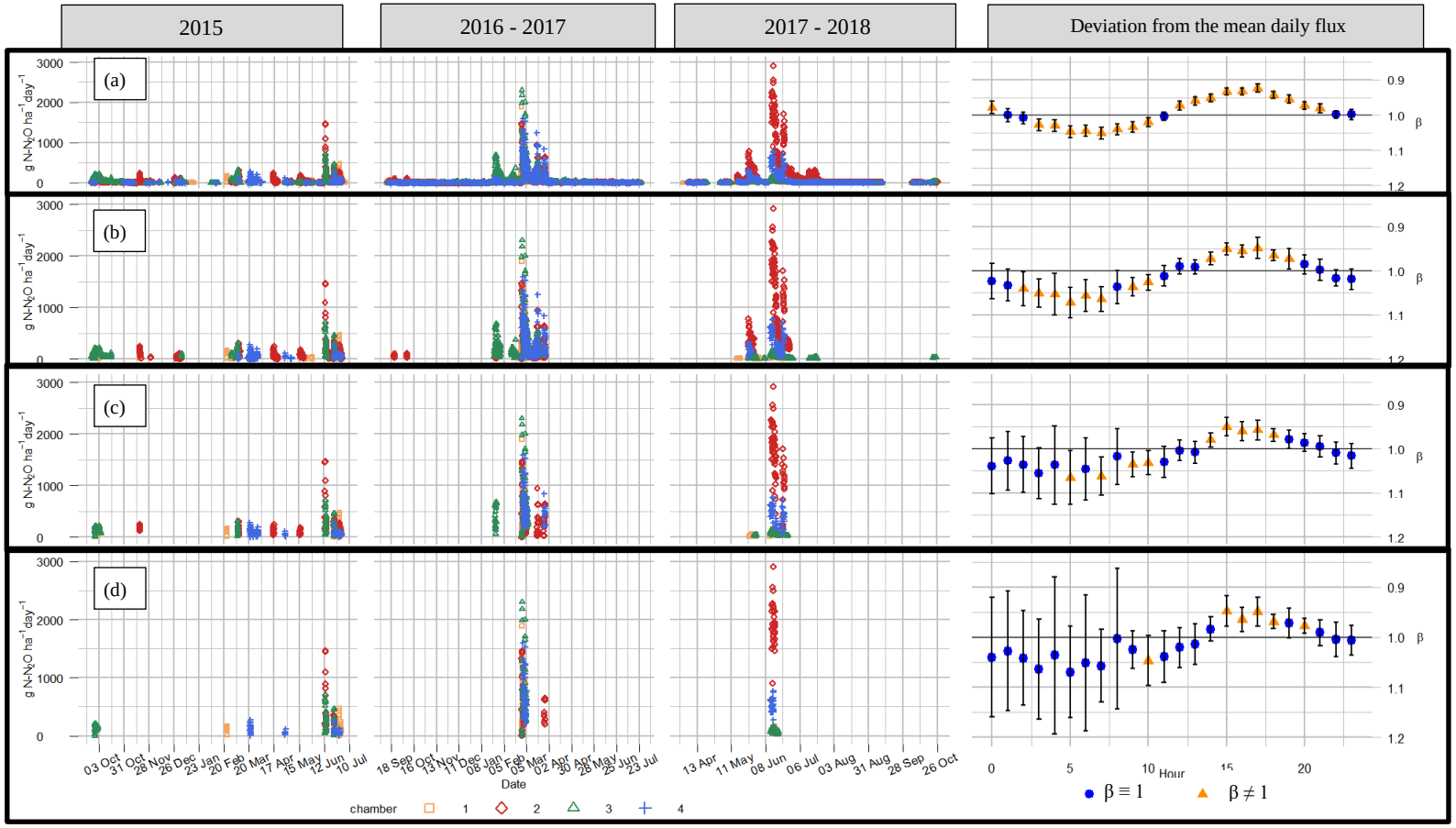


**Figure 1. $N_2O$ fluxes from three sampling campaigns (left columns) and the diurnal deviation of the mean hourly flux from the mean daily flux (far right column).** The rows (a, b, c and d) are the fluxes and diurnal deviation of the largest fluxes that account for a cumulative contribution of 100%, 75%, 50% and 25% of total emissions, respectively. These account for 100%, 15%, 6% and 3% of the total observations, respectively. The deviation coefficient β was computed by least squared regression of the logarithm of the mean daily flux on the logarithm of the flux measured during certain hour of the day $\boldsymbol{log_{10}(mean\ daily\ flux_{chamber,day}) = \beta_{hour} \times log_{10}(hourly\ flux_{chamber,day,hour})}$. Blue circles indicate no significant difference between β and 1 (p value >0.05). Vertical bars are 95% confidence intervals. Variability and uncertainty of the deviation coefficient β is highest for the largest fluxes (shown in row (d): 25% of the total flux from 3% of the total observations).

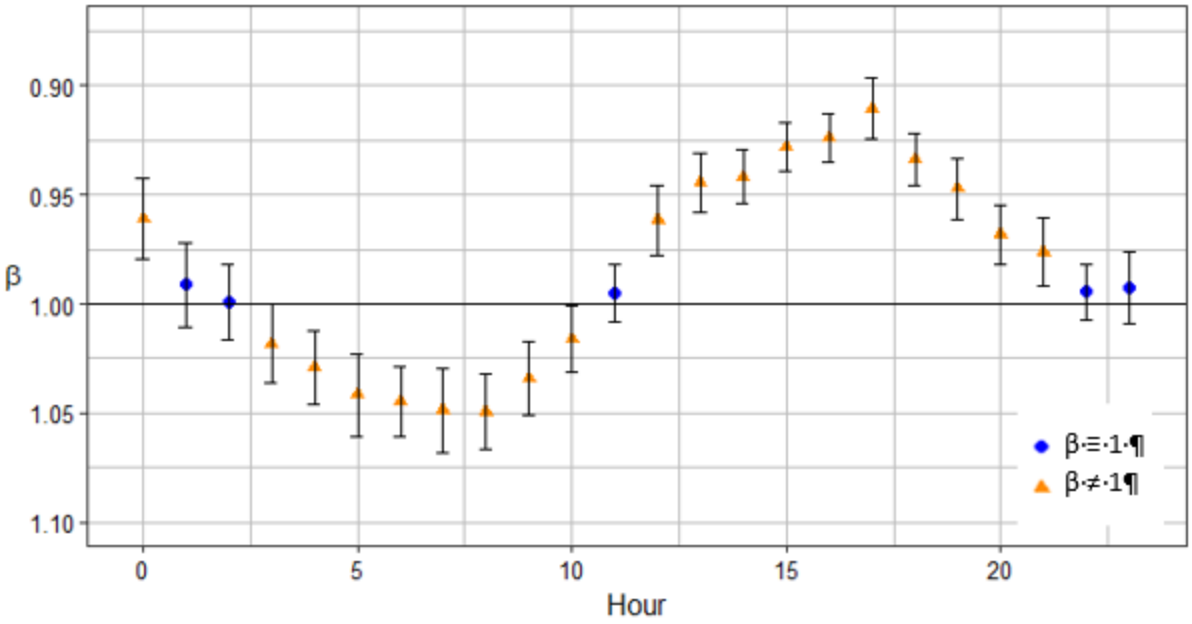


**Figure 2.** Diurnal deviation of average hourly flux relative to the mean daily flux for the smallest fluxes. The diurnal deviation coefficient, β, was computed by least squares regressions of the logarithm of the mean daily flux on the logarithm of the flux measured at a certain hour of the day $\boldsymbol{log_{10}(mean\ daily\ flux_{chamber,day})} = \boldsymbol{\beta_{hour}} \times \boldsymbol{log_{10}(hourly\ flux_{chamber,day,hour})}$. Blue circles indicate no significant difference between β and 1 (p value < 0.05), and vertical bars are 95% confidence intervals. The β values shown were computed for low flux periods (the smallest fluxes which contributed to 50% of the total emissions, representing 85% of the total observations) they are relatively consistent across the hours of the day and their associated uncertainties are also relatively uniform and small.

The β values computed for all hourly sampling periods and data subsamples (HCC, LCC, seasons and sampling campaigns) were significant (p value < 0.05); β values ranged from 0.82 to 1.1. The coefficients of determination ($r^2$) ranged from 0.78 to 1, indicating that the variability of the mean daily flux was well explained by the flux measured during each period. In general the $r^2$ values for regressions of the fluxes measured between 00:00 to 12:00 were smaller than the $r^2$ associated with fluxes measured between 12:00 to 23:00 (data not shown).The largest variability of β values was observed at the subsampling levels of 50% and 25% HCC, for regressions of the fluxes measured between 00:00 and 09:00 (Fig. 1 Panels (c) and (d), right)

When examined as a whole, the $N_2O$ flux estimates exhibited a clear diurnal pattern. Relative to the mean daily flux, $N_2O$ flux was generally lower in the morning and higher in the afternoon. The β values computed from fluxes observed during the sampling intervals beginning between 03:00 and 10:00 were greater than 1, while the values of β for the sampling intervals beginning between 13:00 and 22:00 were less than 1 (Fig. 1, Panels (a) and (b), right, and Fig. 2).

The maximum β value (1.052) was associated with fluxes observed during the 07:00 sampling interval. The β values for sampling intervals after 07:00 decreased monotonically toward the minimum (0.923) in the 17:00 interval. The value of β for fluxes observed at sampling intervals beginning at 01:00, 02:00, 11:00, 22:00, and 23:00 were not significantly different from one (p value > 0.05) (Fig. 1, panel (a) right).

The β values observed from the subsamples at 75%, 50%, and 25% HCC level were largest at 05:00 and smallest at 15:00; except for the subsample at 75% HCC level which exhibited a minimum β at 07:00 (Fig. 1 Panels (b), (c) and (d), right). The β values for the high cumulative contribution (50% and 25% HCC) subsamples did not follow a smooth diurnal pattern as observed in the full data set.

## *5. Discussion*

To our knowledge this is the first multiyear study of diurnal variability of soil $N_2O$ emissions in highly fertilized agronomic systems in which ephemeral bursts of $N_2O$ emissions (e.g. 'hot moments') were measured at high temporal resolution. The results show that the diurnal variability of $N_2O$ soil fluxes varies with flux intensity, represented here as the cumulative contribution to cumulative emissions.

In the 50% LCC group, $N_2O$ soil fluxes exhibited a diurnal pattern in which $N_2O$ fluxes increased beginning at sunrise and decreased during the night (Fig. 2). In this experiment, PMTs were during the hours beginning at 01:00, 02:00, 11:00, 22:00 and 23:00 (Fig. 2). The diurnal pattern and PMTs identified during analysis of the set of all flux estimates were the same as those identified through analysis of the set of low flux estimates (Fig. 1, Panel (a), Right). This is not surprising since the low flux estimates represent approximately 85% of the total number of estimated fluxes. Since low emissions are the most common state and these tend to show diurnal variability, studies that use small data sets are likely to find PMTs (Table S1). The tendency of $N_2O$ soil flux to exhibit a diurnal pattern has been observed in many previous studies, however, these studies have often identified different PMTs (Table S1).

Because the diurnal pattern of $N_2O$ emissions is usually related to soil temperature (Table S1), it is expected that under different experimental conditions (e.g. location, season, etc.), PMTs will occur at different times of the day (Akiyama, Tsuruta & Watanabe, 2000; Flessa et al., 2002; Thies et al., 2019). Analysis of our flux data grouped by season showed that a diurnal pattern was evident during all four seasons, and the duration and timing of the PMTs varied between seasons (data not shown). To our knowledge Alves et al., (2012) is the only study of diurnal variability in which PMTs coincide for contrasting locations (UK and Brazil), this might result from equivalent diurnal temperature patterns at both locations during the observation periods. When we analyzed our data at a chamber level we observed that generally the diurnal pattern of the fluxes and the PMTs from all chambers within a season were equivalent (data not shown). The only exception occurred during the 2015 sampling season, when fluxes from one chamber exhibited an inverted diurnal pattern with respect to the other three chambers (i.e., flux decreased after sunrise and increased during the night). This inverted pattern could be related

to limited soil nitrogen availability and the role of plants in regulating the microbial processes associated with $N_2O$ exchange as suggested by Shurpali et al. (2016). Because N fertilization and emissions rates in our experiments were much higher than those of Shurpali et al. (2016), we believe that a more logical explanation is that the dominant source of $N_2O$ production in this chamber was at a depth where soil temperature changes lagged the other three chambers as suggested by Dusza et al., (2020) and Parkin (1987). Although the fluxes measured in this one chamber exhibited an inverted diurnal pattern relative to the others, the PMTs found for the four chambers were the same.

Although the experimental conditions of the studies that have reported a diurnal pattern of $N_2O$ flux vary widely, the range of $N_2O$ fluxes observed during these experiments is mostly within the range of the set of low emissions (50% LCC) defined in this study (0.04 to 723, 0.08 to 90.64, and 0.04 to 344.6 g of N-$N_2O$ $ha^{-1}$ $day^{-1}$ for the sampling seasons of 2015, 2016-2017, and 2017-2018 respectively). This is consistent with the hypothesis that low emissions systems tend to exhibit a diurnal pattern (summarized for the literature cited in Table S1).

During the high emissions periods of our experiments, $N_2O$ fluxes did not exhibit a diurnal pattern and thus there was no PMT (Fig. 1, Panels (c) and (d), right). During these periods, measuring in the afternoon between 14:00 and 18:00 tends to overestimate the mean daily flux. Our observations of increasing fluxes in the afternoon are supported by Christensen (1983) and Parkin (2008). We suggest avoiding afternoon sampling when possible. In this study, high emission periods were the result of peaks of $N_2O$ flux lasting from one to several days (Fig. 1, Panels (c) and (d), left). These very high fluxes were triggered by precipitation events following fertilization and/or soil thaw, but forecasting when (e.g. day) the flux peak will occur is extremely difficult (Molodovskaya et al., 2012; Singurindy, Molodovskaya, Richards, & Steenhuis, 2009). Although high emissions periods observed in this study

represent less than 6% of the total flux data, they contributed as much as 50% of total annual emissions. Peak $N_2O$ fluxes like those observed during the high emission periods in this study have been characterized as 'hot moments' or 'hot periods' which occur most frequently in highly fertilized crops and have been observed most frequently in the upper Midwest region of the US (Groffman et al., 2009; Molodovskaya et al., 2012; Wagner-riddle et al., 2007). This study is the first to analyze diurnal variability of $N_2O$ soil emissions during hot moments and hot periods from multiple years and under a range of weather conditions and occurring following both summer fertilization and spring soil thaw. Diurnal variability studies carried out in crop systems in which peak emission events occur, support our observations during high emissions periods. Blackmer et al., (1982) measured $N_2O$ soil emissions from highly fertilized corn systems in the Midwest of the US, at sub-daily intervals during short sampling campaigns (i.e. days); the observed fluxes did not exhibit a PMT. Laville et al., (1999) studied the diurnal variability of $N_2O$ soil emissions measured during a 'hot period' lasting six days and occurring after precipitation following the injection of 200 kg N $ha^{-1}$ in a corn crop in the south-west of France. During this high emission period, $N_2O$ fluxes were highly variable at the hourly scale and did not exhibit a diurnal pattern. Šimek, Brůček, & Hynšt, (2010) measured $N_2O$ fluxes from a cattle overwintering area, the extremely high $N_2O$ emissions observed during soil thaw did not exhibit a diurnal pattern.

In our experiments, high emissions periods (25% HCC), represent only 6% of the total observations but 25% of the cumulative emissions (Fig. 1, Panels (d), left). On average across the three years, the beta coefficient for each hour during the 25% HCC is computed from data gathered on just 27 days. In average the amount of $N_2O$ emitted in one day during the high emission period, account for 0.93% (i.e., 25% / 27) of the cumulative emissions. This is similar for the 50% HCC fluxes, one day's measured emissions during this period is 0.91% (i.e., 50% / 55) of the cumulative emissions. On the other hand,

emissions during low emissions periods represent 50% of the cumulative emissions, and on average, emissions data from 912 days are used to compute the beta coefficients. One day's measured emissions during low emissions periods (LCC 50%) is only 0.056% (50% / 912) of the cumulative emissions. Thus, getting one accurate measurement during the high emissions periods (50% and 25% HCC) is more important than measuring 17 times during low emissions periods (50% LCC) (0.91% / 0.056% = 16.6). Our observations related with the importance of capturing high emissions periods are supported by others (Barton et al., 2015; Parkin, 2008; Rowlings, Grace, Kiese, & Weier, 2012; Saha, Kemanian, Rau, Adler, & Montes, 2017). This is the first study in which the importance of capturing high emissions periods is quantified with analysis of fluxes measured over extended periods with high temporal resolution.

An important question for those with limited sampling capacity is how less frequent sampling at a PMT impacts the accuracy of the estimated cumulative emissions. This question, however, is difficult to answer even with our large dataset. The accuracy of estimates made with a particular sampling interval depends on the relative timing of the emissions peaks and flux measurements. Because the emissions profile (i.e., the number, size and duration of the emissions peaks) changes with the local soil conditions, crop management, and weather, the impact of less frequent sampling is not consistent from year-to-year or from location-to-location. For example, the relative accuracy of cumulative emissions estimated by sub-sampling our high temporal resolution data once every three days during the 11:00 PMT ranged from 29% below, to 45% above, the cumulative emissions estimated from the high temporal resolution flux measurements, depending on the year and which day of the three-day sampling cycle the sampling began (details provided in supplement S2). The accuracy of a cumulative emissions estimate based on infrequent sampling depends on the duration of the peak emission events and when the fluxes were

measured relative to those peak emissions. Depending on the relative timing of measurement and peak emissions, peak events may be fully, partially, or not captured at all (see Figure S1). In highly fertilized systems like the one studied here, accurate estimates of annual cumulative emissions require sub-daily sampling during peak emissions periods.

Because in the crop system studied in this article ephemeral high emissions periods did not exhibit a diurnal pattern of $N_2O$ flux and represented up to 50% of the cumulative flux, measuring $N_2O$ fluxes once a day during a PMT would not guarantee accurate estimation of cumulative flux. That is to say that during high emissions periods measuring frequently is more important than choosing the time of day to sample. We do not dispute the benefit of sampling at the PMT when a diurnal cycle is observed. In other systems in which episodic peaks of $N_2O$ emissions are absent or are very rare (Barton et al., 2015; Pennock, Yates, & Braidek, 2006), measuring soil $N_2O$ flux at the PMT could possibly be an appropriate way to estimate daily and cumulative emissions (Reeves, Wang, Salter, & Halpin, 2016; Reeves & Wang, 2015). However, the recommendations of a PMT sampling in previous research, based on very limited data (Table S1) engender false confidence that sampling daily at a particular time is sufficient to yield good estimates of daily and cumulative emissions. We emphasize that such confidence is misplaced.

### *6. Conclusion*

This is the first study in which multi-year and high temporal resolution $N_2O$ soil flux data from a highly fertilized corn system in the Midwest US were used to study diurnal variability. Our goal was to develop reasonable sampling strategies to reduce sampling frequency or to improve sampling estimates. We found that in this system, diurnal variability of $N_2O$ emissions is closely related to flux intensity. We did not, however, find any clear relationships between the soil flux intensity and observed soil

temperature, soil moisture, or air temperature. During low emission periods, $N_2O$ soil fluxes exhibited a diurnal pattern so that flux during the PMTs was not significantly different from the mean daily emissions. During high emission periods, however, $N_2O$ soil fluxes did not exhibit a diurnal pattern and there was no PMT. High emission periods were observed every year and comprised both single and multi-day $N_2O$ flux peak events that contributed up to half of the cumulative $N_2O$ emissions while representing less than 6% of the total observations. Because emissions during peak events did not exhibit a diurnal pattern and PMTs, accurate estimation of cumulative emissions during these events required $N_2O$ flux measurements at sub-daily sampling intervals. In highly managed cropping systems of this type that account for a majority of anthropogenic $N_2O$ emissions, peak flux periods often dominate cumulative emissions. In such systems, accurate cumulative $N_2O$ flux estimates require frequent sampling, particularly during peak flux periods. The high temporal resolution data collected in this study can improve the ability of $N_2O$ emissions models to predict peak emission periods and enable the deployment of increased sampling when it is most valuable.

## *7. Acknowledgments*

The authors are grateful to the personnel of the Arlington Agricultural Research Station. We thank our colleagues: Mark Allie, Kody Habeck, Lawrence G. Oates, Andy Larson, Todd. W. Andraski and Carrie Laboski for material and intellectual support in this research. This material is based upon work that was supported by the National Institute of Food and Agriculture, U.S. Department of Agriculture, Hatch projects under accession numbers 1001805 and 1009785.

## *8. References*


Akiyama, H., Tsuruta, H., & Watanabe, T. (2000). N2O and NO emissions from soils after the application of different chemical fertilizers. *Chemosphere - Global Change Science*, *2*(3–4), 313–320. https://doi.org/10.1016/S1465-9972(00)00010-6

Alves, B. J. R., Smith, K. A., Flores, R. A., Cardoso, A. S., Oliveira, W. R. D., Jantalia, C. P., Urquiaga, S., & Boddey, R. M. (2012). Selection of the most suitable sampling time for static chambers for the estimation of daily mean $N_2O$ flux from soils. *Soil Biology and Biochemistry*, *46*, 129–135. https://doi.org/10.1016/j.soilbio.2011.11.022

Anex, R. P., Francis Clar, J., Anex, B. B. (December 2015). Near-Continuous Isotopic Characterization of Soil $N_2O$ Fluxes from Maize Production. Measurements and Modeling of Stable Isotopes to Advance Understanding of Non-$CO_2$ Greenhouse Gas Cycling and Budgets Posters. American Geophysical Union (AGU) Fall Meeting 2015, San Francisco, CA.

Baggs, E. M., Richter, M., Hartwig, U. A., & Cadisch, G. (2003). Nitrous oxide emissions from grass swards during the eighth year of elevated atmospheric pCO2 (Swiss FACE). *Global Change Biology*, *9*(8), 1214–1222. https://doi.org/10.1046/j.1365-2486.2003.00654.x

Barton, L., Wolf, B., Rowlings, D., Scheer, C., Kiese, R., Grace, P., Stefanova, K., & Butterbach-Bahl, K. (2015). Sampling frequency affects estimates of annual nitrous oxide fluxes. *Scientific Reports*, *5*(1), 15912. https://doi.org/10.1038/srep15912

Blackmer, A. M., Robbins, S. G., & Bremner, J. M. (1982). Diurnal Variability in Rate of Emission of Nitrous Oxide from Soils1. *Soil Science Society of America Journal*, *46*(5), 937. https://doi.org/10.2136/sssaj1982.03615995004600050011x

Christensen, S. (1983). Nitrous oxide emission from a soil under permanent grass: Seasonal and diurnal fluctuations as influenced by manuring and fertilization. *Soil Biology and Biochemistry*, *15*(5), 531–536. https://doi.org/10.1016/0038-0717(83)90046-9

Christiansen, J. R., Outhwaite, J., & Smukler, S. M. S. M. (2015). Comparison of CO2, CH4 and N2O soil-atmosphere exchange measured in static chambers with cavity ring-down spectroscopy and gas chromatography. *Agricultural and Forest Meteorology*, *211–212*, 48–57. http://linkinghub.elsevier.com/retrieve/pii/S0168192315001835

Cosentino, N. V. R., Fernandez, P. L., Figueiro Aureggi, S. A., & Taboada, M. A. (2012). N2O emissions from a cultivated mollisol: optimal time of day for sampling and the role of soil temperature. *Revista Brasileira de Ciência Do Solo*, *36*(6), 1814–1819. https://doi.org/10.1590/S0100-06832012000600015

Dusza, Y., Sanchez-Cañete, E. P., Galliard, J. F. Le, Ferrière, R., Chollet, S., Massol, F., Hansart, A., Juarez, S., Dontsova, K., Haren, J. van, Troch, P., Pavao-Zuckerman, M. A., Hamerlynck, E., & Barron-Gafford, G. A. (2020). Biotic soil-plant interaction processes explain most of hysteric soil CO2 efflux response to temperature in cross-factorial mesocosm experiment. *Scientific Reports*, *10*(1), 1–11. https://doi.org/10.1038/s41598-019-55390-6

Flessa, H., Ruser, R., Schilling, R., Loftfield, N., Munch, J. C., Kaiser, E. A., & Beese, F. (2002). N2O and CH4 fluxes in potato fields: Automated measurement, management effects and temporal variation. *Geoderma*, *105*(3–4), 307–325. https://doi.org/10.1016/S0016-7061(01)00110-0

Francis Clar, J., Anex, R. P., Allie M., Elwood, C., Rigel, I., & Lunzer, B. (November 2015). A Novel System for High-Resolution, Near-Continuous Measurement of Soil N2O Isotope Fluxes. Improving Accuracy and Precision of Soil Carbon and Greenhouse Gas Emission Measurements and Quantification: I. Synergy in Science: Partnering for solutions (ASA, CSSA & SSSA) 2015 Annual Meeting. Minneapolis, MN.

Francis Clar, J., & Anex, R. P. (July 2018). Automatic system for long-term monitoring of soil N2O isotope flux at high temporal and spatial resolution. Crop and Soil Sensing - Part 1. *ASABE 2018 Annual International Meeting*. Detroit, MI. https://doi.org/10.13031/aim.201800878

Groffman, P. M., Butterbach-Bahl, K., Fulweiler, R. W., Gold, A. J., Morse, J. L., Stander, E. K., Tague, C., Tonitto, C., & Vidon, P. (2009). Challenges to incorporating spatially and temporally explicit phenomena (hotspots and hot moments)

in denitrification models. *Biogeochemistry*, *93*(1–2), 49–77. https://doi.org/10.1007/s10533-008-9277-5

Hutchinson, G. L., & Livingston, G. P. (2001). Vents and seals in non-steady-state chambers used for measuring gas exchange between soil and the atmosphere. *European Journal of Soil Science*, *52*(4), 675–682. https://doi.org/10.1046/j.1365-2389.2001.00415.x

IPCC. (2011). Intergovernmental Panel on Climate change, Special Report on Renewable Energy Sources and Climate Change Mitigation. In Prepared by Working Group III of the Intergovernmental Panel on Climate Change . Cambridge Univ. Press, Cambridge, UK and New York, NY. https://www.ipcc.ch/report/renewable-energy-sources-and-climate-change-mitigation/

Kladivko, E. J., Helmers, M. J., Abendroth, L. J., Herzmann, D., Lal, R., Castellano, M. J., Mueller, D. S., Sawyer, J. E., Anex, R. P., Arritt, R. W., Basso, B., Bonta, J. V., Bowling, L. C., Cruse, R. M., Fausey, N. R., Frankenberger, J. R., Gassman, P. W., Gassmann, A. J., Kling, C. L., … Villamil, M. B. (2014). Standardized research protocols enable transdisciplinary research of climate variation impacts in corn production systems. *Journal of Soil and Water Conservation*, *69*(6), 532–542. https://doi.org/10.2489/jswc.69.6.532

Laboski, C. A. M., & Peters, J. B. (2011). Nutrient application guidelines crops in Wisconsin. *UW Extension. Cooperative Extension*, 94. https://www.rockriverlab.com/file_open.php?id=123

Laville, P., Lehuger, S., Loubet, B., Chaumartin, F., & Cellier, P. (2011). Effect of management, climate and soil conditions on N2O and NO emissions from an arable crop rotation using high temporal resolution measurements. *Agricultural and Forest Meteorology*, *151*(2), 228–240. https://doi.org/10.1016/J.AGRFORMET.2010.10.008

Laville, P., Jambert, C., Cellier, P., & Delmas, R. (1999). Nitrous oxide fluxes from a fertilised maize crop using micrometeorological and chamber methods. *Agricultural and Forest Meteorology*, *96*(1–3), 19–38. https://doi.org/10.1016/S0168-1923(99)00054-4

Maag, M., & Vinther, F. P. (1996). Nitrous oxide emission by nitrification and denitrification in different soil types and at different soil moisture contents and temperatures. *Applied Soil Ecology*, *4*(1), 5–14. https://doi.org/10.1016/0929-1393(96)00106-0

Machado, P. V. F., Wagner-Riddle, C., MacTavish, R., Voroney, P. R., & Bruulsema, T. W. (2019). Diurnal Variation and Sampling Frequency Effects on Nitrous Oxide Emissions following Nitrogen Fertilization and Spring-Thaw Events. *Soil Science Society of America Journal*, *83*(3), 743–750. https://doi.org/10.2136/sssaj2018.10.0365

Molodovskaya, M., Singurindy, O., Richards, B. K., Warland, J., Johnson, M. S., & Steenhuis, T. S. (2012). Temporal Variability of Nitrous Oxide from Fertilized Croplands: Hot Moment Analysis. *Soil Science Society of America Journal*, *76*(5), 1728. https://doi.org/10.2136/sssaj2012.0039

Parkin, T. B. (1987). Soil Microsite as a Source of Denitrification Variability. *Soil Science Society of America Journal*, *51*(5), 1194. https://doi.org/10.2136/sssaj1987.03615995005100050019x

Parkin, T. B. (2008). Effect of Sampling Frequency on Estimates of Cumulative Nitrous Oxide Emissions. *Journal of Environment Quality*, *37*(4), 1390. https://doi.org/10.2134/jeq2007.0333

Parkin, T. B., Mosier, A., Smith, J., Venterea, R., Johnson, J., Reicosky, D., Doyle, G., Mccarty, G., & Baker, J. (2003). *U.S. Department of Agriculture - Agricultural ressearch service Greenhouse gas Reduction through Agricultural Carbon Enhancement network (USDA-AR S GRAC Enet) Chamber-based Trace Gas Flux Measurement Protocol*.

Parkin, T. B., Venterea, R. T., & Hargreaves, S. K. (2012). Calculating the detection limits of chamber-based soil greenhouse gas flux measurements. *Journal of Environmental Quality*, *41*(3), 705–715. https://doi.org/10.2134/jeq2011.0394

Pattey, E., Edwards, G. C., Pennock, D. J., Smith, W., Grant, B., & MacPherson, J. I. (2007). Tools for quantifying N2O emissions from agroecosystems. *Agricultural and Forest Meteorology*, *142*(2–4), 103–119. https://doi.org/10.1016/J.AGRFORMET.2006.05.013

Pennock, D. J., Yates, T. T., & Braidek, J. T. (2006). Towards optimum sampling for regional-scale $N_2O$ emission monitoring in Canada. *Canadian Journal of Soil Science*, *86*(3), 441–450. https://doi.org/10.4141/S05-104

Reeves, S., & Wang, W. (2015). Optimum sampling time and frequency for measuring $N_2O$ emissions from a rain-fed cereal cropping system. *Science of the Total Environment*, *530–531*, 219–226. https://doi.org/10.1016/j.scitotenv.2015.05.117

Reeves, S., Wang, W., Salter, B., & Halpin, N. (2016). Quantifying nitrous oxide emissions from sugarcane cropping systems: Optimum sampling time and frequency. *Atmospheric Environment*, *136*, 123–133. https://doi.org/10.1016/j.atmosenv.2016.04.008

Rowlings, D. W., Grace, P. R., Kiese, R., & Weier, K. L. (2012). Environmental factors controlling temporal and spatial variability in the soil-atmosphere exchange of CO2, CH4 and N2O from an Australian subtropical rainforest. *Global Change Biology*, *18*(2), 726–738. https://doi.org/10.1111/j.1365-2486.2011.02563.x

Saha, D., Kemanian, A. R., Rau, B. M., Adler, P. R., & Montes, F. (2017). Designing efficient nitrous oxide sampling strategies in agroecosystems using simulation models. *Atmospheric Environment*, *155*, 189–198. https://doi.org/10.1016/j.atmosenv.2017.01.052

Sehy, U., Ruser, R., & Munch, J. C. (2003). Nitrous oxide fluxes from maize fields: relationship to yield, site-specific fertilization, and soil conditions. *Agriculture, Ecosystems & Environment*, *99*(1–3), 97–111. https://doi.org/10.1016/S0167-8809(03)00139-7

Shurpali, N. J., Rannik, Ü., Jokinen, S., Lind, S., Biasi, C., Mammarella, I., Peltola, O., Pihlatie, M., Hyvönen, N., Räty, M., Haapanala, S., Zahniser, M., Virkajärvi, P., Vesala, T., & Martikainen, P. J. (2016). Neglecting diurnal variations leads to uncertainties in terrestrial nitrous oxide emissions. *Scientific Reports*, *6*(1), 25739. https://doi.org/10.1038/srep25739

Šimek, M., Brůček, P., & Hynšt, J. (2010). Diurnal fluxes of CO2 and N2O from cattle-impacted soil and implications for emission estimates. *Plant, Soil and Environment*, *56*(10), 451–457. https://www.agriculturejournals.cz/publicFiles/127_2010-PSE.pdf

Singurindy, O., Molodovskaya, M., Richards, B. K., & Steenhuis, T. S. (2009). Nitrous oxide emission at low temperatures from manure-amended soils under corn (Zea mays L.). *Agriculture, Ecosystems and Environment*, *132*(1–2), 74–81. https://doi.org/10.1016/j.agee.2009.03.001

Syakila, A., & Kroeze, C. (2011). The global nitrous oxide budget revisited. *Greenhouse Gas Measurement and Management*, *1*(1), 17–26. https://doi.org/10.3763/ghgmm.2010.0007

Thies, S., Bruggeman, S., Clay, S. A., Mishra, U., Hatfield, G., Kumar, S., & Clay, D. E. (2019). Midmorning point sampling may not accurately represent nitrous oxide emissions following fertilizer applications. *Soil Science Society of America Journal*, *83*(2), 339–347. https://doi.org/10.2136/sssaj2018.08.0313

Van der Weerden, T., Clough, T., & Styles, T. (2013). Using near-continuous measurements of N 2 O emission from urine-affected soil to guide manual gas sampling regimes. *New Zealand Journal of Agricultural Research*, *56*(1), 60–76. https://doi.org/10.1080/00288233.2012.747548

Venterea, R. T., Spokas, K. A., & Baker, J. M. (2009). Accuracy and Precision Analysis of Chamber-Based Nitrous Oxide Gas Flux Estimates. *Soil Science Society of America Journal*, *73*(4), 1087. https://doi.org/10.2136/sssaj2008.0307

Wagner-riddle, C., Furon, A., Mclaughlin, N. L., Lee, I., Barbeau, J., Jayasundara, S., Parkin, G., von Bertoldi, P., & Warland, J. (2007). Intensive measurement of nitrous oxide emissions from a corn-soybean-wheat rotation under two contrasting management systems over 5 years. *Global Change Biology*, *13*(8), 1722–1736. https://doi.org/10.1111/j.1365-2486.2007.01388.x

WMO. (2014). *World Meteorological Organization Greenhouse gas bulletin No.8 Based on observations trough 2011*. WMO GHG Bulletin No 8. https://www.wmo.int/pages/mediacentre/press_releases/documents/GHG_Bulletin_No.8_en.pdf

Yanai, Y., Toyota, K., & Okazaki, M. (2004). Effects of successive soil freeze-thaw cycles on nitrification potential of soils. *Soil Science and Plant Nutrition*, *50*(6), 831–837. https://doi.org/10.1080/00380768.2004.10408543

## *9. Appendix*

### *9.1. Supplement S1 (next page)*

**Table S1. Summary of literature reporting a diurnal pattern of $N_2O$ soil emissions and PMTs**

| Reference | Flux range (g of N-$N_2O$ $ha^{-1}$ $day^{-1}$) | Reso-lution | Number of days observed | PMTs (Preferred Measuring Times) | Corre-lation with temp. | Soil cover | Location |
|---|---|---|---|---|---|---|---|
| **This study** | **Low emissions** (LCC 50%) 0 to 723.16 (median = 4.3) | 2.5 h | 1909 (LCC 50%) | 01:00 - 02:00, 11:00, 22:00 - 23:00 | No | Maize | Arlington, Wisconsin, USA |
| Akiyama et al. 2000 | 0.6 - 1 | 4 h | 6 | 08:00 - 12:00 | Yes | Carrots | Tsukuba, Japan |
| Flessa et al. 2002 | 1.8 - 6 | 12 h | 8 | 08:00 - 12:00 | yes | Potato | Munich, Germany |
| Williams et al. 1999 | 0.36 – 0.4 | 2.67 h | 3 | 12:00 - 14:40 | Yes | Perennial grass | Cumbria, UK |
| Jantalia et al. 2008 | 2.5 – 33.5 | 3 h | 3 | 07:00 - 10:00 | Yes | Perennial grass | Paso Fundo, Brazil |
| Denmead 1979 | 2.3 – 3 | < 1h | 2 | 09:00 - 12:00 | Yes | Perennial grass | Camberra, Australia |
| Rosa et al. 2012 | 1.5 – 3.5 | 3 h | 3 | 09:00 - 12:00 | Yes | Soybeans | Buenos Aires, Argentina |
| Laville et al. 2011 | 17.3 – 103.4 | < 1 h | 9 | 07:30 - 09:00 and 16:00 - 19:30 | Yes | Maize | Gignon, France |
| Alves et al. 2012 | 0 – 10.8 | 3 & 6 h | 35 | 09:00 - 10:00 and 21:00 - 22:00 | Yes | Perennial grass/ Potato | Seropedica, Brazil / Edinburgh, Scotland |
| Reeves and Wang 2015 | 20 – 140 | < 1h | 3 yrs. | 09:00 - 12:00 and 21:00 - 24:00 | Yes | Wheat/ barley | Queensland, Australia |
| Reeves et al. 2016 | 0 - 550 | 2-3 h | 1yr | 09:00 - 12:00 and 21:00 - 24:00 | Yes | Sugarcan e | Queensland, Australia |
| Savage, et al. 2014 | 0 – 4.8 | 1 h | 74 | 09:00 - 10:00 | Yes | Forest wetland | Bangor, Maine |
| Maljanen et al. 2002 | 0 - 24 | 6 h | 38 | NA | Yes | Multiple | Eastern Finland |
| Shurpali et al. 2016 | 0 - 350 | 1 h | 214 | NA | Yes / No | Perennial grass | Eastern Finland |
| Machado et al. 2019 | -16 - 496 | 0.5, 1, 2, 4 h | 2280 | 09:00 - 12:00 and 18:00 - 02:00 | Yes | Corn, soybean, wheat | Ontario, Canada |

### *9.2. Supplement S2*

For researchers with limited sampling capacity it is important to know how less frequent sampling at a PMT impacts the accuracy of cumulative emissions estimates. We explored this question using our data. Predictably, the answer depends on the sampling frequency, but also on which particular sequence of days is sampled.

We evaluated the accuracy of estimates of annual cumulative emissions made by subsampling the high frequency resolution flux data every three days at the 11:00 PMT. The error in these cumulative emissions estimates was computed as the ratio of the cumulative emissions estimated from the subsampled flux data to the cumulative emissions estimated from high temporal resolution flux measurements (i.e., approximately every 2 hours) expressed as a percentage.

Cumulative emissions were computed for each sampling season as the sum of the estimated daily emissions. In the subsampled data, the daily emission from each chamber was the flux observed at the 11:00 PMT. In the high temporal resolution flux data, the daily emissions were computed for each chamber as the integral of the hourly fluxes measured over the 24 hour period. In both cases, the emissions of the four chambers were averaged to give the daily emission. If measurements were missing for a particular day, the daily emissions were estimated by linear interpolation between the two nearest available data. There are three sampling sequences possible when using a three-day sampling interval. In our analysis, Sequence 1 is the case when sampling started on the first day of the sampling season, with Sequence 2 and Sequence 3 starting on the second and third days, respectively. The results of this analysis are presented in Figure S1 for sampling seasons 2015, 2016-17, and 2017-18 (panels A, B, and C, respectively.

Figure S1 shows that during high emissions periods, measuring at the 11:00 PMT was often a poor estimate the average daily flux. This is most apparent in the two largest peaks of the 2017-18 season (Figure S1, panel C). The peaks, 750 and 600 g $N\text{-}N_2O$ $ha^{-1}$ $day^{-1}$, are only two days apart, occurring on March 1st 2018 and March 3rd 2018. The only sampling sequence with a flux measurement at the 11:00 during the first peak event was sequence 3, in this day the average daily emission, estimated from high temporal resolution measurements, was 750 g $N\text{-}N_2O$ $ha^{-1}$ $day^{-1}$ while the flux measured at the PMT was 350 g $N\text{-}N_2O$ $ha^{-1}$ $day^{-1}$. Similarly sequence 1 was the only sampling sequence with a flux measurements during the second peak, in this case the average daily emission was 600 g $N\text{-}N_2O$ $ha^{-1}$ $day^{-1}$ while the flux measured at the PMT was 280 g $N\text{-}N_2O$ $ha^{-1}$ $day^{-1}$. Sampling sequence 2 does not include flux measurements during either of these two peak events. Overall, the arbitrary timing of intermittent sampling leads to underestimation of the cumulative emissions during the 2017-18 season by 29, 23, and 3% for sampling sequences 1, 2, and 3 respectively (Figure S1, panel C). These underestimations are the results of the arbitrary timing of intermittent sampling and the lack of accuracy of flux measurements at a PMT to representing the daily mean emission during high emissions periods. Sequence 2 of sampling season 2016-17 (Figure S1, panel B), is another example of the disadvantage of using fluxes measured at a PMT to estimate cumulative emissions. In this case, the fluxes measured at 11:00 during peak events usually overestimate the daily emissions computed using high temporal resolution flux measurements. This lack of accuracy in the estimation of daily emissions by a PMT during peak emissions lead to an overall overestimation of the cumulative emissions of 45% (Figure S1, panel B).

These results are suggestive, but do not provide definitive information about the impact of sampling interval on the accuracy of cumulative emissions estimates. The accuracy of estimates made with a particular sampling interval depends on the number, size and duration of the emissions peaks. This

emissions profile, in turn, will vary with the local soil conditions, crop management, and weather. It is clear that in highly fertilizes systems like the one studied here, accurate estimates of annual cumulative emissions requires sub-daily sampling during peak emissions periods.

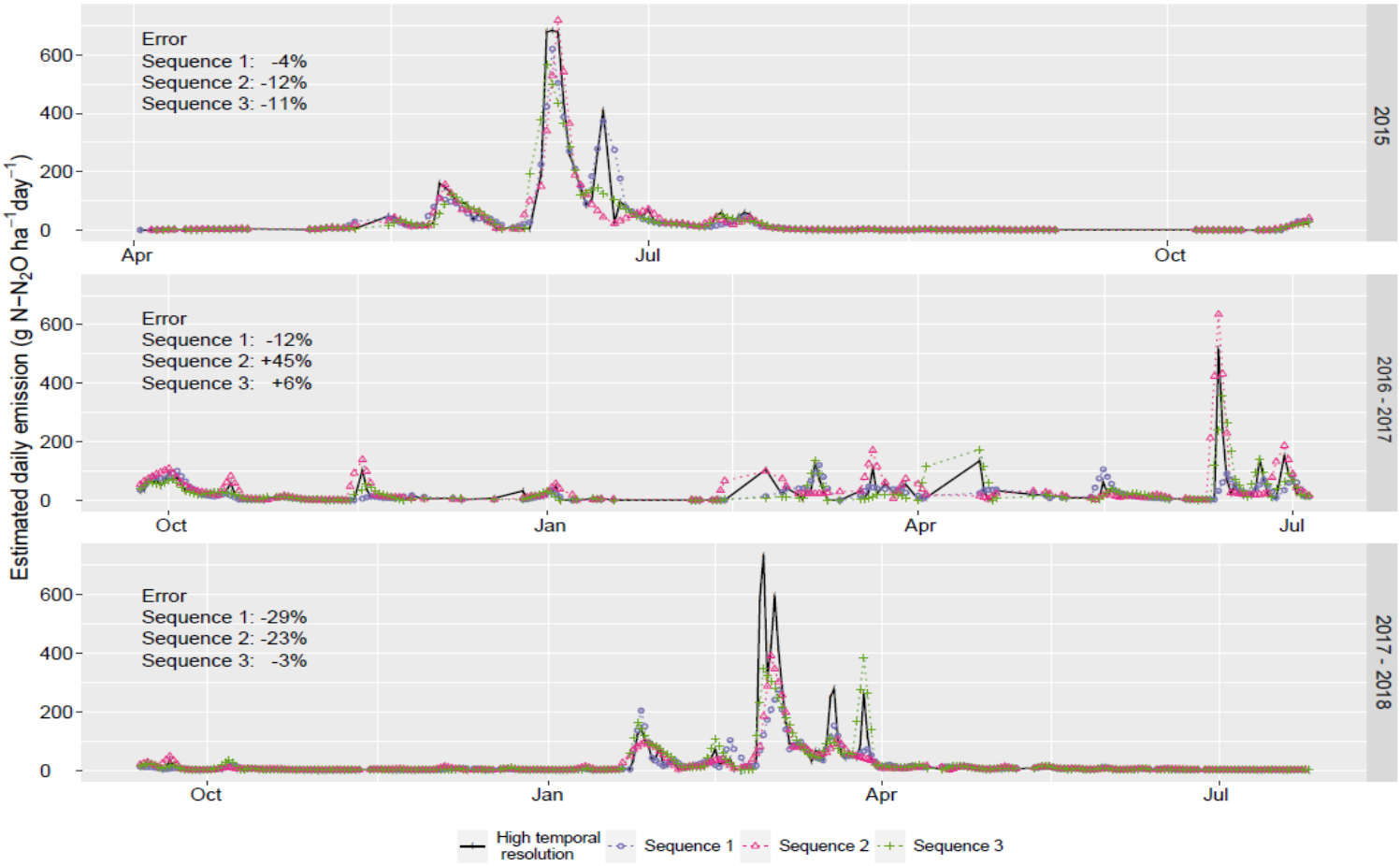


**Figure S1.** Soil N2O flux estimated by subsampling the high temporal resolution flux data every third day at the 11:00 PMT. Vertical panels A, B, and C show the estimated daily flux (y-axis) for sampling seasons 2015, 2016-17 and 2017-18, respectively. The three different sampling sequences correspond to the day sampling begins within the three-day cycle. The solid black line is the daily emissions estimated from the high temporal resolution flux measurements. The error in estimated cumulative emissions for each sampling sequence is computed relative to, and as a percentage of, the cumulative emissions estimated from the high temporal resolution data

## ***Chapter 5: Quantifying trade-offs of nitrogen loss as NO3- and N2O between early and late fall dairy slurry application.***

### *1. Abstract*

Fall manure application is a common practice in the Midwest of the US, because it offers economical and logistical advantages to farmers. Due to the large time between nutrient availability and plant uptake, fall application creates a risk of nitrogen (N) losses that can have serious negative health and environment consequences. Timing of manure application during the fall has been used as a strategy to minimize nitrate ($NO_3^-$) losses but there is little information available about its effect on soil emissions of nitrous oxide ($N_2O$). Our objectives were to evaluate how the timing of fall application of dairy slurry affected $N_2O$ emissions and $NO_3^-$ leaching below the root zone, and to test if the impact of recommended strategies for reducing $NO_3^-$ leaching on $N_2O$ emissions and total N losses. We measured $N_2O$ emissions and $NO_3^-$ leaching year-round during 4 years in corn grown in Columbia County, WI. Dairy slurry was applied early (Mid-September), and late in the fall (Mid-November). Later application of manure had opposite effects on N loss as $NO_3^-$ and N loss through cumulative $N_2O$ gas emissions. Relative to late fall application, early fall application led to higher $NO_3^-$ leaching losses below the root zone, lower peak $N_2O$ losses during soil freeze-thaw cycles (FTC) and lower cumulative $N_2O$ emissions. Overall N losses from plots that received early manure application were larger than those from late manured plots because N losses via $NO_3^-$ leaching were larger than the cumulative N losses as $N_2O$ gas emissions in all cases.

In our experiments later application of dairy slurry application reduced both $NO_3^-$ leaching losses and overall N ($N_2O$ + $NO_3^-$) loss but increased the cumulative $N_2O$ emissions due to larger peak emissions during winter FTC. Late application of manure is the preferred practice to

minimize $NO_3^-$ leaching losses from fall-applied manure. Late fall application combined with the FTCs associated with Wisconsin's cold continental climate led to a concomitant increase in $N_2O$ emissions, however. Climate change has led to more frequent FTCs, a trend which is expected to continue (Henry, 2008). Additional research is needed to better understand the mechanisms of the $N_2O$ emissions associated with FTCs and to devise mitigation strategies to avoid a positive feedback between climate change and the emission of $N_2O$ which is a powerful greenhouse gas.

## *2. Introduction*

The Midwest of the US is a major producer of animal feed and livestock (Grace et al., 2011; Hatfield, 2012, USDA-NASS, 2018). Using the manure produced in livestock operations to fertilize crops provides multiple economic and agricultural advantages (Talarczyk et al., 1996; van Es et al., 2006). In this region, farmers prefer to apply manure during the fall rather than during the spring, because fall manure applications offer logistical advantages (Williams et al., 2012). Fall applications of manure allow time for the breakdown of the organic portions of the manure before the high crop nutrient demand in the spring, but fall applications also increase the risk of contamination of groundwater by nitrate ($NO_3^-$) (Rabotyagov et al., 2010; van Es et al., 2006) and has the potential to increase nitrous oxide ($N_2O$) emissions from the soil (Abalos et al., 2016; Cambareri et al., 2017; Schwager et al., 2016). This manuscript investigates the trade-offs between nitrogen (N) losses as $NO_3^-$ and $N_2O$ associated with the timing of dairy slurry application during the fall in the upper Midwest of the US in a corn grain production system.

Elevated nitrate ($NO_3^-$) levels in surface and ground water are a major health and environmental concern. High levels of nitrate ingestion with drinking water have been associated with birth defects, child mortality, and increased risk of cancer (Gupta et al., 2000). In

Wisconsin, where 68% of the population uses groundwater as the primary source of water, 10% of the private wells exceed the 10 mg/L $NO_3^-$-N limit for drinking water (Dieter et al., 2017). Approximately 90% of the total groundwater contamination in Wisconsin is derived from agricultural sources (Shaw 1994, WGCC 2019). Nonetheless $NO_3^-$-N contamination extend far beyond the limits of Wisconsin, recent studies have linked the hypoxic zone of the Gulf of Mexico with excessive N loss from cropland in the Mississippi River Basin, an area that is comprised of more than 30 mostly agricultural states (Andraski et al., 2000; Jones et al., 2018; Porter et al., 2015). Between 10 to 55% of the N applied in manure is lost in the form of nitrate leached below the root zone, increasing the risk of ground and drinking water contamination, and contributing to eutrophication of marine habitats (Goolsby et al., 2001; Paul & Zebarth, 1997; Stoddard et al., 2005). Implementing agricultural practices that reduce $NO_3^-$ losses to water is crucial to reduce the adverse impacts of $NO_3^-$-N on human health and environmental degradation.

Nitrous oxide is an important atmospheric gas because it is a long-lived greenhouse gas (GHG) with a global warming potential 289 times that of carbon dioxide. Its breakdown in the atmosphere is a major source of stratospheric NO which destructively reacts with the stratospheric ozone layer (Ravishankara et al., 2009). The atmospheric concentration of $N_2O$ is increasing at 0.6 – 0.9 ppbv $yr^{-1}$ (IPCC, 2011). Agriculture is estimated to contribute around 80% of global anthropogenic $N_2O$ emissions, approximately 45% of which result from the spreading of animal waste on agricultural soils (Syakila & Kroeze, 2011). Developing agricultural practices that reduce $N_2O$ is crucial to mitigate climate change and to reverse the thinning of the stratospheric ozone layer.

Organic amendments, such us liquid dairy manure, provide the soil with large quantities of organic carbon (C) and N, mostly in organic and ammoniacal ($NH_4$ and urea) forms, where $NH_4$ and urea could represent up to 40% of the total N from manure (Pettygrove et al., 2009). If manure it is not rapidly incorporated after application, $NH_4$ and urea can be converted into ammonia ($NH_3$) as pH increases and the manure begins to dry, leading to important N losses via $NH_3$ volatilization. Ammonia volatilization increases with increasing temperatures and wind speed and is reduced when manure application is followed by rain, as rain increases the infiltration of $NH_4$ and urea into the soil (Chadwick et al., 2011). If manure is effectively incorporated in the soil, $NH_4$ can be converted into $NO_3^-$ which if it is not intercepted by the plants roots is subject to leaching or loses via denitrification. $NH_4$ is converted to $NO_3^-$ via nitrification the rate of which increases with soil temperature. Fall applications of manure allow time for the breakdown of the organic portions of the manure before the high crop N demand in the spring, but fall applications also provide more time for possible loss of nitrogen through leaching and $N_2O$ volatilization via nitrification and denitrification (van Es et al., 2006; Gupta et al., 2004; Williams et al., 2012). The same C required for heterotrophic denitrification stimulates biological oxygen demand, leading to low oxygen conditions and substantially increasing $N_2O$ emissions due to denitrification when $NO_3^-$ is available in the soil (Miller et al., 2009; Rochette et al., 2000). Rates of mineralization and the main $N_2O$ production pathways in soils, nitrification and denitrification, are strongly influenced by soil temperature and soil moisture levels (i.e., water filled pore space), because the amount of water in the soil regulates oxygen availability (Grundmann et al., 1995; Guntiñas et al., 2012; Williams et al., 2012). Because temperature and rainfall change seasonally, timing of manure application during the fall is expected to have a significant impact on the dynamics of $NO_3^-$ and $N_2O$ production and loss.

Nitrous oxide emissions in managed crop systems are highly episodic, exhibiting long periods of low $N_2O$ emissions that are interrupted by short lived peak emissions events that represent the majority of cumulative emissions (Francis Clar & Anex, 2020; Molodovskaya et al., 2011). These peak $N_2O$ emissions that are triggered by brief transitory biogeochemical changes during dry-wet (DW) and freeze-thaw cycles (FTC) can contribute up to 70% of annual cumulative emissions (Congreves et al., 2018; Kariyapperuma et al., 2012; Wagner-Riddle et al., 2017). Peak emissions triggered by DW cycles happen when precipitation occurs soon after fertilization. Their duration and magnitude are related to substrate availability, temperature, and soil moisture (Congreves et al., 2018; Molodovskaya et al., 2012). For the same soil nutrient conditions, $N_2O$ emissions significantly increase with higher soil and air temperatures (Benckiser et al., 2015; Rudaz et al., 1999). Peak emissions triggered by FTC occur during the winter and spring. The mechanisms regulating FTC peak emissions are not fully understood but $NO_3^-$ and organic C availability are widely accepted as the largest contributors to their magnitude and duration as $NO_3^-$ and organic C are the main substrates for denitrification (Congreves et al., 2018; Risk et al., 2013). Because peak emissions represent the largest part of cumulative emissions, measuring them accurately is crucial for comparing the effects of manure application timing. Nonetheless peak emissions, especially during the winter and spring, are often overlooked as they are difficult to measure with conventional soil trace gas measurement strategies (i.e., infrequent manual sampling of static chambers) (Barton et al., 2015; Francis Clar & Anex, 2020; Schwager et al., 2016; Wagner-Riddle, 2019). Therefore, the effect of timing manure application in the fall, early versus late, on peak and cumulative $N_2O$ emissions remains uncertain.

The strategy recommended by USDA extension services and industry professionals to reduce nitrate losses and increase N soil retention is to apply manure late in the fall *"when the soil temperature at 10 cm is below 10° C and falling"* (e.g., late fall, approximately Mid-November in south Wisconsin) rather than in the early fall (approximately Mid-September in south Wisconsin). Because low soil temperatures reduce $NH_4$ volatilization, N mineralization, and N leaching. In cold climates, this recommendation practice has been shown to be effective in reducing $NO_3^-$ leaching below the root zone and in increasing overall $NO_3^-$ soil retention, especially during the winter and spring months (Gupta et al., 2004; van Es et al., 2006, Williams et al., 2012). If delaying manure application increases $NO_3^-$ soil concentrations during soil thaw it is possible that it also leads to an increase in the magnitude, duration, and frequency of $N_2O$ emissions during winter and spring FTC. However, the effect of timing of fall manure application on $NO_3^-$ leaching and $N_2O$ emissions have not previously been studied simultaneously. Here we investigated if cumulative and peak $N_2O$ soil emissions will increase as a result of applying manure in late rather than early fall and (2) if the effect of the recommended strategies aimed at reducing $NO_3^-$ leaching are counter-productive in terms of $N_2O$ emissions and total N losses.

Relative to early fall (Mid-September) manure application, $N_2O$ emissions resulting from late fall (Mid-November) manure application are expected to be lower during the fall due to lower soil temperatures and larger during the winter and spring due to the presence of more available soil $NO_3^-$ that can enable denitrification during FTC. On the other hand, N losses via $NO_3^-$ leaching from early manured plots are expected to be larger than those from late manured plots due to higher temperatures leading to higher mineralization rates during the warm period after early fall manure application.

The goals of this study are to: (1) assess the effects of fall manure application timing in N losses via $N_2O$ emissions and $NO_3^-$ leaching; (2) investigate if cumulative and peak $N_2O$ soil emissions increase as a result of applying manure late rather than early during the fall; and, (3) examine if the recommendations strategies for reducing $NO_3^-$ leaching are counter-productive in terms of $N_2O$ soils emissions and total N losses.

To achieve these goals, we monitored $N_2O$ soil emissions and $NO_3^-$ leaching below the root zone from plots manured during the early fall (Mid-September) or late fall, *"when the soil temperature at 0.1 m is below 10° C and falling"*, approximately Mid November in South Wisconsin. Losses of $N_2O$ and $NO_3^-$ were measured at high temporal resolution during four years in soils representative of soils used for corn grain production in the upper Midwest of the US. The results showed that timing of dairy slurry application during the fall came with a clear trade-off between $NO_3^-$ loss and $N_2O$ emissions. Relative to late fall application, early fall application of dairy slurry led to higher $NO_3^-$ leaching loss below the root zone, lower peak $N_2O$ losses during freeze-thaw cycles (FTC) and lower cumulative $N_2O$ emissions. For the conditions of this study, late fall manure application resulted lower N losses than early fall manure application due to lower $NO_3^-$ losses via leachate.

## *3. Materials and Methods*

### *3.1. Experimental Site and set up*

The experiment examining the trade-offs in $NO_3^-$-N and $N_2O$-N losses between two different times of dairy slurry application during the fall in fields used for corn production on grain in the upper Midwest of the US was performed at the University of Wisconsin Agricultural Research Station - Arlington (ARS-A) (43°17'41.2"N 89°21'28.1"W) in Columbia County (WI). The

experiment lasted four years, from 2016 to 2020, comprising four 12-month sampling campaigns that began in September one year and finished in September of the following year. The four sampling campaigns are referred as 2016-17, 2017-18, 2018-19 and 2019-20.

The study was a randomized complete block design with subsampling with one treatment: time of dairy slurry application during the fall at two different times, early or late. Two experimental plots were monitored during each sampling campaign and the time of manure application was randomly assigned. Each 3.04 m wide plot contained four rows of corn with 0.76 m spacing and was 12.2 m long. During each sampling season the two treatment plots were adjacent to each other sharing a long edge.

To avoid interference from previous manure amendments new experimental sites were chosen for each sampling campaign. The selected sites had no manure application history for at least the three years immediately preceding our experiment and the previous crop was corn silage managed with pre-planting shallow tillage (i.e., 0.1 m depth). The four sites were in close proximity to one another (< 0.5 km). The soil in all plots was Plano silt loam and Ringwood slit loam complex (fine-silty, mixed, superactive, mesic Typic Argiudoll). The soil texture was silty clay loam at a depth between 0 to 0.4 m and varied between loam and sandy loam between 0.4 to 0.9 m.

Early fall slurry was applied in Mid-September as soon as the previous crop, corn silage, was harvested. The late manure application occurred when the soil temperature at a depth of 0.1 m was below 10°C and falling, which in Arlington, WI. usually happened in Mid-November. Dairy slurry was collected from a single concrete pit which had been mixed thoroughly prior to collection on the same day of the application. To improve slurry incorporation in the soil, 24-

hours before slurry application the plots were tilled with a shallow soil finisher (0.1 m depth). The rate of slurry application for all campaigns was 66,325 L $ha^{-1}$. Manure was surface applied using a custom-made tank and hose mounted on a tractor, manure was incorporated within 24-hours of application by tilling the plot with the same shallow soil finisher used prior manure application. The rate of manure application and application method were based recommendations in *Nutrient Application Guidelines for Crops in Wisconsin* (Laboski & Peters, 2011).

Immediately before each manure application one sample of thoroughly agitated dairy slurry manure was collected in a 1-liter HDPE container and placed into a freezer right away. The frozen manure sample was sent for analysis of total N, $NH_4$-N, total solids, pH, ash and C:N to the 'UW Soil and Forage Lab' (2611 Yellowstone Dr. Marshfield, WI, 54449). All fertilizer was applied as dairy slurry during the fall, early or late. The quantity of total N applied varied between application due to manure composition variability, results of manure analysis and the quantities of total N applied are presented in the appendix in table A4.

During all sampling campaigns corn grain was planted at a rate of 87,500 seeds $ha^{-1}$ (Pioneer Seed ID# P0157AMX) with row spacing of 0.76 m. Weed control was performed using labelled rates of glyphosate applied post-emergence. Dates of manure application, corn planting and harvest are presented in Table 1.

At corn physiological maturity ("black layer") above ground biomass plant samples were collected by cutting at ground level and hand harvesting 10 random plants per plot. The plants were weighted and chopped at size of 9.5 to 19 mm using a tractor mounted hand-feed chopper. A representative sample of the chopped biomass from the 10 plants was transferred to a 1-liter paper bag, weighed and oven dried in a force-draft dryer at 66º C for at least one week. Dried

plant samples were weighted and sent for analysis of Total Nitrogen and Dry matter to the 'UW Soil and Forage Lab' (2611 Yellowstone Dr. Marshfield, WI, 54449). Biomass yield was computed in a dry basis by multiplying the biomass yield of one plant by the number of plants in a hectare, which was assumed to be the planting rate (87,500 seeds $ha^{-1}$). The results of above ground biomass yield and total N in above ground biomass are presented in Table A6 in Appendix 1.

Corn grain was harvested from the center two rows of each plot with a plot combine which measured yield, moisture, and test weight. The combine mass flow sensor was calibrated by harvesting two rounds of corn that at least weighted 1375 kg per round. The weight of each load was compared with the eight measured by an accurate scale at the ARS-Arlington. Grain yield was adjusted to a 15.5% moisture in a dry basis and presented in Mg $ha^{-1}$ by multiplying the weight of corn harvested in the area occupied by the two center rows of the experimental plot by the ratio of the experimental plot area to hectare (Lauer, 2002). The results of corn grain yield are presented in Table A6 in Appendix 1.

Weather data (air temperature, precipitation, Reference Evapotranspiration, etc.) with a 30-minute resolution were obtained from the Arlington-ARS Weather Station (43°17'48.0"N 89°23'03.4"W) located within 500 m of the experimental sites.

Soil temperature and moisture were recorded following the method of Kladivko et al. (2014): measured at the quarter-row position (less than 4 meters radius from the soil chambers) every 15 minutes using five soil probes (5TM, Decagon Inc.) installed at depths of 0.05, 0.1, 0.2, 0.4, and 0.6 m. All soil measurements were recorded using an em50 data logger (Decagon Inc.).

Soil samples were collected twice during each sampling campaign: in September before the experiments started, and at vegetative corn growth stage V6. At the beginning of the sampling season soil samples were collected at four depths, from 0 to 0.1, 0.1 to 0.2, 0.2 to 0.4 and 0.4 to 0.6. At V6 soil samples were collected to a depth of 0.9 m at 0.3 m intervals. At each soil sampling depth, a soil composite sample was formed by mixing soil samples from seven different locations within the plot. Composite soil samples were frozen and sent for analysis to the 'UW Soil and Forage Lab' (2611 Yellowstone Dr. Marshfield, WI, 54449), where the quantities of Total Nitrogen, $NO_3^-$, $NH_4$, Total Organic Carbon and a wide range of basic elements were measured, the results are presented in Appendix 1 in Table A5.

### *3.2. $NO_3^-$ leaching losses*

#### *Soil-water sampling*

Soil-water sampling started immediately after early fall manure application and ended the first of August of the following year. Soil-water samples were not collected when the soil was frozen. The soil-water samplers were installed at the start of each sampling campaign one week before early fall manure application. Samplers were installed at a depth of 0.75 m, below the root zone.

Soil-water samplers from two manufacturers were used. These were the Prenart Super Quartz standard (Prenart Equipment ApS, Frederiksberg, Denmark), and 'pressure/vacuum soil water samplers' (Part #1920F1L24-B02M2, Soilmoisture Equipment Corp. Santa Barbara, CA). For

simplicity, these will be referred as ‘prenart’ and ‘soilmoisture’ lysimiters respectively. Both water samplers were suction lysimeters consisting of a porous ceramic cup connected to a sample reservoir. Soil-water samples is collected by applying vacuum in the water reservoir, this generates a suction in the other side of the porous ceramic cup and force waterflow from the soil through the porous ceramic cup into the soil-water sample reservoir. The main differences between the two brands of lysimeters were the shape of the suction cup, the type of reservoir and the angle of installation. The Prenart lysimeters had a long and narrow cylindrical suction cup (outside diameter of 21 mm, length 95 mm), which was connected to a polypropylene collecting bottle/vacuum container through a 1.2 m long polyethylene tube (outside diameter 3.175 mm). Prenart lysimeters were installed at a 45º angle, following the manufacturer recommendations. Soilmoisture lysimeters had a wider and shorter suction cup (Outside diameter 48 mm, length 50 mm), the reservoir was a 0.6 m long food-grade PVC pipe seamlessly bonded to the suction cup forming a unique lysimeter body. Soilmoisture lysimeters were installed vertically following the recommendations of the manufacturer. Between sampling campaigns, the soil-water samplers were cleaned using diluted acid (1 N HCl) and repeatedly rinsed with deionized water (Curley et al., 2010). Compatibility between these two designs of suction cup lysimeter have been tested previously. Differences in $NO_3^-$-N concentration in soil-water samples collected with the suction cups during field experiments were not found to be significant (Lord & Shepherd, 1993).

During the sampling campaigns of 2016-17 and 2017-18, one prenart lysimeter was installed between the two center corn rows of each plot. During these two sampling campaigns soil-water samples were collected every two weeks and after rain events greater than 10 mm $day^{-1}$. Due to the lack of replication in $NO_3^-$-N soil-water sampling during 2016-17 and 2017-18 the statistical analysis used to quantify differences in N losses among early and late fall manured plots losses

was conducted using a simple paired *t*-test between the [$NO_3^-$-N] concentration of the soil-water samples. It is common for field lysimeter data to be un-replicated and for their results to qualitatively interpreted (Basso & Ritchie, 2005; Martin et al., 1994; Rasse et al., 2000; Ritchie, 1972). The results of $NO_3^-$-N losses in 2016-17 and 2017-18 are used to support the 2018-19 and 2019-20 results that utilized substantial subsampling (n=7) with soil water sampling performed twice per week.

During 2018-19 and 2019-20, seven lysimeters, 3 prenart and 4 soilmoisture, were installed uniformly throughout each plot between the corn rows. In these sampling campaigns soil-water samples were collected twice per week and after rain events greater than 10 mm $day^{-1}$.

During all four sampling campaigns, soil-water samples were collected by applying a vacuum of 0.6 Pa to the collection bottle or sampler body using a portable vacuum pump (Prenart Equipment ApS, Frederiksberg, Denmark). The amount of water collected from each water sampler was recorded and a soil-water subsample of more than 5 ml was transferred to 20 ml HDPE scintillation vial with a polypropylene screw cap. The 20 ml scintillation vials were stored at -20ºC within 48-hours after the application of the vacuum. Soil-water samples were transported from the field to the freezer in a covered cooler with cold packs.

***Soil-water analysis***

During 2016-17 and 2017-18, standard method 353.2 of the United States Environmental Protection Agency (USEPA) was followed to measure the concentration of N in the soil-water samples as the combination in N in the $NO_3^-$ and $NO_2$ ions (e.g., N- $NO_3^-$ + N-$NO_2^-$). For this technique, the Method Detection Limit (MDL) for $NO_3^-$-N + $NO_2^-$-N was 0.0005 mg $L^{-1}$ applicable within a range of 0.005 to 10 mg $L^{-1}$ ($NO_3^-$-N + $NO_2^-$-N). When needed, the

measuring range was extended by diluting the original soil-water sample with deionized water. Samples were analyzed using an automated injected Segmented Flow Analyzer FS 3100 (Oi Analytical, College Station, TX). Analysis of each soil-water sample was performed in triplicate.

Soil-water samples collected during 2018-19 and 2019-20 were analyzed for $NO_3^-$ concentration at the Rock River Laboratory (Watertown, WI) using a $NO_3^-$ ion selective electrode that offered comparable MDL, precision, and applicable range than that used to analyze the soil-water samples in the two previous sampling campaigns.

For all four sampling campaigns, the N concentration in soil-water was referred as $NO_3^-$-N. It is a common practice to measure the N concentration in soil-water as $NO_3^-$-N + $NO_2^-$-N and refer to it only as $NO_3^-$-N, this is because the chemical analysis determine both source of N ($NO_3^-$-N + $NO_2^-$-N) together and because, the amount of $NO_2^-$-N is usually very in small in comparison to that of $NO_2^-$-N due to its higher reactivity (Francis Clar & Anex, 2020; Francis Clar et al., 2015).

***Quantification of leachate volume***

The quantity of $NO_3^-$-N leached below the corn root zone was calculated on a daily basis as the $NO_3^-$-N concentration of the soil-water samples collected with the porous cup lysimeter multiplied by the volume of soil water that drained at a 0.75 m depth.

When drainage occurred between soil-water sampling dates, linear interpolation between soil-water samples was used to estimate the $NO_3^-$-N concentration of the soil-water. Quantities of $NO_3^-$-N leached below the root zone are presented for each campaign as the sum of daily $NO_3^-$ over four periods, the starting and end dates of which were determined by soil conditions and management events, and therefore had variable length. The events used as breakpoints for these

four periods were: early manure application (i.e., starting), soil freeze, soil thaw, planting, V6, and the campaign end (i.e., August 1st).

Daily drainage below the root zone was estimated using a water balance approach which considered precipitation inputs, changes in soil water storage, and evapotranspiration similar to the method used by Andraski et al. (2000), in which,

If $TSW_{(t-1)} + P_t - Et_t > TSW_{FMC}$, then (1)

$$(TSW_{(t-1)} + P_t - Et_{t)} - \ TSW_{FMC} = \ D_t \quad (2)$$

Where *TSW* is the Total Stored Water, *P* is precipitation amount and *Et* is water lost due to evapotranspiration and *D* is drainage, all units in millimeters. The subscript *t* represents the current day and *FMC* the Field Moisture Capacity (Matric Potential = -33 J/kg). According to this model, drainage (*D*) will only occur if the amount of precipitation minus the losses due to evapotranspiration are greater than the volume of water that the soil can store on the specific date ($TSW_{FMC} - TSW_{(t-1)}$). Where $TSW_{FMC}$ at 0.75 m depth for a Silty Clay Loam soil was 300 mm (Campbell & Norman, 1998). When the condition in Eq. 1 was not met $D_t$ was zero.

Reference evapotranspiration ($ET_{Ref}$) and precipitation were retrieved from the Arlington Agricultural Research Station weather station located within 500 meters south from the experimental plots. Daily Evapotranspiration ($Et_t$) was computed by multiplying $ET_{Ref}$ by $K_{c,t}$ (the crop coefficient) (Equation 3).

$$Et_t = \ k_{c,t} \times \ ET_{Ref,t} \quad (3)$$

During the growing season, crop coefficients for corn were taken from FAO paper No. 56 (Allen et al., 2006) according to the corn growing stage which was calculated relative to the planting date and Growing Degree Units (GDU) (McMaster & Wilhelm, 1997). During the non-growing season, a value of 0.3 was used for $K_{c,t}$ as recommended by FAO paper No. 56 (Allen et al., 2006).

During the winter and spring months when the soil was frozen and soil-water samples could not be retrieved water budgeting was interrupted and the amount of drainage was assumed to be zero. Since the porous-cup sampling method does not capture leaching occurring through macropore flow, the amounts of nitrate leached based on water budget calculations must be viewed as a conservative estimate of the actual quantity of nitrate lost by leaching (Wang et al., 2012).

### *3.3. $N_2O$ measurements*

Soil $N_2O$ emissions were measured during each sampling campaign from immediately after early manure application during the fall until mid-September of the following year using two static soil chambers per plot. One chamber was placed between plant rows and the other directly on the row. Any vegetation that grew within the chambers was removed by hand.

From immediately after early manure application until mid-summer, $N_2O$ soil emissions were measured using an automatic $N_2O$ flux measurement system which comprises a Los Gatos Research model 914-0027 $N_2O$ analyzer and four automatic soil chambers (Francis Clar & Anex, 2020). In mid-summer when $N_2O$ soil fluxes were low and non-episodic, the automated $N_2O$ monitoring system was brought to the lab for calibration and maintenance. From mid-summer

until mid-September, soil trace gas flux was measured at 10-day intervals using a standard manual sampling technique described below.

The automatic monitoring system measured soil fluxes every day at high sampling resolution of (i.e., ~10 fluxes per day and chamber). The high sampling frequency was maintained throughout the winter and spring months. During the winter months only the snow that exceeded the chamber height was removed. Removing snow from the interior of the soil chambers due to snow fall was rare and always occurred when soil fluxes were low.

The ability to measure $N_2O$ concentration at both high rate and precision was key to keeping deployment times short (i.e., 10 to 20 minutes) and high sampling resolution and thereby capturing short lived peak emissions events. In continuous flow mode, the analyzer computes in 'real time' the $N_2O$ concentration of a gas stream (i.e., 100 cc $min^{-1}$) by integrating multiple laser absorption measurements (<3 milliseconds) over a user selected averaging time. An averaging time of 20 seconds was used, yielding a measurement precision (i.e., one standard deviation) of 1/1500 of the measured gas concentration ($1\sigma < 0.2$pbb at $[N_2O] \approx 300$ ppb). With these settings (sampling rate, deployment time and analytical precision) and the chamber dimensions described below, the Minimum Detectable Flux (MDF) of the system is $9.2 \times 10^{-5}$ g of $N_2O$-N $ha^{-1}$ $day^{-1}$ for deployment times of 20 minutes and $3.7 \times 10^{-4}$ g of $N_2O$-N $ha^{-1}$ $day^{-1}$ for deployment times of 10 minutes. MDFs were computed following the method of Francis Clar & Anex (2018).

In the automatic monitoring system, the chambers were 0.35 m long by 0.20 m wide by 0.25 m tall ferromagnetic stainless steel open-ended boxes. After the 2016-2017 sampling campaign the soil chambers were rebuilt. The redesigned chamber volume was slightly larger. Chambers used in the sampling campaigns of 2017-18, 2018-19 and 2019-20 were 0.30 m long by 0.30 m

wide by 0.20 m tall and the chamber lid levers were redesigned as two parallel four bar linkages. The analyzer was connected to each of the four soil chambers with a gas path composed of two manifold valve assembles at the inlet and the outlet of the analyzer which diverted the continuous gas flow from the analyzer to the soil chambers and vice versa via a 30-meter-long closed loop made of Chemfluor ®FEP tubing (6.35 mm OD, 0.79 mm wall). The automatic monitoring system included an interruption sequence triggered by an optical rain sensor that halted gas sampling and opened all chambers during (and for 1 hour after) precipitation events. A more detailed description of the automatic $N_2O$ monitoring system can be found in (Francis-Clar & Anex, 2018).

From mid-summer to mid-September, soil fluxes were measured by hand every 10 days using the materials and methods described by Duncan et al., (2019). These chambers were 0.285 m in diameter and 0.22 m tall stainless steel, open-ended cylinders. The chamber lids were made of a 12.7 mm thick HDPE plate and were fitted with a septum for gas extraction. For each chamber, four headspace gas samples of 10 ml were collected, the firs samples were collected immediately upon chamber closure, the other three subsequently at 20 min intervals. Samples were placed in glass 5.9 ml Exetainer vials (Labco Limited, Buckinghamshire, UK), using 20 ml of sample to flush the vial before over pressurizing with another 10 ml. $N_2O$ concentration was measured within two months from sample collection using an electron capture detector (micro-ECD, Agilent 7890A GC System, Santa Clara, CA, USA). The MDF of the manual soil chambers was computed following the method of Parkin et al., (2012) attending to analyzer precision, number of $N_2O$ measurements and flux calculation method (explained below). The MDF for the manual sampling technique was 0.1 g of $N_2O$-N $ha^{-1}$ $day^{-1}$.

All chambers were equipped with a vent tube for pressure equilibration, the vent was made of a 0.02 m outside diameter and 0.2 m long coiled stainless-steel tube. The soil chambers were pushed into the soil approximately 0.05 m and were only removed from the field during manure application, planting and when switching between $N_2O$ sampling systems. Soil chambers were placed back in their original position as soon as feasible (a few hours to two days) after manure application or planting and on the same day after switching between $N_2O$ monitoring systems.

The temporal coverage of the automatic $N_2O$ monitoring systems was evaluated as the average flux temporal resolution. The average flux temporal resolution was computed by dividing the total number of reliable flux measurements (section 2.3) by the number of days between the start and the end of the automatic monitoring period (Table 2). These dates include days with sampling interruptions shorter than 5 consecutive days that occurred due to precipitation events such as rain, snow, or sleet, and short system failures. When the $N_2O$ monitoring system stopped for more than 5 consecutive days, gas samples were collected manually through a septum fitted on the lid of the automatic soil chambers. Manual gas collection and analysis was performed as previously described.

### *3.4. $N_2O$ flux estimation*

Soil $N_2O$ gas flux was estimated from the change in gas concentration in the chamber headspace over time. Gas flux per unit soil area was estimated from the slope obtained by least-squares linear regression of the concentration of $[N_2O]$ versus time (t) to estimate $d[N_2O]/dt$, as in Equation (4).

$$N_2O_{flux} = H \frac{d[N_2O]}{dt} \quad (4)$$

where *H* is the ratio of the internal chamber volume to area of soil surface enclosed by the chamber. Flux of $N_2O$ is generally expressed in units of mole or mass of N-$N_2O$ per units of area and time (e.g., mol $N_2O$-N $ha^{-1}$ $day^{-1}$ or g $N_2O$-N $ha^{-1}$ $day^{-1}$) (Parkin et al., 2012; Venterea et al., 2009).

During automatic $N_2O$ flux monitoring, total chamber closure times were either 20 minutes or 10 minutes, depending on flux intensity, and the corresponding effective chamber deployment (i.e., sampling) times after accounting for gas transport time in the sampling system, were 15 or 5 minutes, respectively. The analyzer sampling rate was set to 20 seconds yielding an approximate precision of 0.2 ppb and recording 45 or 15 $N_2O$ concentration measurements per a 15- or 5-minute chamber deployment time, respectively. Having such a large number of measurements allowed us to reliably detect and eliminate chamber effects (Parkin et al., 2012; Venterea et al., 2009) by testing for linearity in the flux calculation and subsampling the data when necessary, to assure flux linearity. The first step in the adaptive linear flux calculation was to estimate the flux (change in chamber headspace $N_2O$ concentration vs. time) and the corresponding coefficient of determination ($r^2$) using all data collected during the effective sampling period. If $r^2$ was smaller than 0.95, a new flux estimate (i.e., slope of $N_2O$ concentration vs. time) and corresponding $r^2$ were calculated using a subsample of the data. Subsamples were created by sequentially eliminating the last $N_2O$ concentration datum until the computed $r^2$ was larger than 0.95, with a minimum of 6 time-concentration data points. This adaptive linear flux calculation allowed us to minimize chamber effects without compromising the precision or accuracy of the flux estimates.

Fluxes during the period of manual $N_2O$ gas sampling were estimated using equation 4 fit to the four $N_2O$ concentration measurements (Parkin et al., 2012).

### *3.5. $N_2O$ data selection*

Soil $N_2O$ flux estimates calculated from the chamber concentration measurements were screened to eliminate unreliable and *de minimis* flux measurements prior to statistical analysis. Estimated fluxes that were below the MDF corresponding to the chamber closure time (e.g., < $3.7 \times 10^{-4}$ g $N_2O$-N $ha^{-1}$ $day^{-1}$ for 20-minute closure) were indistinguishable from zero flux and were removed from the flux dataset. These fluxes were removed rather than included as zero flux because in the unsupervised system it is impossible to differentiate between fluxes below the MDF and those resulting from a chamber failure. In addition, we screened for unreliable flux estimates resulting from occasional malfunctions of the unsupervised measurement system that occurred when a chamber failed to open or failed to close. For example, a chamber might not close or open if ice build-up blocked the chamber lid linkage during a freezing rain. A flux estimate was deemed unreliable and rejected due to failure of a chamber to close when the measured chamber $N_2O$ concentrations at the beginning and end of the sampling period were both within ± 2 times the instrument precision (0.4 ppbv) of the ambient atmospheric $N_2O$ concentration. If a chamber failed to open, it would remain closed through a complete 2-hour cycle of sampling all four chambers, and the chamber headspace $N_2O$ concentration would be in equilibrium with the $N_2O$ concentration in the soil or very nearly to. Therefore, a flux estimate was deemed rejected due to failure of a chamber to open when the measured chamber $N_2O$ concentration at the beginning of the sampling period was greater than the ambient atmospheric $N_2O$ concentration by +2 times the instrument precision and the chamber $N_2O$ concentration at the end of the sampling period was within ± 2 times the instrument precision (0.4 ppbv) of the chamber $N_2O$ concentration at the beginning of the sampling period. Ambient atmospheric $N_2O$ concentration was measured by sampling the ambient air 2 m above the instrumentation trailer

during the 5 minutes prior to chamber closure. After data filtering no negative fluxes were observed.

### *3.6. Cumulative $N_2O$ emissions*

The magnitude of soil $N_2O$ flux can be highly variable on weekly, monthly, seasonally, and annual scales due to variations in the levels of available oxygen, nitrogen, and carbon in the soil and temperature. The mechanisms controlling the availability of these limiting resources, and therefore the size of the soil $N_2O$ flux, are expected to vary both seasonally and with events like precipitation, tillage, and fertilization. To better understand the effect of time of dairy manure application on $N_2O$ emissions, cumulative emissions were first estimated as cumulative emissions for each sampling campaign and time of manure application. And then divided into four periods representing contrasting soil and weather conditions which could have a significant effect on $N_2O$ daily emission (e.g., soil freeze-thaw cycles, increasing temperatures, crop growing stages, etc.,). $N_2O$ emissions in highly fertilized crops such as corn grain, are characterized by short-lived peak emissions events which contribute to most of the cumulative emissions. Because peak events contribute to the largest fraction of cumulative emissions, they were characterized for each sampling campaign and time of manure application during the fall. All in all, cumulative emissions were divided in different periods according to soil and crop condition and peak emissions during each period were identified.

Cumulative fluxes for each chamber were computed as the sum of the daily fluxes over the sampling campaign duration. When using the automatic system, the daily flux of $N_2O$ at each chamber (g $N_2O$-N $ha^{-1}day^{-1}$) was computed as the integral over 24 hours of the individual flux estimates at that chamber on a specific day. When the fluxes were measured manually, the

estimated flux was used as daily flux on the measuring date. Linear interpolation was used between $N_2O$ manual sampling dates and to fill occasional short data gaps of the automatic $N_2O$ monitoring system. Cumulative emissions were computed as the sum of daily fluxes.

### *3.7. Peak $N_2O$ emissions*

High fertilized corn systems are characterized by episodic extreme peak emissions that can contribute up to 70% of the cumulative emission while representing less than 10% of the total observations (Francis Clar & Anex, 2020; Molodovskaya et al., 2012). Because peak emission events contribute the majority of cumulative emissions, characterizing these peak events is crucial to understanding the differences in cumulative $N_2O$ emissions due to timing of manure application during the fall.

Daily emissions were categorized as peak emissions using a functional approach based in normalized cumulative daily flux size as described in Francis Clar & Anex, (2020). Normalized cumulative daily flux size was calculated for each sampling campaign and chamber as the ratio between the daily flux and the cumulative flux. To estimate the flux value used as threshold to classify daily emissions as peak emission a new variable referred to here as cumulative contribution was computed. Cumulative contribution was computed as the result of successive additions of normalized cumulative daily fluxes that were sorted by size in descending order. For example, if the 3 top normalized daily fluxes were 2%, 1.5% and 1% the resulting cumulative contributions for each successive normalized daily flux would be 2%, 3.5% and 4.5%. The daily flux value chosen as the peak emissions threshold was that with a cumulative contribution equal or greater than 50% of the cumulative contribution. Threshold daily fluxes were different for each sampling campaign, timing of manure application during the fall and chamber, for

simplicity, based in the previously explained calculations two threshold values where chosen. During the 2016-17 and 2017-18 daily fluxes greater than 50 g $N_2O$-N $ha^{-1}$ $day^{-1}$ were classified as peak emissions, during the 2018-19 and 2019-20 daily fluxes greater than 20 g $N_2O$-N $ha^{-1}$ $day^{-1}$ were classified as peak emissions.

### *3.8. Statistical analysis*

Statistical analyses were conducted using SAS 9.3 (SAS Institute, 2011) using the MIXED procedure. The experimental design was a randomized complete block design with subsampling with one fixed treatment, time of dairy slurry application during the fall at two different times, early or late. The blocking factor was sampling campaign, it was treated as a random effect, the experimental unit was plot and the subsampling units were the number of samplers per plot. The number of samplers per plot were 2 soil chambers for $N_2O$ emissions during all 4 sampling campaigns. For $NO_3^-$ losses via leachate, during the sampling campaigns of 2018-19 and 2019-20, seven soil-water samplers were installed at each plot, therefore subsampling was 7.

Differences between early and late fall manured plots in $N_2O$ cumulative emissions for all four sampling campaigns and in $NO_3^-$-N losses during 2018-19 and 2019-20 were evaluated using the least squares means using the LSMEAN method for a 90% confidence level (p_value < 0.05). The statistical analyses were applied to cumulative campaign results and to the different periods in which sampling campaigns were divided (i.e., fall, winter, etc.,).

During the 2016-17 and 2017-18 one soil-water sampler was installed at each plot. Due to lack of subsampling in the two first sampling campaigns, the differences in the amount of $NO_3^-$-N leaching between early and late manured plots were statistically assessed only for the sampling

campaigns of 2018-19 and 2019-20. The observations made during the two first sampling campaigns were used to qualitatively support the results 2018-19 and 2019-20.

During all sampling campaigns the differences in [$NO_3^-$-N] of soil-water samples collected on the same date but from different treatments were analyzed using a paired *t*-test at a significance level of 0.1. As explained in section 2.2 this is a common approach when soil-water [$NO_3^-$-N] measurement are not replicated.

To provide a reference for the variability of the [$NO_3^-$-N] in soil-water samples we calculated the Coefficient of Variability (CV) of the soil-water [$NO_3^-$-N] collected on the same day from each within each plot, early or late fall manured. The CV between [$NO_3^-$-N] from the different suctions cups samplers from early manured plots was 51% and 81% in 2016-17 and 2017-18 respectively, and 50% and 53% in 2016-17 and 2017-18 respectively for late manured plots. For both treatments, the CV varied randomly along the sampling campaign, I did not observe any pattern in the variability of [$NO_3^-$-N] among different sampling periods (i.e., before soil freeze and after soil thaw). On average across all sampling campaigns and treatments, the mean CV was 59%. This CV is a representative value for the spatial variability in $NO_3^-$-N concentration measurements using ceramic suction cups below the root zone in agricultural loamy sand soils (Lord & Shepherd, 1993). The 59% CV is used later as a reference for $NO_3^-$-N variability for the non-replicated [$NO_3^-$-N] measurements obtained in 2016-17 and 2017-18.

During the first sampling campaign, 2016-17 the early and late fall manured plots were accidentally fertilized at corn growth stage V6 on July 13$^{th}$. Fertilization at V6 did not occur in the following three sampling campaigns. In 2016-17, fertilization at V6 was followed by a large peak in $N_2O$ emissions. To avoid misleading comparisons between treatments across all

sampling campaigns, the $N_2O$ and $NO_3^-$ data collected between the V6 fertilization event (July 13th, 2017) and the end of the sampling campaign (September 15th, 2017) were discarded. Rejecting these data did not impact the quality of the experimental results or limit the conclusions drawn from these results. The results of soil analysis, grain and above ground biomass yields for 2016-17 seasons were not included.

**Table 1. Date of relevant fields events during the four soil sampling campaigns**

| Season | Dairy slurry app (Early/Late) | Soil Freeze | Soil Thaw | Planting | Switch to manual | Harvest |
|---|---|---|---|---|---|---|
| 2016-17 | 9/20/2016<br>11/16/2016 | 1/3/2017 | 3/10/2017 | 5/8/2017 | 7/05/2017 | 10/30/2017 |
| 2017-18 | 9/12/2017<br>11/13/2017 | 12/1/2017 | 4/25/2018* | 5/8/2018 | 8/22/2018 | 10/29/2018 |
| 2018-19 | 9/14/2018<br>11/24/2018 | 12/19/2018 | 3/25/2019 | 5/14/2019 | 8/19/2019 | 10/30/2019 |
| 2019-20 | 9/18/2019<br>11/5/2019 | 12/21/2019 | 3/15/2020 | 5/6/2020 | Ended as automatic | 11/04/2020 |

## *4. Results*

### *4.1. Weather conditions*

During each of the sampling campaigns the total amount of precipitation, rain and snow, was higher than the average of the 30 previous years. During all sampling campaigns we often recorded more precipitation that the monthly average for the previous 30 years. In comparison to the rest of sampling campaigns and to the historic monthly averages of the previous 30 years, the sampling campaign of 2017-18 had a drier fall and a wetter spring and summer (Table A1 and A2).

The average air temperature in November 2016 and February 2017 was up to 5ºC higher than during the same months of the other sampling campaigns. In April 2017 the average temperature was 4ºC lower than the average air temperature in April during the rest of sampling campaigns. Snow fall in April 2017 was also unusually large. In general, average monthly temperatures during the observed sampling campaigns were warmer than the 30-year average. This was especially noticeable at the beginning and the end of the winters (Table A2 and A3).

### *4.2.* ***Soil and manure analysis***

Manure analysis showed that the N, C, and solid fraction of dairy slurry applications were variable throughout the study period. The rates of total nitrogen (TN) applied ranged from 99 to 163 Kg $ha^{-1}$, the fraction of mineral N (i.e., $NH_4$-N) ranged from 60% to 42% of the TN, and C to N ratios (C/N) ranged from 5 to 12. Differences in the rates of TN and the $NH_4$-N applied to the early and late manured plot within each sampling campaign were small and did not exhibit a consistent trend across sampling campaigns (Table A4). The observed differences in manure composition did not confound the study of the effect of timing of manure application during the fall on N losses (Table A4).

Differences in soil $NH_4$-N, $NO_3^-$-N, TN and TOC between experimental plots before the experiments started, (i.e., before early manure application) were not significant. Although these differences were not significant, it is worth noting that the $NH_4$ concentration at depths of 0.2-0.4 m and 0.4-0.6 m in the plots used in 2017-18 were two and three times greater than in the plots from the other sampling campaign (Table A5).

Differences in soil $NH_4$-N and $NO_3^-$-N concentrations between early and late manured plots at V6 were not significant. During the same season, differences between early and late manured

plots in the change of soil nitrogen ($NO_3^-$-N and $NH_4$-N) from pre-manured to V6 soil samples analysis were smaller than 10 Kg $ha^{-1}$ except for $NO_3^-$ changes in the topsoil layer in 2019-20. During this sampling campaign the soil top layer in the early manured plot lost 22 $NO_3^-$-N Kg $ha^{-1}$ while the topsoil layer of the early manured plot gained 6 $NO_3^-$-N Kg $ha^{-1}$ , the difference in $NO_3^-$-N change from pre-manure application to V6, between early and late manured was 28 $NO_3$-N Kg $ha^{-1}$ (Table A5).

### *4.3. $NO_3^-$ leaching losses*

The quantity of $NO_3^-$-N leached outside of the corn system was calculated by multiplying the volume of soil-water drainage below the corn root zone (0.75 m) by the $NO_3^-$-N concentration of the soil-water ([$NO_3^-$-N]). During 2018-19 and 2019-20 seven soil-water samplers per plots were used to capture the spatial variability of [$NO_3^-$-N] while only one sampler per plot was used in 2016-17 and 2017-18. The $NO_3^-$-N leaching results from 2018-19 and 2019-20 are presented first.

Due to the variability of both volume of water leached below the root zone and [$NO_3^-$-N] of the soil-water samples, the amount of $NO_3^-$-N leached out of the system varied widely (Table 2, Table 3). When averaged across all sampling campaigns, early manured plots lost larger amounts of $NO_3^-$-N than plots manured late in the fall. During 2018-19 and 2019-20 $NO_3^-$-N losses from early manured plots were significantly higher (p_value = 0.042) than those from late manured plots. On average in 2018-19 and 2019-20 early manured plots lost 4.55 $NO_3^-$-N Kg $ha^{-1}$ (or 20%) more $NO_3^-$-N than plots manured later during the fall (Table 2). During 2016-17, the late manured plot lost 7.51 $NO_3^-$-N kg $ha^{-1}$ more that the early manured plot, this difference represented 13% of the total $NO_3^-$-N losses in the late manured plot. During 2017-18, the early

manured plot lost 99 $NO_3^-$-N kg $ha^{-1}$ more that the early manured plot. This difference represented 59% of the total $NO_3^-$-N losses in the late manured plot (Table 3).

The $NO_3^-$-N concentration in soil-water samples varied widely across sampling campaigns and treatments, average [$NO_3^-$-N] for all sampling campaigns ranged from 0.02 to 94.46 mg $L^{-1}$ (Figure 1, Figure 2). The average [$NO_3^-$-N] during 2016-17, 2018-19, and 2019-20 were similar, average [$NO_3^-$-N] measurements during 2019-20 were 6 and 2 times smaller than those from 2016-17 and 2018-19 respectively (Figures 1 and 2). The average [$NO_3^-$-N] during 2017-18 were large, especially during the spring, average [$NO_3^-$-N] measurements ranged from 0.04 to 94.46 $NO_3^-$-N mg $L^{-1}$; retrieving soil-water samples during 2017-18 was troublesome, specially at the beginning of the season and after soil thaw (Figure 1).

During the period between early manure application and soil freeze, the pattern in differences between [$NO_3^-$-N] in water-samples collected from late and early manured plots on the same day was the same for all sampling seasons. The [$NO_3^-$-N] of soil-water samples collected from early manured plots were higher than those measured from the late manured plot, and on most days these differences were significant (*t*-test, p_value < 0.1) (non-overlapping error bars in Figures 1 and 2). After early manure application [$NO_3^-$-N] in soil water samples exhibit a characteristic pattern during all sampling seasons, in which [$NO_3^-$-N] increased following manure application, then decreased and then increased again, describing two peaks of [$NO_3^-$-N], the size of the peaks and their timing was different in each sampling campaign.

The pattern in differences between [$NO_3^-$-N] in water-samples collected from late and early manured plots on the same day after soil thaw varied among the different sampling campaigns. During 2018-19 and 2019-20 these differences were smaller than 2 $NO_3^-$-N mg $L^{-1}$ and not

significant (p_value > 0.1) (overlapping error bars in Figure 1). During 2016-17, the [$NO_3^-$-N] of soil-water samples collected from late manured plots were higher than those measured from the early manured plot, these differences were not significant (*t*-test, p_value > 0.1) (overlapping error bars in Figure 2). The contrary was true during 2017-18, the [$NO_3^-$-N] of soil-water samples collected from early manured plots were higher than those measured from the late manured plot, these differences were significant in most days (*t*-test, p_value < 0.1) (non-overlapping error bars in Figure 2).

Across all sampling campaigns the largest losses in $NO_3^-$-N occurred during the period of the largest volume of water leached below the root zone; this period varied among the sampling campaigns. During 2018-19 and 2019-20, the largest fraction of leaching occurred during fall, between early manure application and soil freeze (Table 2). During these two sampling campaigns the [$NO_3^-$-N] in the period between early manure application and soil freeze was greater than after soil thaw (Figure 1). During 2016-17 and 2017-18, the largest fraction of leaching occurred during spring, between soil thaw and planting (Table 3). During these two sampling campaigns the [$NO_3^-$-N] in the period between early manure application and soil freeze was smaller than after soil thaw (Figure 2)

**Table 2.** $NO_3$-N losses, precipitation and leachate for sampling periods at plots manured with dairy slurry early and late during the fall for the sampling campaigns (SC) of 2018-19 and 2019-20**.**

| SC | Period | Date (m/d/y) | #Days | Rain (mm) | Leachate (mm) | $NO_3^-$-N kg $ha^{-1}$ Early | Late | Early - Late |
|---|---|---|---|---|---|---|---|---|
| 2018-19 | Early manure app | 9/14/18 | | | | | | |
| | Starting date | 9/24/18 | 10 | 40 | | | | |
| | Start to Soil Freeze (Fall) | 12/19/18 | 96 | 270 | 207 | 9.4 ± 4 | 3.5 ± 0.4 | 5.9 |
| | Soil Freeze to Thaw | 3/25/19 | 96 | 0 | | | | |
| | Soil Thaw to Planting | 5/14/19 | 50 | 177 | 55 | 4.5 ± 1.7 | 2.9 ± 1.4 | 1.6 |
| | Planting to V6 | 6/13/19 | 30 | 115 | 92 | 1.8 ± 0.5 | 2.9 ± 1.6 | -1.1 |
| | V6 to End | 8/1/19 | 49 | 390 | 85 | 1.7 ± 0.6 | 1.7 ± 0.6 | 0 |
| | Total | | 225 | 952 | 439 | 14.7 ± 4.8 | 10.9 ± 2.7 | 3.8 |
| 2019-20 | Early manure app | 9/18/19 | | | | | | |
| | Starting date | 9/20/19 | 2 | 2.5 | | | | |
| | Start to Soil Freeze (Fall) | 12/21/19 | 94 | 285 | 253 | 6.3 ± 2.6 | 0.8 ± 0.5 | 5.5 |
| | Soil Freeze to Thaw | 3/15/20 | 85 | 0 | | | | |
| | Soil Thaw to Planting | 5/6/20 | 52 | 135 | 84 | 0.8 ± 0.3 | 1.1 ± 0.6 | -0.3 |
| | Planting to V6 | 6/13/20 | 38 | 168 | 101 | 1.7 ± 0.5 | 1.6 ± 0.6 | 0.1 |
| | V6 to End | 8/1/20 | 49 | 374 | 30 | 0.3 ± 0.2 | 0.3 ± 0.2 | 0 |
| | Total | | 233 | 962 | 468 | 8 ± 2.8 | 3.7 ± 1.4 | 5.3 |
| | | | | | | | Mean diff | 4.55 |

**Table 3.** $NO_3$-N loses, precipitation and leachate for sampling periods at plots manured with dairy slurry early and late during the fall for the sampling campaigns (SC) of 2016-17 and 2017-18.

| SC | Period | Date (m/d/y) | #Days | Rain (mm) | Leachate (mm) | $NO_3^-$-N kg $ha^{-1}$ | | Early - Late |
|---|---|---|---|---|---|---|---|---|
| | | | | | | Early | Late | |
| 2016-17 | Early manure app | 9/20/16 | | | | | | |
| | Starting date | 9/29/16 | 9 | 41 | - | | | |
| | Start to Soil Freeze (Fall) | 1/3/17 | 105 | 224 | 129 | 20.90 | 6.87 | 14.03 |
| | Soil Freeze to Thaw | 3/10/17 | 66 | | | | | |
| | Soil Thaw to Planting | 5/8/17 | 59 | 324 | 173 | 14.20 | 27.30 | -13.10 |
| | Planting to V6 | 6/13/17 | 36 | 78 | 41 | 5.20 | 9.50 | -4.30 |
| | V6 to End | 8/1/17 | 49 | 183 | 60 | 9.12 | 13.26 | -4.14 |
| | Total | | 249 | 809 | 403 | 49.42 | 56.93 | -7.51 |
| 2017-18 | Early manure app | 9/12/17 | | | | | | |
| | Starting date | 10/23/17 | 47 | 107 | - | | | |
| | Start to Soil Freeze (Fall) | 12/6/17 | 85 | 131 | 96 | 3.01 | 2.48 | 0.53 |
| | Soil Freeze to Thaw | 4/25/18 | 140 | | | | | |
| | Soil Thaw to Planting | 5/14/18 | 19 | 153 | 130 | 86.80 | 27.66 | 59.14 |
| | Planting to V6 | 6/13/18 | 30 | 76 | 27 | 24.41 | 11.77 | 12.64 |
| | V6 to End | 8/1/18 | 49 | 161 | 57 | 53.38 | 26.69 | 26.69 |
| | Total | | 183 | 521 | 310 | 167.60 | 68.60 | 99 |

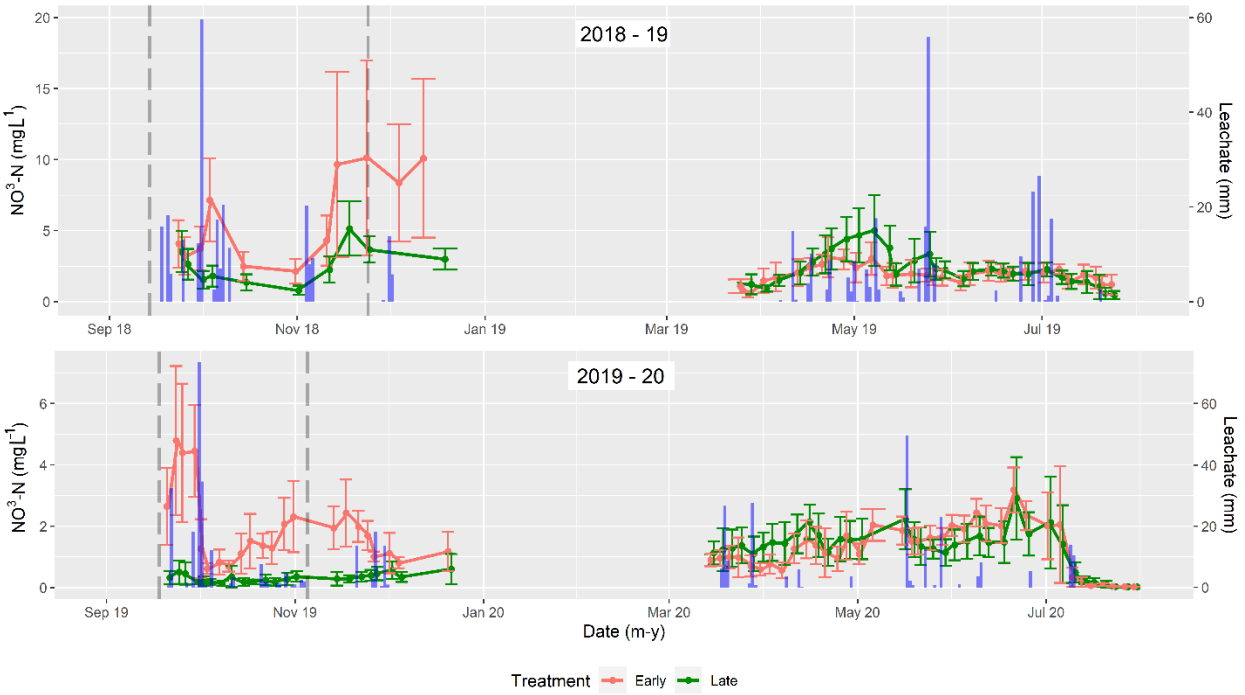


**Figure 1.** Volume of leachate (blue columns) and [$NO_3^-$-N] concentration measured from plots receiving dairy slurry early (red) and late (dark green) during the fall for the 2018-19 and 2019-20 sampling campaigns. Errors bars indicate 90% confidence intervals. Notice different y-axis scale between upper and lower plots. Leachate sampling was halted during soil freeze (Table 2). In general, during the fall, [$NO_3^-$-N] form water samples collected from the early manured plot were larger than those collected from the late manured plot in the same day.

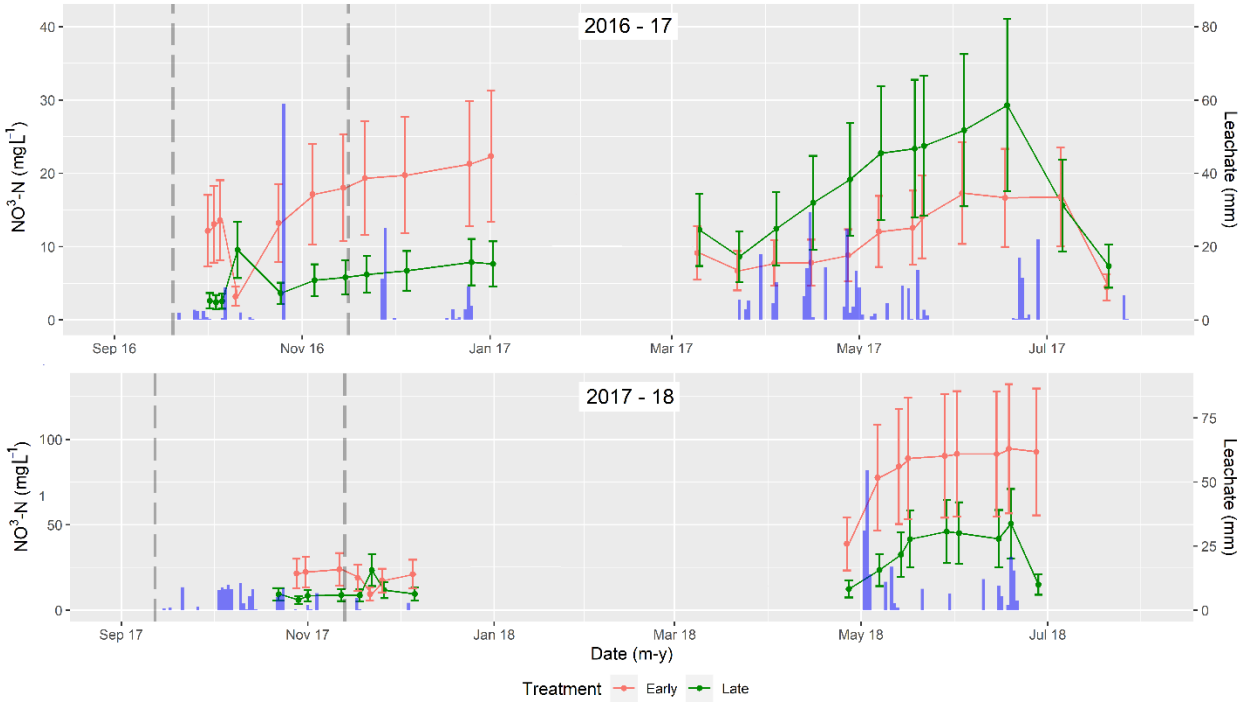


**Figure 2.** Volume of leachate (blue columns) and [$NO_3^-$-N] from plots receiving dairy slurry early (red) and late (dark green) during the fall for the 2016-17 and 2017-18 sampling campaigns. Errors bars indicate 90% confidence intervals, error bars were computed based in the variability in $NO_3^-$ soil-water samples measured during 2018-19 and 2019-20. Leachate sampling was halted during soil freeze (Table 3). Notice different y-axis scale between upper and lower plots. In general, during the fall, [$NO_3^-$-N] form water samples collected from the early manured plot were larger than those collected from the late manured plot in the same day.

### *4.4. $N_2O$ measurements*

During the four-year experiment, automatic sampling was only interrupted for more than 5 consecutive days on three occasions and only two of them were related to failure of a component of the monitoring system (Table 4). The average sampling resolution during the operational time, which includes periods during which sampling was interrupted for less than five consecutive days, was 7.2 times per chamber and day across all sampling campaigns (Table 4). This is important because accurate estimation of daily and therefore cumulative $N_2O$ emissions requires (1) daily sampling to capture peak emissions and (2) $N_2O$ measurements at sub-daily frequencies to accurately estimate daily emissions during peak events (Francis Clar & Anex 2020).

During 2016-17, a $N_2O$ sampling interruption of 25 days occurred in the winter, this was triggered by several days of unusually high temperatures and rain in January. These events resulted in flooding of the experimental plots which was followed immediately by freezing temperatures. The flood resulted in standing water and subsequently sheet ice formation which caused damage to the automatic soil chambers and delayed the restart of automatic $N_2O$ sampling. Once the standing water froze, soil fluxes were measured manually. Due to the soil and weather conditions (i.e., water and ice cover) and based on the magnitude of the $N_2O$ fluxes measured manually, it is unlikely that significant $N_2O$ soil emissions were missed due to intermittent sampling during this period (Figure 1).

Sampling interruptions due to systems failure occurred during 2018-19 and 2019-20 lasting 30 and 17 days, respectively (Table 4). On both occasions the system failed because the diaphragm of the analyzer internal vacuum pump required replacement. Loss of vacuum in the measuring cell can be observed from the analyzer user interface. During these two sampling interruptions, $N_2O$ fluxes were measured manually every 5 days. Due to the soil condition and weather conditions and based on the magnitude of the $N_2O$ fluxes measured manually during this period, it is very unlikely that we missed significant $N_2O$ soil emissions due to intermittent manual sampling during either of these periods (Figure 1).

**Table 4. Performance of the automatic $N_2O$ monitoring system and days sampled at high temporal resolution**

| Sampling campaign | Date early slurry app | Automatic monitoring starts | Automatic monitoring ends | Operational time in days | Average resolution (flux $day^{-1}$ $chamber^{-1}$) | Sampling interruptions dates (#days – cause) |
|---|---|---|---|---|---|---|
| 2016-17 | 9/20/16 | 9/22/16 | 7/5/17 | 285 | 6.5 | 1/18/17 to 2/5/17 (25 – flood/freeze) |
| 2017-18 | 9/12/17 | 9/11/17 | 8/22/18 | 334 | 6.7 | none |
| 2018-19 | 9/14/18 | 9/13/18 | 7/15/19 | 279 | 7.9 | 6/4/19 to 6/30/19 (30 - Analyzer fail) |
| 2019-20 | 9/18/19 | 9/18/20 | 9/10/20 | 358 | 7.8 | 10/19/19 to 11/5/19 (17 - Analyzer fail) |

All manually measured fluxes were below 10 g $N_2O$-N $ha^{-1}$ $day^{-1}$. The fluxes measured during August and September of the 2018-19 sampling campaign were below the MDF (< 0.1 g of $N_2O$-N $ha^{-1}$ $day^{-1}$) and thus equivalent to a zero flux. Soil $N_2O$ fluxes at the end of the sampling campaign (i.e., July to September) when the soil is depleted of available N are low and stable (Table 3, Figure 2). Given the soil and weather conditions at the end of the sampling campaign and the magnitude of the manually measured fluxes, intermittent manual sampling during the end of the sampling campaign did not affect the accuracy of our cumulative estimates.

### *4.5. **Cumulative $N_2O$ emissions***

Cumulative emissions varied widely across sampling campaigns (Table 5). The largest cumulative emissions occurred in 2017-18, in this sampling campaign the average cumulative $N_2O$ emissions from early and late manured plots was 4,794.5 $N_2O$-N kg $ha^{-1}$. Cumulative emissions from 2016-17 were 34% smaller than those from 2017-18. Cumulative emissions in 2018-19 and 2019-20 were much smaller than those from the previous seasons, being 64% and 66% smaller than those observed in 2017-18 (Table 5), respectively.

The difference in cumulative emissions between early and late manured plots did not follow the same pattern in all years. Averaged across the four sampling campaigns, cumulative $N_2O$ emissions from plots receiving dairy slurry manure late were 1692 ± 1963 (μ ± σ) $N_2O$-N g $ha^{-1}$ larger than $N_2O$ emissions from plots that received manure early (Table 5). The difference in cumulative $N_2O$ emissions due to timing of manure applications during the fall across the four sampling campaigns was not significant (p-value = 0.2). In this statistical analysis, the significance of the blocking factor *'sampling campaign'* was low (p-value = 0.07).

During the first three sampling campaigns (2016-17, 2017-18, and 2018-19), $N_2O$ emissions from late manured plots were significantly higher (p-value = 0.035) than cumulative emissions from early manured plots (Table 5). On average, across the first three sampling campaigns, cumulative emissions from late manured plots were 2,763 ± 743 g $N_2O$-N $ha^{-1}$ (μ ± σ) larger than cumulative emissions from early manured plots (Table 5). In this statistical analysis, the blocking factor sampling campaign was significant (p-value = 0.023).

During 2019-20 cumulative emissions from late manured plot were 1,520 $N_2O$-N g $ha^{-1}$ smaller than those from the early manured plot (Table 5). In 2019-20, the effect of manure application time on cumulative $N_2O$ emissions was reversed respect that observed in the three previous sampling campaigns.

### *4.6.* ***Peak $N_2O$ emissions***

Peak $N_2O$ emission events contributed between 42 to 74% of the cumulative emissions and between 5 to 9% of the total observed time (i.e., < 31 days per year) (Table 5).

Timing of manure application in the fall affected the timing, magnitude, duration, and frequency of peak emissions. Across the four sampling campaigns, peak emissions usually occurred during the fall following dairy slurry application and soon after precipitation and during Freeze-Thaw cycles (FTC) in the winter and spring (Figure 3 and Table 5).

During the fall, peak emissions from early and late manured plots occurred within two to three weeks after manure application. Fall peak emissions from early manured plots were greater and last longer than those from late manured plots. In 2017-18, the late manured plot did not exhibit peak emissions after manure application (Figure 3 and Table 5). Relative to late manured plots, peak emissions after manure application from early manured plots occurred usually under higher air and soil temperatures and received larger amounts of precipitations in the days following manure application. Peak emissions after early manure application occurred during days when air temperatures ranged between 5º to 22º C and soil temperatures at a depth of 0.1 m ranged from 19.8º to 22.6ºC (Figure 3). For all sampling campaigns, except for 2017-18, more than 10 mm of rainfall occurred within 3 days of the early manure application, rising the VWC of the soil at a depth of 0.05 m to ~30% (i.e., field capacity) (Figure 3). Late fall manure application occurred when soil temperatures at a depth of 0.1 m ranged from 8.8º to 0.1ºC. Peak emissions after late manure application occurred during days when air temperatures ranged from 7º to 0ºC, except during 2016-17, when peak emissions occurred the same day of manure application at a mean daily air temperature of 13.4ºC. Peak emissions after late manure application in 2017-16 were the highest peak emissions after late manure application across all sampling campaigns. Accumulated rainfall during the week after late manure application was below 10 mm, during all sampling campaigns. The soil at 0.05 m depth froze (reach and stayed at 0 ºC or below for a week or more) within 4 weeks of late manure application (Figure 3).

Peak emissions occurring during FTC in the winter and spring were larger, lasted longer and occurred more frequently than peak emissions occurring during the fall for both early and late fall manured plots (Figure 3 and Table 5). During the first three sampling campaigns, peak emissions occurring during FTC from late manured plots were greater, lasted more days and occurred more frequently that those from early manured plots. By the contrary, FTC peak emissions in 2019-20 from the early manure plot were greater, lasted more days and occurred more frequently that those from early manured plot. The differences in FTC peak emissions between early and late manured plot during the first 3 sampling campaigns were between 4 and 9 times greater than those observed in 2019-20 (Figure 3 and Table 5).

Peak emissions during FTC tend to occur within the same week or days and under similar soil temperature and moisture conditions. The largest FTC peak emissions tend to occur at the end of the winter when soil temperature at a depth of 0.05 m increased to 0ºC or above and when soil moisture (VWC) increased (Figure 3).

**Table 5**. Cumulative and peak $N_2O$ emissions from plots manured early and late during the fall. $N_2O$ emissions are divided in 4 different periods according to soil and crop conditions. Percentages indicate the portion of cumulative emissions and total observed time represented by peak emissions. Peak $N_2O$ emissions contributed to more than 40% of the cumulative emissions and to less than 10% of the total observed time. For all sampling campaigns, except for the 2019-20, cumulative emission from late manured plots were greater than those from early manured plots. Time of dairy slurry application influenced the magnitude, frequency, and timing of $N_2O$ cumulative and peak emission. $N_2O$ emissions from 'V6 to end' in 2016-17 are not included because the plots were accidentally fertilized at V6. (next page)

| Season | Period | Date (m/d/y) | #Days | Cumulative emissions (g $N_2O$-N $ha^{-1}$) | | | Peak emissions (g $N_2O$-N $ha^{-1}$) | | | |
|---|---|---|---|---|---|---|---|---|---|---|
| | | | | Early | Late | Late - Early | Early | Early (days) | Late | Late (days) |
| 2016-17 | Sampling begins (Date of Early app) | 9/20/16 | | | | | | | | |
| | Soil Freeze (End of Fall) | 12/22/16 | 93 | 1,160 | 843 | | 392 | 6 | 103 | 1 |
| | Soil Thaw to Planting (Winter and Spring) | 5/8/17 | 137 | 2,444 | 4,547 | | 1,168 | 8 | 3,111 | 20 |
| | Planting to V6 | 6/13/17 | 36 | 134 | 461 | | 0 | 0 | 56 | 1 |
| | **Total** | | **266** | **3,738 ±353** | **5,851 ±1415** | **2,113 ±1459** | **1,560 (42%)** | **14 (5%)** | **3,270 (56%)** | **22 (8%)** |
| 2017-18 | Sampling begins | 9/12/17 | | | | | | | | |
| | End of Fall | 12/6/17 | 85 | 555 | 278 | | 116 | 2 | 0 | 0 |
| | Winter and Spring | 5/8/18 | 153 | 5,316 | 8,904 | | 4,504 | 25 | 6,727 | 30 |
| | Planting to V6 | 6/13/18 | 36 | 409 | 319 | | 0 | 0 | 0 | 0 |
| | V6 to End | 9/15/18 | 94 | 208 | 220 | | 0 | 0 | 0 | 0 |
| | **Total** | | **368** | **6,281 ±525** | **9,721 ±1421** | **3,440 ±1946** | **4,620 (74%)** | **27 (7%)** | **6,727 (69%)** | **30 (8%)** |
| 2018-19 | Sampling begins | 9/14/18 | | | | | | | | |
| | Fall | 12/19/18 | 96 | 697 | 443 | | 255 | 6 | 53 | 2 |
| | Winter and Spring | 5/14/19 | 146 | 1,193 | 3,128 | | 720 | 20 | 1,760 | 29 |
| | Planting to V6 | 6/13/19 | 30 | 97 | 143 | | 20 | 1 | 0 | 0 |
| | V6 to End | 9/9/19 | 88 | 169 | 174 | | 0 | 0 | 0 | 0 |
| | **Total** | | **360** | **1,986 ±271** | **3,714 ±583** | **1,732 ±854** | **975 (49%)** | **26 (7%)** | **1,813 (49%)** | **31 (9%)** |
| 2019-20 | Sampling begins | 9/18/19 | | | | | | | | |
| | Fall | 12/21/19 | 94 | 1,508 | 457 | | 988 | 14 | 21 | 1 |
| | Winter and Spring | 5/6/20 | 137 | 1,804 | 1,353 | | 1,064 | 16 | 829 | 25 |
| | Planting to V6 | 6/13/20 | 38 | 128 | 109 | | 0 | 0 | 24 | 1 |
| | V6 to End | 9/4/20 | 83 | 135 | 143 | | 0 | 0 | 0 | 0 |
| | **Total** | | **352** | **3,440 ±395** | **1,920 ±494** | **-1,520 ±889** | **2,052 (60%)** | **30 (9%)** | **874 (46%)** | **27 (8%)** |
| | Cumulative emissions all four sampling campaigns (2016-2020) (μ±σ) | | | 3,899± 1,544 | 5,498± 2,910 | 1,692± 1,963 | | | | |
| | Cumulative emissions first three sampling campaigns (2016-2019) (μ±σ) | | | 4,052± 1,757 | 5,553± 2,453 | 2,763± 743 | | | | |

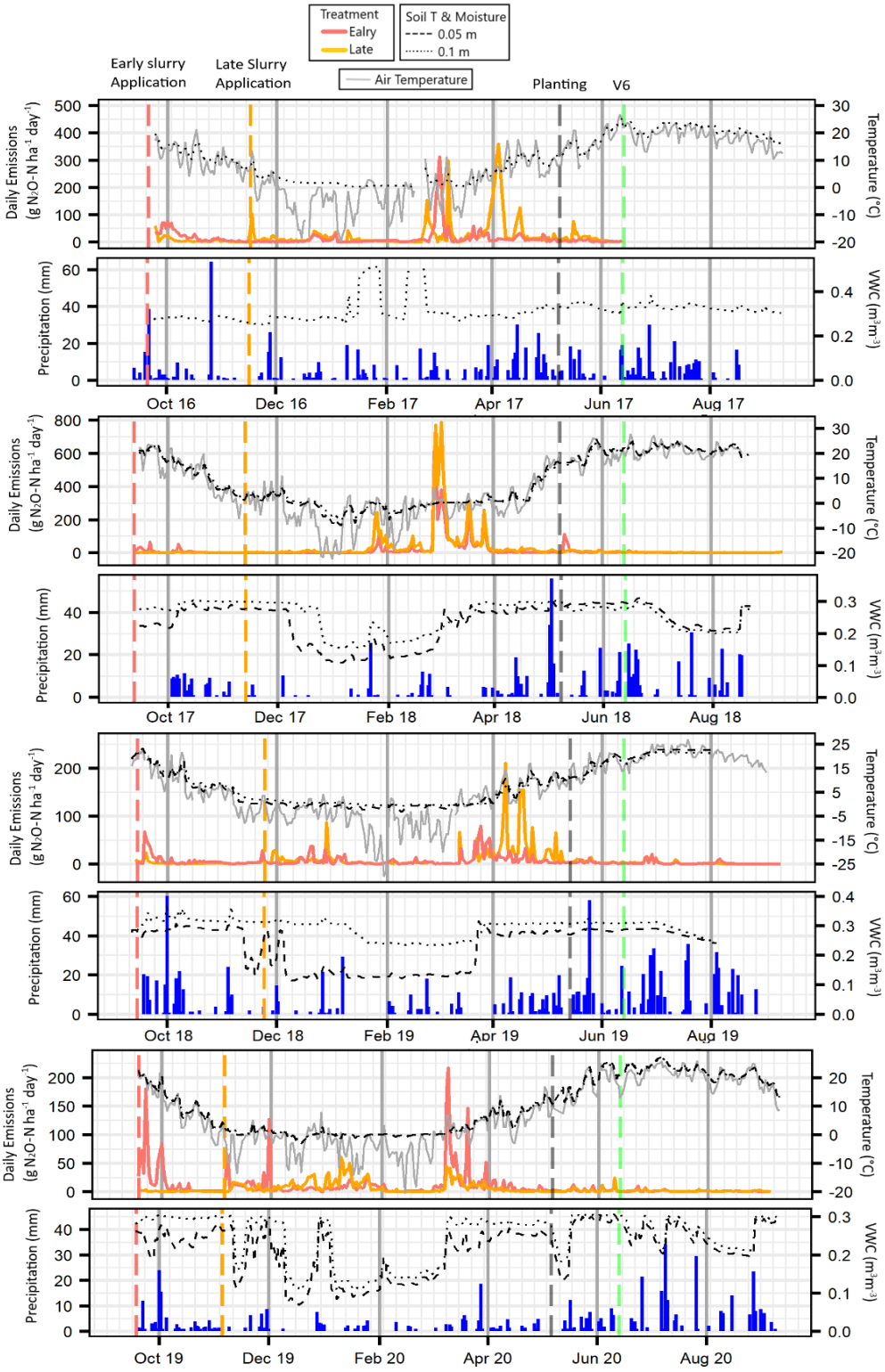


**Figure 3.** Daily $N_2O$ emissions from corn plots manured early and late during the fall with dairy slurry during 4 sampling campaigns (x-axis indicates month and year). $N_2O$ emissions data is accompanied with precipitation, air temperature and soil temperature and moisture (Volumetric Water Content – VWC $m^3m^{-3}$) at 0.05 and 0.1 m depth. Peak emissions occurred during fall soon after manure application and precipitation and during winter and spring during and soon after soil thaw. Time of dairy slurry application affected the magnitude, frequency, and timing of $N_2O$ peak emission.

### *4.7. **Overall $N_2O$ and $NO_3$- losses***

Total N losses varied among all sampling seasons, total N losses in 2018-19 and 2019-20 were similar and much smaller than those from 2016-17 and 2017-18. Nitrate loss, represented between 96% to 66% of the total N losses measured as $N_2O$ and $NO_3^-$. When considering total N losses $NO_3^-$-N and $N_2O$-N was did not exhibit an apparent relationship. Compared with the variability between sampling campaigns, differences in total N loss between early and late manured plots within the same sampling campaign were small and driven by total N losses $NO_3^-$-N that represented the majority of N loss. In 2016-17, the late manured plot lost 9.6 kg $ha^{-1}$ (or 17%) more N than the early manured plot. During 2017-18, 2018-19 and 2019-20 early manured plots lost 95.6, 2.1 and 5.82 kg $ha^{-1}$ (or 76, 13 and 68%) more N than late manured plots (Figure 4).

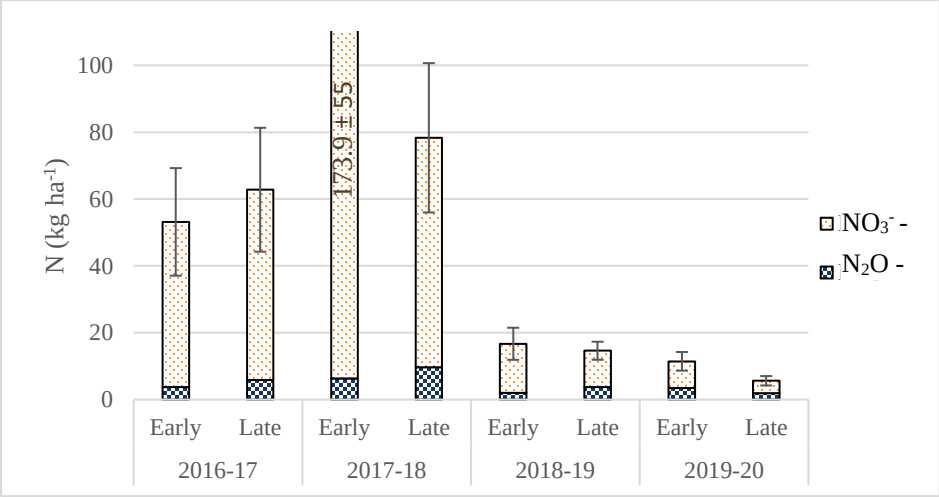


**Figure 4.** Overall N loss as $N_2O$ and $NO_3^-$, in Kg of N $ha^{-1}$during each sampling campaign for early and late fall dairy slurry plots. Notice series 'Early 2017-18' extends out of the plot area. Error bars indicated the standard deviation (SD) of the subsampling units, 2 soil chambers, 7 suction cups per plot. SD of NO3 in 2016-17 and 2017-18 was estimated based in the variability of $NO_3^-$measurments of 2018-19 and 2019-20. N losses via $NO_3^-$are much larger than losses via N losses via $N_2O$.

### *4.8. **Grain and biomass yields***

Differences in corn grain yield, above ground biomass and nitrogen content in above ground biomass between plots were not significant. The corn grain yields measured in our experiments

varied from 8.27 to 4.11 Mg $ha^{-1}$. The corn grain yield measured in the early fall manured plots was 8.27 Mg $ha^{-1}$. Above ground biomass yield varied from 16.18 to 24.42 Mg $ha^{-1}$ (Table A6, Table A3).

## *5. Discussion*

### *5.1. $NO_3$ leaching losses*

Relative to late application, early fall dairy slurry application increased the risk of $NO_3^-$-N loss via leaching due to significantly higher [$NO_3^-$-N] in soil-water samples in the months between early manure application and soil freeze, referred to here as fall. These large differences in [$NO_3^-$-N] were created by a rapid increase in [$NO_3^-$-N] observed immediately after early manure application followed by a second peak several weeks later, while [$NO_3^-$-N] of soil-water samples from late manured plot remained low throughout the fall period. This pattern in [$NO_3^-$-N] in soil-water samples after fall manure application was recurrent across all four sampling campaigns.

Our observations of the variability of [$NO_3^-$-N] after early and late fall manure application illustrates the rationale for the standard recommendations for timing of fall manure application (Aguirre-Villegas et al., 2017). The rates of N-mineralization and nitrification significantly decrease when soil temperature falls below 10ºC (Guntiñas et al., 2012; Robertson & Groffman, 2015). Early manure application in warm soils allows nitrification and mineralization and therefore the loss of manure N via $NO_3$ leaching. On the other hand, applying manure late during the fall, when the soil temperature at 0.1 m depth was below 10ºC and falling, reduces the conversion of organic- and ammonium-N in manure into more easily leachable $NO_3^-$, leading to low $NO_3^-$ losses after manure application in cold soils and higher N soil content during the

winter. Our observations and explanation of the pattern of variability of [$NO_3^-$-N] after early and late fall manure application are supported by microcosm studies (Williams, et al., 2012) and field experiments (Chadwick et al., 2000; van Es et al., 2006; Cambareri et al., 2017; Sawyer, 2020). The increased soil N retention resulting from late fall manure application will have important consequences in $N_2O$ soil emissions during the winter and spring as discussed below.

The pattern in variability of [$NO_3^-$-N] after fall manure application was important and was consistent through the four years of observation, but it did not always dominate the total amount of $NO_3^-$-N loss via leachate and therefore $NO_3$-N loss via leachate from early manured plots was not always significantly higher than that from late manured plots. $NO_3$-N losses were also influenced by the differences in [$NO_3^-$-N] before and after soil thaw and the total volume of leachate lost during different periods along the sampling campaign (Table 2, Table 3, Figure 1, and Figure 2).

In 2018-19 and 2019-20, $NO_3^-$-N loss via leachate from early manured plots was significantly higher than that from late fall manure plots due to the combinations of the three factors mentioned above. These are: (1) the recurrent pattern of significantly higher [$NO_3^-$-N] in soil-water samples from early relative to late fall manured plots; (2) the overall higher [$NO_3^-$-N] in soil-water samples in the fall relative to the spring and summer; and (3) the larger fraction of water leaching occurring during the fall relative to spring and summer (Table 2, Figure 1). Our results of higher $NO_3^-$-N loss via leachate from early manured plots relative to late fall dairy slurry manured plots in the Midwest US is supported by the observations of Sawyer (2020) and van Es, et al. (2006), which to my knowledge are the only publications that have studied the differences in $NO_3^-$-N losses between early and late dairy manure application in the Midwest. In

contrast to Sawyer (2020), that only presents total $NO_3^-$-N loss via leachate, van Es, et al. (2006) present measurements that support the 3 causes of higher $NO_3^-$-N loss in early relative to late manured plots.

In 2016-17, late manured plots exhibited $NO_3^-$-N loss via leachate that were 13% larger than those from early manured plots; this difference is relatively small in comparison with the average difference of 20% observed, with an opposite trend (early larger than late) in 2018-19 and 2019-20. Larger losses in $NO_3^-$-N loss from late manured plots were the result of similar [$NO_3^-$-N] in soil-water samples in the fall, spring, and summer, and a larger fraction of water leaching occurring during the spring and summer relative to the spring. This is the opposite of what we observed in 2018-19 and 2019-20 (Table 2, Figure 1). It is possible that the change in the pattern of [$NO_3^-$-N] differences between early and late manured plots after spring thaw was caused by the unusual flood that occurred in these plots during January 2017.

Although the results from 2017-18 support our results of larger $NO_3^-$-N loss via leachate from early manured plots relative to late fall manured plots from 2018-19 and 2019-20, these results should be taken with caution for two reasons. First, the soil samplers were not always able to collect a soil-water sample and the sampling season was significantly reduced (Figure 2). Brye et al. (2001) had similar problems using the same samplers in a close location. And second, the measured [$NO_3^-$-N] were above 75 g $m^{-3}$ during most of the summer and spring. These [$NO_3^-$-N] were between 3 and 10 times greater than those observed during the other sampling campaigns and much higher than values reported in the literature in similar locations and under similar conditions (Andraski et al 2000; Brye et al., 2000; Brye et al., 2001).

### *5.2. $N_2O$ emissions*

$N_2O$ emissions were highly variable, characterized by episodic and hard to predict $N_2O$ peak emissions that fluctuated widely in magnitude, frequency, and duration (Table 5, Figure 3). The temporal variability of our observations is consistent with the pattern of $N_2O$ soil emissions observed from managed agricultural soils in similar conditions (Barton et al., 2015; Chantigny et al., 2016; Laville et al., 2011; Molodovskaya et al., 2012).

Although averaged across all sampling campaigns $N_2O$ emissions from late manure plots were 29% higher than those from early manured plots, this difference was not statistically significant. The lack of statistical significance was a result of the influence of timing of manure application in the last sampling campaign was opposite to that observed in the first three sampling campaigns (Table 5). The differences in cumulative $N_2O$ emissions due to timing of manure applications during the fall were driven by differences in peak emission events because peak events represented a large fraction of the total cumulative emissions (Table 5, Figure 3).

Although there are no other studies that compare the effect of early and late manure application during the fall, the few studies that have measured $N_2O$ emissions regularly (i.e., weekly) during the non-growing season support our observations that: (1) fall manure application leds to peak emissions occurring at two different times, soon after manure application and during soil FTC; (2) these $N_2O$ peak fluxes occurring outside of the growing season were the majority of annual emissions; and, (3) peak emissions during soil FTC cycles are larger than peak emissions occurring after manure application.

In a two-year experiment where liquid dairy manure was injected in the fall, Cambareri, et al. (2017) observed that $N_2O$ emissions increased soon after manure application in the fall and

peaked during soil thaw in the spring. The $N_2O$ emissions occurring during the non-growing seasons contributed to 86%, 68%, and 78% of the total emissions. Similarly, in a two-year experiment where liquid dairy manure was applied (i.e., broadcast and incorporated within 24 hours) in the fall, Schwager et al., (2016) observed $N_2O$ emissions peaked twice, first during the days following fall dairy slurry application and then again during soil FTC in the winter and spring. Schwager et al., (2016) indicated that $N_2O$ emissions occurring between fall manure application and planting represented 68% and 69% of the cumulative emissions in two consecutive years. Wagner-Riddle & Thurtell, (1998) observed that different fall field operations, some including manure application, resulted in multiple coincidental peak emissions during soil FTC in the spring, fluxes occurring during these times again represented the majority of the annual emissions in fall manured plots.

***Peak $N_2O$ emissions soon after manure application***

During each sampling campaign, peak emission events observed soon after manure applications occurred under different soil temperature and moisture conditions due to different time of manure application, but they received equal amounts of manure that had similar composition (Figure 3, Table A4). This suggests that within a sampling campaign the differences in peak emissions soon after manure application between early and late manured plots were the result of differences in soil and weather conditions at the time of manure application. Our observations suggest that soil temperature and precipitation events controlled the magnitude of peak emissions occurring soon after manure application. Relative to late manure application, warmer and wetter soil conditions in early fall caused larger $N_2O$ emissions than manure application late in the fall on colder and dryer soils.

Our findings are consistent with those reported in the literature where manure applications in warmer and wetter soils resulted in higher $N_2O$ emissions that manure applications in cold and dry soils. Cambareri, et al. (2017), Chantigny, et al. (2016), Lin, et al. (2017) and Schwager, et al. (2016) applied manure late in the fall within a month a soil freeze, when air temperature was below 10ºC and soils were dry, they did not always observe increasing fluxes after manure application and when an increase in flux was observed it was always small (i.e., < 100 g N-$N_2O$ $ha^{-1}$ $day^{-1}$). On the contrary, Chadwick, et al. (2000), Kariyapperuma, et al. (2012), and Rochette, et al, (2004) applied manure early in the fall at soil temperatures above 12ºC, and manure application was soon followed by rain and resulted in large peak emissions.

Our results suggest that $N_2O$ emissions after manure application were the result of a complicated interplay between nitrification, mineralization, and denitrification, and that their magnitude and duration was controlled by soil temperature and precipitation. I hypothesize that, as manure was incorporated in the soil, $NH_4$ was exposed to aerobic conditions and was converted into $NO_3$ via nitrification resulting in an increase of $N_2O$ emissions soon after application. These peaks in $N_2O$ emissions soon after manure application occurred after rainfall and were most likely the result of denitrification. Rates of mineralization and nitrification increase with temperature, optimal conditions being around 25ºC, and emissions are very small at soil temperatures below 10ºC (Guntiñas et al., 2012; Maag & Vinther, 1996). Therefore, higher $N_2O$ emissions via nitrification and higher accumulations of soil $NO_3$ and available carbon were expected after early manure application than after late manure application in soils below 10ºC. Because soil $NO_3^-$ and available carbon are necessary substrates for denitrification the magnitude of $N_2O$ emissions via denitrification are somehow contingent on soil temperature. This logic of N dynamics leading to $N_2O$ emissions after manure application is supported by the

observations of Chadwic, et al. (2000) and Cambareri, et al. (2017) of changes in $N_2O$ fluxes and soil $NO_3$ and $NH_4$ after manure application early in the fall.

***Peak $N_2O$ emissions during FTC***

Contrary to what we observed during peak emissions that came soon after manure application in the fall, peak emissions occurring during FTC tended to be larger from plots manured late than from plots manured early during the fall. During 2016-17, 2017-18 and 2018-19, peak $N_2O$ emissions induced by soil FTC in late manured plots were approximately 2, 2/3 and 2 times greater than peak emission occurring early after manure application and during FTC in early manured plots. In 2019-20, peak emissions during FTC from the early manured plot were 22% greater than those from late manured plot (Table 5). Our observations of large and generally coincidental $N_2O$ peak emissions during soil FTC as a result as soil thaw are consistently supported by the literature (Cui et al., 2016; Müller et al., 2002; Wagner-Riddle, 2019).

Peak FTC emissions from late and early manured plots that occurred at approximately the same time as soil thaw and soil moisture increases, indicated that $N_2O$ was mostly produced via denitrification and that differences in the magnitude, duration, and frequency of these emissions were due to differences in the availability of denitrification substrates, $NO_3^-$ and organic C, rather than differences in weather conditions. Although apportioning $N_2O$ fluxes among source pathways is difficult, field and laboratory studies of $N_2O$ emissions during FTC support that denitrification tends to be the dominant process responsible for the largest peak emissions observed during soil FTC and that the differences between the magnitude, duration, and frequency during FTC peak emissions are related to differences in available organic carbon and $NO_3$ (Congreves et al., 2018; Risk et al., 2013, Gao et al., 2018; Wagner-Riddle et al., 2017).

In soil incubations experiments Muller, et al. (2002) attributed $N_2O$ peak to denitrification, pointing out that soil amended with $NO_3$ before soil freeze exhibited $N_2O$ emissions 20 times larger than those unfertilized or fertilized with $NH_4$. Cambareri, et al. (2017) observed that the magnitude of the $N_2O$ peak events was larger in fall manured plots in which soil $NO_3^-$ content increased during the winter than in non-manured plots in which soil $NO_3^-$ content remained low during the winter. Similarly, in a three-year experiment, Wagner-Riddle et al. (1998) observed a strong correlation ($r = 0.7$) with nitrate concentration in soil measured during the previous fall. According to Wagner-Riddle et al. (1998), it was obvious that the level of nitrate in soils was limiting $N_2O$ production by denitrification.

During the last sampling campaign, 2019-20, peak emissions during FTC from the early manured plot were 22% greater than those from the late manured plot (Table 5). During late manure application in 2019-20, air temperature drastically dropped on the day of manure application. On this occasion manure incorporation was delayed until the next day when the top layer of soil was frozen, making manure incorporation difficult (Figure 3). The reduced or non-incorporation of the slurry into the soil could have led to high N losses via ammonia volatilization during the days following manure application. Although ammonia volatilization rates decrease with temperature, high losses have been observed at near freezing temperatures (Perin et al., 2020; Thies et al., 2020). The lack of N incorporation could also have led to N loss via runoff (Chadwick et al., 2011; Williams et al., 2012). This would also explains the low $NO_3^-$ losses observed during the fall of 2019 from the late manured plot (Table 2). All in all, we hypothesize that lack of manure incorporation in the late manured plot depleted $NH_4$ after manure application and prevented an increase in $NO_3^-$ in the soil via nitrification during the winter, leading to low peak emissions via FTC during the winter. This rational is consistent with

the attribution of peak emissions during FTC to denitrification and their magnitude to the availability of denitrification substrates (i.e., available carbon and $NO_3^-$).

### *5.3. $N_2O$ and $NO_3^-$ losses*

Total N losses were very variable, losses via $NO_3^-$-N represented by far the majority of the emissions. It is important to remember that soil-water below the root zone was sampled using suction cups which do not capture macropore flow and that water percolation was estimated using a functional approach therefore the estimated $NO_3^-$-N loss should be considered as a conservative estimate of the actual quantity of $NO_3^-$-N lost via leachate (Andraski et al., 2000, Brye et al., 2001).

To our knowledge there is only one study that have simultaneously measured $NO_3^-$N and $N_2O$-N losses from fall dairy manure applications (Schwager et al., 2016). The results of Schwager et al. (2016) support our observations of that $N_2O$-N loss represent a small fraction of total N loss ($N_2O$-N + $NO_3^-$-N) and that there was no relationship between total $N_2O$-N and $NO_3^-$N loss. The few studies in which $NO_3^-$N and $N_2O$-N losses from fertilized fields have been measured simultaneous support our results that $NO_3^-$N represent the majority of N losses and they are highly variable across different years (Molina-Herrera et al., 2016; Sanz-Cobena et al., 2012; Wallace, 2015).

## *6. Conclusions*

The timing of dairy slurry application during the fall resulted in a clear trade-off between $NO_3^-$ loss and $N_2O$ emissions. Relative to early fall application, late fall application of dairy slurry led to lower $NO_3^-$ leaching loss below the root zone, higher peak $N_2O$ emissions during freeze-thaw cycles (FTC), and therefore higher cumulative $N_2O$ emissions.

$NO_3^-$-N losses were much larger (>5x) than $N_2O$-N losses. In general, late manured plots lost less $NO_3^-$ via leaching than early manured plots. Lower $NO_3^-$ loss in late manured plots relative to early manure plots before soil freeze, was the driver of the majority of $N_2O$ emissions which occurred during peak emissions during soil FTC. Continuous and high temporal $N_2O$ measurements were crucial to capture and quantify total $N_2O$ emissions which have been oversight in previous research.

Our results indicate that the USDA recommendation to reduce $NO_3^-$ loss during fall manure application are effective but lead to higher $N_2O$ than early fall manure application. In Wisconsin $NO_3^-$ contamination from agricultural fields endangers the livelihood of almost ¾ of the state population while $N_2O$ emissions have a large impact in stratospheric ozone destruction and climate change.

The trade-off between $NO_3^-$ loss and $N_2O$ emissions brings difficult decisions that maybe result in different outcomes. Nonetheless this dilemma bring an opportunity for new research based in reducing $N_2O$ emissions from late fall manured fields; which ultimate could result in the reduction of both $N_2O$ emissions and $NO_3^-$ loss. Overall, more research is needed to better understand the mechanisms of, and conditions that result in large $N_2O$ emissions during FTC.

Verification of our results at larger scales and in additional locations is recommended to better understand the impacts of the timing of fall manure application and to allow formulation of strategies to reduce $NO_3^-$ and $N_2O$ losses.

## *7. References*


Abalos, D., Brown, S. E., Vanderzaag, A. C., Gordon, R. J., Dunfield, K. E., & Wagner-Riddle, C. (2016). Micrometeorological measurements over 3 years reveal differences in N2O emissions between annual and perennial crops. *Global Change Biology*, *22*(3), 1244–1255. https://doi.org/10.1111/gcb.13137

Aguirre-Villegas, H., Larson, R. A., & Ruark, M. D. (2017). Managing Manure Nitrogen to Reduce Loses. *Sustainable Dairy*, 2–2. https://doi.org/10.4159/harvard.9780674183803.c2

Allen, R. G., Pereira, L, S., Raes, D., Smith, M. (2006). guidelines for computing crop water requirements. FAO Irrigation and Drainage Paper Crop by. *Remote Sensing of Environment*, *300*(No. 56), 173. https://www.kimberly.uidaho.edu/water/fao56/fao56.pdf

Andraski, T. W., Bundy, L. G., & Brye, K. R. (2000). Crop Management and Corn Nitrogen Rate Effects on Nitrate Leaching. *Journal of Environment Quality*, *29*(4), 1095. https://doi.org/10.2134/jeq2000.00472425002900040009x

Barton, L., Wolf, B., Rowlings, D., Scheer, C., Kiese, R., Grace, P., Stefanova, K., & Butterbach-Bahl, K. (2015a). Sampling frequency affects estimates of annual nitrous oxide fluxes. *Scientific Reports*, *5*, 15912. https://doi.org/10.1038/srep15912

Basso, B., & Ritchie, J. T. (2005). Impact of compost, manure and inorganic fertilizer on nitrate leaching and yield for a 6-year maize-alfalfa rotation in Michigan. *Agriculture, Ecosystems and Environment*, *108*(4), 329–341. https://doi.org/10.1016/j.agee.2005.01.011

Benckiser, G., Schartel, T., & Weiske, A. (2015). Control of NO3 − and N2O emissions in agroecosystems: A review. *Agronomy for Sustainable Development*, *35*(3), 1059–1074. https://doi.org/10.1007/s13593-015-0296-z

Brye, K. R., Norman, J. M., Bundy, L. G. & Gower, S. T. (2000). *Ground Water Quality Nitrogen and Carbon Leaching in Agroecosystems and Their Role in Denitrification Potential*. https://doi.org/10.2134/jeq2001.30158x

Brye, K. R., Norman, J. M., Bundy, L. G. & Gower, S. T. (2001). Nitrogen and Carbon Leaching in Agroecosystems and Their Role in Denitrification Potential. *Journal of Environmental Quality*, *30*(1), 58–70. https://doi.org/10.2134/jeq2001.30158x

Cambareri, G., Drury, C., Lauzon, J., Salas, W., & Wagner-Riddle, C. (2017). Year-Round Nitrous Oxide Emissions as Affected by Timing and Method of Dairy Manure Application to Corn. *Soil Science Society of America Journal*, *81*(1), 166–178. https://doi.org/10.2136/sssaj2016.05.0160

Campbell, G. S., & Norman, J. M. (1998). *Introduction to environmental biophysics*. Springer.

Chadwick, D., Sommer, S., Thorman, R., Fangueiro, D., Cardenas, L., Amon, B., & Misselbrook, T. (2011). Manure management: Implications for greenhouse gas emissions. *Animal Feed Science and Technology*, *166–167*, 514–531. https://doi.org/10.1016/J.ANIFEEDSCI.2011.04.036

Chantigny, M. H., Rochette, P., Angers, D. A., Goyer, C., Brin, L. D., & Bertrand, N. (2016). Nongrowing season N2O and CO2 emissions — temporal dynamics and influence of soil texture and fall-applied manure. *Canadian Journal of Soil Science*, *97*(3), 452–464. https://doi.org/10.1139/cjss-2016-0110

Congreves, K. A., Wagner-Riddle, C., Si, B. C., & Clough, T. J. (2018). Nitrous oxide emissions and biogeochemical responses to soil freezing-thawing and drying-wetting. *Soil Biology and Biochemistry*, *117*, 5–15. https://doi.org/10.1016/J.SOILBIO.2017.10.040

Cui, Q., Song, C., Wang, X., Shi, F., Wang, L., & Guo, Y. (2016). Rapid N2O fluxes at high level of nitrate nitrogen addition during freeze-thaw events in boreal peatlands of Northeast China. *Atmospheric Environment*, *135*, 1–8. https://doi.org/10.1016/J.ATMOSENV.2016.03.053

Curley, E. M., O'Flynn M.G., & McDonnell K.P. (2010). Porous Ceramic Cups: Preparation and Installation of Samplers for Measuring Nitrate Leaching. *International Journal of Soil Science*, *5*(1), 19–25. http://docsdrive.com/pdfs/academicjournals/ijss/2010/19-25.pdf

Duncan, D. S., Oates, L. G., Gelfand, I., Millar, N., Robertson, G. P. & Jackson, R. D. (2019). Environmental factors function as constraints on soil nitrous oxide fluxes in bioenergy feedstock cropping systems. *GCB Bioenergy*, *11*(2), 416–426. https://doi.org/10.1111/gcbb.12572

Francis Clar, J., Anex, R. P. ;, Allie, M., Elwood, C., Rigell, I., & Lunzer, B. (2015, October 17). *A Novel System for High-Resolution, Near-Continuous Measurement of Soil N2O Isotope Fluxes. (ASA, CSSA and SSSA International Annual Meetings (2015))*. https://scisoc.confex.com/crops/2015am/webprogram/Paper94435.html

Francis-Clar, J. T., & Anex, R. P. (2018). Automatic system for long-term monitoring of soil N2O isotope flux at high temporal and spatial resolution. *2018 Detroit, Michigan July 29 - August 1, 2018*, 1-. https://doi.org/10.13031/aim.201800878

Francis Clar, J. T., & Anex, R. P. (2020). Flux intensity and diurnal variability of soil $N_2O$ emissions in a highly fertilized cropping system. *Soil Science Society of America Journal*, saj2.20132. https://doi.org/10.1002/saj2.20132

Gao, D., Zhang, L., Liu, J., Peng, B., Fan, Z., Dai, W., Jiang, P. & Bai, E. (2018). Responses of terrestrial nitrogen pools and dynamics to different patterns of freeze-thaw cycle: A meta-analysis. *Global Change Biology*, *24*(6), 2377–2389. https://doi.org/10.1111/gcb.14010

Goolsby, D. A., Battaglin, W. A., Aulenbach, B. T., & Hooper, R. P. (2001). Nitrogen Input to the Gulf of Mexico. *Journal of Environment Quality*, *30*(2), 329. https://doi.org/10.2134/jeq2001.302329x

Grace, P. R., Philip Robertson, G., Millar, N., Colunga-Garcia, M., Basso, B., Gage, S. H., & Hoben, J. (2011). The contribution of maize cropping in the Midwest USA to global warming: A regional estimate. *Agricultural Systems*, *104*(3), 292–296. https://doi.org/10.1016/j.agsy.2010.09.001

Grundmann, G. L., Renault, P., Rosso, L., & Bardin, R. (1995). Differential Effects of Soil Water Content and Temperature on Nitrification and Aeration. *Soil Science Society of America Journal*, *59*(5), 1342. https://doi.org/10.2136/sssaj1995.03615995005900050021x

Guntiñas, M. E., Leirós, M. C., Trasar-Cepeda, C., & Gil-Sotres, F. (2012). Effects of moisture and temperature on net soil nitrogen mineralization: A laboratory study. *European Journal of Soil Biology*, *48*, 73–80. https://doi.org/10.1016/J.EJSOBI.2011.07.015

Gupta, S. K., Gupta, R. C., Gupta, A. B., Seth, A. K., Bassin, J. K., & Gupta, A. (2000). Recurrent acute respiratory tract infections in areas with high nitrate concentrations in drinking water. *Environmental Health Perspectives*, *108*(4), 363–366. https://doi.org/10.1289/ehp.00108363

Gupta, S., Munyankusi, E., Moncrief, J., Zvomuya, F., & Hanewall, M. (2004). Tillage and Manure Application Effects on Mineral Nitrogen Leaching from Seasonally Frozen Soils. *Journal of Environment Quality*, *33*(4), 1238. https://doi.org/10.2134/jeq2004.1238

Hatfield, J. (2012). Agriculture in the Midwest. *U.S. National Climate Assessment Midwest Technical Input Report*, *March*, 1–8. http://glisa.msu.edu/docs/NCA/MTIT_Agriculture.pdf.

Henry, H.A., (2008). Climate change and soil freezing dynamics: historical trends and projected changes. Climatic Change, 87(3), pp.421-434.

IPCC. (2011). Intergovernmental Panel on Climate change, Special Report on Renewable Energy Sources and Climate Change Mitigation. In *Prepared by Working Group III of the Intergovernmental Panel on Climate Change [O. Edenhofer, R. Pichs-*

*Madruga, Y. Sokona, K. Seyboth, P. Matschoss, S. Kadner, T. Zwickel, P. Eickemeier, G. Hansen, S. Schlömer, C. von Stechow (eds)]*.

Jones, C. S., Nielsen, J. K., Schilling, K. E., & Weber, L. J. (2018). Iowa stream nitrate and the Gulf of Mexico. *PLOS ONE*, *13*(4), e0195930. https://doi.org/10.1371/journal.pone.0195930

Kariyapperuma, K. A., Furon, A., & Wagner-Riddle, C. (2012). Non-growing season nitrous oxide fluxes from an agricultural soil as affected by application of liquid and composted swine manure. *Canadian Journal of Soil Science*. http://www.nrcresearchpress.com/doi/pdf/10.4141/cjss2011-059

Laboski, C. A. M., & Peters, J. B. (2011). Nutrient application guidelines crops in Wisconsin. *UW Extension. Cooperative Extension*, 94. https://www.rockriverlab.com/file_open.php?id=123

Lauer, J. (2002). *University of Wisconsin-Extension United States Department of Agriculture Wisconsin Counties Cooperating and Providing Equal Opportunities in Employment and Programming Methods for Calculating Corn Yield*.

Laville, P., Lehuger, S., Loubet, B., Chaumartin, F., & Cellier, P. (2011). Effect of management, climate and soil conditions on N2O and NO emissions from an arable crop rotation using high temporal resolution measurements. *Agricultural and Forest Meteorology*, *151*(2), 228–240. https://doi.org/10.1016/J.AGRFORMET.2010.10.008

Lin, S., Hernandez-Ramirez, G., Kryzanowski, L., Wallace, T., Grant, R., Degenhardt, R., Berger, N., Lohstraeter, G. & Powers, L.-A. (2017). Timing of Manure Injection and Nitrification Inhibitors Impacts on Nitrous Oxide Emissions and Nitrogen Transformations in a Barley Crop. *Soil Science Society of America Journal*, *81*(6), 1595–1605. https://doi.org/10.2136/sssaj2017.03.0093

Lord, E. I., & Shepherd, M. A. (1993). Developments in the use of porous ceramic cups for measuring nitrate leaching. *Journal of Soil Science*, *44*(3), 435–449. https://doi.org/10.1111/j.1365-2389.1993.tb00466.x

Maag, M., & Vinther, F. P. (1996). Nitrous oxide emission by nitrification and denitrification in different soil types and at different soil moisture contents and temperatures. *Applied Soil Ecology*, *4*(1), 5–14. https://doi.org/10.1016/0929-1393(96)00106-0

Martin, E. C., Loudon, T. L., Ritchie, J. T., & Werner, A. (1994). Use of drainage lysimeters to evaluate nitrogen and irrigation management strategies to minimize nitrate leaching in maize production. *Transactions of the American Society of Agricultural Engineers*, *37*(1), 79–83. https://arizona-pure-elsevier-com.ezproxy.library.wisc.edu/en/publications/use-of-drainage-lysimeters-to-evaluate-nitrogen-and-irrigation-ma

McMaster, G. S., & Wilhelm, W. W. (1997). Growing degree-days: one equation, two interpretations. *Agricultural and Forest Meteorology*, *87*(4), 291–300. https://doi.org/10.1016/S0168-1923(97)00027-0

Miller, M. N., Zebarth, B. J., Dandie, C. E., Burton, D. L., Goyer, C., & Trevors, J. T. (2009). Influence of Liquid Manure on Soil Denitrifier Abundance, Denitrification, and Nitrous Oxide Emissions. *Soil Science Society of America Journal*, *73*(3), 760. https://doi.org/10.2136/sssaj2008.0059

Molina-Herrera, S., Haas, E., Klatt, S., Kraus, D., Augustin, J., Magliulo, V., Tallec, T., Ceschia, E., Ammann, C., Loubet, B., Skiba, U., Jones, S., Brümmer, C., Butterbach-Bahl, K., & Kiese, R. (2016). A modeling study on mitigation of N2O emissions and NO3 leaching at different agricultural sites across Europe using LandscapeDNDC. *Science of the Total Environment*, *553*, 128–140. https://doi.org/10.1016/j.scitotenv.2015.12.099

Molodovskaya, M., Singurindy, O., Richards, B. K., Warland, J., Johnson, M. S., & Steenhuis, T. S. (2012). Temporal Variability of Nitrous Oxide from Fertilized Croplands: Hot Moment Analysis. *Soil Science Society of America Journal*, *76*(5), 1728. https://doi.org/10.2136/sssaj2012.0039

Molodovskaya, M., Warland, J., Richards, B. K., Öberg, G., & Steenhuis, T. S. (2011). Nitrous Oxide from Heterogeneous Agricultural Landscapes: Source Contribution Analysis by Eddy Covariance and Chambers. *Soil Science Society of America Journal*, *75*(5), 1829. https://doi.org/10.2136/sssaj2010.0415

Müller, C., Martin, M., Stevens, R. J., Laughlin, R. J., Kammann, C., Ottow, J. C. G., & Jäger, H.-J. (2002). Processes leading to N2O emissions in grassland soil during freezing and thawing. *Soil Biology and Biochemistry*, *34*(9), 1325–1331. https://doi.org/10.1016/S0038-0717(02)00076-7

Parkin, T. B., Venterea, R. T., & Hargreaves, S. K. (2012). Calculating the detection limits of chamber-based soil greenhouse gas flux measurements. *Journal of Environmental Quality*, *41*(3), 705–715. https://doi.org/10.2134/jeq2011.0394

Paul, J. W., & Zebarth, B. J. (1997). Denitrification and nitrate leaching during the fall and winter following dairy cattle slurry application. *Canadian Journal of Soil Science*, *77*(2), 231–240. https://doi.org/10.4141/S96-052

Perin, V., Santos, E. A., Lollato, R., Ruiz-Diaz, D., & Kluitenberg, G. J. (2020). *A R T I C L E Impacts of ammonia volatilization from broadcast urea on winter wheat production*. https://doi.org/10.1002/agj2.20371

Pettygrove, G. S. & Heinrich, A. L. (2009). Dairy Manure Nutrient Content and Forms. *Technical Guide Series for Crop Management Professionals*. http://manuremanagement.ucdavis.edu/files/134369.pdf

Porter, P. A., Mitchell, R. B., & Moore, K. J. (2015). Reducing hypoxia in the Gulf of Mexico: Reimagining a more resilient agricultural landscape in the Mississippi River Watershed. *Journal of Soil and Water Conservation*, *70*(3), 63A-68A. https://doi.org/10.2489/jswc.70.3.63A

Rabotyagov, S., Campbell, T., Jha, M., Gassman, P. W., Arnold, J., Kurkalova, L., Secchi, S., Feng, H., & Kling, C. L. (2010). Least-cost control of agricultural nutrient contributions to the Gulf of Mexico hypoxic zone. *Ecological Applications*, *20*(6), 1542–1555. https://doi.org/10.1890/08-0680.1

Rasse, D. P., Ritchie, J. T., Peterson, W. R., Wei, J., & Smucker, A. J. M. (2000). Rye Cover Crop and Nitrogen Fertilization Effects on Nitrate Leaching in Inbred Maize Fields; Rye Cover Crop and Nitrogen Fertilization Effects on Nitrate Leaching in Inbred Maize Fields. *Journal of Enviromental Quality*, *29*, 298–304. https://doi.org/10.2134/jeq2000.00472425002900010037x

Ravishankara, A. R., Daniel, J. S., & Portmann, R. W. (2009). Nitrous oxide (N2O): the dominant ozone-depleting substance emitted in the 21st century. *Science (New York, N.Y.)*, *326*(5949), 123–125. https://doi.org/10.1126/science.1176985

Risk, N., Snider, D., & Wagner-Riddle, C. (2013). Mechanisms leading to enhanced soil nitrous oxide fluxes induced by freeze–thaw cycles. *Canadian Journal of Soil Science*, *93*(4), 401–414. https://doi.org/10.4141/cjss2012-071

Ritchie, J. T. (1972). Model for predicting evaporation from a row crop with incomplete cover. *Water Resources Research*, *8*(5), 1204–1213. https://doi.org/10.1029/WR008i005p01204

Robertson, G. P., & Groffman, P. M. (2015). Chapter 14 - Nitrogen Transformations. *Soil Microbiology Ecology and Biochemistry*, 421–446. https://doi.org/10.1016/B978-0-12-415955-6.00014-1

Rochette, P., van Bochove, E., Preˊvost, D., Angers, D. A., Coˆteˊ, D., & Bertrand, N. (2000). Soil Carbon and Nitrogen Dynamics Following Application of Pig Slurry for the 19th Consecutive Year. *Soil Science Society of America Journal*, *64*(4), 1396. https://doi.org/10.2136/sssaj2000.6441396x

Rochette, P., Angers, D. A., Chantigny, M. H., Bertrand, N. & Côté, D. (2004). Carbon Dioxide and Nitrous Oxide Emissions following Fall and Spring Applications of Pig Slurry to an Agricultural Soil. *Soil Science Society of America Journal*, *68*(4), 1410. https://doi.org/10.2136/sssaj2004.1410

Rudaz, A. O., Wälti, E., Kyburz, G., Lehmann, P., & Fuhrer, J. (1999). Temporal variation in N2O and N2 fluxes from a permanent pasture in Switzerland in relation to management, soil water content and soil temperature. *Agriculture, Ecosystems & Environment*, *73*(1), 83–91. https://doi.org/10.1016/S0167-8809(99)00005-5

Sanz-Cobena, A., Sánchez-Martín, L., García-Torres, L., & Vallejo, A. (2012). Gaseous emissions of N 2 O and NO and NO 3 − leaching from urea applied with urease and nitrification inhibitors to a maize (Zea mays) crop. *Ecosystems and Environment*, *149*, 64–73. https://doi.org/10.1016/j.agee.2011.12.016

Sawyer, J. (2020). *Effect of Manure Application Timing and Cover Crops on Nitrogen and Phosphorus Leachingin*.

Schwager, E. A., VanderZaag, A. C., Wagner-Riddle, C., Crolla, A., Kinsley, C., & Gregorich, E. (2016). Field Nitrogen Losses Induced by Application Timing of Digestate from Dairy Manure Biogas Production. *Journal of Environmental Quality*, *45*(6), 1829–1837. https://doi.org/10.2134/jeq2016.04.0148

Stoddard, C. S., Grove, J. H., Coyne, M. S., & Thom, W. O. (2005). Fertilizer, tillage, and dairy manure contributions to nitrate and herbicide leaching. *Journal of Environmental Quality*, *34*(4), 1354–1362. https://doi.org/10.2134/jeq2004.0226

Syakila, A., & Kroeze, C. (2011). The global nitrous oxide budget revisited. *Greenhouse Gas Measurement and Management*, *1*(1), 17–26. https://doi.org/10.3763/ghgmm.2010.0007

Talarczyk, K. A., Kelling, K. A., Wood, T. M. & Hero, D. E. (1996, January). Timing of manure application to cropland to maximize nutrient value. *Wisconsin Fertilizer, Aglime, and Pest Management Conference, Madison, WI (Vol. 257263).*

Thies, S., Joshi, D. R., Bruggeman, S. A., Clay, S. A., Mishra, U., Morile-Miller, J., & Clay, D. E. (2020). Fertilizer timing affects nitrous oxide, carbon dioxide, and ammonia emissions from soil. *Soil Science Society of America Journal*, *84*(1), 115–130. https://doi.org/10.1002/saj2.20010

USDA-NASS. (2018). *United States Department of Agriculture National Agricultural Statistics Service. 2017 State Agriculture Overview - Kansas*. http://www.nass.usda.gov/.

van Es, H. M., Sogbedji, J. M., & Schindelbeck, R. R. (2006). Effect of Manure Application Timing, Crop, and Soil Type on Nitrate Leaching. *Journal of Environmental Quality*, *35*(2), 670–679. https://doi.org/10.2134/jeq2005.0143

Venterea, R. T., Spokas, K. A., & Baker, J. M. (2009). Accuracy and Precision Analysis of Chamber-Based Nitrous Oxide Gas Flux Estimates. *Soil Science Society of America Journal*, *73*(4), 1087. https://doi.org/10.2136/sssaj2008.0307

Wagner-Riddle, C., & Thurtell, G. W. (1998). Nitrous oxide emissions from agricultural fields during winter and spring thaw as affected by management practices. *Nutrient Cycling in Agroecosystems*, *52*(2/3), 151–163. https://doi.org/10.1023/A:1009788411566

Wagner-Riddle, Claudia. (2019, April 15). Nitrous oxide emissions induced by freeze/thaw: importance and potential mechanisms. *Climate Change, Reactive Nitrogen, Food Security and Sustainable Agriculture* .

Wagner-Riddle, Claudia, Congreves, K. A., Abalos, D., Berg, A. A., Brown, S. E., Ambadan, J. T., Gao, X., & Tenuta, M. (2017). Globally important nitrous oxide emissions from croplands induced by freeze-thaw cycles. *Nature Geoscience*, *10*(4), 279–283. https://doi.org/10.1038/ngeo2907

Wallace, B. M. (2015). Thesis: C*haracterizing nitrogen losses to air and drainage water from red clover managed as green manure or forage*. Department of Soil Science, University of Saskatchewan, Saskatoon, Saskatchewan (Canada). April 28, 2015.

Wang, Q., Cameron, K., Buchan, G., Zhao, L., Zhang, E. H., Smith, N., & Carrick, & S. (2012). Comparison of lysimeters and porous ceramic cups for measuring nitrate leaching in different soil types. *New Zealand Journal of Agricultural Research*, *55*(4), 333–345. https://doi.org/10.1080/00288233.2012.706224

Williams, M. R., Feyereisen, G. W., Beegle, D. B., & Shannon, R. D. (2012). Soil Temperature Regulates Nitrogen Loss from Lysimeters following Fall and Winter Manure Application. *Transactions of the ASABE*, *55*(3), 861–870. https://doi.org/10.13031/2013.41520

## *8. Appendix*

**Table A17.** Monthly average and total rainfall (mm), at Arlington WI, for all sampling seasons, 2016-17, 2017-18, 2018-19 and 2019-20 and 30-years historic values.

| | 2016-17 | 2017-18 | 2018-19 | 2019-20 | 30-YEARS |
|---|---|---|---|---|---|
| SEPT | 157 | 20 | 118 | 138 | 83 |
| OCT | 86 | 94 | 136 | 165 | 72 |
| NOV | 41 | 18 | 39 | 60 | 52 |
| DEC | 33 | 15 | 40 | 48 | 39 |
| JAN | 63 | 38 | 54 | 44 | 32 |
| FEB | 42 | 44 | 76 | 24 | 33 |
| MARCH | 72 | 19 | 26 | 87 | 51 |
| APRIL | 133 | 66 | 74 | 35 | 93 |
| MAY | 83 | 181 | 177 | 109 | 100 |
| JUNE | 154 | 134 | 103 | 111 | 138 |
| JULY | 118 | 61 | 137 | 137 | 104 |
| AUG | 43 | 240 | 123 | 91 | 99 |
| **TOTAL** | **1025** | **929** | **1102** | **1048** | **894** |

**Table A2.** Monthly and seasonal snowfall (mm), at Arlington WI, for all sampling seasons, 2016-17, 2017-18, 2018-19 and 2019-20 and 30-years historic values.

| | 2016-17 | 2017-18 | 2018-19 | 2019-20 | 30-YEARS |
|---|---|---|---|---|---|
| SEPT | 0 | 0 | 0 | 0 | 0 |
| OCT | 0 | 0 | 0 | 165 | 9 |
| NOV | 0 | 0 | 69 | 256 | 75 |
| DEC | 510 | 71 | 47 | 81 | 283 |
| JAN | 316 | 183 | 543 | 445 | 280 |
| FEB | 64 | 333 | 580 | 356 | 272 |
| MARCH | 223 | 94 | 63 | 77 | 127 |
| APRIL | 0 | 435 | 99 | 5 | 51 |
| MAY | 0 | 0 | 0 | 0 | 3 |
| JUNE | 0 | 0 | 0 | 0 | 0 |
| JULY | 0 | 0 | 0 | 0 | 0 |
| AUG | 0 | 0 | 0 | 0 | 0 |
| **TOTAL** | **1113** | **1116** | **1401** | **1385** | **1100** |

**Table A3.** Monthly and season average air temperature (ºC), at Arlington WI, for all sampling seasons, 2016-17, 2017-18, 2018-19 and 2019-20 and 30-years historic values**.**

| | **2016-17** | **2017-18** | **2018-19** | **2019-20** | **30-YEARS** |
|---|---|---|---|---|---|
| SEPT | 17.9 | 17.4 | 17.6 | 17.9 | 16.2 |
| OCT | 11.3 | 10.9 | 8.1 | 8.4 | 9.2 |
| NOV | 6.3 | 0.9 | -1.1 | -1.5 | 1.7 |
| DEC | -6.1 | -6.3 | -2.5 | -1.4 | -4.6 |
| JAN | -5.5 | -8.2 | -9.2 | -4.7 | -7.9 |
| FEB | -1.2 | -7 | -8.6 | -6.2 | -6.1 |
| MARCH | 0 | 0 | -1.9 | 2.3 | 0.5 |
| APRIL | 9.7 | 1.9 | 7.1 | 6.1 | 7.2 |
| MAY | 12.7 | 17.8 | 12.2 | 13.1 | 14.0 |
| JUNE | 20 | 20.4 | 18.8 | 20.4 | 19.3 |
| JULY | 21 | 21.9 | 23 | 23.4 | 21.4 |
| AUG | 18.6 | 21.6 | 19.7 | 20.9 | 20.3 |
| **AVERAGE** | **8.73** | **7.61** | **6.93** | **8.23** | **7.6** |

**Table A4.** Manure N application rates based on N analysis and dairy slurry application rates of 66,325 L $ha^{-1}$. The table includes the precentage of Dry Matter (DM) and the Carbon:nitrogen ratio of the dairy slurry.

| Season | Variable | Early | Late | Early - Late |
|---|---|---|---|---|
| 2016-17 | App. date | 09/20/16 | 11/16/16 | 57 (days) |
| | Total N (kg $ha^{-1}$) | 137.3 | 158.4 | -21.1 |
| | N-$NH_4$ (kg $ha^{-1}$) | 63.6 | 91.7 | -28.2 |
| | % N-$NH_4$ | 46% | 58% | -12% |
| | DM (%) | 6% | 5% | 1% |
| | C:N | 15 | 12 | 3.0 |
| 2017-18 | App. date | 09/12/17 | 11/17/17 | 66 (days) |
| | Total N (kg $ha^{-1}$) | 163.0 | 99.0 | 64.0 |
| | N-$NH_4$ (kg $ha^{-1}$) | 74.0 | 42.1 | 31.9 |
| | % N-$NH_4$ | 46% | 42% | 4% |
| | DM (%) | 7% | 4% | 3% |
| | C:N | - | 10 | - |
| 2018-19 | App. date | 09/14/18 | 11/24/18 | 71 (days) |
| | Total N (kg $ha^{-1}$) | 100.3 | 165.5 | -65.2 |
| | N-$NH_4$ (kg $ha^{-1}$) | 59.9 | 80.7 | -20.8 |
| | % N-$NH_4$ | 60% | 49% | 11% |
| | DM (%) | 2% | 6% | -4% |
| | C:N | 5 | 11 | 6 |
| 2019-20 | App. date | 09/18/19 | 11/05/19 | 48 (days) |
| | Total N (kg $ha^{-1}$) | 146.0 | 143.8 | 2.2 |
| | N-$NH_4$ (kg $ha^{-1}$) | 61.5 | 67.3 | -5.8 |
| | % N-$NH_4$ | 42% | 47% | -5% |
| | DM (%) | 6% | 5% | 1% |
| | C:N | 12 | 10 | -2 |

**Table A5.** Nitrogen and total organic carbon content of the soil profile at the beginning of the experimental trial before manure application and at corn stage V6. And the difference between V6 and pre fall manure application values, two last columns (Table is next page)

| | | | Pre fall manure app - Soil depth (m) | | | | V6 | | V6 - Pre fall | |
|---|---|---|---|---|---|---|---|---|---|---|
| Season | Treat. | Variable | 0-0.1 | 0.1-0.2 | 0.2-0.4 | 0.4-0.6 | 0-0.3 | 0.3-0.6 | 0-0.3 | 0.3-0.6 |
| 2016-17 | Early | $NO_3$-N (kg $ha^{-1}$) | 12 | 8 | 8 | 3 | - | - | - | - |
| | | $NH_4$-N (kg $ha^{-1}$) | 5 | 5 | 9 | 5 | - | - | - | - |
| | | TN (%) | 0.44 | 0.42 | 0.44 | 0.24 | - | - | - | - |
| | | TOC (%) | 3.37 | 3.13 | 3.75 | 2.28 | - | - | - | - |
| | Late | $NO_3$-N (kg $ha^{-1}$) | 10 | 4 | 6 | 2 | - | - | - | - |
| | | $NH_4$-N (kg $ha^{-1}$) | 5 | 3 | 6 | 5 | - | - | - | - |
| | | TN (%) | 0.41 | 0.39 | 0.40 | 0.24 | - | - | - | - |
| | | TOC (%) | 3.39 | 3.09 | 3.80 | 2.59 | - | - | - | - |
| 2017-18 | Early | $NO_3$-N (kg $ha^{-1}$) | 9 | 7 | 12 | 10 | 21 | 15 | -1 | +5 |
| | | $NH_4$-N (kg $ha^{-1}$) | 9 | 6 | 21 | 20 | 18 | 16 | -7.5 | -15 |
| | | TN (%) | 0.18 | 0.12 | 0.08 | 0.03 | - | - | | |
| | | TOC (%) | 2.05 | 1.27 | 0.67 | 0.37 | - | - | | |
| | Late | $NO_3$-N (kg $ha^{-1}$) | 11 | 6 | 12 | 11 | 26 | 25 | +3 | +5 |
| | | $NH_4$-N (kg $ha^{-1}$) | 9 | 7 | 27 | 15 | 22 | 17 | -8 | -12 |
| | | TN (%) | 0.18 | 0.11 | 0.06 | 0.05 | - | - | | |
| | | TOC (%) | 2.02 | 1.17 | 0.71 | 0.44 | - | - | | |
| 2018-19 | Early | $NO_3$-N (kg $ha^{-1}$) | 11 | 6 | 10 | 6 | 12 | 16 | -10 | +4 |
| | | $NH_4$-N (kg $ha^{-1}$) | 5 | 4 | 6 | 8 | 21 | 20 | +9 | -9 |
| | | TN (%) | 0.22 | 0.22 | 0.13 | 0.12 | 1.75 | 0.79 | +1.56 | +0.66 |
| | | TOC (%) | 2.19 | 1.55 | 0.94 | 0.59 | 0.2 | 0.12 | | |
| | Late | $NO_3$-N (kg $ha^{-1}$) | 8 | 4 | 8 | 6 | 17 | 23 | +1 | +13 |
| | | $NH_4$-N (kg $ha^{-1}$) | 5 | 4 | 8 | 8 | 32 | 22 | +19 | +10 |
| | | TN (%) | 0.22 | 0.18 | 0.13 | 0.12 | 1.96 | 0.83 | +1.78 | +0.7 |
| | | TOC (%) | 2.07 | 1.26 | 0.80 | 0.54 | 0.22 | 0.12 | | |
| 2019-20 | Early | $NO_3$-N (kg $ha^{-1}$) | 5 | 3 | 4 | 4 | 4 | 4 | +6 | +2 |
| | | $NH_4$-N (kg $ha^{-1}$) | 8 | 7 | 13 | 11 | 22 | 19 | +1 | +2 |
| | | TN (%) | 0.22 | 0.15 | 0.11 | 0.10 | 0.15 | 0.06 | -0.01 | -0.04 |
| | | TOC (%) | 2.03 | 1.26 | 0.59 | 0.84 | 1.44 | 0.55 | | |
| | Late | $NO_3$-N (kg $ha^{-1}$) | 10 | 11 | 11 | 6 | 5 | 8 | -22 | -4 |
| | | $NH_4$-N (kg $ha^{-1}$) | 9 | 9 | 14 | 12 | 20 | 16 | -5 | -3 |
| | | TN (%) | 0.23 | 0.17 | 0.13 | 0.08 | 0.16 | 0.07 | -0.02 | -0.01 |
| | | TOC (%) | 2.06 | 1.22 | 0.63 | 0.49 | 1.48 | 0.8 | | |

**Table A6.** Corn grain and above ground biomass (harvested at R6) for plot receiving dairy slurry manure early and late during the fall. Values in parenthesis are presented as reference, these indicate $\mu \pm \sigma^2$ of 4 plots receiving the same treatment in an experiment performed in the same field (Tetter et al., 2019).

| | 2017-18 | | | 2018-19 | | | 2019-20 | | | **Avg. Diff** |
|---|---|---|---|---|---|---|---|---|---|---|
| | Early | Late | **Early - Late** | Early | Late | **Early - Late** | Early | Late | **Early - Late** | |
| Grain yield (≈ 15.5% moisture content) (Mg $ha^{-1}$) | 8.27 (16.3 ± 0.21) | 7.31 | **0.96** | 4.11 | 6.6 | **-2.49** | 5.45 | 4.93 | **0.52** | **-0.25** |
| Biomass yield (dry mass) (Mg $ha^{-1}$) | 22.20 (19.5) | 24.42 | **-2.22** | 16.18 | 19.04 | **-2.86** | 21.62 | 22.55 | **-0.93** | **-2.00** |
| Total nitrogen % of dry mass | 0.91 (0.83) | 0.87 | **0.04** | 0.65 | 0.66 | **-0.01** | 0.57 | 0.57 | **0** | **0.01** |

## ***Chapter 6: General conclusions***

Fertilized cropping systems are the largest source of anthropogenic $N_2O$ which is the third most important greenhouse gas and the most significant ozone-depleting emission. Development of agronomic mitigation strategies is crucial to reduce the increasing rate of anthropogenic $N_2O$ emissions. Nonetheless, assessment of these mitigation strategies is extremely difficult due to spatial and temporal variability of $N_2O$ soil emissions. The development of new technologies in the field of trace gas analyzers brings the opportunity to build new automated monitoring systems capable of measuring $N_2O$ soil emissions at the necessary temporal and spatial rates over extended periods of time.

This dissertation focusses on the design and validation of a state-of-the-art $N_2O$ isotopic monitoring system for field research that combines the capabilities of: (1) performing long sampling campaigns with enough temporal and spatial resolution to evaluate mitigation strategies; and, (2) measuring changes in the isotope ratios of soil $N_2O$ emissions to elucidate the underlying biological $N_2O$ production and consumption processes. The system is based on a new Laser Absorption Spectroscopy (LAS) technology, known as Off-Axis Integrated Cavity Output Spectroscopy (Off-Axis ICOS) which measures variations in $N_2O$ concentration and $N_2O$ isotope ratios simultaneously and in real time. The validation process went beyond traditional in-laboratory tests and included assessing the usability of the system in real-time field experiments, providing valuable insight to the N-cycle in corn production systems in the U.S. Upper Midwest. The key characteristics of the new $N_2O$ monitoring system and the main findings of our field research were summarized below:

1) **The combination of LAS with automatic soil chambers enables high temporal resolution and long term in-field $N_2O$ flux measurements with minimal maintenance.**

The LAS analyzer measures variations in $N_2O$ concentration at atmospheric levels with high accuracy and precision at high sampling frequencies, allowing to obtain precise flux estimations during very short chamber deployment times ( ~ 10 min). short deployment times reduced the inherit inaccuracies of chamber methodologies (i.e., chamber effects) and allowed to increase temporal and spatial resolution ~ 10 fluxes measurements per day from four different soil chambers (Chapter 3).

In addition to the high quality of the data generated, the system is easy to manage, automation is centralized and customizable to user specifications from the analyzer interface, similarly calibrations and measurement corrections, which only need to be performed annually, are also initiated from the analyzer interface. The Custom Digital Logic used to synchronize the different components of the monitoring systems was reliable under field conditions during long crop seasons and provided component (i.e. soil chamber, gas path, analyzer) isolation that in case of electrical failure, prevented its propagation. Because rain is a main trigger of $N_2O$ soil emissions, the Custom Digital Logic included a sampling sequence interruption during rain events that warranty rain-soil interaction. Custom Digital Logic did not limiting the flexibility of the gas analyzer and allow to connect up to 15 automatic soil chambers to a single LAS analyzer. Maintenance of the mechanical parts, which were exposed to the elements during 3 years of near-continuous operation, usually consisted in cleaning and lubrication. Sampling interruption due to soil chamber failure was unusual and when it happened it was in most cases solved easily by replacing immediately available spare parts (e.g., fuses, switches). The components of the gas path were tested for leaks annually, gas pumps were replaced every two years

through preventive maintenance. The autonomous $N_2O$ monitoring system provided accurate $N_2O$ flux measurements continuously at high temporal resolution with minimal user supervision.

Future efforts to maximize the efficiency of the system should include setting up an internet connection to access the analyzer remotely. This will allow the user to detect system failure in real time and increase the already high performance of the system while reducing travel to the experimental location. Remote access also warranty data protection by direct data storage in a more secure location than the analyzer hard drive. Furthermore, in real time flux estimation combined with remote data access would be useful to develop adaptive sampling decisions (e.g., setting chamber deployment time and dispatching soil or water sampling effort) to improve agricultural data acquisition and overall research.

2) **In high fertilized corn systems, accurate estimation of cumulative emissions requires continuous, all year-round, high frequency flux measurements.**

In highly fertilized crops the majority of the cumulative emissions occur in short lived, hard to predict peak emissions events, during three years of observations these represented up to 50% of the total cumulative emissions but only lasted from hours to a few days (i.e., < 6% of the total observations) (Chapter 3). Despite peak emissions tend to occur soon after fertilization and rain or during soil Freeze Thaw Cycles it is not possible to anticipate during which hours or days these peak emissions will occur, therefore capturing these peak events requires continuous sampling (i.e., daily). Due to the large hourly flux variability during peak emissions events, obtaining precise estimates of daily mean emission requires sub-daily sampling frequencies (i.e., hourly). In highly fertilized crop systems where peak emissions represent the majority of the emissions, obtaining accurate cumulative emissions estimates requires both continuous and high frequently sampling that can only be achieved with automatic monitoring systems.

3) ***In situ* isotopic measurement of soil emitted gases using LAS instruments is likely to remain a qualitative tool for $N_2O$ source partitioning**

The variability of LAS isotopic ratio measurements is inversely related to $N_2O$ concentration leading to high uncertainty in soil emitted $N_2O$ isotope ratios estimated using the Keeling plot method in which low concentration measurements have the largest influence. In-field systems performance under a range of conditions was evaluated through Monte Carlo simulations based in the instrument precision which was evaluated using reference gases. The most relevant Monte Carlo predictions of in-field measurement accuracy were evaluated with soil flux simulations using soil emitted gases. Isotope ratios derived using LAS measurements during soil flux simulations deviated markedly from IRMS measurements and from the Monte Carlo predictions. In-field system performance was limited by the concentration dependence of $N_2O$ isotope ratio measurements and the suspected presence of interferents in soil emitted gases. These characteristics of the LAS isotopic analyzer make it poorly suited for *in situ* source partitioning of $N_2O$ emitted from soil. Until we overcome these limitations in field $N_2O$ isotopic ratio measurements by LAS are best used qualitatively.

4) **In soil systems that experiences freeze-thaw cycles during the winter, measuring $N_2O$ fluxes frequently during the winter and spring is more important than sampling during the growing season.**

Seasonal freezing induces large peak $N_2O$ emissions related to soil freeze-thaw cycles (FTC) but the contribution of these peak emissions to cumulative $N_2O$ emissions is poorly quantified; this is mostly due to the lack of year-round measurements and because the short-lived $N_2O$ peaks are elusive to traditional measuring methods (i.e., manual soil chamber sampling) (Wagner-Riddle, et al., 2017). It is

also in these cold climate regions where it is common to apply manure during the fall rather than in the spring because it offers practical and economic advantages and allow the N forms in manure to become available to the crop for the next growing season (van Es, et al. 2006). However, fall manure application can lead to increased N soil content during the winter and enhance $N_2O$ peak emissions during soil FTC. During 4 years of continuous and high frequency $N_2O$ flux measurements, $N_2O$ peak events linked to soil Freeze Thaw Cycles occurring in the winter and spring represented between 42% to 74% of the total cumulative emissions while $N_2O$ emissions during the growing season were low and did not exhibit peak emissions (Chapter 4). Because in cold climates fall manure application enhances peak $N_2O$ emissions associated to FTC during the winter and spring and these represent a larger portion of total cumulative emissions that $N_2O$ emissions during the growing season, in these regions sampling frequently during the winter and spring is more important than sampling frequently during the growing season.

5) **The effect of dairy slurry application timing during the fall is counter-productive in terms of $NO_3^-$ and $N_2O$ losses, delaying manure application reduced $NO_3^-$ and overall N losses but increased cumulative $N_2O$ emissions due to larger peak emissions during FTC.**

Nitrate leachates represent by far the largest amount of N losses in fall manured plots. The main strategy recommended by USDA extension services and industry professionals to reduce nitrate losses is applying manure late (mid-November) rather than early (Mid-September) during the fall. Late fall manure application was effective in reducing $NO_3^-$ and total N losses ($NO_3^-$ and $N_2O$), however, $N_2O$ emissions from late manured plots were significantly larger than those from early fall manured plots.

Choosing between early or late fall dairy manure application is troublesome due to the trade-off between $NO_3^-$ and $N_2O$ losses associated with manure application timing. On one hand, nitrous oxide is

the third most important GHG and the most important anthropogenic Ozone depletion substance in the stratosphere (Stocker et al., 2013; Ravishankara et al., 2009). On the other hand, nitrate leaching from agricultural field is to the most widespread groundwater contaminant in Wisconsin where groundwater serves as the primary water source for 68% of residents (Mathewson et al., 2020). Reducing $NO_3^-$ and $N_2O$ contamination requires further investigation and the development of techniques to reduce losses of both N forms.

Dairy manure application in Wisconsin, the "Dairyland" is unavoidable and plays a crucial role in farm management and profitability and environmental impact. Nutrient cycling could offer important economic and environmental advantages when properly managed, but more investigation is needed to develop mitigation strategies that reduce N losses, especially in the forms of $NO_3^-$ and $N_2O$.

Studies as the one presented in chapter 5, are a rare however they are crucial to developing and evaluating the effect of fertilization on $NO_3^-$ and $N_2O$ losses. The accuracy in the estimation of N loss in Chapter 5 could be improved by using monolithic lysimeters instead of ceramic suctions cups (Wang et al., 2012), and quantifying ammonia volatilization in the days following manure application. Combining these with soil analyses and $N_2O$ isotope analysis scheduled in real time based in $N_2O$ flux intensity is a promising tool to improve our understanding of the soil N cycle. Further investigations will also benefit from including a wider range of treatments (different fertilization rates, the use of cover crops and/or nitrifier inhibitors, manure pre-treatment, etc.,) and as climate affect N losses they should be performed in different locations to develop better fertilization strategies at different locations.

The result of chapter 5, unveiled the trade-off in $NO_3^-$ and $N_2O$ losses after fall manure application and point that $N_2O$ emissions during FTC are the largest source of emissions and offer an opportunity to

significantly reduce cumulative $N_2O$ emissions and N losses. We have characterized the complexity of the problem presenting a new path of research to reduce $NO_3^-$ and $N_2O$ loss and environmental contamination from agricultural fields in Wisconsin.

Overall, this thesis has improved our understanding of $N_2O$ soil emissions in agriculture by:

- Developing a very powerful $N_2O$ monitoring tool for evaluating soil nitrous oxide mitigation strategies and improving estimates of annual nitrous oxide flux.
- Identifying the limitations and pitfalls of new laser absorption spectrometers for use in estimating the isotope ratios of soil emitted $N_2O$ use direct soil chamber measurements and the Keeling plot method.
- Pointing out the needs and goals in the development of LAS technologies for in-field and in real time $N_2O$ isotope research.
- Providing knowledge about the seasonal and daily variability of $N_2O$ emissions in highly fertilized corn systems in the Midwest U.S.
- Determining the effect of timing of manure application during the fall on $N_2O$ soil emissions and nitrate leaching loss and quantifying the N losses for both forms.
- Identifying the trade-off of the USDA recommendation for reducing $NO_3^-$ leaching in terms of $N_2O$ emissions and unveiling the need for new research to reduce $N_2O$ emissions after fall manure application in climates that experience winter freeze.

Collectively this thesis provides valuable information that led to reducing the impacts of agriculture on the environment and especially in the mitigation of $N_2O$ soil emissions

## *References*

Aguirre-Villegas, H., Larson, R. A. & Ruark, M. D. (2017). Managing Manure Nitrogen to Reduce Loses. *Sustainable Dairy*, 2–2. https://doi.org/10.4159/harvard.9780674183803.c2

Mathewson, P. D., Evans, S., Byrnes, T., Joos, A. & Naidenko, O. v. (2020). Health and economic impact of nitrate pollution in drinking water: a Wisconsin case study. *Environmental Monitoring and Assessment*, *192*(11). https://doi.org/10.1007/s10661-020-08652-0

Ravishankara, A. R., Daniel, J. S. & Portmann, R. W. (2009). Nitrous oxide (N2O): the dominant ozone-depleting substance emitted in the 21st century. *Science (New York, N.Y.)*, *326*(5949), 123–125. https://doi.org/10.1126/science.1176985

Stocker, T.F., Qin, D., Plattner, G.-K., Tignor, M., Allen, S. K., Boschung, J., Nauels, A., Xia, Y., Bex, V. & Midgley, P. M. (eds. ). (2013). *IPCC, 2013: Climate change2013: The Physical Science Basis. Contribution of Working Group I to the Fifth Assesment Report of the Intergovernmental Panel on Climate Change*. https://www.ipcc.ch/report/ar5/wg1/

van Es, H. M., Sogbedji, J. M. & Schindelbeck, R. R. (2006). Effect of Manure Application Timing, Crop, and Soil Type on Nitrate Leaching. *Journal of Environmental Quality*, *35*(2), 670–679. https://doi.org/10.2134/jeq2005.0143

Wagner-Riddle, C., Congreves, K. A., Abalos, D., Berg, A. A., Brown, S. E., Ambadan, J. T., Gao, X. & Tenuta, M. (2017). *Globally important nitrous oxide emissions from croplands induced by freeze-thaw cycles*. https://doi.org/10.1038/NGEO2907

Wang, Q., Cameron, K., Buchan, G., Zhao, L., Zhang, E. H., Smith, N. & Carrick, & S. (2012). Comparison of lysimeters and porous ceramic cups for measuring nitrate leaching in different soil types. *New Zealand Journal of Agricultural Research*, *55*(4), 333–345. https://doi.org/10.1080/00288233.2012.706224